

# **Modulated Waveform Design for Optimal Microwave Simultaneous Wireless Information and Power Transfer**

by **Perna Dhull**

Thesis submitted in fulfilment of the requirements for  
the degree of

**Doctor of Philosophy**

under the supervision of Prof. Dominique Schreurs, A/Prof.  
Negin Shariati, and Prof. Mehran Abolhasan

University of Technology Sydney  
Faculty of Engineering and Information Technology

December 2024



# **Modulated Waveform Design for Optimal Microwave Simultaneous Wireless Information and Power Transfer**

**Perna DHULL**

Examination Committee at KU Leuven:

Prof. Dr. Ir. Paul Sas, Chair (Dept. of Mechanical Engg., KU Leuven, Belgium)

Prof. Dr. Ir. Dominique Schreurs (ESAT-WaveCore, KU Leuven, Belgium)

A/Prof. Dr. Negin Shariati (University of Technology Sydney, Australia)

Prof. Dr. Mehran Abolhasan (University of Technology Sydney, Australia)

Prof. Dr. Ir. Sofie Pollin, Secretary (ESAT-WaveCore, KU Leuven, Belgium)

Prof. Dr. Ir. Alessandra Costanzo (University of Bologna, Italy)

Prof. Dr. Ir. Paul Leroux (FIIW-ESAT-ECS, KU Leuven, Belgium)

A/Prof. Dr. Daniel Franklin (University of Technology Sydney, Australia)

Prof. Dr. Ir. Massimo Piccardi (University of Technology Sydney, Australia)

External Examiners for UTS:

Prof. Dr. Xuejun Li (Auckland University of Technology, New Zealand)

A/Prof. Dr. Ir. Simon Hemour (University of Bordeaux, France)

September 2024

*“Live as if you were to die tomorrow.  
Learn as if you were to live forever.”*

- Mahatma Gandhi

# Dedication

*Dedicated to my parents, Promila Dhull and Sunil Dhull,  
and brother Ujjwal Dhull*

मेरे माता-पिता, प्रोमिला ढुल और सुनील ढुल,  
और भाई उज्जवल ढुल को समर्पित

मम मातापितरौ प्रोमिला ढुल तथा सुनील ढुल इत्यस्मै समर्पितः,  
तथा भ्राता उज्जवल ढुल ।

# Acknowledgements

My doctoral adventure at the University of Technology Sydney (UTS) and KU Leuven is about to end and it has definitely been a transformative journey for me in every way. I would like to express my gratitude to everyone whom I met during this journey and I learnt something from them whether it is personal or professional, small or big, everything matters to my heart. I am grateful to UTS for providing me with the financial support of the UTS President's Scholarship and International Research Scholarship, which gave me the opportunity and freedom to do what I wanted to do. I would like to express my sincere gratitude to Dominique Schreurs for the opportunity of double PhD degrees. I am grateful to her for taking care of my finances and accepting my request to extend my stay in Leuven.

I am extremely grateful to my supervisor, Dominique Schreurs, for supervising me and for her constant guidance and support through every challenge during the journey. I joined PhD just to do pure research and learn, and Dominique is the perfect supervisor for doing in-depth research, and I am lucky to have her. I started my PhD as a communication system engineer and knew nothing about microwave circuit designing and measurements, but I wanted to learn. I am thankful to her for her confidence in me that I could do it. I remember in my first year, I would discuss with her every small step I had learned, and she would listen to me with so much curiosity and patience, provide her critical feedback and guide me through the problems. Then, after a few months, I would laugh at those small problems. She discusses research with so much ease and critical depth that even a big research problem feels like a small problem.

---

While working with her, I just enjoyed the research and the process of learning about the integration of microwave research and communication research. I got the opportunity to explore research to satisfy my curiosity. She likes to know and learn every aspect of the fundamental research problem, whether it is small or big. She is a true researcher, a perfect Guru to follow your passion, and open to all challenging ideas. I never really felt lost in my research only because of her patience. After every discussion, I always feel so happy about research. I always feel excited to have discussions with her.

I am grateful to Dominique for all her help in the administrative process at both UTS and KU Leuven. I am thankful for her consistent efforts during the long period of signing a proper, well-defined double-degree agreement with UTS, which helped me in the end. She guided me in fulfilling both universities' requirements step-by-step from my first year of PhD. I was just focusing on research, and I was not aware of the importance of the agreement, but in the end I learnt how important the agreement was to go through the challenges at UTS.

Dominique's passion, discipline, and dedication to novel research motivated me to go through all the challenges and learn more and more. I really admire her integrity, research ethics, her consistent pursuit of excellence, and her leadership skills, and she does everything with her 100% best efforts. She supports risk-taking, following your passion, and encourages your dreams and adventure. I knew nothing about hardware measurements at the start of my PhD. Her commitment, confidence, and incredible patience through all challenges made me keep going and gave me the courage to solve the problems. I learnt everything from her during this journey from research discussions to measurements. I enjoyed my research and PhD journey only because of her. Whether I was in Sydney or in Leuven, she supported me at every step. She did so much for me I will always be grateful to her for my whole life. Now, I cannot imagine my life without sharing new learnings, failures, successes, and experiences with her. Dominique is a friend and family to me now. I just love her!

---

I would like to thank my UTS supervisors, Negin Shariati and Mehran Abolhasan, for their help and support during this journey. I am thankful to Negin for all the support and for all the equipment facilities in the RFCT lab.

I would like to thank Sofie Pollin for all the discussions and for providing an atmosphere for research discussions with intellectual freedom. I admire the way Sofie discusses complex communication technologies in such a simple and practical way that even a newcomer can understand. I would also like to thank Sofie for supporting my request to extend my stay at Leuven. I would like to thank Giacomo Paolini and Alessandra Costanzo for all the help and our discussions about the WPT circuit design. My work would not have been possible without Giacomo's help in the design of the efficient microwave receiver hardware. I started circuit designing with his help. I admire his patience and humbleness.

I am extremely grateful to Qiang Wu, my Responsible Academic Officer at UTS, for helping me in the final times of my PhD and for supporting research ethics and research integrity at UTS. I am thankful for his time in discussing the requirements of both degrees, his involvement in structuring a plan, and his guidance for the thesis submission toward the end of my PhD. It was really helpful for the successful submission of my thesis at UTS.

I would like to thank my examiners, Massimo Piccardi, Sofie Pollin, Alessandra Costanzo, Paul Leroux, Daniel Franklin, and Paul Sas, for the KU Leuven defence, and Xuejun Li and Simon Hemour for the UTS examination. Their feedback really helped me to improve the thesis.

I would like to thank Maede, Christos, Marie, Matko, and Ben for a very nice and friendly atmosphere in Belgium. I got friends the day I arrived in Leuven. I am really happy and appreciate all the lunches, discussions, get-togethers, and their dedication to our commitment to eating together in front of the castle every day irrespective of the urgency of the individual's work (personal time is important 😊). For me, it was really a breath of fresh air and helpful for my mental health, especially

---

after going through a tough lockdown in Sydney.

I am thankful to Yasser, Ali, and Vladimir for all our insightful discussions, measurement suggestions, and all the fun. I am thankful for all of their suggestions and for helping me through the challenges. I really enjoyed our office time at ESAT.

I would like to thank my friends Vincent, Zhang, and Sophie, who helped me in adjusting and settling down in Sydney and made me feel at home when I did not know anyone in Australia. I never stayed in a big city before, and it was challenging for me. I am also thankful to them for helping me with the cooking and introducing me to the various adventurous activities of beautiful Sydney.

I am thankful to Amanath, Majid, and Kevin Sharp for being at UTS during my PhD time and being available whenever I needed any suggestions, information, and help. Special thanks for the help through the challenging times at the end.

My decision to pursue a PhD in Australia was motivated by the National Geographic to explore Australia while pursuing research. Thanks to Dominique, I also traveled to beautiful Belgium and experienced so many different cultures in Europe. I would like to thank my friends, Ravi, Debi, and Rishabh, for making all the spontaneous travel plans, for their company, and for the enjoyment we had on all our trips across Europe. The day I met them, their bags got stolen thanks to my mistake, but somehow I got great friends after the chase :-). I really admire Ravi's 'not to miss a single moment of life and live life to the full potential' attitude.

I am thankful to Dominique for my Leuven stay, where I had a wonderful time, the best of my PhD journey. I really admire the quality of open and direct communication of the Flemish culture. I was lucky to get accommodation in Studentenwijk Arenberg on such short notice and experience a beautiful and peaceful campus life full of greenery, canals, and raw nature. In the past ten years, Leuven has been the most similar place to my hometown, among the places I lived. I could experience the peace of working on what I loved the most with so many nice people. The satisfaction I got from working in Leuven is more than every skydive.

---

I am thankful to my years-old friends Pulkit and Arpita for their support through the challenging times, for always being there with me, and for always listening to my dreamy plans for life.

I am also thankful to Rippy bhaiya and Swati didi for all the care and support, and for being my family in Sydney.

Finally, I would like to express my sincere gratitude to my loving family: my mother, Promila Dhull; my father, Sunil Dhull; my brother, Ujjwal; and my aunt, Sushila Dhull. This journey would not have been possible without their unconditional love, support, and blessings. I am also thankful to my grandparents Mahinder Dhull and Sudhi Devi for all their love and guidance throughout my life. My parents always encouraged me to continuously learn through life and explore new experiences. I am forever indebted to my father for imbibing integrity and moral values in me and teaching me the importance of having a good character. My father is my best friend. He gave me courage, and my family always had my back through all the challenges. I am also thankful to all my uncles and aunts (my extended family members) for their support. Although I could not spend much time with them during this journey, I wish to spend more time with my family in the future.

Overall, my doctoral journey has been very fulfilling, and I really enjoyed it. I am grateful to everyone whom I met during this time and we laughed together. I am thrilled that I had an opportunity to pursue double degrees, which gave me the opportunities to learn, visit Australia and Europe, interact with brilliant people from different backgrounds and cultures, and it transformed my perspective on life. It was a rollercoaster of different experiences and emotions. Every challenge taught me some lessons, and without them, the journey would not have been the same. Everything happens for the best. Life is just so beautiful and full of surprises!

Prerna Dhull

November 6, 2024

# Abstract

The Internet of Things (IoT) envisions a global wireless network where trillions of wireless sensors are connected via the Internet, generating data from a diverse range of applications. Wireless standards such as 5G and beyond will underpin the growth in the ubiquitous deployment of IoT devices. To make such deployments feasible, there is a need for sustainable batteryless energy sources. One promising technology aiming to provide both power and data transfer is Simultaneous Wireless Information and Power Transfer (SWIPT).

SWIPT provides an energy-efficient solution by exploiting the same communication signal for data transfer as well as Wireless Power Transfer (WPT). The transferred output power to the sensor is not only a function of received signal power but also of the received signal shape. Therefore, high peak-to-average power ratio (PAPR) waveforms came into the picture to increase WPT. However, these high PAPR waveforms deteriorate the Wireless Information Transfer (WIT) performance due to the saturation of the non-linear amplifier at the transmitter, and the transmission of data over these waveforms reduces WPT. Therefore, it is necessary to design waveforms to maximize the trade-off between the information rate and extracted power at the receiver.

This thesis aims to design modulated waveforms carrying information while simultaneously maximizing the output power. A Multitone PSK waveform has been proposed for the rectifier-receiver so that information detection is possible with only a rectifier reducing the overall power consumption at the sensor node. A rectifier

---

circuitry with an optimum power conversion efficiency over a required bandwidth is designed and fabricated. The SWIPT performance of the designed waveform signal is studied with the measurements.

Next, a Multitone ASK waveform is proposed by transmitting information in tones' amplitude levels. The WPT and WIT performances of the waveform are analyzed. The performance of the designed signal with the symbol level and the effect of different distributions for symbol levels is analyzed for increasing WPT performance.

Finally, a combined Multitone QAM is proposed by using both phases and amplitudes for information transfer offering a higher data rate. QAM symbol constellation is redesigned and two asymmetric QAM constellations are introduced to enhance the WPT performance of the system due to varying amplitudes.

The designed waveforms offer the benefit of reducing the overall power consumption at the sensor nodes for future SWIPT-enabled IoT WSNs.

**KEYWORDS:** Amplitude shift keying (ASK); Baseband; Batteries; Data transfer; Information decoding; Energy harvesting; Envelope detector; Integrated information-energy receiver; Internet of things; Local oscillator; Low-power electronics; Multi-tone; Microwave devices; Modulation technique; OFDM; Peak to average power ratio; Phase shift keying (PSK); Quadrature amplitude modulation (QAM); Radio frequency; Receiver architecture; Receivers; Rectifiers; Sensors; Signal design; Simultaneous wireless information and power transfer (SWIPT); Symbols; Waveform design; Wireless communication; Wireless power transfer (WPT); Wireless sensor networks

# Beknopte Samenvatting

Internet der dingen (IoT) voorziet een wereldwijd draadloos netwerk waarin biljoenen draadloze sensoren via internet zijn verbonden en gegevens genereren uit een breed scala aan toepassingen. Draadloze standaarden zoals 5G en hoger zullen de groei van de alomtegenwoordige inzet van IoT-apparaten ondersteunen. Om dergelijke toepassingen mogelijk te maken is er behoefte aan duurzame batterijloze energiebronnen. Een veelbelovende technologie die zowel stroom als gegevensoverdracht wil bieden, is gelijktijdige draadloze informatie en vermogenoverdracht (SWIPT).

SWIPT biedt een energiezuinige oplossing door hetzelfde communicatiesignaal te benutten voor gegevensoverdracht en draadloze vermogenoverdracht (WPT). Het overgedragen uitgangsvermogen naar de sensor is niet alleen een functie van het ontvangen signaalvermogen, maar ook van de ontvangen signaalvorm. Daarom kwamen golfvormen met een hoge piek-tot-gemiddelde vermogensverhouding (PAPR) in beeld om de WPT te verhogen. Deze hoge PAPR-golfvormen verslechteren echter de prestaties van de draadloze informatie overdracht (WIT) als gevolg van de verzadiging van de niet-lineaire versterker bij de zender, en de overdracht van gegevens via deze golfvormen vermindert de WPT. Daarom is het noodzakelijk om golfvormen te ontwerpen om de wisselwerking tussen de informatiesnelheid en het onttrokken vermogen bij de ontvanger te maximaliseren.

Dit proefschrift heeft tot doel gemoduleerde golfvormen te ontwerpen die informatie dragen en tegelijkertijd het uitgangsvermogen maximaliseren. Voor de gelijkrichter-ontvanger is een meertonige PSK-golfvorm voorgesteld, zodat informatiedetectie

---

mogelijk is met alleen een gelijkrichter, waardoor het totale energieverbruik bij het sensorknooppunt wordt verminderd. Er wordt een gelijkrichterschakeling met een optimale efficiëntie van de energieomzetting over een vereiste bandbreedte ontworpen en vervaardigd. Met de metingen wordt de SWIPT-prestatie van het ontworpen golfvormsignaal bestudeerd.

Vervolgens wordt een Multitone ASK-golfvorm voorgesteld door informatie in de amplitudeniveaus van de tonen te verzenden. De WPT- en WIT-prestaties van de golfvorm worden geanalyseerd. De prestaties van het ontworpen signaal met het symboolniveau en het effect van verschillende distributies voor symboolniveaus worden geanalyseerd om de WPT-prestaties te verbeteren.

Ten slotte wordt een gecombineerde Multitone QAM voorgesteld door zowel fasen als amplitudes te gebruiken voor informatieoverdracht, wat een hogere datasnelheid oplevert. De QAM-symboolconstellatie is opnieuw ontworpen en er zijn twee asymmetrische QAM-constellaties geïntroduceerd om de WPT-prestaties van het systeem te verbeteren vanwege variërende amplitudes.

De ontworpen golfvormen bieden het voordeel dat ze het totale energieverbruik op de sensorknooppunten voor toekomstige SWIPT-compatibele IoT WSN's verminderen.

# List of Abbreviations

**4G** Fourth Generation

**5G** Fifth Generation

**6G** Sixth Generation

**AC** Alternating Current

**ADC** Analog-to-Digital Converter

**ADSK** Amplitude Difference Shift Keying

**ARSK** Amplitude Ratio Shift Keying

**ASK** Amplitude Shift Keying

**AWGN** Additive White Gaussian Noise

**BER** Bit Error Rate

**BPF** Band Pass Filter

**BS** Base Station

**CP** Cyclic Prefix

**CW** Continuous Waveform

**DC** Direct Current

**DFT** Discrete Fourier Transform

**EH** Energy Harvesting

**EVM** Error Vector Magnitude

**FFT** Fast Fourier Transform

**FSK** Frequency Shift Keying

**GCD** Greatest Common Divisor

**HCS** Hybrid Constellation Shaping

**ID** Information Detection

**IM** Intermodulation

**IoT** Internet of Things

**IT** Information Transfer

**LPF** Low Pass Filter

**NOMA** Non-orthogonal Multiple Access

**OFDM** Orthogonal Frequency Division Multiplexing

**PA** Power Amplifier

**PAPR** Peak to Average Power Ratio

**PCE** Power Conversion Efficiency

**PDF** Probability Density Function

**PS** Power Splitting

**PSK** Phase Shift Keying

**QAM** Quadrature Amplitude Modulation

**QPSK** Quadrature Phase Shift Keying

**R&S** Rohde & Schwarz

**RF** Radio Frequency

**RFID** Radio Frequency Identification

**SER** Symbol Error Rate

**SNR** Signal-to-Noise Ratio

**SVM** Support Vector Machine

**SWIPT** Simultaneous Wireless Information and Power Transfer

**TS** Time Switching

**VSG** Vector Signal Generator

**WIT** Wireless Information Transfer

**WPT** Wireless Power Transfer

**WSN** Wireless Sensor Networks

# List of Symbols

$\alpha$	Parameter to redesign $M/4$ inner constellation points for asymmetric QAM
$\alpha_c$	Parameter to redesign $M/4$ inner constellation points for compressed asymmetric QAM
$\alpha_e$	Parameter to redesign $M/4$ inner constellation points for expanded asymmetric QAM
$\alpha_{\sqrt{M}}$	Column vector consisting of parameter $\alpha$
$\beta$	Parameter to redesign $3M/4$ outer constellation points for asymmetric QAM
$\beta_c$	Parameter to redesign $3M/4$ outer constellation points for compressed asymmetric QAM
$\beta_e$	Parameter to redesign $3M/4$ outer constellation points for expanded asymmetric QAM
$\beta_{\sqrt{M}}$	Column vector consisting of parameter $\beta$
$\Delta \mathbf{B}_{\sqrt{M}}$	Column vector for designing asymmetric $\sqrt{M}$ -PAM constellation
$\Delta \mathbf{F}_i$	Column vector consisting of $(N - 1)$ frequency spacings between consecutive tones of $N$ -tones multitone RF signal
$\mathbf{B}_{\text{asym}, \sqrt{M}}$	Column vector consisting of redesigned asymmetric $\sqrt{M}$ -PAM constellation
$\mathbf{B}_{\sqrt{M}}$	Square matrix having the symmetric $\sqrt{M}$ -PAM constellation symbols
$\mathbf{S}$	Available information symbol set
$\mathbf{U}_i$	Upper triangular matrix of order $i \times i$ having non-zero elements as 1
$\Delta f_n$	Frequency spacing between $(n + 1)^{\text{th}}$ and $n^{\text{th}}$ tones
$\delta$	Considered phase range to allocate the information symbol in terms of phases
GCD	Greatest common divisor among $f_n$ s of multitone RF signal
$\phi_n$	Phase of the $n^{\text{th}}$ tone frequency $f_n$ of $N$ -tone multitone RF signal
$\Phi_x$	Lower bound of the symbols constellation for phases of multitone RF signal
$\Phi_y$	Upper bound of the symbols constellation for phases of multitone RF signal
$\text{IM}_2$	Second order intermodulation frequency component

$\text{PAPR}_{\text{exp}}$	PAPR of transmitted multitone signal $x(t)$ for exponentially distributed information amplitude levels
$\text{PAPR}_{\text{linear}}$	PAPR of transmitted multitone signal $x(t)$ for linearly distributed information amplitude levels
$\text{PAPR}_{\text{log}}$	PAPR of transmitted multitone signal $x(t)$ for logarithmically distributed information amplitude levels
$\text{Pr}(x)$	Probability at $x$
$A$	Amplitudes of tones of multitone PSK RF signal
$b_i$	$i^{\text{th}}$ symbol of $\sqrt{M}$ PAM symbol constellation
$C_1$	Input capacitance of rectifier
$C_{\text{out}}$	Capacitance of RC-LPF of rectifier
$D_1$	Diode 1 of the rectifier
$D_2$	Diode 2 of the rectifier
$f_c$	Center frequency of the multitone RF signal
$f_n$	Frequency of the $n^{\text{th}}$ tone of multitone RF signal
$f_{\text{cutoff}}$	Cut-off frequency of low pass filter
$gf_{\text{exp}}$	Growth factor for exponentially distributed information amplitude levels
$gf_{\text{log}}$	Growth factor for logarithmically distributed information amplitude levels
$L$	ASK modulation order for the information symbol set for a particular designed modulation scheme
$l_{\text{max}}$	Maximum level of information symbols for multitone ASK signal
$l_{\text{min}}$	Minimum level of information symbols for multitone ASK signal
$l_i$	$i^{\text{th}}$ information symbol from the available information symbol set $\mathcal{S}$ for multitone ASK
$l_L$	Maximum transmitted information symbol level for multitone ASK
$l_{s_i}$	Transmitted ASK symbol over the $n^{\text{th}}$ tone frequency $f_n$ of $x(t)$
$M$	Overall modulation order of available information symbol set for a particular designed modulation scheme
$N$	Number of tones in multitone RF signal
$P_{\text{avg,max}}$	Maximum possible average power for the transmitted multitone ASK signal $x(t)$ after embedding the information
$P_{\text{avg,min}}$	Minimum possible average power for the transmitted multitone ASK signal $x(t)$ after embedding the information
$P_{\text{avg}}$	Average power for the transmitted multitone ASK signal $x(t)$ after embedding the information

$P_{\text{in}}$	Input power for the transmitted signal $x(t)$
$P_{\text{sym\_avg}}$	Average symbol power for multitone ASK signal $x(t)$
$r$	BW spreading factor for multitone RF signal
$r(t)$	Reference multitone signal with all tones having equal powers
$R_{\text{load}}$	Load resistance of the rectifier
$s_i$	$i^{\text{th}}$ information symbol from available information symbol set $\mathbf{S}$
$s_n$	Information symbol transmitted over the $n^{\text{th}}$ tone for a particular designed modulation scheme
$S_{11}$	Reflection coefficient of the rectifier
$s_{\text{inner}}$	Inner $M/4$ symbols of QAM constellation
$s_{\text{outer}}$	Outer $3M/4$ symbols of QAM constellation
$s_{i,k}$	QAM information from a set of $M$ information symbols as a combination of two $\sqrt{M}$ PAM symbol constellations
$T$	Time-period of waveform $x(t)$
$T_{\text{PSK}}$	Time-period of multitone PSK signal
$T_{\text{p}}$	Throughput of multitone RF signal $x(t)$
$V_{\text{th}}$	Threshold voltage of diode
$X(f)$	Frequency spectrum of multitone RF signal $x(t)$
$x(t)$	Time-domain designed multitone RF signal
$Y(f)$	Frequency spectrum of baseband signal output $y(t)$ after the rectifier
$y(t)$	Time-domain baseband signal output after the rectifier
$y_{\text{dc}}$	dc voltage of the received signal $y(t)$
BW	Bandwidth of multitone RF signal

# Contents

<b>Certificate of Authorship / Originality</b>	<b>i</b>
<b>Examination Committee</b>	<b>ii</b>
<b>Dedication</b>	<b>iv</b>
<b>Acknowledgements</b>	<b>v</b>
<b>Abstract</b>	<b>x</b>
<b>Beknopte Samenvatting</b>	<b>xii</b>
<b>List of Abbreviations</b>	<b>xiv</b>
<b>List of Symbols</b>	<b>xvi</b>
<b>Contents</b>	<b>xix</b>
<b>List of Figures</b>	<b>xxiii</b>
<b>List of Tables</b>	<b>xxxii</b>
<b>1 Introduction</b>	<b>1</b>
1.1 Motivation . . . . .	1
1.2 Scope of the PhD Thesis . . . . .	6
1.2.1 Aim . . . . .	6
1.2.2 Challenges and Research Questions . . . . .	6
1.3 Contributions . . . . .	7

1.3.1	Contribution 1: Multitone PSK modulated waveform design for SWIPT . . . . .	8
1.3.2	Contribution 2: Multitone ASK modulated waveform design for SWIPT . . . . .	9
1.3.3	Contribution 3: Multitone QAM modulated waveform design for SWIPT . . . . .	9
1.4	Publications . . . . .	10
1.5	Thesis Outline . . . . .	11
<b>2</b>	<b>Literature Review</b>	<b>14</b>
2.1	Background . . . . .	14
2.1.1	WPT and SWIPT . . . . .	14
2.1.2	Non-linear Energy Harvester Model . . . . .	17
2.2	Waveforms for WPT and SWIPT . . . . .	19
2.2.1	Impulsive Wireless Power Transmission . . . . .	20
2.2.2	Spatial Power Combining . . . . .	21
2.2.3	Multitone Transmission . . . . .	22
2.2.3.1	Tone Separation . . . . .	24
2.2.3.2	Number of Tones . . . . .	24
2.2.3.3	Phase . . . . .	24
2.2.3.4	Input Power Range . . . . .	25
2.2.3.5	Low-pass RC Filter Cut-off Frequency ( $f_{\text{cutoff}}$ ) . . . . .	25
2.2.3.6	Effect of Load . . . . .	25
2.2.4	Modulated Waveform . . . . .	26
2.2.4.1	Modulation Scheme . . . . .	27
2.2.4.2	Bit rate . . . . .	27
2.2.4.3	Modulation Order . . . . .	27
2.3	Modulation Techniques for SWIPT . . . . .	28
2.3.1	PAPR Based Detection . . . . .	32
2.3.1.1	Dual Mode Adaptive SWIPT System . . . . .	34

---

2.3.1.2	Tone-index Modulation . . . . .	34
2.3.2	Amplitude Based Detection . . . . .	35
2.3.2.1	Biased ASK . . . . .	35
2.3.2.2	Ratio ASK . . . . .	36
2.3.3	Frequency Based Detection . . . . .	38
2.3.3.1	Non-coherent Multitone FSK . . . . .	39
2.3.3.2	ASK-OFDM . . . . .	41
2.4	Input Distribution . . . . .	42
2.4.1	Asymmetric Modulation . . . . .	44
2.4.2	Constellation Rotation . . . . .	47
2.5	Conclusion . . . . .	50
<b>3</b>	<b>Multitone PSK</b>	<b>51</b>
3.1	Introduction . . . . .	51
3.2	Signal Model . . . . .	56
3.2.1	Multitone PSK Frequencies . . . . .	58
3.2.2	Multitone PSK Phases . . . . .	60
3.3	Multitone PSK Phase distribution and PAPR . . . . .	64
3.4	Receiver Model . . . . .	73
3.4.1	Rectifier Design . . . . .	75
3.4.2	Measurement Setup . . . . .	77
3.5	Performance Analysis of Multitone PSK . . . . .	80
3.6	Conclusion . . . . .	96
<b>4</b>	<b>Multitone ASK</b>	<b>98</b>
4.1	Introduction . . . . .	98
4.2	Signal Model . . . . .	102
4.3	Amplitude Levels Distribution and PAPR . . . . .	112
4.4	Performance Analysis of Multitone ASK . . . . .	119
4.5	Conclusion . . . . .	129

---

<b>5</b>	<b>Multitone QAM</b>	<b>130</b>
5.1	Introduction . . . . .	130
5.2	Signal Model . . . . .	134
5.2.1	Signal Design . . . . .	134
5.2.2	PAPR Analysis . . . . .	139
5.3	Asymmetric QAM Constellation . . . . .	143
5.3.1	QAM Constellation Redesign . . . . .	143
5.3.2	Expanded Multitone QAM symbols constellations . . . . .	145
5.3.3	Compressed Multitone QAM symbols constellations . . . . .	147
5.4	Performance Analysis of Multitone QAM . . . . .	149
5.5	Conclusion . . . . .	160
<b>6</b>	<b>Conclusions and Recommendations for Future Work</b>	<b>162</b>
6.1	Conclusions . . . . .	163
6.2	Recommendations & Future Works . . . . .	165
	<b>Bibliography</b>	<b>167</b>
	<b>Biography</b>	<b>185</b>

# List of Figures

1.1	A simultaneous wireless information and power transfer system model.	3
1.2	Base station transmitting to a sensor node consisting of a rectifier, PMU (power management unit), storage unit for power extraction, and backscattering for information transfer from the received signal.	4
2.1	Rectenna block diagram.	15
2.2	Separated information and energy receiver architecture for SWIPT.	16
2.3	Integrated information and energy receiver architecture for SWIPT.	16
2.4	A wireless power transfer communication system model.	17
2.5	A non-linear energy harvesting rectifier receiver model.	18
2.6	Impulsive wireless power transmission with the same average power $P_{avg}$ .	20
2.7	OFDM frequency spectrum and corresponding receiver architecture.	29
2.8	Frequency spectra of multisine superimposed upon the OFDM information signal and corresponding receiver architecture.	29
2.9	CP-OFDM information symbol superimposed on the rectangular pulse power signal.	29
2.10	Frequency spectrum of unmodulated power signal superimposed on modulated information signal.	32
2.11	PAPR-based waveform for (a) $N = 4$ , (b) $N = 8$ , and its (c) receiver architecture.	33
2.12	Dual mode SWIPT system block diagram.	34
2.13	Biased 4-ASK with increasing minimum symbol power.	36
2.14	Dual ASK SWIPT system with two half-wave rectifiers.	37

---

2.15	Multitone FSK waveform and receiver architecture. . . . .	39
2.16	Symbol construction for uniform multitone FSK with tone $N = 3$ and modulation order $M = 4$ . . . . .	40
2.17	Symbol construction for non-uniform multitone FSK with tone $N = 3$ and modulation order $M = 4$ . . . . .	40
3.1	SWIPT integrated receiver rectifier. . . . .	56
3.2	5-tone multitone PSK RF input signal spectrum $X(f)$ centered around carrier frequency $f_c = 2.45$ GHz and rectified baseband output spec- trum $Y(f)$ consisting of IM frequency tones (in MHz) used for infor- mation decoding (colored) and extra IM components (black). . . . .	56
3.3	Multitone PSK tone phase constellation for $n^{th}$ tone, (a) $n = 2$ , (b) $n = 3$ , (c) $n = 4$ , and (d) $n = 5$ , for $M = 4$ and $\delta = [-90^\circ, 90^\circ]$ . . . . .	61
3.4	Multitone PSK tone phase constellation for $n^{th}$ tone, (a) $n = 2$ , (b) $n = 3$ , (c) $n = 5$ , and (d) $n = 6$ , for $M = 4$ and $\delta = [-45^\circ, 45^\circ]$ . . . . .	62
3.5	Multitone PSK tone phase constellation for $n^{th}$ tone, (a) $n = 2$ and (b) $n = 3$ , for $M = 4$ and $\delta = [-180^\circ, 180^\circ]$ . . . . .	62
3.6	Irwin-Hall Probability density function (PDF) for a random variable $t$ with increasing $n$ . . . . .	65
3.7	Probability density function (PDF) for Irwin-Hall distribution and Gaussian distribution for a random variable $t$ with (a) $n = 1$ , (b) $n = 2$ , (c) $n = 3$ , (d) $n = 4$ , (e) $n = 5$ , (f) $n = 6$ , (g) $n = 7$ , and (h) $n = 8$ . . . . .	66
3.8	Irwin-Hall Probability density function (PDF) for $n^{th}$ tone of multi- tone PSK for (a) $n = 2$ , (b) $n = 4$ , (c) $n = 6$ , (d) $n = 8$ , (e) $n = 10$ , and (f) $n = 16$ for $\delta = [-45^\circ, 45^\circ]$ . . . . .	69
3.9	Irwin-Hall Probability density function (PDF) for $n^{th}$ tone of multi- tone PSK for (a) $n = 2$ , (b) $n = 4$ , (c) $n = 8$ , and (d) $n = 16$ for $\delta = [-90^\circ, 90^\circ]$ . . . . .	70

---

---

3.10	Irwin-Hall Probability density function (PDF) for $n^{\text{th}}$ tone of multi-tone PSK for (a) $n = 2$ and (b) $n = 3$ for $\delta = [-180^\circ, 180^\circ]$ . . . . .	70
3.11	Probability density function (PDF) for $n^{\text{th}}$ tone of multitone PSK for (a) $n = 2$ , (b) $n = 4$ , (c) $n = 6$ , (d) $n = 8$ , (e) $n = 10$ , and (f) $n = 16$ for $\delta = [-45^\circ, 45^\circ]$ . . . . .	71
3.12	Probability density function (PDF) for $n^{\text{th}}$ tone of multitone PSK for (a) $n = 2$ , (b) $n = 4$ , (c) $n = 6$ , (d) $n = 8$ , (e) $n = 10$ , and (f) $n = 16$ for $\delta = [-90^\circ, 90^\circ]$ . . . . .	72
3.13	Probability density function (PDF) for $n^{\text{th}}$ tone of multitone PSK for (a) $n = 2$ and (b) $n = 3$ for $\delta = [-180^\circ, 180^\circ]$ . . . . .	73
3.14	Multitone PSK PAPR with varying $N$ for $M = 4$ , GCD = 1 MHz and 1000 multitone streams for each $N$ and $\delta$ . . . . .	74
3.15	Rectifier simulation model for SWIPT for a matched BW of 100 MHz with $C_1 = 1$ pF, two Schottky diodes (Skyworks SMS7630-079LF), and a LPF ( $C_{\text{out}} = 0.1$ pF and $R_{\text{load}} = 4.4$ k $\Omega$ ). . . . .	74
3.16	(a) Fabricated integrated receiver rectifier and (b) Measurement setup with VSG R&S SMW200A, power splitter, rectifier, and oscilloscope R&S RTO2044. . . . .	76
3.17	Measured multitone PSK PAPR with varying $N$ for $M = 4$ , GCD = 1 MHz, and 50 multitone streams for each $N$ and $\delta$ . . . . .	78
3.18	Oscilloscope measured transmitted $x(t)$ and received $y(t)$ waveforms with (a) all phases aligned (b) with information symbol transmission, and (c) frequency spectra. . . . .	79
3.19	Simulated PCE for multitone PSK centred around 2.45 GHz with $N = 5$ , GCD = 1 MHz, and $M = 4$ for 100 multitone streams, i.e., 1000 bits. . . . .	81
3.20	Measured PCE for multitone PSK with $N = 6$ , GCD = 1 MHz, and $M = 4$ for 100 multitone streams, i.e., 1000 bits. . . . .	81

---

---

3.21	Simulated BER using multitone PSK with $N = 6$ , $M = 4$ , GCD = 1 MHz, $r = 0$ , and for 100 multitone streams, i.e., 1000 bits. . . . .	84
3.22	Measured BER using multitone PSK with $N = 6$ , $M = 4$ , GCD = 1 MHz, $r = 0$ , and for 100 multitone streams, i.e., 1000 bits. . . . .	84
3.23	Symbols constellations at baseband tone of 1 MHz for $N = 6$ , $M = 4$ , $\delta = [-180^\circ, 180^\circ]$ , received input power (a) $P_{\text{in}} = -21$ dBm, (b) $P_{\text{in}} = -16$ dBm, (c) $P_{\text{in}} = -11$ dBm, and (d) $P_{\text{in}} = -6$ dBm for 100 multitone streams, i.e., 500 symbols. . . . .	85
3.24	Simulated PCE using multitone PSK with $N = 3$ , GCD = 1 MHz, $\delta = [-180^\circ, 180^\circ]$ , $r = 0$ , and 100 multitone streams for different $M$ . . . . .	86
3.25	Simulated BER using multitone PSK with $N = 3$ , GCD = 1 MHz, $\delta = [-180^\circ, 180^\circ]$ , $r = 0$ , and 100 multitone streams for different $M$ . . . . .	87
3.26	Measured BER using multitone PSK with $N = 3$ , GCD = 1 MHz, $\delta = [-180^\circ, 180^\circ]$ , $P_{\text{in}} = -6$ dBm, $r = 0$ , and 100 multitone streams for $M = 2$ , $M = 4$ , and $M = 8$ . . . . .	87
3.27	Measured PCE using multitone PSK with $M = 4$ , GCD = 1 MHz, $\delta = [-180^\circ, 180^\circ]$ , $P_{\text{in}} = -6$ dBm, $r = 0$ , and 100 multitone streams for $N = 3$ , $N = 4$ , $N = 5$ , and $N = 6$ . . . . .	88
3.28	Simulated BER using multitone PSK with $M = 4$ , GCD = 1 MHz, $\delta = [-180^\circ, 180^\circ]$ , $P_{\text{in}} = -6$ dBm, $r = 0$ , and 100 multitone streams for $N = 3$ , $N = 4$ , $N = 5$ , and $N = 6$ . . . . .	89
3.29	Measured BER using multitone PSK with $M = 4$ , GCD = 1 MHz, $\delta = [-180^\circ, 180^\circ]$ , $P_{\text{in}} = -6$ dBm, $r = 0$ , and 100 multitone streams for $N = 3$ , $N = 4$ , $N = 5$ , and $N = 6$ . . . . .	89
4.1	Integrated receiver rectifier for SWIPT. . . . .	102
4.2	Four-tone Multitone ASK RF signal spectrum $X(f)$ centered around frequency $f_c$ and rectified baseband output spectrum $Y(f)$ consisting of intermodulations frequency tones (in MHz) carrying information (colored) and extra intermodulations components (black). . . . .	103

---

---

4.3	Magnitude variation of first baseband tone ( $\Delta f_1 = 1$ MHz) for Multitone ASK centered around 2.45 GHz with $N = 3$ , $L = 2$ , and $l_{\min} = 0.1$ for different information symbol patterns over multitone streams by varying symbol $l_{s_2}$ . . . . .	110
4.4	Magnitude variation of first baseband tone ( $\Delta f_1 = 1$ MHz) for Multitone ASK centered around 2.45 GHz with $N = 3$ , $L = 4$ , and $l_{\min} = 0.1$ for different information symbol patterns over multitone streams by varying symbol $l_{s_2}$ . . . . .	110
4.5	Magnitude variation of second baseband tone ( $\Delta f_2 = 2$ MHz) for Multitone ASK centered around 2.45 GHz with $N = 3$ , $L = 4$ , and $l_{\min} = 0.1$ for different information symbol patterns over multitone streams by varying symbol $l_{s_2}$ . . . . .	111
4.6	Analytical PAPR for Multitone ASK centred around 2.45 GHz with $N = 6$ and linearly distributed amplitudes with variation in $l_{\min}$ . . . . .	114
4.7	Simulated PAPR for Multitone ASK centred around 2.45 GHz with $N = 6$ and linearly distributed amplitudes with variation in $l_{\min}$ for 100 multitone streams. . . . .	114
4.8	Linearly distributed, exponentially distributed, and logarithmically distributed symbols with $gf = 10$ for $l_{\min} = 0.1$ and $L = 4$ . . . . .	116
4.9	PAPR for Multitone ASK centred around 2.45 GHz with $N = 6$ and exponentially distributed amplitudes with variation in $l_{\min}$ for 100 multitone streams. . . . .	117
4.10	PAPR for 6-tone Multitone ASK centred around 2.45 GHz with logarithmic amplitudes ( $gf = 10$ ) with variation in $l_{\min}$ for 100 multitone streams. . . . .	118
4.11	PAPR for 6-tone Multitone ASK centered around 2.45 GHz with linearly distributed, exponentially distributed, and logarithmically distributed levels ( $gf = 10$ ) with variation in $l_{\min}$ and $L = 4$ for 100 multitone streams. . . . .	118

---

---

4.12	Magnitude variation of first baseband tone ( $\Delta f_1 = 1$ MHz) for Multitone ASK centred around 2.45 GHz with $N = 3$ , $L = 2$ , and $l_{\min} = 0.1$ for different patterns of logarithmically distributed information symbol over multitone streams by varying symbol $l_{s_2}$ . . . . .	119
4.13	Magnitude variation of first baseband tone ( $\Delta f_1 = 1$ MHz) for Multitone ASK centred around 2.45 GHz with $N = 3$ , $L = 4$ , and $l_{\min} = 0.1$ for different patterns of logarithmically distributed information symbol over multitone streams by varying symbol $l_{s_2}$ . . . . .	120
4.14	Magnitude variation of second baseband tone ( $\Delta f_2 = 2$ MHz) for Multitone ASK centred around 2.45 GHz with $N = 3$ , $L = 4$ , and $l_{\min} = 0.1$ for different patterns of logarithmically distributed information symbol over multitone streams by varying symbol $l_{s_2}$ . . . . .	120
4.15	4-tone Multitone ASK waveform $x(t)$ centred around 2.45 GHz having all tones power equal and maximum for a data transfer of $[1\ 0\ 1\ 0\ 1\ 0]$ . . . . .	122
4.16	4-tone Multitone ASK waveform $x(t)$ centred around 2.45 GHz for $l_{\min} = 0.1$ and $L = 4$ for a data transfer of $[0\ 0\ 0\ 0\ 0\ 0]$ . . . . .	123
4.17	4-tone Multitone ASK waveform $x(t)$ centred around 2.45 GHz for $l_{\min} = 0.5$ and $L = 4$ for a data transfer of $[0\ 0\ 0\ 0\ 0\ 0]$ . . . . .	123
4.18	4-tone Multitone ASK waveform $x(t)$ centred around 2.45 GHz for $l_{\min} = 0.1$ and $L = 4$ for a data transfer of $[0\ 0\ 1\ 1\ 0\ 1]$ . . . . .	124
4.19	6-tone Multitone ASK waveform $x(t)$ centred around 2.45 GHz for $l_{\min} = 0.3$ and $L = 4$ for a data transfer of $[0\ 1\ 1\ 1\ 1\ 0\ 1\ 0\ 1\ 0]$ . . . . .	124
4.20	PCE for 4-tone Multitone ASK centred around 2.45 GHz with $L = 4$ for 600 multitone streams, i.e., 3600 bits data transfer for $l_{\min} = 0.1$ , $l_{\min} = 0.3$ , $l_{\min} = 0.5$ , and $l_{\min} = 0.7$ . . . . .	125
4.21	PCE for 4-tone Multitone ASK centred around 2.45 GHz with $L = 4$ and $P_{\text{in}} = 0$ dBm for 600 multitone streams, i.e., 1800 symbols with the variation in $l_{\min}$ . . . . .	126

---

---

4.22	PCE for Multitone ASK centred around 2.45 GHz with $l_{\min} = 0.1$ and $L = 4$ for 600 multitone streams for $N = 3$ , $N = 4$ , and $N = 6$ . . . . .	127
4.23	BER for Multitone ASK centred around 2.45 GHz with $N = 6$ , $l_{\min} =$ 0.1, and $L = 4$ for 600 multitone streams, i.e., 3000 symbols. . . . .	127
5.1	Integrated information-energy receiver rectifier for SWIPT. . . . .	134
5.2	Four-tone multitone QAM RF signal frequency spectrum $X(f)$ centered around frequency $f_c = 2.45$ GHz and rectified baseband output spectrum $Y(f)$ consisting of dc, IM frequency tones used for information decoding (colored), and extra IM components (black). . . . .	134
5.3	Symbol constellation for multitone QAM with modulation order of $M = 16$ . . . . .	138
5.4	Rotated symbols constellations for QAM multitone for a modulation order of $M = 16$ with a phase shift of $45^\circ$ . . . . .	141
5.5	Normalized symbols constellations for $M = 16$ QAM (a) conventional and (b) with phase rotation of $45^\circ$ . . . . .	141
5.6	Multitone QAM signal PAPR with conventional QAM symbols constellation and the QAM symbols constellation rotated with $45^\circ$ . . . . .	142
5.7	(a) Modified expanded Multitone QAM symbols constellations with $\alpha_e \leq 1$ (blue starred) and (b) Modified compressed Multitone QAM symbols constellations with $\beta_c \leq 1$ (blue starred) with respect to conventional Multitone QAM symbols constellations (orange dots) for $M = 16$ . . . . .	146
5.8	Multitone QAM expanded symbols constellations for (a) $\alpha_e = 0.9$ , (b) $\alpha_e = 0.7$ , (c) $\alpha_e = 0.5$ , and (d) $\alpha_e = 0.3$ , for $M = 16$ . . . . .	148
5.9	(a) Modified expanded Multitone QAM symbols constellations with $\alpha_e \leq 1$ (blue starred) and (b) Modified compressed Multitone QAM symbols constellations with $\beta_c \leq 1$ (blue starred) with respect to conventional Multitone QAM symbols constellations (orange dots) for $M = 64$ . . . . .	150

---

---

5.10	Multitone QAM symbols constellations for (a) $\beta_c = 0.96$ , (b) $\beta_c = 0.92$ , (c) $\beta_c = 0.9$ , and (d) $\beta_c = 0.88$ , for $M = 16$ . . . . .	151
5.11	PCE for a 6-tone multitone signal without information data and with a 16-QAM simultaneous information flow with a transmission rate of 20 Mbps varying with average input power $P_{in}$ . . . . .	154
5.12	PCE comparison for 6-tone multitone signal with no information flow, using conventional QAM, and the asymmetric expanded QAM symbols constellations for outer symbols with $M = 16$ with a transmission rate of 20 Mbps and average input power $P_{in} = 0$ dBm. . . . .	155
5.13	PCE comparison for a 6-tone multitone signal with no information flow, using conventional QAM, and the asymmetric expanded QAM symbols constellations for inner symbols with $M = 16$ with a transmission rate of 20 Mbps and average input power $P_{in} = 0$ dBm. . . . .	156
5.14	PCE comparison for a 6-tone multitone signal with no information flow, using conventional QAM, and the asymmetric compressed QAM symbols constellations for outer symbols with $M = 16$ with a transmission rate of 20 Mbps and average input power $P_{in} = 0$ dBm. . . . .	157
5.15	PCE comparison for a 6-tone multitone signal with no information flow, using conventional QAM, and the asymmetric compressed QAM symbols constellations for inner symbols with $M = 16$ with a transmission rate of 20 Mbps and average input power $P_{in} = 0$ dBm. . . . .	158
5.16	PCE comparison for a 6-tone multitone signal with 16-QAM expanded constellation ( $\alpha_e = 0.7$ ) and compressed constellation ( $\beta_c = 0.92$ ) for $\Pr(s_{inner}) = p$ for a transmission rate of 20 Mbps. . . . .	159

# List of Tables

2.1	Effect of various multisine parameters on wireless power transfer. . .	26
2.2	Transmission designs for separated information-energy receiver architecture. . . . .	31
2.3	Transmission designs for integrated information-energy receiver architecture. . . . .	43
2.4	Summary of existing modulation methods for integrated information-energy receiver architecture. . . . .	48
3.1	Transmission strategies for integrated information and energy receiver architecture. . . . .	91
3.2	SWIPT performance for Multitone PSK with various parameters. . .	95
4.1	Different patterns of $(N - 1)$ transmitted symbols for Multitone ASK with $N = 3$ , $L = 4$ , and $l_{\min} = 0.1$ . . . . .	108
4.2	Different patterns of $(N - 1)$ transmitted symbols for Multitone ASK with $N = 4$ , $L = 4$ , and $l_{\min} = 0.1$ . . . . .	109

# Chapter 1

## Introduction

A revolution in wireless communication occurred in 1990s which completely transformed the earlier way how people communicated. An era of advancements in digital wireless communications started which provided mobility to telephones and the freedom from wires. Since then, wireless information technology has been constantly evolving for decades in the pursuit of higher and higher spectral efficiency and currently moving towards its sixth generation ([6G](#)). However, communication devices' freedom from power cords/ batteries is still in its infancy and we have not even achieved a first generation for far-field wireless power transfer ([WPT](#)). This thesis investigates wireless communication and power transfer technology moving towards a standard for simultaneous wireless information and power transfer ([SWIPT](#)).

In this chapter, the motivation for this thesis is discussed, followed by an exploration of the challenges and research objectives. Subsequently, the original contributions of this research work are summarized, followed by a discussion of the thesis outline. Finally, a list of publications resulting from this research study is presented.

### 1.1 Motivation

The Internet of Things ([IoT](#)) envisions a global wireless network where trillions of wireless sensors are connected via the Internet and communicate with each other

sharing data for various applications in defense, biomedical implants, vehicular communications, home automation, agriculture, smart cities, etc [1–4]. The development of 5G, 6G, and beyond international wireless communication standards for higher data rates with low latency networks over the fourth generation (4G) will see the rise of this enormous IoT wireless sensor network (WSN) of low-power wireless sensors [5].

In addition to providing a robust connection between these large networks of wireless sensors, a sustainable and reliable energy source for these sensors is also required. As technology becomes smaller and mobility becomes more important to consumers, energy supply through wired connections becomes infeasible due to a large number of sensors. Another traditional way is to use built-in batteries for sensors. However, this traditional way is quite challenging for low-power WSNs as these batteries have a limited lifespan and large amounts of energy-consuming applications may quickly drain these batteries, and it becomes difficult to replace these batteries frequently. Also, these replaceable batteries would produce huge amounts of e-waste. Future technologies need to be developed while having a minimal contribution to global warming and climate change. Therefore, a more energy-efficient green solution needs to be provided to protect the environment and minimize the carbon footprint while using the large WSN infrastructure.

Energy harvesting provides a promising solution for charging these low-power electronic devices. Energy harvesting for these small sensors may be possible through many ambient environmental sources such as wind, solar, thermal, vibration, and the present radio frequencies. However, these ambient sources depend upon the available environmental conditions and may change frequently. Therefore, a more reliable and sustainable way is to have a dedicated radio frequency (RF) power transmitter for these sensors which is called wireless power transfer (WPT). For users with a small distance, WPT can be provided by capacitive, inductive, or magnetic resonance [6,7]. For WSNs having low-power sensors spread over a wider area, radiative far-field WPT using the RF signals provides a viable solution for remote

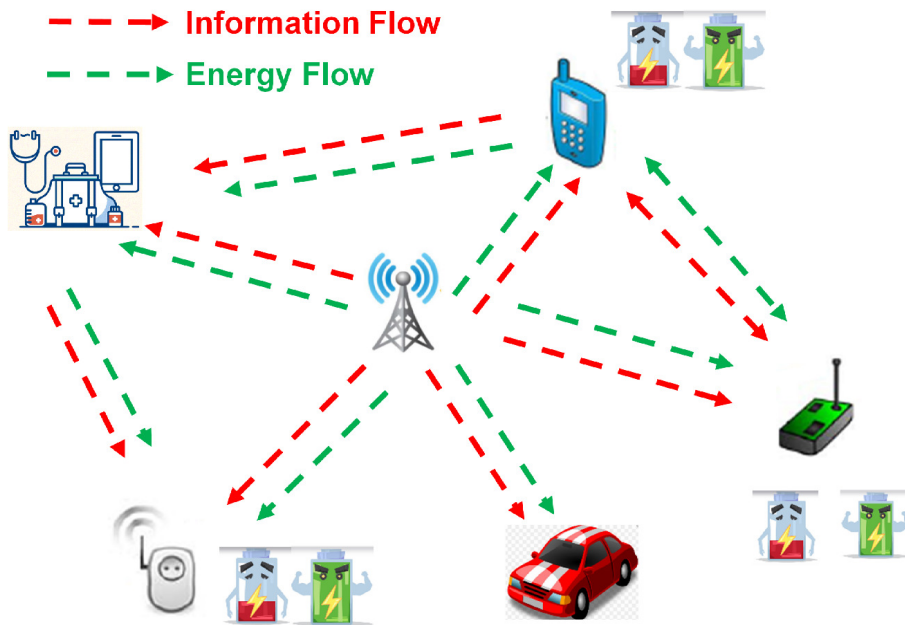


Fig. 1.1. A simultaneous wireless information and power transfer system model.

charging [8,9]. However, the transmitted power needs to be carefully controlled to minimize the health risks to the ecosystem, for avoiding interference in adjacent frequency bands, and also to allow spectrum reuse.

In the real-world scenario, deploying base stations (BSs) solely for transferring wireless power to sensors for RF WPT is not practical and does not use the resources efficiently. Therefore, the already existing infrastructure for wireless information communication can be utilized for the feasibility of WPT technology which would also be helpful from the environmental perspective. As IoT devices are embedded in Wireless Sensor Networks (WSNs) and communicate with a Base Station (BS), the logical step is to have the BS transmit both power and information wirelessly to the IoT devices using the same Radio Frequency (RF) signal, as demonstrated in Fig. 1.1, while the sensor node performs information detection and energy harvesting operations over the same RF signal. This approach has been termed simultaneous wireless information and power transfer (SWIPT), from Wireless Information Transfer (WIT) and Wireless Power Transfer (WPT). In WIT, a signal is utilized only for information transmission, whereas in WPT, the signal is used only to deliver power to the node. SWIPT provides a bridge between these two technologies by exploiting

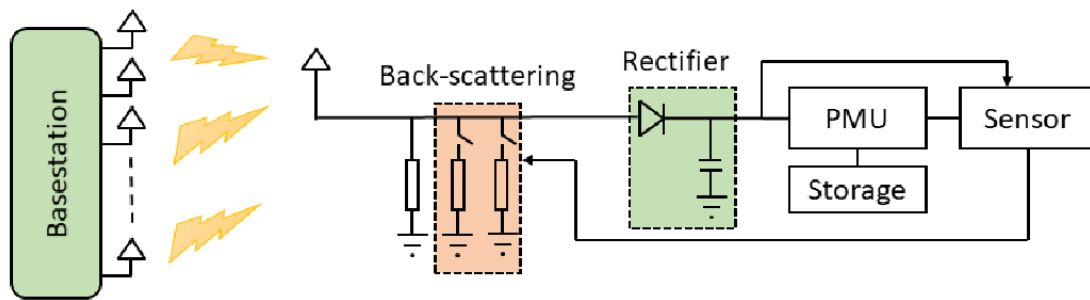


Fig. 1.2. Base station transmitting to a sensor node consisting of a rectifier, PMU (power management unit), storage unit for power extraction, and backscattering for information transfer from the received signal.

the same signal to provide both information and power to IoT devices.

In this thesis, the focus has been on downlink WIT only. The IoT sensor node would typically send sensed data to the BS, using backscattering or another approach, representing uplink WIT. Further, as seen in Fig. 1.2, there has to be a power management unit between the information receiver and power storage unit, which consumes very low power levels [10]. However, this is considered as part of the power storage system in order to keep the receiver architecture representation simple.

In addition to signal coverage, it is essential to take into account the IoT node architecture. Prior to SWIPT, receiver structures were being studied separately either for wireless communication purposes only or for energy harvesting purposes only, whereas now these operations need to be performed on the same signal at the IoT node side. Therefore, the problem of integrating these two processes in an efficient manner arises [11]. Initially, in 2013, two types of receiver setups were introduced as shown in (a) a separated information-energy receiver architecture where the signal is divided between two streams, one for information decoding and the other for energy harvesting. Various signal-splitting techniques can be considered, such as time switching (TS) and power splitting (PS); (b) an integrated information-energy receiver where signal splitting is performed only after passing the whole signal through the rectifying circuit (i.e., no RF mixer is required at the receiver [12]).

For both SWIPT architectures, there is a trade-off between the achievable informa-

tion rate and the amount of harvested power, as both metrics cannot be maximized simultaneously [12]. Further, the use of an energy harvester (rectifying circuitry consisting of diodes) at the receiver introduces non-linearity into the SWIPT system, and this non-linearity significantly affects the power conversion efficiency (PCE) performance at the output [13]. Earlier, most of the research related to WPT and SWIPT was focused on characterizing the rate-energy tradeoff assuming the linear energy harvester model. However, these findings have been shown as an overestimated performance when the realistic non-linear model energy harvester model is considered. Due to the non-linearity, the output power is not only a function of received signal power but also of the received signal shape. For example, a waveform having a higher peak-to-average power ratio (PAPR) with the same average input power is able to turn on the diode earlier, resulting in an increased PCE at the output [13, 14].

However, these high PAPR waveforms deteriorate the WIT performance because of the saturation of the non-linear amplifier at the transmitter. From a SWIPT system perspective, the performance of both the WIT and the WPT is important and it is therefore necessary to maximize the rate-energy trade-off at the receiver. Thus, for a complete SWIPT system, we need to co-design not only the transmitter and receiver hardware but also the transmitted waveform for a particular type of IoT node architecture to enhance the SWIPT performance.

Integrated information-energy receiver architecture consists of passive elements whereas a separated receiver architecture contains an RF mixer (active component) in addition to the passive components consuming higher power for signal processing compared to the separated one. Therefore, in this research, the main focus would be on designing efficient modulation techniques for the integrated type of receiver architecture where information demodulation would occur in the baseband. The research in this area has been limited to the basic low-bit rate schemes which are quite far from the practical requirements such as Orthogonal Frequency Division Multiplexing (OFDM). This research would provide a step closer to the high data rate while

simultaneously meeting the power demands of WSNs.

## 1.2 Scope of the PhD Thesis

### 1.2.1 Aim

To design efficient modulated transmission schemes optimized for an IoT receiver architecture so that the strongly energy-constrained IoT node can receive both information and power efficiently for SWIPT systems.

### 1.2.2 Challenges and Research Questions

In the area of SWIPT, for the past few years, the research has mainly focused on maximizing the rate-energy trade-off for a separated information-energy receiver architecture. This type of architecture provides better results from an information transfer perspective as conventional standard modulation transmission schemes can be utilized. However, considering the overall power consumption of the circuit, this is not a reliable and practical solution. Hence, recently, an integrated information-energy rectifier receiver architecture has emerged as a more practical solution. This architecture allows power, as well as information, to be retrieved from the same rectified baseband signal without the need for a mixer. Based on the conducted literature review, a few limitations are highlighted below:

- Till now, most of the modulation schemes designed for integrated receivers are suitable only for short distances and low bit-rate systems. Therefore, there is a requirement for more practical schemes closer to OFDM which can provide a higher data rate.
- For integrated information-energy receivers, transmission of information over the same signal used for WPT also affects the WPT performance and a trade-off exists between WIT and WPT performances.
- WPT performance decreases for the signal where information is embedded in

amplitude levels because of an increase in IMs amplitude level.

- It has been seen that the non-linearity of the rectifier improves the WPT performance with the use of multisine but ‘how this non-linearity can be exploited from the information reception perspective’ is still a question.

The following key issues are identified as the research gaps which would be addressed in this study:

1. How can the effect of WIT over the WPT be minimized to improve rate-energy trade-off while still utilizing the same communication signal for both WPT and WIT with high data rates for integrated information-energy receivers?
2. How the information can be encoded in multitone phases for lower ripples in received DC voltage while also having a higher data rate resulting in enhanced rate-energy trade-off?
3. How can the multitone amplitude levels be utilized for information while having a minimum impact on WPT performance?
4. How can the tone amplitude levels together with phase modulation be utilized for WIT resulting in a higher data rate and having a minimum impact on WPT performance?
5. How can the symbol constellation range for the proposed modulation transmission schemes be increased by exploiting the non-linearity of the rectifier?

## 1.3 Contributions

This Ph.D. thesis research work results in three main contributions. All of these contribute to the design of modulated transmission schemes for integrated information-energy receiver architecture SWIPT systems. These communication techniques lower the power consumption at the sensor nodes by removing mixers and local oscillators earlier needed for information detection and moving towards more prac-

tically feasible SWIPT systems.

The answers to the earlier mentioned five research questions are contributed in this research work.

### 1.3.1 Contribution 1: Multitone PSK modulated waveform design for SWIPT

For integrated information-energy receiver SWIPT architecture, a novel multitone PSK transmission scheme has been proposed for simultaneous information detection with only a rectifier reducing the power consumption at the sensor node. The rectifier is used to extract the power as well as downconvert the information. WPT performance and WIT performance of the designed communication signal over rectifier circuitry are studied. A suitable rectifier circuitry is fabricated and the SWIPT performance is verified with the measurements.

Research question 1 is addressed by proposing the transmission of  $(N - 1)$  symbols over an  $N$ -tone multitone signal which can be closely related to the standard OFDM used for WIT. Measurements confirm that it is possible to transmit the information in the form of tones' phases and detect using just a simple rectifier. Research question 2 is addressed by showing that the information transmission in terms of tones' phases does not affect the WPT performance and results in the maximum power efficiency of the rectifier. This makes the WPT performance independent of WIT performance. Therefore, it is possible to attain a high PCE while simultaneously transmitting an increased data rate for the sensor networks. Performance of the waveform according to various key parameters such as phase range, number of tones, and modulation order is studied. In addition, a multitone PSK signal is shown to improve the end-to-end SWIPT performance by reducing the chances of saturation of the transmitter power amplifier. The research work is discussed in Chapter 3, concluded in Chapter 6, and published in [15].

### 1.3.2 Contribution 2: Multitone ASK modulated waveform design for SWIPT

Multitone PSK offers the advantage of a minimum effect of information transfer over WPT performance. However, transmitting information in tones' amplitude levels offers the benefit of a simpler transmitter circuitry compared to the one required for transmitting information in tones' phases as in the latter case, phase synchronization is more critical. Therefore, a novel multitone ASK transmission scheme for an integrated information-energy receiver SWIPT architecture has also been proposed where information is embedded by varying the tones' power levels of the multitone signal.

Research question 1 is addressed by proposing the transmission of  $(N - 1)$  symbols over an  $N$ -tone multitone signal to increase the data rate. The effect of varying average power of transmitted signal with the varying information patterns is evaluated. The WPT and WIT performances of the proposed transmission scheme are analyzed in terms of PCE and bit error rate (BER), respectively. Further, the effect of different distributions for symbol levels for a modulation order due to the non-linearity of the rectifier circuitry is observed. For research question 3, the performance of the designed transmitted signal with a minimum level of symbols is analyzed for increasing WPT performance. Multitone ASK communication scheme can perform better for noisy and mobile channel environments compared to multitone PSK. Therefore, the desired SWIPT transmission signal scheme can be chosen depending on the present environmental conditions requirements. The research work is discussed in Chapter 4, concluded in Chapter 6, and published in [16].

### 1.3.3 Contribution 3: Multitone QAM modulated waveform design for SWIPT

Multitone PSK and Multitone ASK transmission schemes exploit a multitone sig-

nal's either phases or amplitudes, respectively, one at a time. However, the usage of both phases and amplitudes together for information transfer offers a higher data rate. Therefore, a combined Multitone QAM is proposed by exploiting the non-linearity of the receiver-rectifier, and both amplitudes and phases are used for information transfer offering an advantage of a higher degree of freedom to optimize WPT and WIT performances. Research Question 4 has been addressed by Multitone QAM by transmitting a higher number of bits per multitone stream by exploiting both amplitudes and phases for information symbols.

The effect of orientation of QAM symbol constellation has been analysed over the PAPR of the designed waveform. Further, variations of magnitudes of the different symbols of the QAM constellation have been shown to affect WPT performance significantly. Therefore, two asymmetric QAM constellation designs, asymmetric expanded QAM constellation and asymmetric compressed QAM constellation, are proposed to enhance WPT performance according to the application-specific requirement, such as whether a higher level of minimum continuous power transfer is critical or if a high-power transfer in short bursts is preferred for the SWIPT's operation. Research Question 5 has been addressed by the proposed asymmetric QAM constellation by locating symbols closer to each other. Therefore, a higher modulation order for a higher information rate can be used with the same WPT performance. It has been shown that WPT and WIT performances can be enhanced according to the IoT node's requirements by varying the transmission probabilities of inner symbols and outer symbols of the QAM constellation. The research work is discussed in Chapter 5, concluded in Chapter 6, and published in [17].

## 1.4 Publications

1. **Prerna Dhull**, Andrea P. Guevara, Maral Ansari, Sofie Pollin, Negin Shariati and Dominique Schreurs, "Internet of Things Networks: Enabling Simultaneous Wireless Information and Power Transfer," *IEEE Microwave Magazine*,

- vol. 23, no. 3, pp. 39-54, March 2022, doi: [10.1109/MMM.2021.3130710](https://doi.org/10.1109/MMM.2021.3130710).
2. **Prerna Dhull**, Dominique Schreurs, Giacomo Paolini, Alessandra Costanzo, Mehran Abolhasan and Negin Shariati, “Multitone PSK Modulation Design for Simultaneous Wireless Information and Power Transfer,” *IEEE Transactions on Microwave Theory and Techniques*, vol. 72, no. 1, pp. 446-460, Jan. 2024, doi: [10.1109/TMTT.2023.3294008](https://doi.org/10.1109/TMTT.2023.3294008).
  3. Steven Claessens, **Prerna Dhull**, Dominique Schreurs and Sofie Pollin, “WiLO-OFDM Transmission Scheme for Simultaneous Wireless Information and Power Transfer,” *IEEE Open Journal of the Communications Society*, vol. 5, pp. 6261-6278, 2024, doi: [10.1109/OJCOMS.2024.3467680](https://doi.org/10.1109/OJCOMS.2024.3467680).
  4. **Prerna Dhull**, Dominique Schreurs, Sofie Pollin, Mehran Abolhasan and Negin Shariati, “Multitone ASK Waveform Design for Simultaneous Wireless Information and Power Transfer,” *IEEE Access*, 2024, doi: [10.1109/ACCESS.2024.3519316](https://doi.org/10.1109/ACCESS.2024.3519316) (early access).
  5. **Prerna Dhull**, Negin Shariati, Sofie Pollin, Mehran Abolhasan and Dominique Schreurs, “Multitone QAM Modulation Design for Simultaneous Wireless Information and Power Transfer,” *IEEE Access*, 2024, doi: [10.1109/ACCESS.2024.3520104](https://doi.org/10.1109/ACCESS.2024.3520104) (early access).

## 1.5 Thesis Outline

This doctoral thesis has been organized into six chapters.

Chapter 1 presents an overview of the research area regarding SWIPT, the motivation of the Ph.D. thesis, identifies the challenges and research problems, and highlights the main contributions with their significance.

Chapter 2 presents a background of WPT and SWIPT research and its challenges. Waveforms for WPT and their key parameters affecting WPT are discussed. This is followed by a discussion of modulated waveforms consisting of information as

well as power. Waveforms for both SWIPT receiver architectures: a separated information-energy receiver architecture and an integrated information-energy receiver architecture, are discussed. Further, the effect of input distribution of transmitting information over SWIPT performance is discussed. In the end, the existing transmission schemes for different receiver architectures are compared in Table 2.2, Table 2.3, and Table 2.4.

Chapter 3 presents a multitone PSK SWIPT transmission scheme for an integrated information-energy receiver architecture. Multitone signal parameters such as frequency spacings and tones' phases are designed accordingly to increase the waveform PAPR. WPT performance and WIT performance for SWIPT are measured with the attained power conversion efficiency and bit-error rate at the rectifier output. Performance of the waveform according to various key parameters such as phase range, number of tones, and modulation order is studied from both WIT and WPT perspectives for the overall SWIPT performance of a system. A comparison of the proposed multitone PSK communication scheme with the existing schemes is presented in Table 3.1.

Chapter 4 proposes a novel multitone ASK transmission scheme for an integrated information and energy receiver SWIPT architecture. The effect of varying information patterns resulting in the variation of the average power of transmitted signal is evaluated. The WPT and WIT performances of the proposed transmission scheme are analyzed in terms of PCE and BER, respectively. The performance of the designed transmitted signal with the minimum level of the symbols is analyzed. Further, the effect of different distributions for symbol levels for a modulation order due to the non-linearity of the rectifier circuitry is observed.

Chapter 5 probes into the utilization of both amplitude and phase of a multitone signal for information transfer while simultaneously transferring power with an integrated information and energy receiver SWIPT architecture. The effect of symbol constellation orientation over the PAPR of the designed waveform is studied. Two

asymmetric QAM constellation designs have been proposed to enhance the power transfer performance according to the transmission probabilities of the inner symbols and outer symbols of the QAM constellation. It has been shown that it is necessary to redesign the QAM constellation to exploit the non-linearity of the rectifier for the performance requirement of the SWIPT system.

Chapter 6 provides the conclusion of this Ph.D. thesis, highlighting the summary of contributions in this research work, and further, discusses some possible future research avenues for standardizing the SWIPT waveforms for future IoT networks and designing efficient SWIPT systems in the future.

# Chapter 2

## Literature Review

In this chapter, a review of waveforms for WPT and SWIPT technologies is presented. The literature about modulated waveforms for both SWIPT receiver architectures: a separated information-energy receiver architecture and an integrated information-energy receiver architecture, is discussed. Afterward, a brief comparison of existing transmission schemes is performed. This chapter also consists of some of the author’s work published [18]:

- **Prerna Dhull**, Andrea P. Guevara, Maral Ansari, Sofie Pollin, Negin Shariati and Dominique Schreurs, “Internet of Things Networks: Enabling Simultaneous Wireless Information and Power Transfer,” *IEEE Microwave Magazine*, vol. 23, no. 3, pp. 39-54, March 2022, doi: [10.1109/MMM.2021.3130710](https://doi.org/10.1109/MMM.2021.3130710).

## 2.1 Background

### 2.1.1 WPT and SWIPT

Energy harvesting (EH) is a method of using the surrounding waste energy present in the ambient sources such as heat, wind, RF signal, etc., to match up the power requirement of a system. However, environmental conditions are not stationary for a long time duration making EH from ambient sources unreliable. Installing a fully

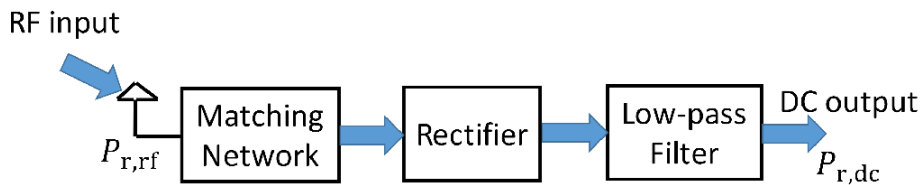


Fig. 2.1. Rectenna block diagram.

controlled dedicated power source for the nodes present in the communication network can solve this problem which is known as wireless power transfer (WPT) [19]. Depending upon the applications, WPT may be near-field (short distance) and far-field (long distance) [20]. Near-field WPT using inductive resonant coupling is mostly suitable for the indoor environment. However, in a communication network, the distance between the node and the base station is a critical factor. Therefore, prospects of far-field WPT need to be explored [21–24].

Rectenna is the basic element of the RF energy harvester circuit at the receiver. Fig. 2.1 illustrates the basic rectenna components consisting of an antenna, an impedance matching network, a rectifier, and a low pass filter (LPF). The performance of a rectenna is often measured by its RF-DC conversion capability  $\eta_3$ , defined as

$$\eta_3 = \frac{P_{r,dc}}{P_{r,rf}} = \frac{V_{r,dc}^2}{P_{r,rf}R} \quad (2.1)$$

where  $P_{r,rf}$  represents received input RF power at the antenna terminals,  $P_{r,dc}$  represents received DC power at the load after rectenna,  $V_{r,dc}$  is the output DC voltage, and  $R$  is the output load.

In wireless information transfer (WIT), a signal is only utilized for information transmission whereas in WPT, the signal is only used to deliver power to the node. Simultaneous wireless information and power transfer (SWIPT) provides a bridge between these two technologies by exploiting the same signal for providing information as well as power to the system. The idea of a signal carrying information and power simultaneously in additive white Gaussian noise (AWGN) channel is firstly introduced in [8] and then further extended to an AWGN channel under the

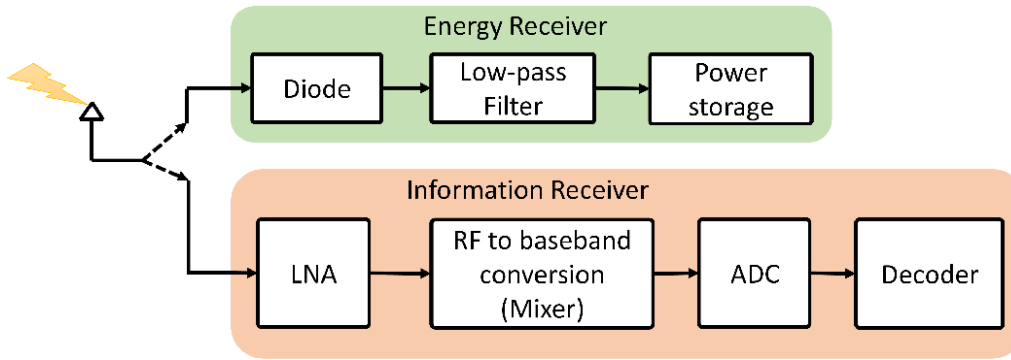


Fig. 2.2. Separated information and energy receiver architecture for SWIPT.

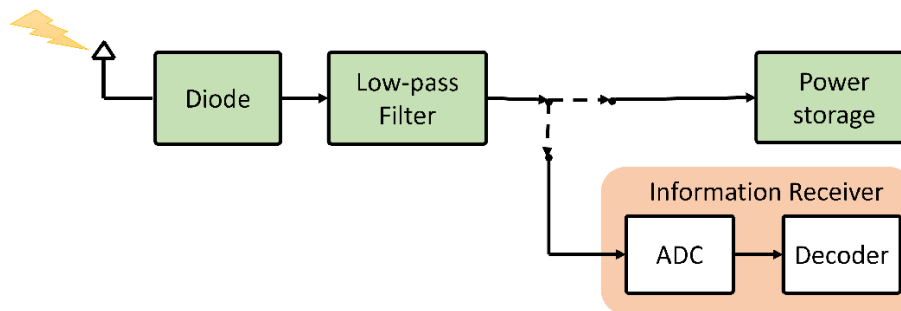


Fig. 2.3. Integrated information and energy receiver architecture for SWIPT.

transmitted power constraints in [25]. It is shown that a trade-off exists between achievable rate and the amount of energy harvested and both can not be maximized simultaneously. Further, it is also shown that energy harvesters can not be directly used as information decoders, giving rise to the research problem of integrating these two processes [11].

In 2013, Zhang proposed two types of receiver setups— separated information energy receiver architecture (Fig. 2.2) and integrated information energy receiver architecture (Fig. 2.3) [12]. In the former one, the signal is divided among two streams, one for information decoding and the other for energy harvesting before passing the signal to the energy harvester, and for this, various signal splitting schemes such as time switching (TS), power splitting (PS), and antenna switching have been introduced [26]. In the case of an integrated information energy receiver, the signal splitter is used only after passing the whole signal through the rectifying circuit, and a non-coherent detection is performed, i.e., no mixer is needed at the receiver. Therefore, the energy consumed by the integrated receiver structure is far less than



Fig. 2.4. A wireless power transfer communication system model.

that for the separated structure case.

## 2.1.2 Non-linear Energy Harvester Model

A communication system consists of a transmitter, a channel, and a receiver, as shown in Fig. 2.4. The overall efficiency of a WPT system can be defined in terms of the individual efficiency of these systems as [27]

$$\eta = \eta_1 \cdot \eta_2 \cdot \eta_3 = \frac{P_{t,\text{rf}}}{P_{t,\text{dc}}} \times \frac{P_{r,\text{rf}}}{P_{t,\text{rf}}} \times \frac{P_{r,\text{dc}}}{P_{r,\text{rf}}}, \quad (2.2)$$

where  $\eta_1$ ,  $\eta_2$ , and  $\eta_3$  represents DC-RF PCE, RF-RF PCE, and RF-DC PCE. These efficiencies can be maximized separately by using an efficient power amplifier (PA), proper signal design according to channel conditions, and an efficient rectenna design, respectively. In earlier research, the problem of maximizing the overall PCE of the system referred to improve  $\eta_1$ ,  $\eta_2$ , and  $\eta_3$  independent to each other. This was possible only when EH model was considered as a linear function of input signal power for making analytical solution much easier [28–32]. For such type of linear EH model,  $\eta_3$  becomes constant and the received power is calculated as

$$P_{r,\text{dc}} = \eta_3 \times P_{r,\text{rf}}. \quad (2.3)$$

In reality, the rectenna present at the receiver consists of a diode which introduces non-linearity in  $\eta_3$ . A non-linear energy harvesting rectifier receiver model is depicted in Fig. 2.5. PCE found by (2.3) does not relate with the practically achievable value. Hence a study of non-linear characteristics of the diode model was needed. Based on the logistic function, a non-linear EH model is also introduced in [33]. Further, a quadratic non-linear model having convex properties with input power [34]

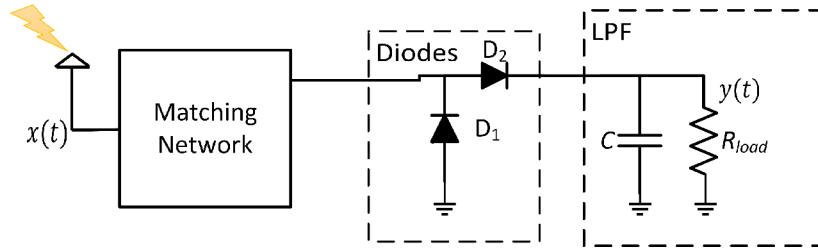


Fig. 2.5. A non-linear energy harvesting rectifier receiver model.

is compared with the linear models and is found to be closer to the practical measurements. In short, here in [33, 34], PCE non-linearity is characterized by input power variation.

Rate-energy trade-off for SWIPT considering a non-linear energy harvester is calculated in [35] and found that for PS scheme, the declining rate of maximum energy harvested with the increasing rate is higher compared to TS, where the declining rate remains almost constant. Furthermore, the performances of non-linear energy harvester model with the various signal splitting schemes are evaluated and compared [36].

Another model is introduced in [37, 38] where an analytical diode model using Taylor series expansion is considered. Received power  $z_{DC}$  for the received signal  $x(t)$  at the output is derived as

$$z_{DC} = \sum_{i=\text{even}, i \geq 2}^{n_0} k_i E[x(t)^i] \quad (2.4)$$

where  $k_i$  are the non-linearity coefficients and  $E\{\cdot\}$  refers to the expected value of  $\{\cdot\}$ . After truncating (2.4) at  $n_0 = 2$ ,  $z_{DC}$  can be represented by

$$z_{DC} = k_2 E[x(t)^2]. \quad (2.5)$$

This is the linear model of the rectifier as  $k_2$  is constant and  $z_{DC}$  is solely dependent upon input signal power  $E[x(t)^2]$ . Now, truncating (2.4) at a higher order term, for instance  $n_0 = 4$ ,  $z_{DC}$  can be represented by

$$z_{DC} = k_2 E[x(t)^2] + k_4 E[x(t)^4]. \quad (2.6)$$

(2.6) represents the non-linear model of the rectifier as now  $z_{\text{DC}}$  not only depends upon the input signal power  $E[x(t)^2]$  but also upon the  $E[x(t)^4]$  which is also determined by the input signal shape. Hence, the problem of maximizing  $\eta_2\eta_3$  can not be solved by maximizing only  $\eta_2$  and keeping  $\eta_3$  constant.

In the case of **SWIPT**, the effect of non-linearity on the information rate also needs to be considered. In [39, 40], it is mentioned that although the Shannon Capacity theorem provides the limit for the linear channels, it is still possible to achieve higher capacity for non-linear channels. Therefore, non-linearity is beneficial for power transfer as well as information transfer.

## 2.2 Waveforms for WPT and SWIPT

Most of the research related to the **WPT** and **SWIPT** system considered a linear energy harvester model [12, 28]. Enhancement of overall system performance focused on the improvement of  $\eta_1$ ,  $\eta_2$ , and  $\eta_3$  individually. However, PCE is a non-linear function of input power because of the presence of a diode in the rectifying circuit. Therefore, the output voltage is not only a function of the input voltage level but also depends upon the shape of the input waveform [14, 41]. Therefore, the effect of signal shape on all three efficiencies needs to be studied.  $\eta_1$  is influenced by the distortion introduced by the signal at the power amplifier,  $\eta_2$  is a function of channel state as well as input signal, and  $\eta_3$  is a function of input signal shape, power, and rectenna design.

In WPT systems, the threshold voltage of the diode present in the rectenna imposes a requirement for the minimum input voltage for turning on the diode [13]. This problem can be solved by raising the peak voltage levels in the input waveforms [42]. This is where high Peak to Average Power Ratio (**PAPR**) signals come into the picture. For a signal **PAPR** can be defined as

$$\text{PAPR} = 10 \log \left( \frac{\max[x(t)]^2}{\langle x(t)^2 \rangle} \right) \quad (2.7)$$

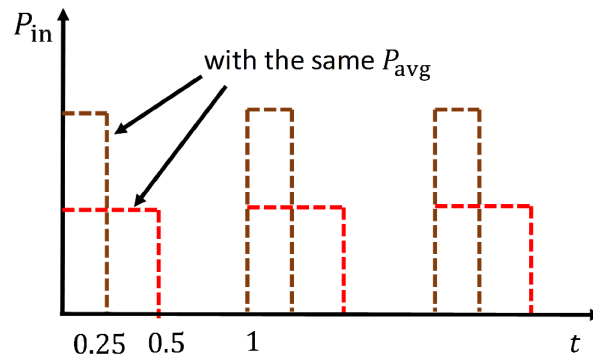


Fig. 2.6. Impulsive wireless power transmission with the same average power  $P_{\text{avg}}$ .

where  $x(t)$  is the time-domain representation of the signal.

For information transmission in communication systems, high PAPR signals are not preferred as they introduce distortions at the power amplifier of the transmitter because of their higher peak voltage. But schottky diodes' threshold voltage can easily be overcome by these high PAPR signals to have relatively higher available voltage levels for the shorter duration for the same average power. Therefore, the same PCE level can be achieved even at the lower input power by utilizing PAPR signals. Although high PAPR offers the benefit of an increased output PCE, large bandwidth of the multitone signal would result in lower RF input matching efficiency. Therefore, receiving circuitry would be required to be designed for a large input RF matching bandwidth.

### 2.2.1 Impulsive Wireless Power Transmission

One way to take advantage of high PAPR is by using intermittent transmission. In [43], RFID read range capability and power efficiency are improved by transmitting a waveform where power is concentrated within a shorter duration, which means power is transmitted only for a while and not for the whole time duration. Intermittent waveform is generated by multiplying a square pulse by the continuous waveform. Here, the distance between the reader and the tag is increased by using the same amount of transmitted average power by increasing PCE as the activation of the diode is achieved at a relatively lower input power.

Further, in [44–47], another method to increase the PAPR, impulsive transmission of the signal power is introduced for PCE enhancement. Here, the duty cycle of a pulse waveform is reduced resulting in a higher voltage level for a short duration with the same average power  $P_{\text{avg}}$  as shown in Fig. 2.6. As the duty cycle is decreased from 1 to 0.5 for the same input power level, higher voltage levels are available for the shorter duration which can easily turn on the rectifying component. However, signal representations in the time domain and frequency domain have a reverse relationship. A reduction of the duty cycle in the time domain has the effect of converting a narrow-band spectrum to a wide-band spectrum in the frequency domain and this large bandwidth signal would impose some limitations on the matching network [47]. The reason for this is if the same matching network is used for this wide-band spectrum, most of the energy will be filtered out. Hence, PCE would start declining if the duty cycle is further reduced. This can be overcome by the use of a wide-band matching network.

In [48], it is shown that signals having high PAPR or having lower duty cycle increase PCE only up to a certain point after which the diode breakdown voltage starts dominating, and in consequence, the PCE starts approaching zero. Further, a similar effect is observed by increasing the input power greater than 10 dBm where higher input powers result in lower PCE.

### 2.2.2 Spatial Power Combining

High PAPR signals offer the advantage of high transferred power at the receiver but simultaneously these signals suffer from distortion, spectrum regrowth, etc., at the transmitter because of the signal clipping by the power amplifier [49, 50]. Spatial power combining provides a way to receive high PAPR signals at the receiver while minimizing the distortion at the transmitter. In this, tones of multitone signal are amplified individually and transmitted by the separate antennas. These tones are received as a combined high PAPR multisine signal by the single antenna at the receiver. However, this approach becomes inefficient with the increasing number of

tones as each tone uses a separate power amplifier at the receiver.

### 2.2.3 Multitone Transmission

High **PAPR** signals offer the advantage of increased PCE in WPT systems by exploiting non-linear characteristics of the diode. Hence, different waveform shapes are designed to make it have high **PAPR**. One such method is to use a signal having multiple tones instead of a single tone [13] as

$$\text{PAPR} \propto N \quad (2.8)$$

where  $N$  is the number of tones. A basic polynomial model of diode behavior is studied similar to Taylor series polynomial as previously mentioned. As it was seen from (2.6) only even order terms contribute to the output DC power, therefore the diode DC output voltage  $y(t)$  can be written in terms of input voltage  $x(t) = A \cos(2\pi f_1 t + \phi)$  as

$$y_{\text{DC}} = \frac{A^2 k_2}{2} + \frac{3A^4 k_4}{8}. \quad (2.9)$$

In (2.9), only second-order and fourth-order harmonics are represented. There would also be an impact of higher-order harmonics on DC. However, it would be significantly smaller compared to second-order harmonics [51].

Now if  $y(t)$  is a multitone with  $N = 4$  having equal amplitudes, i.e.,  $A_1 = A_2 = A_3 = A_4 = B = A/2$ , phases  $\phi_1$ , having tone phases  $\phi_2$ ,  $\phi_3$ , and  $\phi_4$ , and having an equal spacing between tones such as  $f_1$ ,  $f_2 = f_1 + \Delta f$ ,  $f_3 = f_1 + 2\Delta f$ , and  $f_4 = f_1 + 3\Delta f$ , then  $x(t)$  can be represented as

$$x(t) = B \cos(2\pi f_1 t + \phi_1) + B \cos(2\pi f_2 t + \phi_2) + B \cos(2\pi f_3 t + \phi_3) + B \cos(2\pi f_4 t + \phi_4). \quad (2.10)$$

The output DC voltage after filtering out all the frequency components would be

$$y_{\text{DC}} = \frac{4B^2k_2}{2} + \frac{21B^4k_4}{2} + \frac{3B^4k_4}{2} \cos(2\phi_3 - \phi_2 - \phi_4) + \frac{3B^4k_4}{2} \cos(\phi_1 + \phi_3 - 2\phi_2) + 3B^4k_4 \cos(\phi_1 - \phi_2 - \phi_3 + \phi_4). \quad (2.11)$$

By comparing (2.9) and (2.11), it can be seen that a multitone signal enhances the amount of DC voltage at the receiver and it can further be increased by increasing the number of tones. Besides the effect of  $N$  on the output DC voltage, the effect of phases of individual tones can also be seen from (2.11). Alignment of the tone phases, i.e.,  $\phi_1 = \phi_2 = \phi_3 = \phi_4 = 0$  also enhances the rectified voltage level.

In [42, 52–54], few other high PAPR waveforms having time-varying envelope, such as a chaotic signal, harmonically spaced multisine, Orthogonal Frequency Division Multiplexing (OFDM), modulated waveform, white noise, radar waveforms are introduced and shown that indeed, these waveforms are able to cross the diode threshold with much lower average input power compared to a single tone continuous wave. One other way of using multisine for WPT is using multisine with harmonically spaced tones to enhance RF-DC efficiency [55]. Harmonic-spaced multisine waveforms exhibit asymmetrical behavior having lower negative amplitude peaks and higher positive amplitude peaks. Therefore, Harmonic spaced multisine performs better when the breakdown region is in focus.

As the rectifier exhibits the non-linearity due to the presence of diodes, different tones present in the multisine signal would undergo intermodulation resulting into different frequency components. The presence of these intermodulations would affect the output DC voltage level and WPT efficiency [56]. There are several parameters related to the multitone such as tone spacing, bandwidth, etc., that can influence the amount and the magnitude of these intermodulations, a few of these are highlighted below:

### 2.2.3.1 Tone Separation

The rectifier output voltage also contains some ripple voltage due to intermodulation between the different tones in addition to the required DC voltage [57]. The lower the magnitude of this ripple voltage, the better would be the PCE. In a multisine signal, the peak occurrence rate is inversely proportional to  $\Delta f$  (frequency spacing between tones), such as the time period  $T$  of the signal  $T = 1/\Delta f$ . If the distance between peaks of the time-varying signal is too large, then the capacitor would have a longer time duration to get discharged. Therefore,  $\Delta f$  is kept at maximum for the higher average DC output voltage. In a consequence of this, another constraint of having a wider bandwidth would be imposed on the matched filter. In addition, an output filter with a higher time constant ( $\tau$ ) needs to be used for further minimizing the voltage ripples [57].

### 2.2.3.2 Number of Tones

In general, as the number of tones increases, the PCE increases as shown in (2.11) but only up to a certain optimum  $N$ , above this optimum value of  $N$ , the PCE starts to show a downward trend [58]. There are two reasons for this: first, as signal bandwidth BW is a function of  $N$  such as  $BW = (N - 1) \times \Delta f$ , circuit mismatching increases with the increasing  $N$  resulting in a reduction in the PCE.

Second, in [58], the probability density function (PDF) of the instantaneous available amplitude levels at the diode input is studied. Although PAPR increases with the increase in  $N$ , the probability of occurrence of high amplitude level reduces for the same average input power signal. Consequently, there would be frequent cases where the instantaneous amplitude would not turn on the diode. Therefore,  $N$  should be chosen as an optimum value after considering the above-mentioned factors.

### 2.2.3.3 Phase

As shown by (2.11), the magnitude of DC voltage is a function of phases of different tones. Therefore, to maximize the output DC voltage and enhance PCE, all tones

must be aligned i.e.  $\phi_1 = \phi_2 \dots = \phi_N = 0$  [13].

#### 2.2.3.4 Input Power Range

Multisine waveforms perform better compared to single-tone waveforms in the ultra-low power range. However, the output DC voltage is always lower than that in the case of a single sine wave for the medium power range [59–61]. The reason for this is the inductive effect of the LPF which resists the relatively sudden change in current because of relatively higher peak voltage at the diode. Thus, a multitone waveform is beneficial only in the ultra-low power range and if multisine waveform needs to be used at the medium level, more diodes can be used in the rectifier circuit to raise the  $V_{th}$  level [59].

#### 2.2.3.5 Low-pass RC Filter Cut-off Frequency ( $f_{cutoff}$ )

It has been previously discussed that tone separation ( $\Delta f$ ) affects the PCE at the output. In [56], the effect of filter bandwidth is also taken into consideration by introducing a ratio  $\Delta f/f_{cutoff}$ . It is shown that if  $\Delta f/f_{cutoff}$  is too large, then most of the signal would be filtered out by the low-pass filter, and on the other hand, if  $\Delta f/f_{cutoff}$  is too small, then the peak repetition frequency in time-domain would be too large resulting into excessive ripples. Therefore, an optimum value of the  $\Delta f/f_{cutoff}$  needs to be selected for the required WPT efficiency.

#### 2.2.3.6 Effect of Load

There exist different optimum load values for the maximum achievable PCE for a time-varying multisine [62]. It has been shown that although optimal load shifts to a larger value as the PAPR of the multitone signal increases, this optimum load value reduces as the input signal power increases. Therefore, there exists a range of an optimum load for a particular input power and number of tones for maximum RF–DC efficiency. In [63], it is shown that although multitone signals do not increase PCE with higher PAPR after a certain limit these signals provide higher output voltage

and peak efficiency over a wider load range, i.e., RF-DC efficiency reduces but DC-DC efficiency increases, further eliminating the need of a voltage booster for the system. At high input power, the PCE reduces due to the diode's early breakdown. A reconfigurable rectifier having high breakdown voltage and low threshold voltage is proposed in [64]. Table 2.1 highlights the effect of the above-discussed various parameters on wireless power transfer.

Table 2.1: Effect of various multisine parameters on wireless power transfer.

Ref.	Multitone Parameter	Ripple Voltage	WPT	Bandwidth
[58]	$N$	Increases	Increases upto a maximum then decreases	Increases
[57]	$\Delta f$	Decreases	Increases	Increases
[59]	Input power	Increases	Increases for low power range and decreases for medium power range	-
[56]	$f_{\text{cutoff}}$	Increases	Decreases	-

### 2.2.4 Modulated Waveform

Modulated waveforms result in lower power efficiency at the rectifier compared to a multisine waveforms because of the increased ripples in the output voltage [65]. However, in a SWIPT system where both information transmission and power transmission are required, these additional ripples can be exploited from the information perspective. There are several parameters related to the modulated waveform that can affect the energy harvester's performance and these can be chosen according to

the communication system requirement such as whether the power transfer or information transfer is critical for the system. Some of these parameters are mentioned below:

#### 2.2.4.1 Modulation Scheme

In [65] and [66], performances of the different modulated waveforms such as [FSK](#), [QPSK](#), [QAM](#) are compared with continuous waveforms ([CW](#)). A decline in PCE is observed when an FSK signal is used for WPT instead of the CW signal. The reason for this is: that when a multiple tone signal is passed through the rectifier, mixing of the different frequency components occurs resulting in intermodulations at the output because of the non-linear characteristics of the diode.

QPSK and QAM waveforms also result in lower PCE compared to CW waveforms. As in QPSK and QAM, information is encoded in amplitude as well as phase. Because of different phases for different symbols, there exists phase discontinuity among QPSK and QAM waveforms thus, the diode does not turn on and turn off cyclically. For a particular symbol rate, [QPSK](#) gives a better PCE compared to 16-QAM as in the case of QPSK, information is embedded only in the phase of the signal keeping amplitude level constant whereas, in the case of [QAM](#), information is embedded in amplitude as well as phase. Therefore, for QAM more ripple voltage is generated at the rectifier output further lowering the PCE.

#### 2.2.4.2 Bit rate

PCE is more dependent on [PAPR](#) when the symbol rate is high [67] and [PAPR](#) reduces with the increasing symbol rate. Degradation in QAM [PAPR](#) is more than QPSK when the bit-rate is increased.

#### 2.2.4.3 Modulation Order

Error vector magnitude ([EVM](#)) doesn't get affected for PSK by increasing the modulation order resulting in the same PCE [68]. However, for QAM, as the modulation

order is increased, the difference between the power of the innermost symbol and the outermost symbol increases. While transmitting information in the worst-case scenario, if these lowest and highest power symbols occur consecutively, high voltage ripples are induced in the output voltage decreasing the overall PCE.

## 2.3 Modulation Techniques for SWIPT

In 2013, the idea of a single-tone energy modulation was introduced [12] where information symbols can be transmitted using different energy levels and the detection at the receiver is performed by identifying different received energy levels for the corresponding symbols [12]. This is the simplest information transmission method for integrated receivers. However, it does not take advantage of the previously discussed multi-tone carrier to enhance the power transfer. Recently, a research area for designing practical efficient modulation schemes while taking all the above factors into consideration, emerged. In [69], a simple multi-antenna environment for energy as well as information is introduced where information is encoded in the antenna patterns not on the RF wave. Therefore, this low-complexity structure can be used for separated as well as integrated receiver architectures.

It has been shown that high PAPR signals play a major role in WPT systems by significantly improving wireless power transmission efficiency. A simple model for using high PAPR OFDM signal for power transfer is introduced in [70], where OFDM subcarriers are divided into two parts, one for information transfer and another for energy transfer as shown in Fig. 2.7. This is achieved by using well-designed bandpass filters (BPFs), and therefore eliminating the need for power splitting or time switching at the receiver [71]. It is possible to harvest 18 mW for 4 bps/Hz from the transmitted signal power of 1 W using this OFDM subcarrier splitting technique. However, here, the required BPFs need to be really sharp to support an OFDM signal having smaller sub-carrier frequencies. This increases the computational complexity at the receiver because of the increased Discrete Fourier Transform

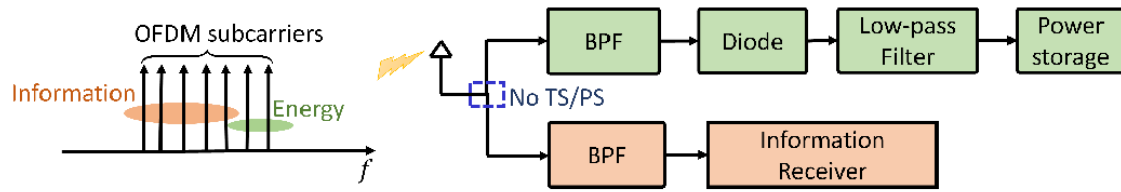


Fig. 2.7. OFDM frequency spectrum and corresponding receiver architecture.

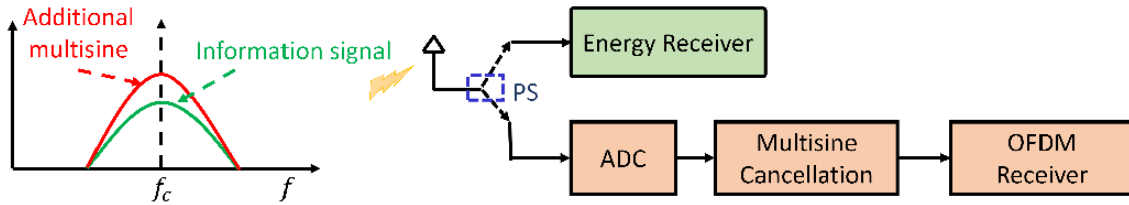


Fig. 2.8. Frequency spectra of multisine superimposed upon the OFDM information signal and corresponding receiver architecture.

(DFT) length [72]; consequently, increasing the power consumption at the receiver. Therefore, it is necessary to monitor the signal processing power consumption at the receiver in order to check the feasibility of this scheme.

An alternative, tailored for the PS configuration, is to superimpose an additional multisine on the OFDM waveform, as illustrated in Fig. 2.8, to further enhance its PAPR [73]. For a 20 dB SNR, information and power performance of 1 bit/s/Hz and around  $1.8 \mu\text{A}$  current can be attained for the combination of OFDM and 16-tone deterministic multitone. Although the only modification needed in this receiver architecture is the incorporation of cancellation of this multisine waveform, the drawback of this approach is that the receiver's analog-to-digital-converter (ADC) may suffer from saturation when the power signal level is relatively higher than the information signal.

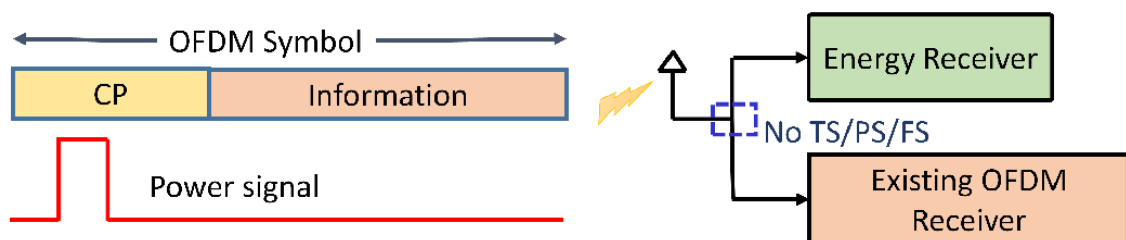


Fig. 2.9. CP-OFDM information symbol superimposed on the rectangular pulse power signal.

Another way to capitalize on the high PAPR OFDM signal for energy harvesting is to exploit its redundant cyclic prefix (CP), as shown in Fig. 2.9. In this approach, a high PAPR rectangular pulse for power transfer can be superimposed on the CP of the OFDM information signal [74]. As the cyclic prefix is discarded for information decoding, no modification is required in the information receiver, and a voltage 1.4 V can be harvested in a  $-15$  dB SNR environment. However, proper functioning of this signal requires optimization of the rectangular pulse width to minimize interference with the information part of the signal. Another approach for using the redundant CP for power transfer is proposed in [75]. Here, instead of transmitting a separate power signal over the OFDM signal, some portion of the information part is utilized for energy harvesting in addition to CP, and the length of this used information part for energy harvesting is optimized according to the energy requirement at the receiver.

In [76], directly superimposing a transmitting DC signal over the OFDM signal to make an OFDM-DC signal is proposed. In such a case, the power can be directly transferred in DC, in addition to the OFDM information signal. It is able to have 2 mW power and a symbol error rate (SER) of  $10^{-1}$  for 10 dB SNR with 2 bits/channel of the quadrature-phase-shift-keying (QPSK) OFDM-DC signal. This technique offers the advantage of the elimination of non-linear rectifying components at the receiver, which saturates the PCE in rectifier-based schemes, and a low-pass filter is sufficient for power conversion. However, the drawback of this transmission technique is that it requires a complete redesign of the transmitter and receiver architectures.

The performance analysis of the above-discussed transmission designs is summarized and compared in Table 2.2, in terms of their advantages, disadvantages, achievable information transfer rate, and harvested energy under different received power levels and SNR scenarios. Note that a separated information-energy receiver architecture offers the advantage of transmitting the information using an OFDM signal, as the portion of the signal being utilized for power delivery can be separated from

Table 2.2: Transmission designs for separated information-energy receiver architecture.

Transmission Approach	Advantages	Drawbacks	Information Rate and Energy
OFDM frequency spectrum splitting [71]	<ul style="list-style-type: none"> <li>No power splitting or time switching needed.</li> </ul>	<ul style="list-style-type: none"> <li>Well-designed BPF needed.</li> <li>Linear energy harvester model considered.</li> </ul>	4 bps/Hz and 18 mW for SNR = 50 dB.
Multisine superimposed on OFDM [73]	<ul style="list-style-type: none"> <li>Higher PAPR.</li> </ul>	<ul style="list-style-type: none"> <li>Saturation of ADC may occur.</li> </ul>	1.8 $\mu$ A for 1 bit/s/Hz for SNR = 20 dB.
Rectangular pulse superimposed on CP-OFDM [74]	<ul style="list-style-type: none"> <li>No modification in information detection.</li> </ul>	<ul style="list-style-type: none"> <li>Interference introduced according to the width of the rectangular pulse.</li> </ul>	1.4 V (maximum) at received input power of -15 dBm.
Partial usage of information part of OFDM [75]	<ul style="list-style-type: none"> <li>No modification in information detection.</li> </ul>	<ul style="list-style-type: none"> <li>Optimization needed for minimum usage of information part for sufficient harvested energy.</li> </ul>	$\sim$ 38% PCE for 2 bit-s/subcarrier channel for SNR = 20 dB.
OFDM-DC signal [76]	<ul style="list-style-type: none"> <li>Rectifying components such as diodes are not required.</li> <li>LPF is sufficient to extract the DC.</li> </ul>	<ul style="list-style-type: none"> <li>Complete redesign of transmitter and receiver.</li> </ul>	2 mW and SER = $10^{-1}$ with 2 bit-s/channel at SNR = 10 dB.

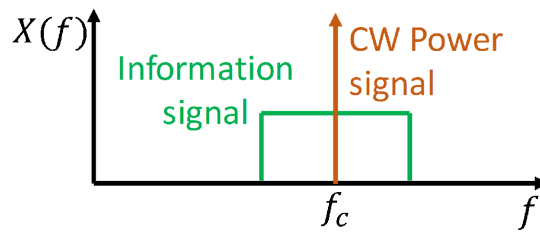


Fig. 2.10. Frequency spectrum of unmodulated power signal superimposed on modulated information signal.

the information signal with the help of distinguishing the information and power frequency bands. After the separation of the information and power signals, information processing can be performed as usual. However, this would not be efficient in a practical SWIPT system, as the power required for OFDM signal processing is quite high. Therefore, it is necessary to consider a practical SWIPT scenario where the transmitter and receiver power consumption is also considered. In this direction, the idea of using an integrated information-energy receiver architecture to reduce receiver power consumption is discussed in the next section.

Furthermore, in [77], a transmission approach is developed from a transmitter perspective. Here, instead of focusing on RF-DC efficiency at the receiver, the DC-RF efficiency at the transmitter is improved. Hence, a low PAPR signal is designed by superimposing a high-power unmodulated continuous wave power signal on the modulated signal, as shown in Fig. 2.10. In this way, interference between the information and energy signals is minimized by allocating power to the narrowband and information to the wider band. This idea might be feasible in practical scenarios where the power signal generally needs to have much higher power compared to the information signal (i.e., 0 dBm for power and -100 dBm for information).

### 2.3.1 PAPR Based Detection

One way of utilizing high PAPR multitone signals for SWIPT systems is to design the multitone waveform with different PAPR levels for each symbol [78]. Although the architecture has a separate information path and energy path, it can be seen

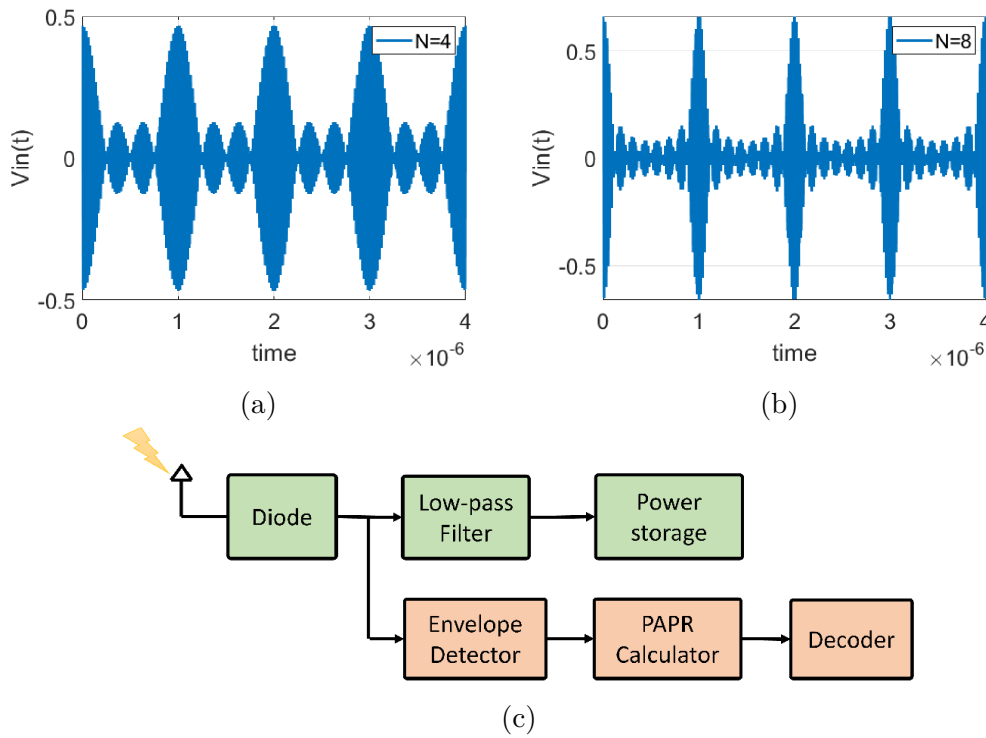


Fig. 2.11. PAPR-based waveform for (a)  $N = 4$ , (b)  $N = 8$ , and its (c) receiver architecture.

that information decoding is performed from the same rectified signal without any signal-splitting scheme as shown in Fig. 2.11. Multiple PAPR levels are produced by varying the number of tones or by varying the tone spacing. Here, the PAPR level is indirectly represented by the number of tones  $N$  as PAPR increases with the increase in  $N$  and the maximum PAPR =  $2N$  is achieved by uniformly allocating the power among all tones and by having the same phase.

A data rate of 0.5 Mbps with  $10^{-2}$  BER and a DC output 3.5 times higher compared to a single tone carrier can be achieved for a 30 dB SNR. For this, matched filtering is performed to achieve maximum PAPR for phase alignment amplitude matching. Although the frequency spacing  $\Delta f$  is kept constant for simpler analysis, the overall signal bandwidth varies for the different symbols. Therefore, the performance of the signal under frequency flat and frequency selective channels are studied and it is shown that no channel estimation is needed as was required in [12].

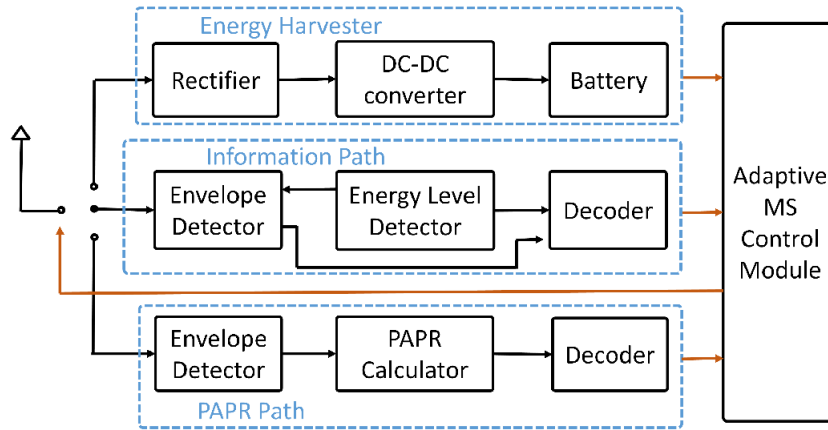


Fig. 2.12. Dual mode SWIPT system block diagram.

### 2.3.1.1 Dual Mode Adaptive SWIPT System

It has been discussed in Section 2.2.3.4 that multi-tone signals enhance PCE only in the ultra-low power region, whereas at high or medium power levels, a single-tone signal outperforms multi-tone signals because the diode enters into saturation region at high input power [79]. Therefore, in [80], a dual-mode adaptive system (Fig. 2.12) is introduced to increase the operational power range by switching between the information paths for single tone and multitone according to the received input power. A power management and information decoding module is used to measure the received power level and then further, the mode is switched between the appropriate information path according to the received feedback signal, i.e., energy-based information path for high received power and PAPR path for low received power. In [81], the input signal is split in the time domain for the energy path and the chosen information path, whereas, in [80], power splitting is employed for signal splitting.

### 2.3.1.2 Tone-index Modulation

In [78], every different symbol requires to be transmitted with different bandwidth, and fading characteristics need to be analyzed. On the contrary, another tone-index-based method is proposed in [82] where frequency spacing between tones gets adjusted for each symbol and the resulting multitone signal bandwidth for

all the transmitting symbols is constant. Additionally, the tone-index demodulation method provides additional benefit over the simple PAPR-based method when low SNR transmission is considered. For this tone-index modulation method, investigation of appropriate tone spacing, number of tones, and bandwidth under practical frequency selective channels is needed in the future.

## 2.3.2 Amplitude Based Detection

Generally, most of the research problems for enhanced PCE in WPT systems revolve around the problem of reducing ripple voltage present in the output voltage with required DC voltage. However, having some amount of ripples may lead to the successful decoding of information using the same rectifier model resulting in a trade-off between WIT and WPT.

### 2.3.2.1 Biased ASK

A system model where information is transmitted through a single tone but with varying amplitudes for various symbols i.e.  $M$ -ary ASK is introduced [83, 84]. The same hardware (envelope detector) is used for information as well as energy. In general ASK, the minimum amplitude is considered as 0 thus, when a symbol having zero energy is being transmitted the receiver just sits idle and is not able to harvest any energy. Here, in [83], a constant bias is added to  $M$ -ary ASK as shown in Fig. 2.13, assigning a minimum amplitude to all the symbols to ensure a minimal continuous power transmission to the receiver irrespective of the symbol. Using this modulation method, 0.13 V voltage (depending on the rectifier) and a quite low BER of  $10^{-4}$  can be achieved for a received input power of  $-20$  dBm.

As in Fig. 2.13,  $A_i$  is varied between  $A_{\min}$  (minimum amplitude) and  $A_{\max}$  (maximum amplitude). The worst case scenario for WPT is when the uppermost symbol ( $A_{\max}$ ) is followed by the lowermost symbol ( $A_{\min}$ ) for the information [84]. In this case, for proper WIT decoding, the detector has to follow the envelope such that the capacitor needs to be discharged from maximum to minimum within a symbol

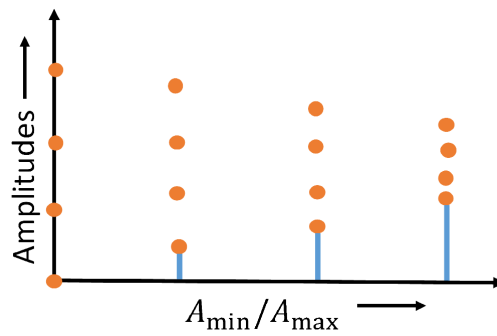


Fig. 2.13. Biased 4-ASK with increasing minimum symbol power.

period. This maximum voltage change would induce the ripple voltage. An upper limit for  $f_{\text{ratio}} = \frac{f_{\text{symbol}}}{f_{\text{cutoff}}}$  is calculated for the proper information decoding where  $f_{\text{symbol}}$  is the symbol rate and output  $f_{\text{cutoff}}$  is the filter cut-off frequency.

It is observed that WPT performance improves with the increase in  $F_{\text{ratio}}$  or  $A_{\text{ratio}}$  as the ripple voltage reduces. However, in this case, the power applied to the matched region is reduced, resulting in a decrease in WIT performance. Therefore, a trade-off between WIT and WPT performance exists depending upon  $F_{\text{ratio}}$ . Also, this transmission technique uses only a single tone for generating amplitude variations, which degrades the PCE and does not make use of a high PAPR multitone signal. A further step towards two-dimensional signaling by combining biased-ASK [84] and PAPR-based detection [78, 85] has also been explored in [86] where two separate paths for information detection one from the amplitude and another from the number of tones present in the signal are provided.

### 2.3.2.2 Ratio ASK

In the previously discussed biased ASK modulation, only a single tone is used for the transmission, while it has been shown that multitone outperforms the single tone in the case of WPT. Thus, exploring the possibility of baseband modulations such as ASK using multitone signals would move the system closer to a practically efficient system. A modulation technique that does use a multitone signal is introduced in [87, 88]. Instead of embedding information directly in the amplitudes of the tones, a model is proposed where the information is embedded in the ratios of the

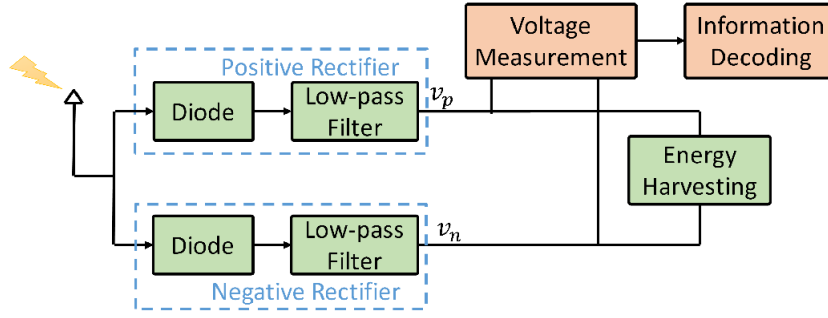


Fig. 2.14. Dual ASK SWIPT system with two half-wave rectifiers.

amplitudes of the different tones rather than in the amplitudes themselves. The transmitted signal is considered as

$$s_i(t) = A_{i,j} \sum_{j=1}^N \cos(2\pi f_j t + \phi_j), \quad (2.12)$$

where  $s_i(t)$  denotes  $i^{\text{th}}$  symbol having tones of  $A_{i,1}, A_{i,2}, \dots, A_{i,N}$  amplitudes.

Although having information in amplitude ratios offers the advantage of making the system independent of transmission distance while providing a 48% PCE for a received signal power of  $-10$  dBm, the drawback of this technique is that it is not suitable for a large  $N$ . As in [88], information is in the ratio of  $A_1$  and  $A_2$ ,  $A_1$  and  $A_2$  need to be found and it is done by measuring direct current (DC) and alternating current (AC) voltage at the output to relate it back to  $A_1$  and  $A_2$ . Therefore, as  $N$  increases, a complete solution of the non-linear equation to find  $A_1$  and  $A_2$  becomes complicated.

Recently, a new integrated receiver architecture using two half-wave rectifiers is introduced, as shown in Fig. 2.14. To further increase the data transmission capacity of the integrated receiver architecture by having a higher degree of freedom for signal amplitudes [89]. By moving from simple energy modulation [12] to biased-ASK [84], output DC voltage is enhanced at the cost of the BER performance. Therefore, an approach for increasing the amplitude range is introduced in Fig. 2.14 where two amplitudes are generated by the rectifiers; one positive voltage  $v_p$  and one negative voltage  $v_n$  and both of these amplitudes are utilized for generating the modulation

symbols [89]. Two possible proposed encoding methods are:

1. **Amplitude difference shift keying (ADSK):**

DC signal with amplitude difference of positive and negative rectifier is calculated for information decoding such as

$$v_{dc} = v_p - v_n \quad (2.13)$$

As  $v_p$  is positive and  $v_n$  is negative so, the achievable range of  $v_{dc}$  is higher than that for the single half-wave rectifier resulting in a wider constellation range available for the amplitudes.

2. **Amplitude ratio shift keying (ARSK):**

In this case, the ratio of  $v_p$  to the  $v_n$  is calculated for decoding the appropriate information symbol.

$$v_{dc} = \frac{v_p}{v_n} \quad (2.14)$$

By using Monte-Carlo simulation, it is shown that ADSK provides better BER compared to both PEM and Biased-ASK. However, the ARSK scheme results in lower BER compared to PEM as here, only linearly spaced ratio  $v_p/v_n$  values are considered. BER for non-linearly spaced ratios may be the future research problem to achieve better BER performance as was achieved in [88]. Also here, only the DC signal is exploited for information decoding, further, different constellation techniques can be studied by the use of more parameters such as frequency spacing and phase.

### 2.3.3 Frequency Based Detection

Nonetheless, amplitude variations in the multitone waveform have benefits in terms of data rate (i.e., with the increase of modulation order) for a SWIPT system, but these variations impose a limit on achievable WPT due to the presence of ripples in the output voltage that degrade the WPT performance [84, 87, 88]. Therefore, the ideal waveform for a SWIPT system would entail minimal variations in the envelope,

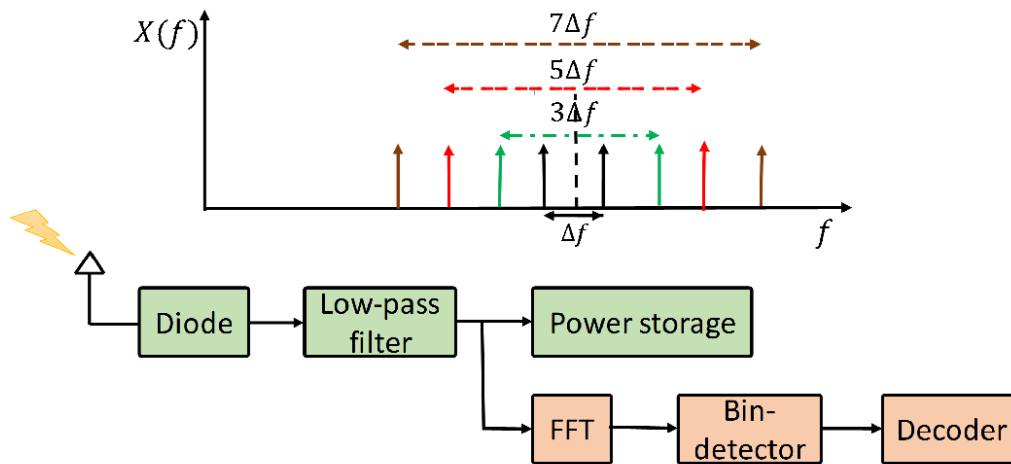


Fig. 2.15. Multitone FSK waveform and receiver architecture.

with the stream of information symbols having a minimum effect on the WPT.

### 2.3.3.1 Non-coherent Multitone FSK

Consequently, a multitone frequency-shift keying (FSK) is proposed in order to reduce the mutual impact of the WPT and WIT on each other [90]. Here, information is transmitted by varying the frequency differences between the tones. Firstly, a two-tone model is recognized [91] where only one tone separation is available for the information transmission. By varying this frequency separation between the tones, it is possible to have intermodulation components at the different frequency values for the different symbols.

For the detection of the signal, the receiver architecture shown in Fig. 2.15 is employed where a Fast Fourier Transform (FFT) block is added to observe the signal in the frequency domain. For each symbol, there exists a particular  $\Delta f$  and the bin detector identifies the frequency corresponding to the highest amplitude which would be  $\Delta f$  for a particular symbol. Therefore,  $f_{\text{cutoff}}$  of the low-pass filter also plays a major role. Further in [90], this idea is extended to the multitone FSK with the transmitted signal as

$$s_{\text{in}}(t) = \sum_{j=1}^N \cos(2\pi f_j t). \quad (2.15)$$

Two multitone FSK schemes are proposed: uniform multitone FSK and non-uniform

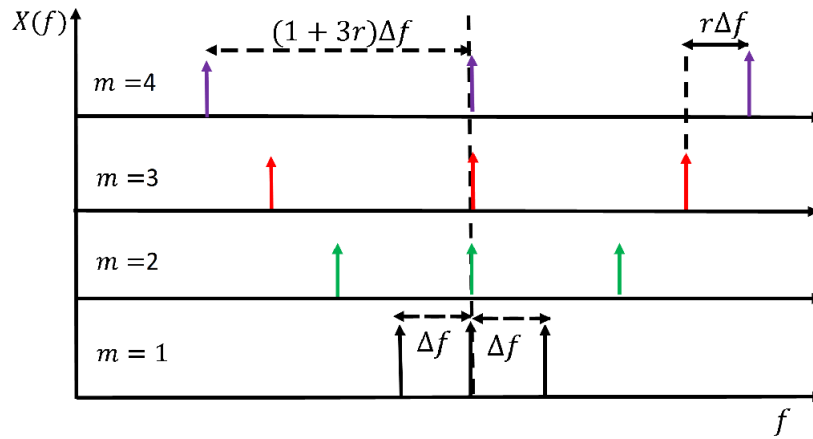


Fig. 2.16. Symbol construction for uniform multitone FSK with tone  $N = 3$  and modulation order  $M = 4$ .

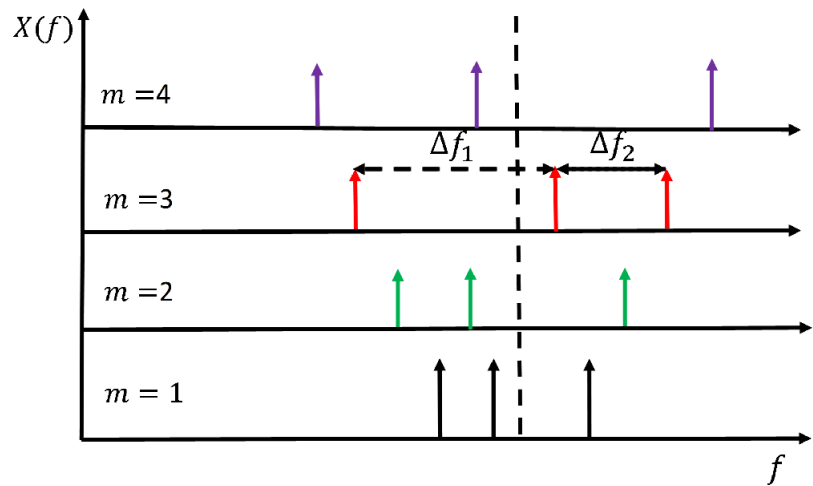


Fig. 2.17. Symbol construction for non-uniform multitone FSK with tone  $N = 3$  and modulation order  $M = 4$ .

multitone FSK. Fig. 2.16 represents the model of uniform multitone FSK where the neighboring tones are separated by the multiple of  $\Delta f$ .

In this simple case of multitone FSK,  $N$  and  $M$  are increased with the equal  $\Delta f$  among tones. Thus, the system is not spectrally efficient for a large modulation order. A 0.55 V output voltage can be attained, which is higher than the amplitude-based biased-ASK waveform. However, SER performance degrades to  $10^{-2}$  compared to  $10^{-4}$  for biased-ASK. Hence, a non-uniform multitone FSK with unequal frequency spacing is introduced to make the SWIPT system more bandwidth efficient as shown in Fig. 2.17. Although the non-uniform multitone FSK fully exploits

the spectrum, the WPT efficiency declines as the bandwidth is not optimally filled with the tones. Uniform FSK provides a higher PAPR signal resulting in higher WPT efficiency and non-uniform FSK provides higher throughput. The above-mentioned FSK schemes pose the advantage of providing a higher symbol rate with less variation in the output power.

Furthermore, decoding at the receiver can be performed by evaluating multitone PAPR levels with the changing frequency spacings to lower the power consumption at the receiver [92] instead of using FFT operation for identifying the strongest baseband signal.

### 2.3.3.2 ASK-OFDM

Biased ASK and multitone FSK are combined to provide a biased OFDM scheme moving closer to full OFDM transmission [93]. As discussed earlier, biased-ASK is an energy-efficient scheme where each symbol carries some minimum amount of energy. Here, an idea of transmission of modulated information over each tone is proposed. The first tone amplitude is kept constant and the information is encoded in the amplitudes of the remaining  $N - 1$  tones relative to the first tone with the help of ratio  $r$ . The received ASK-OFDM signal is given by

$$s(t) = \sin(2\pi f_c t) + r \sum_{n=1}^{N-1} a_n \cos(2\pi(f_c + n\Delta f)t) \quad (2.16)$$

where  $f_c$  is the reference frequency,  $a_n$  is the biased amplitude level, and  $r$  is the maximal amplitude ( $0 \leq r \leq 1$ ) and defined by the modulation order.

It has been discussed that the diode produces intermodulation frequency components, so after passing the signal in (2.16) through the rectifier, various baseband intermodulation components at  $\Delta f$ ,  $2\Delta f$ ,  $\dots$ ,  $(N - 1)\Delta f$  will be present at the output and all other intermodulation would get filtered out by the low-pass filter. For the information decoding,  $a_n$  needs to be calculated for a particular tone. This is done by the use of a reference tone at  $f_c$  keeping its amplitude higher than the

rest of the tones. For example, there will be many intermodulations at  $\Delta f$  as all consecutive tones are separated by the same frequency but the tone closer to  $f_c$  would produce higher amplitude compared to the rest of the tones because all other intermodulations would result in  $r^2$  which is always lower than  $r$ . Similarly, for frequency spacing of  $2\Delta f$ , the next tone would generate the highest amplitude. Therefore, in this way,  $N - 1$  information symbols can be detected by the  $N - 1$  available frequency spacings with respect to  $f_c$ .  $r$  should be the maximum for the WPT keeping in mind acceptable BER for information transmission. Thus, in [93], the upper limit for  $r$  is also analyzed with increasing  $N$ .

The various advantages, disadvantages, and performance analysis of the integrated information-energy receiver architecture-based transmission approaches are summarized in Table 2.3. It can be observed that in most of the transmission approaches and for both the receiver architectures, the PCE is enhanced by giving the transmitted signal a higher PAPR by means of a multitone signal. This is similar to the case of the separated information-energy receiver architecture where a high PAPR OFDM signal is used. Indeed, high PAPR signals offer the advantage of increased power transfer performance. However, these high PAPR signals may saturate the non-linear amplifier at the transmitter and subsequently degrade the information transfer performance [94]. Therefore, a complete transmitter-receiver system analysis is required to attain the actual PCE and information transfer performance of these SWIPT transmission schemes.

## 2.4 Input Distribution

In a SWIPT system, it is required to study optimal operating points to improve rate-energy trade-off characteristics for simultaneous information and energy flow. There exist various sections involved in the measurement of the performance of the whole SWIPT system, such as transmitter distortion, channel performance, hardware design, types of waveform transmitted, etc. One such parameter is the

Table 2.3: Transmission designs for integrated information-energy receiver architecture.

Transmission Approach	Advantages	Disadvantages	Information and Power
PAPR based [78]	<ul style="list-style-type: none"> <li>High PAPR</li> </ul>	<ul style="list-style-type: none"> <li>Performs well only for high SNR.</li> <li>Input matching network for a large BW.</li> </ul>	0.5 Mbps and DC of 3.5 times higher compared to the single carrier input signal for 30 dB SNR.
PAPR based with fixed signal BW [82]	<ul style="list-style-type: none"> <li>Good performance for high SNR as well as low SNR.</li> </ul>	<ul style="list-style-type: none"> <li>Non-uniform frequency spacings.</li> </ul>	0.5 $\mu$ A and BER = $10^{-1}$ for $-10$ dB input power.
Biased-ASK [84]	<ul style="list-style-type: none"> <li>Each symbol has some minimum energy.</li> </ul>	<ul style="list-style-type: none"> <li>Single tone is used.</li> </ul>	$10^{-4}$ BER and 0.13 V at $-20$ dBm received power, for SNR = 18 dB.
Amplitude ratio [88]	<ul style="list-style-type: none"> <li>Independent of transmission distance.</li> </ul>	<ul style="list-style-type: none"> <li>Analysis only for the multitone with a smaller number of tones.</li> </ul>	48% PCE for received power of $-10$ dBm.
Multitone-FSK [90]	<ul style="list-style-type: none"> <li>Lessened envelope variations.</li> <li>Reduced impact of large WPT on WIT.</li> </ul>	<ul style="list-style-type: none"> <li>Power consuming FFT needed.</li> </ul>	SER = $10^{-2}$ and 0.55 V for received power of 0 dBm.
ADSK, ARSK [89]	<ul style="list-style-type: none"> <li>Increased operational range.</li> </ul>	<ul style="list-style-type: none"> <li>Only DC power is considered.</li> </ul>	$10^{-1}$ BER and 0.45 $\mu$ W at $-10$ dBm received power, for SNR = 15 dB.

assumed input distribution at the transmitter side.

In most practical systems, signals are chosen from some group of fixed constellation points such as PSK, QAM. The effect of finite input alphabet signal instead of Gaussian distributed input signal is analyzed on the performance of the point-to-point single user and multi-user SWIPT system model and it is found out that the system does not follow the aforementioned rate-energy trade-off and offers a much lower performance [95]. However, assigning non-uniform probabilities to these input signals is shown to have enhanced rate-energy trade-off and the performance can be optimized with the power splitting factor between the energy signal and the information signal of the receiver architecture.

In [96], rate-energy regions of Gaussian input and discrete input are compared and it is observed that Gaussian input gives maximized region. The reason for this is that in the case of Gaussian input, information increases indefinitely with the increasing SNR whereas for the finite input signal, information gets saturated to a particular value. Thus, the difference between the performances of these two is larger in the case of high SNR compared to low SNR situations. However, this difference can be reduced by increasing the modulation order  $M$ . Furthermore, in [97] also, Gaussian input signals under different transmit power conditions are shown to have overestimated rate-energy region which is not possible to achieve with the finite input set.

Although all the above work focuses on more practical signal design, the energy harvester model is considered to be a linear model which is not practically possible. Some work with the asymmetric modulation for the case of a non-linear energy harvester model has been already explored as below.

### 2.4.1 Asymmetric Modulation

It is shown that the capacity of AWGN channel with non-linear energy harvester is independent of the delivered power constraint for single carrier transmission [98,

99]. In other words, AWGN channel capacity with the transmitter average power constraint and the delivered power constraint depends only upon the transmitter average power constraint when the non-linear energy harvester model is considered. Furthermore, capacity-power regions with zero mean and non-zero mean Gaussian OFDM transmission for separated receiver architecture are evaluated and compared [100, 101]. In these, it is found that non-zero mean Gaussian input attains a larger capacity-power region compared to its zero-mean counterpart and this region can further be expanded by optimizing the asymmetric power distribution among the complex subchannels.

Recently, a signal splitting scheme has been designed for a separated information and energy receiver architecture. Here in [102], instead of a power splitting scheme where all the symbols are used for information transfer (IT) and EH, constellation points are divided into two parts one solely for IT and the other ones solely for the EH and assumed that the receiver already knows the position of IT and EH symbols in the signal stream. A Hybrid Constellation Shaping Scheme (HCS) is used for non-equidistant and non-uniform constellation point design.

For 4-QAM, outer symbols are selected for energy harvesting because of having the largest symbol energy (the distance between the constellation point and the center) and all the remaining 12 symbols are used for the information transfer. HCS makes the constellations such that overall system energy remains the same. Therefore, EH symbols are moved farther for the increased energy transferred per symbol, and consequently, IT symbols move closer to the center. Besides using two separate streams for IT and EH, [102] also makes use of non-uniform symbol distribution by assigning more symbols to the IT and it is shown that this scheme provides better performance compared to previously used power splitting scheme for energy transfer.

The above modulation design method can be implemented in any modulation scheme. However, here in [102] only the linear energy harvester model is discussed. The use of asymmetry in the constellation design is further discussed in [103, 104].

As discussed in [13], multisine waveforms with zero phase difference among tones provide maximum power transfer. However, deviating from the same phase condition opens up the possibility of transmission of information using phase. In [103, 104], rate-energy trade-off region for asymmetric  $M$ -PSK multisine modulation scheme for separated information and energy receiver architecture is shown to be enhanced compared to the uniformly distributed equally spaced M-PSK.

The received signal  $x(t)$  for such a modulation scheme is given by

$$x(t) = \sqrt{\frac{2P}{N}} \sum_{n=0}^{N-1} \cos(2\pi f_n t + \phi_n) \quad (2.17)$$

where  $\phi_n \sim [-\delta, \delta]$  are uniformly distributed random phases with  $\delta \leq \pi$ . It is shown that  $\delta = 0$  provides the maximum power transfer case due to the formation of in-phase multisine and  $\delta = \pi$  provides the benefit of information transfer with the modulated multi-carrier signal [105].

It has also been demonstrated that harvested power is not only depending on the  $\delta$  value but also on the probability masses of symbols. It is shown that there exist two different probability distribution scenarios for the desired information rate and for the desired harvested energy. Wider phase distribution is required for the information transfer, i.e., high probabilities should be assigned to the outermost symbols for the wider decision regions resulting in lower BER. However, from the power transfer perspective, a narrower phase distribution with high probabilities to the innermost symbols to make the signal closer to the deterministic in-phase multisine transmission would be helpful. Therefore, it can be seen that irrespective of the application as information transfer or power transfer, asymmetric probability distribution is favorable. In short, the achieved information rate and harvested energy depend not only on the number of subcarriers  $N$  and modulation order  $M$  but also on the phase range and the probability masses of the symbols.

## 2.4.2 Constellation Rotation

In [106], a non-orthogonal multiple access (NOMA) downlink transmission where different transmit power is assigned to different users is considered. The transmitted signals to these users are combined with each other. As this combination can be constructive or destructive at the receiver, a constellation rotation is performed in a multi-user NOMA system to increase the minimum distance between the symbols to improve BER. Further, this is extended to the improved power transfer in a multi-user NOMA-supported SWIPT system [107]. While designing the constellation, it should also be considered how many symbols have higher voltages than the diode threshold voltage  $V_{th}$  [108]. For example, 16-PAM may outperform 16-PSK for high  $V_{th}$ , but at low  $V_{th}$ , 16-PSK would provide more harvested energy as all the symbols are able to cross the  $V_{th}$  level. Therefore, a higher order modulation performs better for WPT as more symbols are able to overcome threshold voltage [108].

In [107], a two-user system is considered, and symbol  $s_1$  from user 1 and  $s_2$  from user 2 are combined resulting in symbol  $s = s_1 + s_2$ . As  $|s_1 + s_2|^2 \leq |s_1|^2 + |s_2|^2$ . The power carried by symbol  $s$  may be less than that of the  $s_1$  and  $s_2$  and the worst case would be when  $s_1$  and  $s_2$  have the opposite phases and form destructive superposition. For the solution of this problem, here in [107], a rotation angle  $\theta$  is inserted in the constellation such as  $s_1 = |s_1|e^{j\theta}$ . This rotation angle is optimized for maximum energy transfer with the required information rate such that decision regions can still be distinguished. The effect of such rotation in other modulation schemes and for an integrated receiver architecture can be the future research direction. A joint constellation rotation modulator and energy interleaver are designed for the constructive superposition of symbols in the power domain [109].

Table 2.4: Summary of existing modulation methods for integrated information-energy receiver architecture.

Ref.	Modulation Method	Receiver architecture	EH Model	Characteristics
[12]	Energy modulation	Integrated	Linear	<ul style="list-style-type: none"> <li>- Easiest ID using integrated receiver.</li> <li>- Not taking advantage of multi-tone carriers to enhance the power transfer.</li> </ul>
[73]	Multisine superimposed over OFDM signal	Separated	Non-linear	<ul style="list-style-type: none"> <li>- Power signal cancellation required for ID.</li> <li>- Saturation of ADC may occur.</li> </ul>
[74]	Rectangular pulse superimposed over OFDM cyclic prefix	Separated	Linear	<ul style="list-style-type: none"> <li>- No power signal cancellation needed.</li> <li>- No modification in ID.</li> <li>- Interference is introduced according to the width of the rectangular pulse.</li> </ul>
[76]	OFDM-DC signal	—	—	<ul style="list-style-type: none"> <li>- Rectifying components such as diodes are not required.</li> <li>- LPF is sufficient to extract the DC.</li> </ul>

[78]	PAPR based	Integrated	Non-linear	<ul style="list-style-type: none"> <li>- Equal tone spacings resulting into unequal signal bandwidths for the distinct symbols.</li> <li>- Performs well only for high SNR.</li> </ul>
[80] [81]	Dual mode reception	Separated	Non-linear	<ul style="list-style-type: none"> <li>- Dual mode detection for low power and high power signals.</li> <li>- Increased operational range.</li> </ul>
[82]	PAPR based having fixed signal BW	Integrated	Non-linear	<ul style="list-style-type: none"> <li>- Unequal tone spacings for the distinct symbols.</li> <li>- Good performance for high SNR as well as low SNR.</li> </ul>
[84]	Biased-ASK	Integrated	Non-linear	<ul style="list-style-type: none"> <li>- Each symbol having some minimum energy.</li> </ul>
[88], [89]	ADSK, ARSK	Integrated	Non-linear	<ul style="list-style-type: none"> <li>- Only DC power is considered.</li> <li>- Increased operational range with the use of two half-rectifier.</li> </ul>
[90]	Multitone-FSK	Integrated	Non-linear	<ul style="list-style-type: none"> <li>- No envelope variations.</li> <li>- Reduced impact of large WPT on WIT.</li> <li>- High symbol rate</li> </ul>

[93]	ASK-OFDM	Integrated	Non-linear	<ul style="list-style-type: none"> <li>- Practical OFDM transmission is feasible.</li> <li>- Higher data rate.</li> </ul>
[104]	Aymmetric PSK	Separated	Non-linear	<ul style="list-style-type: none"> <li>- Enhanced rate-energy trade-off compared to symmetric PSK.</li> <li>- Higher data rate.</li> </ul>

## 2.5 Conclusion

The discussed transmission waveforms and the corresponding receiver architectures are still far from practical SWIPT systems. Some of the reasons are: (i) OFDM signal waveforms utilizing a separated receiver architecture consume significant power for signal processing at the receiver, (ii) the effect of WIT over WPT is still significant for the modulation methods used for an integrated information-energy architecture due to the presence of ripples at the output, (iii) moving toward more practical SWIPT systems, the constellation range needs to be increased so that the transmission can support higher modulation orders for increasing information rates, and (iv) an end-to-end performance analysis including the transmitter performance for a particular waveform is required.

# Chapter 3

## Multitone PSK

This chapter contributes to the design of a Multitone PSK waveform transmission scheme for an integrated information-energy receiver, and WIT and WPT performances are evaluated. All simulation results are verified by performing measurements over the designed rectifier-receiver circuitry. Contributions in this chapter include the author’s publication [15]:

- **Prerna Dhull**, Dominique Schreurs, Giacomo Paolini, Alessandra Costanzo, Mehran Abolhasan and Negin Shariati, “Multitone PSK Modulation Design for Simultaneous Wireless Information and Power Transfer,” *IEEE Transactions on Microwave Theory and Techniques*, vol. 72, no. 1, pp. 446-460, Jan. 2024, doi: [10.1109/TMTT.2023.3294008](https://doi.org/10.1109/TMTT.2023.3294008).

### 3.1 Introduction

Radio frequency (RF) signals carry information as well as energy. Simultaneous wireless information and power transfer (SWIPT), which is a combination of wireless information transfer (WIT) and wireless power transfer (WPT), has recently gained prominence in making small Internet-of-Things (IoT) devices battery independent [18]. However, till now, most of the SWIPT research treats WIT and WPT performances separately, and either only WIT performance or only WPT perfor-

mance is improved [110, 111].

Recently, high peak to average power ratio (PAPR) signals have been shown to increase power conversion efficiency (PCE) in low-power WPT systems by exploiting the non-linear characteristics of the rectifying circuitry [42]. A multitone waveform is one of such high PAPR waveforms [13, 112, 113]. Several parameters such as tone separations, number of tones, input power range, bandwidth (BW), output filter cut-off frequency, output load, etc., have been shown to affect the achievable PCE at the output [56–59, 62, 68, 114–116].

From an architecture perspective, most of the SWIPT research mainly revolves around a separated information and energy receiver architecture where the main focus is upon the distribution of the received power between information and energy paths according to a power utilization ratio, to optimize the SWIPT receiver performance [110]. Several techniques such as time-switching, power splitting, and frequency-splitting have been introduced to use the received signal in separate information and energy paths [117, 118]. Recently, a symbol-splitting technique has also been introduced for splitting the information and the carrier having no information, with the help of a coupler's isolation port to divide the received signal between information and power components in a better way for power transfer [119]. However, in such an architecture, the information is transmitted using conventional modulation techniques and the information detection is performed using conventional methods involving a local oscillator through a separate information path which involves increased power consumption for information detection at the receiver.

Therefore, an integrated information and energy receiver architecture as shown in Fig. 3.1 has been proposed where the same rectified output signal is used for information decoding as well as power extraction [12]. In this work, this integrated information and energy receiver architecture is utilized. In fact, its main advantage is the reduction of the overall energy consumption at the receiver compared to the separated information and energy receiver architecture, by the removal of the RF

local oscillator needed for information detection. However, in this case, conventional information transmission techniques cannot be utilized. Therefore, new transmission methods are required to be proposed for integrated information and energy receiver architectures.

To address this, a simple energy modulation scheme of transmitting symbols through different energy levels of a single-tone waveform for integrated receiver architecture is introduced [12]. To further increase the available constellation range for the energy symbols, an integrated receiver architecture model consisting of two half-wave rectifiers instead of having only one rectifier is proposed [89]. Two half-wave rectifiers are utilized with two amplitudes at the output, one positive and one negative. Further, information is encoded in the PAPR levels of multitone signals to enhance the WPT performance in [78], and its extended work demonstrated that non-uniformly spaced multitone signals with fixed BW perform better in case of low SNR transmission scenarios compared to uniformly spaced multitone with varying BW [82]. Although [12, 78, 82, 89] introduced new SWIPT transmission techniques for the integrated receiver architecture, their performance has not been verified through measurements. Another way of encoding the information is the use of pulse position modulation which also helps in increasing PAPR to boost harvested power [120].

The non-linearity of the rectifier causes intermodulations among multitone frequency components, resulting in the presence of ripples in the output voltage. A biased amplitude-shift-keying (ASK) waveform has been designed utilizing an integrated information-energy receiver architecture where each symbol carries some minimum energy for continuous energy harvesting at the receiver [84]. Further, a way of embedding information in amplitude ratios of individual tones of a multitone signal is introduced to make this amplitude-based information transfer immune to the transmission distance [88]. Another multitone amplitude transmission scheme has been introduced, utilizing two-dimensional signalling in terms of subcarrier amplitudes and the number of subcarriers [86]. The information is decoded from two separate paths with the help of current intensity and PAPR level. However, for

such amplitude-based modulations, there should be a sufficient distinction in ripple voltage to identify the information symbols. Therefore, the PCE varies significantly depending upon the transmitted symbols, resulting in a significant dependence of WPT upon WIT transmission and, hence, limiting the number of tones and modulation order for proper SWIPT performance.

Amplitude variations offer an advantage for WIT, but in integrated receiver SWIPT systems, it is required to minimize the effect of WIT over WPT. To minimize these ripples, a multitone frequency shift keying (FSK) scheme is introduced, where the tones' frequency spacings are varied according to the transmitted information, and information decoding is performed by Fast Fourier Transform (FFT) [90]. Another way of decoding information from multitone FSK is considering the fact that multitone with different frequency spacings result in different PAPR levels, which further helps in reducing the receiver power consumption by the removal of FFT [92]. A way of utilizing the phase of 2-tone signal is introduced in [88]. However, in this work, the method of information decoding is performed by analyzing the DC and AC components at the output. This way of information transmission and reception becomes very complex even with a signal of three tones. Therefore, the proposed method in [88] is not suitable for an OFDM-type communication where multiple symbols can be transmitted over the same signal. Also, it does not analyze its WIT performance as the focus is solely on WPT performance. A comparison among the existing transmission schemes for separated information and energy receiver architecture and integrated information and energy receiver architecture has been performed in Table 3 and Table 4 of [18], respectively.

In this chapter, a novel multitone phase shift keying (PSK) modulation scheme for the integrated information and energy receiver architecture is introduced. Power transfer, as well as information detection, is performed over the rectified signal. Information is transmitted in the phase differences between consecutive tones of multitone RF signal, and the information decoding at the receiver is performed by observing the phases of corresponding baseband tones of the rectified signal.

Figure-of merits considered for analyzing WPT and WIT performances are PCE and bit-error-rate (BER), respectively. The effect of the chosen symbols constellation, modulation order, and the number of tones over signal PAPR, PCE, and BER are observed, showing a requirement for an optimum design of symbol phases. Further, the simulation results are verified by measurements with a designed receiver rectifier circuitry.

The main advantage of the proposed multitone PSK scheme is the transmission of  $(N - 1)$  symbols over an  $N$ -tone multitone signal which can be closely related to the standard OFDM used for WIT. This entire SWIPT transmission is performed using a simple receiver rectifier circuitry having low power consumption, as information detection does not require an RF local oscillator. Furthermore, the effect of WIT on the WPT performance of a SWIPT system has been reduced with the help of information transmission in the form of the tones' phases instead of amplitudes of the multitone signal. In addition, a multitone PSK signal improves the end-to-end SWIPT performance by reducing the chances of saturation of the transmitter power amplifier. Table. 3.1 in Section 3.5 compares the proposed multitone PSK with the existing transmission schemes for integrated information and energy receiver architecture.

This chapter is organized as follows. Section 3.2 introduces the theoretical model of a multitone PSK signal design with non-uniform spaced tones. Section 3.3 illustrates the relationship between the chosen phase range for symbol constellation and the multitone PSK signal PAPR. Next, in Section 3.4, the rectifier design and measurement setup used for simulations and measurements are presented. Then, the modulation scheme impact on WIT and WPT performances of the SWIPT system is analyzed in Section 3.5. Further, the obtained results are verified with the measurements. In the end, a conclusion is drawn in Section 3.6.



Fig. 3.1. SWIPT integrated receiver rectifier.

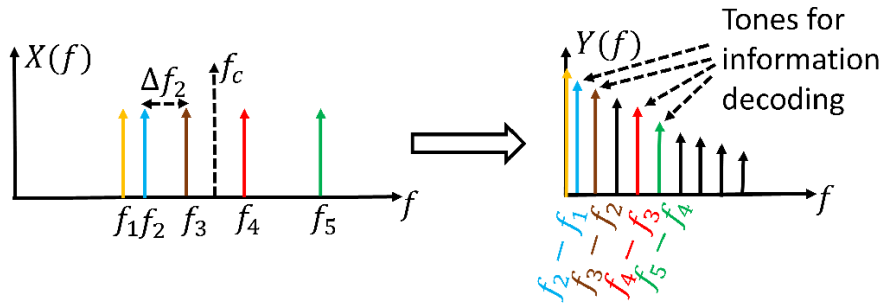


Fig. 3.2. 5-tone multitone PSK RF input signal spectrum  $X(f)$  centered around carrier frequency  $f_c = 2.45$  GHz and rectified baseband output spectrum  $Y(f)$  consisting of IM frequency tones (in MHz) used for information decoding (colored) and extra IM components (black).

## 3.2 Signal Model

The system model is illustrated in Fig. 3.1 and Fig. 3.2 where the multitone PSK RF signal  $x(t)$  is passed through the rectifier circuitry consisting of an input matching network, diodes, and an RC-LPF for both WIT and WPT.  $x(t)$  consists of  $N$  frequency tones at the centre frequency  $f_c$  of 2.45 GHz. After passing through the rectifier,  $x(t)$  results in the baseband output signal  $y(t)$ .  $y(t)$  is used for both power transfer as well as information decoding. Complete  $y(t)$  is used for WPT while information is decoded from phases of some of the baseband tones as shown in Fig. 3.2.

The modulation scheme is designed by making use of the non-linearity of the rectifier. The idea of the multitone PSK comes from the fact that an  $N$ -tones multitone signal passing through the rectifier results in intermodulation frequency components of various orders with the dominant  $2^{nd}$  order intermodulation (IM<sub>2</sub>) component at the rectifier output.

IM<sub>2</sub>s are generated by the mixing between two tones of  $N$ -tones multitone. In this chapter, information is transmitted as phases of IM<sub>2</sub>s between consecutive tones.

The transmitted signal  $x(t)$  can be considered as

$$x(t) = \text{Re} \left\{ A \sum_{n=1}^N e^{j(2\pi f_n t + \phi_n)} \right\}, \quad (3.1)$$

where  $A$  and  $\phi_n$  represent the amplitude and phase of the  $n^{\text{th}}$  tone frequency  $f_n$ , respectively. In order to see the intermodulation behavior, a case of 3-tones with  $N = 3$  in (3.1) can be considered. After transmitting the 3-tone multitone through the model of Fig. 3.1, the filtered output signal  $y(t)$  consists of dc and a combination of baseband intermodulation frequency components. All the harmonics and odd-order intermodulation components are filtered out by the LPF as all these frequencies would be at RF frequencies. Among baseband tones, IM<sub>2</sub> would be dominating compared to 4<sup>th</sup> order, 6<sup>th</sup> order,  $\dots$ , etc., frequency components [51]. Therefore,  $y(t)$  can be represented in terms of dc and IM<sub>2</sub>s as

$$y(t) = \text{dc} + A_1 \cos(2\pi(f_2 - f_1)t + \phi_2 - \phi_1) + A_2 \cos(2\pi(f_3 - f_2)t + \phi_3 - \phi_2) + \\ A_3 \cos(2\pi(f_3 - f_1)t + \phi_3 - \phi_1), \quad (3.2)$$

where  $A_1$ ,  $A_2$  and  $A_3$  represent the amplitudes of IM<sub>2</sub> at  $(f_2 - f_1)$ ,  $(f_3 - f_2)$ , and  $(f_3 - f_1)$ , respectively. In this chapter, the signal is designed in such a way that the information is in the form of phases of IM<sub>2</sub> between consecutive tones only, i.e.,  $(f_2 - f_1)$ ,  $(f_3 - f_2)$ ,  $\dots$ ,  $(f_N - f_{N-1})$  tones phases would carry the information. In this way, it is possible to transmit  $(N - 1)$  information symbols over  $N$ -tone multi-carrier signal as shown in Fig. 3.2. The 5-tone multitone PSK RF signal  $x(t)$  results in a baseband signal consisting of various intermodulation frequency components of which four IM<sub>2</sub> frequency components generated by intermodulations between consecutive frequencies are used for phases information detection. However, multitone frequency spacings  $(\Delta f_n)$  and  $\phi_n$  are required to be properly designed to make this multitone PSK signal feasible. Thus, the required constraints related to multitone PSK frequencies and phases are discussed in Sections 3.2.1 and 3.2.2, respectively.

### 3.2.1 Multitone PSK Frequencies

In order to transmit  $(N - 1)$  symbols with only a single transmission of multitone signal,  $f_n$ 's are chosen in such a way that  $(N - 1)$  IM<sub>2</sub>s between consecutive frequencies do not overlap each other and also do not coincide with other non-consecutive IM<sub>2</sub>s. This results in unique  $(N - 1)$  desired baseband frequencies at the output, and the information symbols are decoded by observing phases of these IM<sub>2</sub>. Therefore, multitone  $f_n$ 's can not be uniformly spaced in (3.1), and require an appropriate selection of  $\Delta f_n$ .

The  $n^{\text{th}}$  tone frequency of multitone PSK signal can be represented by

$$f_n = f_{n-1} + \Delta f_{n-1}, \quad n = 2, 3, \dots, N \quad (3.3)$$

where  $\Delta f_{n-1}$  refers to frequency spacing between  $n^{\text{th}}$  and  $(n - 1)^{\text{th}}$  tone.  $\Delta f_{n-1} \neq \Delta f_n \forall n = 2, 3, \dots, N$  to distinguish the desired  $(N - 1)$  IM<sub>2</sub>s generated by consecutive frequencies of multitone PSK signal and must satisfy

$$\Delta f_{n-1} \notin \mathbf{U}_i \times \Delta \mathbf{F}_i, \quad \forall n = 2, 3, \dots, N \text{ and } i = 1, 2, \dots, n - 1 \quad (3.4)$$

condition where  $\mathbf{U}_i$  represents an upper triangular matrix of order  $i \times i$  having non-zero elements as 1

$$\mathbf{U}_i = \begin{bmatrix} 1 & 1 & 1 & \cdots & 1 \\ 0 & 1 & 1 & \cdots & 1 \\ 0 & 0 & 1 & \cdots & 1 \\ \vdots & \vdots & \vdots & \ddots & \vdots \\ 0 & 0 & 0 & \cdots & 1 \end{bmatrix}, \quad (3.5)$$

and  $\Delta \mathbf{F}_i$  is a column vector as

$$\Delta \mathbf{F}_i = \begin{bmatrix} \Delta f_1 \\ \Delta f_2 \\ \vdots \\ \Delta f_i \end{bmatrix}. \quad (3.6)$$

Here, multitone PSK is considered to be centered around center frequency  $f_c$ , and  $\Delta f_1$  is assumed to be the greatest common divisor (GCD) among  $f_n$ s. Appropriate  $f_n$ 's can be determined by Algorithm 1. A BW spreading factor  $r$  is used to have the signal with minimum BW ( $r = 0$ ) and wider BW ( $r > 0$ ) for a particular  $N$ . Hence, overall signal BW not only is a factor of  $N$  but also depends upon the chosen values of GCD and  $r$ . For example, for  $N = 5$ ,  $f_c = 2.45$  GHz, GCD = 1 MHz, and  $r = 0$ ,  $\Delta f_n$ s would be 1 MHz, 2 MHz, 4 MHz, and 5 MHz from Algorithm 1. Therefore, the corresponding multitone PSK signal  $x(t)$  would be having tones at 2.444 GHz, 2.445 GHz, 2.447 GHz, 2.451 GHz, and 2.456 GHz. After passing this multitone PSK signal through the rectifier, baseband signal having various IM frequency components spaced at minimum 1 MHz apart are generated as GCD = 1 MHz. Four IM frequency tones at 1 MHz, 2 MHz, 4 MHz, and 5 MHz are utilized for information detection.

$\Delta f_n$  increases with an increase in GCD or  $r$ , which is helpful from WIT perspective. The reason for this is that it is relatively easier to identify the required wider-spaced baseband tones at the output. However, the rectifier's matched BW and LPF's cut-off frequency ( $f_{\text{cutoff}}$ ) imposes a limit over allowable multitone  $N$ , GCD, and  $r$  for proper WPT.

**Algorithm 1** Multitone PSK Frequencies**Input:**  $f_c, N, \text{GCD}, r$ **Output:**  $\Delta f_n, \text{BW}, f_n$ *Initialisation* :  $k_1 = 1, i = 1, c = 1$ 1:  $\Delta f_1 = k_1 \times \text{GCD}, \Delta f_1 = \text{GCD}$ *LOOP Process*2: **for**  $n = 2$  to  $N - 1$  **do**3:  $K =$  all combinations of  $k_n = U_j \times k_{j-1} \quad \forall \quad j = \{1, 2, \dots, n - 1\}$ 4: **while** ( $i \in K$ ) **do**5:  $i = i + k_1 + r$ 6: **end while**7:  $k_n = i; i = 1; \Delta f_n = k_n \times \text{GCD}$ 8: **end for**9:  $\text{BW} = \sum_{n=1}^{N-1} \Delta f_n$ 10: Symmetrically align frequencies around  $f_c$ 11: **return****3.2.2 Multitone PSK Phases**

From (3.2), it can be observed that the output baseband tones' phases are phase differences between the corresponding multitone frequencies. Therefore, in multitone PSK, symbols are encoded as the phase differences of the consecutive tones. Hence,  $n^{\text{th}}$  tone phase  $\phi_n$  can be represented in terms of transmitted information symbols as

$$\phi_n = \sum_{i=1}^{n-1} \phi_i + s_{n-1}, \quad n = 2, 3, \dots, N \quad (3.7)$$

with the assumption of the first tone phase,  $\phi_1 = 0$ . In (3.7),  $s_{n-1}$  represents the information symbol, transmitted as the difference between  $\phi_n$  and  $\phi_{n-1}$ .

Let  $\Phi_x$  and  $\Phi_y$  be the lower and upper bound of the symbols constellation such that  $\Phi_y - \Phi_x = \delta$ , where  $\delta$  is defined as a considered phase range to allocate the information symbols within this range as shown in Fig. 3.3(a). Thus, the available information symbols set  $\mathcal{S}$  containing  $M$  symbols can be defined as

$$\mathcal{S} = \left\{ \Phi_x + (2m - 1) \frac{\delta}{2M}, \quad \forall \quad m = 1, 2, \dots, M \right\}, \quad (3.8)$$

in terms of  $\delta$  and modulation order  $M$ . Transmitted  $(N - 1)$  information symbols

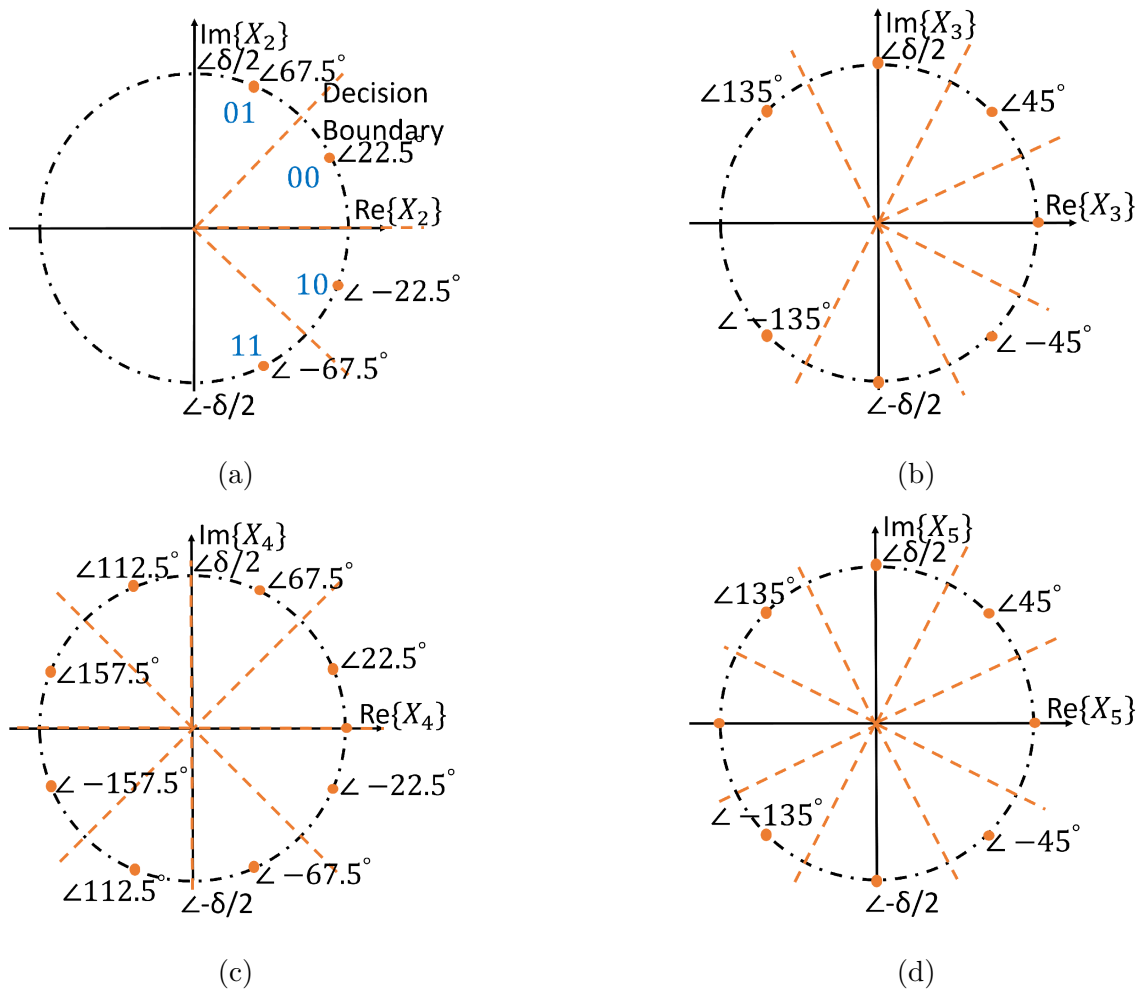


Fig. 3.3. Multitone PSK tone phase constellation for  $n^{\text{th}}$  tone, (a)  $n = 2$ , (b)  $n = 3$ , (c)  $n = 4$ , and (d)  $n = 5$ , for  $M = 4$  and  $\delta = [-90^\circ, 90^\circ]$ .

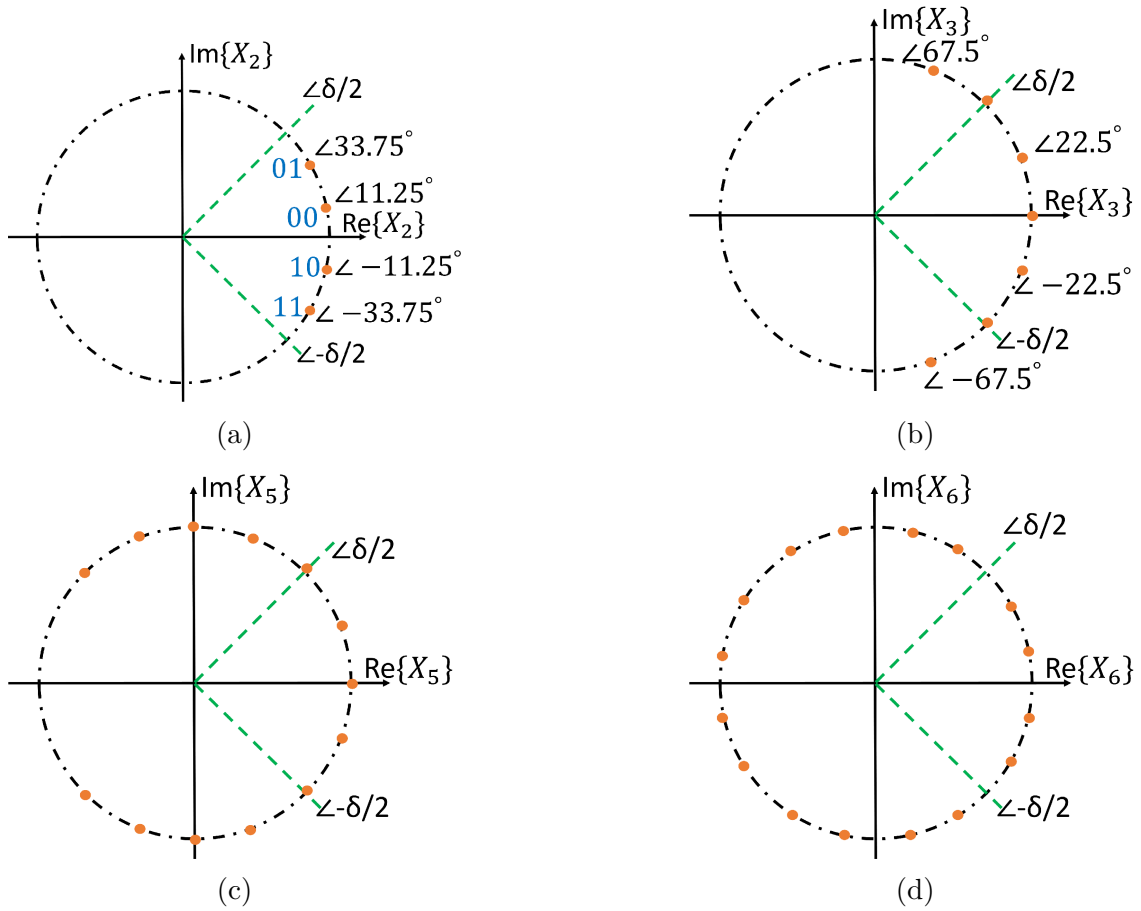


Fig. 3.4. Multitone PSK tone phase constellation for  $n^{th}$  tone, (a)  $n = 2$ , (b)  $n = 3$ , (c)  $n = 5$ , and (d)  $n = 6$ , for  $M = 4$  and  $\delta = [-45^\circ, 45^\circ]$ .

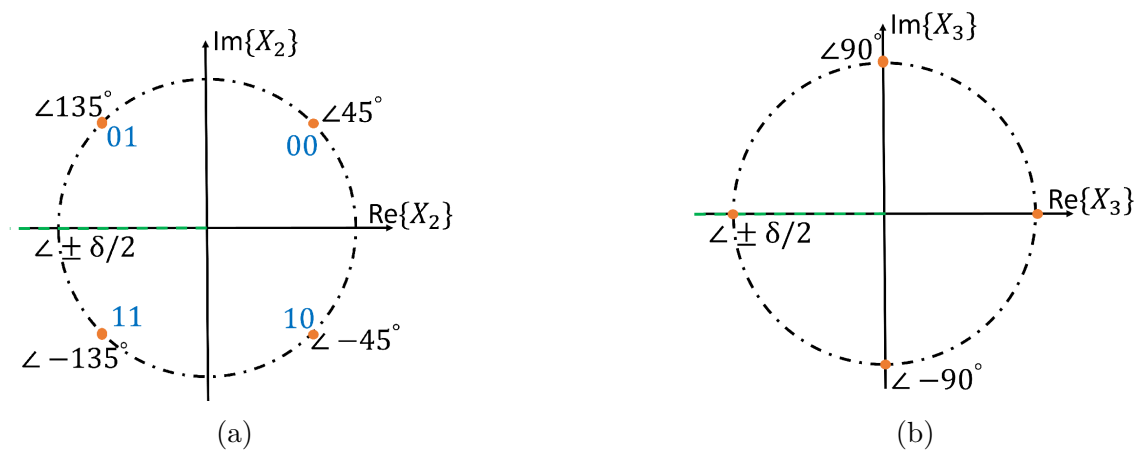


Fig. 3.5. Multitone PSK tone phase constellation for  $n^{th}$  tone, (a)  $n = 2$  and (b)  $n = 3$ , for  $M = 4$  and  $\delta = [-180^\circ, 180^\circ]$ .

over an  $N$ -tone multitone PSK signal would belong to this available information symbols set  $\mathbf{S}$ .

Assuming the symbols to be equidistant and symmetric to  $x$ -axis, i.e.,  $\Phi_x = -\delta/2$ , (3.8) can be rewritten as

$$\mathbf{S} = \left\{ (2m - M - 1) \frac{\delta}{2M}, \quad \forall \quad m = 1, 2, \dots, M \right\}. \quad (3.9)$$

Therefore, for  $\delta = [-90^\circ, 90^\circ]$  and  $M = 4$ , available symbol phases set  $\mathbf{S}$  would be  $67.5^\circ$ ,  $22.5^\circ$ ,  $-22.5^\circ$ , and  $-67.5^\circ$ , as shown in Fig. 3.3(a). Each symbol carries  $\log_2 M$  bits.

Actual possible individual tone phases  $\phi_n$  are different from the chosen transmitted symbol from  $\mathbf{S}$ , as each tone has different choices for its phase as seen in (3.7), varying according to  $\delta$  and  $M$ . As  $\phi_1$  is assumed to be zero, from (3.7),  $f_2$  can have its phase  $\phi_2$  as

$$\phi_2 \in \mathbf{S}, \quad (3.10)$$

and depicted in Fig. 3.3(a) for  $M = 4$  and  $\delta = [-90^\circ, 90^\circ]$ . Further, from (3.7),  $\phi_3$  can be seen as a combination of two symbols as

$$\phi_3 \in \{s_i + s_j, \quad \forall \quad i, j = 1, 2, \dots, M\}, \quad (3.11)$$

where  $s_i$  and  $s_j$  are symbols from  $M$  constellation points defined by (3.9). (3.11) can be rewritten as

$$\phi_3 \in \left\{ (i + j - M - 1) \frac{\delta}{M}, \quad \forall \quad i, j = 1, 2, \dots, M \right\} \quad (3.12)$$

resulting in  $(2M - 1)$  available phases for  $\phi_3$  shown in Fig. 3.3(b), as  $(i + j)$  varies between  $[2, 2M]$ . Generalizing,  $f_n$  has  $((n - 1)M - n - 2)$  phase combinations varying between  $[-(n - 1)(M - 1)\frac{\delta}{2M}, (n - 1)(M - 1)\frac{\delta}{2M}]$ .

However, as seen in Fig. 3.3, these obtained phase combinations are not all dif-

ferent from each other as phases are overall restricted to lie within the interval of  $[-180^\circ, 180^\circ]$ . Therefore, phase combinations of (3.7) start repeating itself after a particular  $n^{\text{th}}$  tone satisfying

$$\left| (n-1)(M-1)\frac{\delta}{2M} \right| \geq 180^\circ, \quad (3.13)$$

and converge to maximum total available tone phases choices of  $(360^\circ/(\delta/M))$ . Fig. 3.3, Fig. 3.4, and Fig. 3.5 illustrate this phase combining behaviour for  $\delta$  as  $[-90^\circ, 90^\circ]$ ,  $[-45^\circ, 45^\circ]$ , and  $[-180^\circ, 180^\circ]$ , respectively for  $M = 4$ . It can be observed that for a particular  $M$ , the smaller the  $\delta$ , the larger is the  $n^{\text{th}}$  tone after which the tones would be able to have phases distributed in the whole  $[-180^\circ, 180^\circ]$  interval. This comparison can be analysed by observing Fig. 3.3(c), Fig. 3.4(d), and Fig. 3.5(b) where phase constellation points start overlapping each other after  $4^{\text{th}}$ ,  $7^{\text{th}}$ , and  $3^{\text{rd}}$  tone for  $\delta$  as  $[-90^\circ, 90^\circ]$ ,  $[-45^\circ, 45^\circ]$ , and  $[-180^\circ, 180^\circ]$ , respectively, for  $M = 4$ .

### 3.3 Multitone PSK Phase distribution and PAPR

In multitone PSK, as the information is being transmitted in the phases, it is important to analyze the effect of these introduced phases on the WIT and WPT performances of the SWIPT system. Although a multitone signal having all its phases aligned performs best for WPT [13], the introduction of phases provides the benefit of transmitting the information to realize a SWIPT operation. Therefore, we need to analyze the extent up to which  $\phi_n$ 's of multitone PSK affect WPT performance. Here, in this section, the effect of phases over the signal PAPR is studied which is one of the figures of merits for WPT performance evaluation [22].

In this chapter, symbol constellations are assumed to be symmetric along the x-axis as discussed in Section 3.2.2. In this way, a multitone signal would have a higher probability of having phases closer to zero which is beneficial for WPT, as described in further discussion.

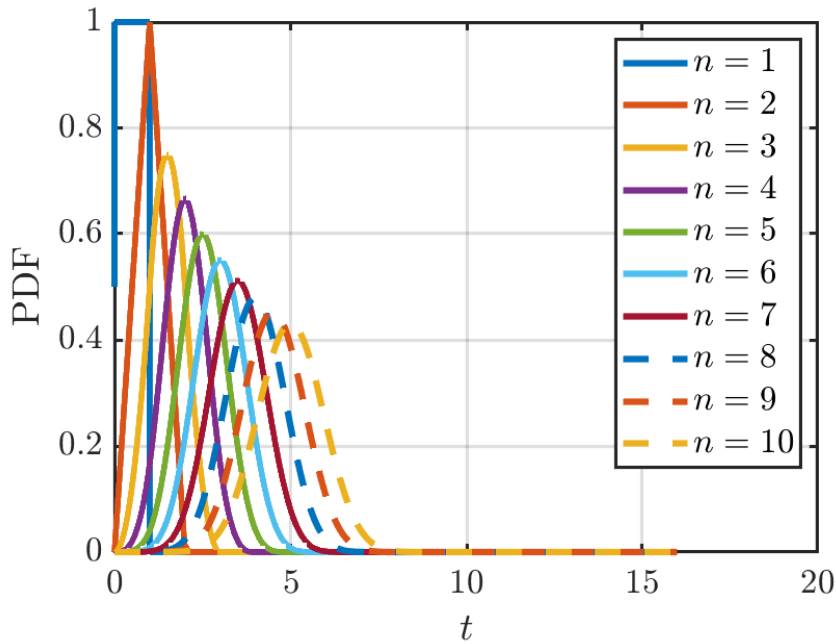


Fig. 3.6. Irwin-Hall Probability density function (PDF) for a random variable  $t$  with increasing  $n$ .

Let  $\mathbf{S}$  defined by (3.9) be uniformly distributed between  $[-\delta/2, \delta/2]$ , i.e., equiprobable symbols with mean 0 and variance  $\delta^2/12$ . From (3.7), phase of an  $n^{\text{th}}$  tone can be seen as the sum of  $(n-1)$  symbol phases. Thus, the probability density function (PDF) of  $\phi_n$  can be evaluated by convolving the  $(n-1)$  uniformly distributed PDFs. Convolution of uniform distribution PDFs can be defined by an Irwin-Hall distribution [121]. The Irwin-Hall distribution is the continuous probability distribution for the sum of  $n$  independent and identically distributed random variables. The PDF for Irwin-Hall distribution for a random variable  $t$  with  $0 \leq t < n$  can be represented by

$$f(t; n) = \frac{1}{(n-1)!} \sum_{i=0}^n (-1)^i \binom{n}{i} (t-i)^{(n-1)} \quad (3.14)$$

Fig. 3.6 represents the convolution of  $n$  uniformly distributed PDFs as a function of a random variable  $t$ . Therefore, the PDF of  $\phi_n$  follows an Irwin-Hall distribution ranging from  $[-(n-1)\delta/2, (n-1)\delta/2]$  with mean 0 and variance  $n \times \delta^2/12$ .

It is well known that the Irwin-Hall distribution closely resembles the Gaussian distribution as  $n$  increases [121]. Fig. 3.7(a) illustrates the comparison between the

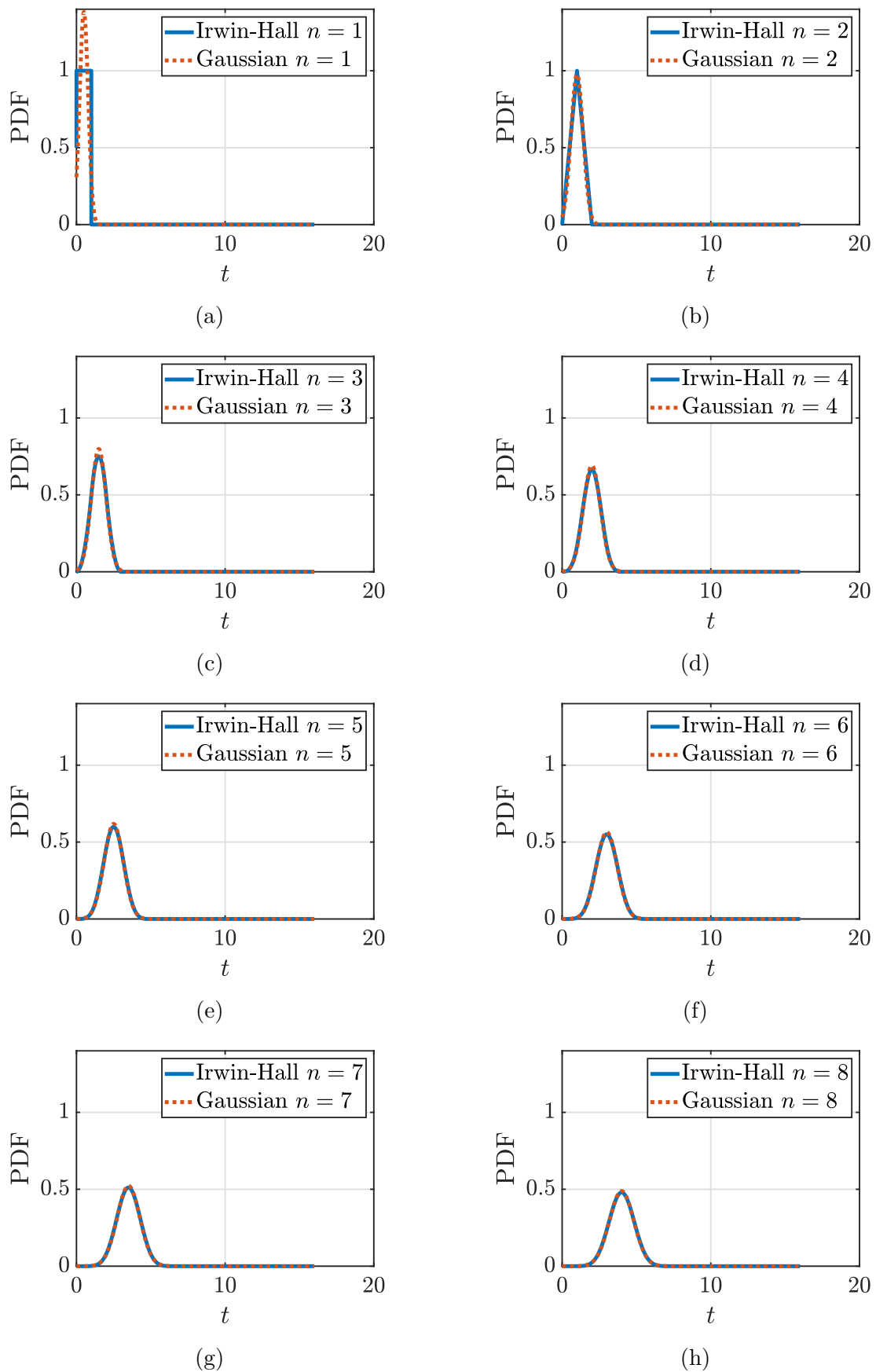


Fig. 3.7. Probability density function (PDF) for Irwin-Hall distribution and Gaussian distribution for a random variable  $t$  with (a)  $n = 1$ , (b)  $n = 2$ , (c)  $n = 3$ , (d)  $n = 4$ , (e)  $n = 5$ , (f)  $n = 6$ , (g)  $n = 7$ , and (h)  $n = 8$ .

Irwin-Hall distribution and Gaussian distribution for  $n = 1$  distribution which are quite distinct from each other. Fig. 3.7(b) compares the Irwin-Hall distribution for  $n = 2$ , i.e., the convolution of two uniform distribution functions and the respective Gaussian distribution. Similarly, Fig. 3.7(h) compares the Irwin-Hall distribution for  $n = 8$ , i.e., the convolution of 8 uniform distribution functions and the corresponding Gaussian distribution which are quite similar to each other. It can be seen that Irwin-Hall distribution approached Gaussian distribution as  $n$  increases. Gaussian distribution implies that there would be a higher probability of occurrence of tones phases closer to zero with the increased number of tones, as seen in Fig. 3.11(b).

However, as discussed in the previous section, the constellation points for a  $\phi_n$  start repeating themselves after a particular  $n$  due to  $[-180^\circ, 180^\circ]$  constraint. Fig. 3.8, Fig. 3.9, and Fig. 3.10 shows the Irwin-Hall PDF for  $\delta = [-45^\circ, 45^\circ]$ ,  $\delta = [-90^\circ, 90^\circ]$ , and  $\delta = [-180^\circ, 180^\circ]$ . As phases can lie within the range of  $[-180^\circ, 180^\circ]$ , these result into Fig. 3.11, Fig. 3.12, and Fig. 3.13. Therefore, all tone phases  $\phi_n$  do not follow Gaussian distribution, and the overall PDF can be found by applying

$$\Pr(x) = \sum_{k=-\infty}^{\infty} \Pr(2\pi k + x), \quad (3.15)$$

over obtained phases, where  $\Pr(x)$  represents the probability at  $x$ .

Fig. 3.11 illustrates the PDF behaviour of  $\phi_2$ ,  $\phi_4$ ,  $\phi_8$ , and  $\phi_{16}$  for  $\delta = [-45^\circ, 45^\circ]$ . It can be seen that PDF for  $\phi_2$  and  $\phi_4$  closely resembles Irwin-Hall distribution, whereas PDF for  $n \geq 7$  starts getting modified as the probability of having phases closer to  $180^\circ$  increases. As  $n$  increases, more and more phases combinations would occur farther from zero phases moving towards uniform distribution PDF as shown in Fig. 3.11(d). The  $n^{\text{th}}$  tone of multitone PSK, after which PDF starts following uniform distribution, depends on the choice of  $\delta$ . From Fig. 3.12, we can see that the PDF of  $\phi_n$  starts moving towards uniform distribution at a faster rate for  $\delta = [-90^\circ, 90^\circ]$  compared to  $\delta = [-45^\circ, 45^\circ]$  (Fig. 3.11(f)), and a uniform distribution is achieved for  $N = 16$ . Further, Fig. 3.13 illustrates PDF for  $\delta = [-180^\circ, 180^\circ]$

where all multitone PSK phases follow uniform PDFs. Therefore, the larger the  $\delta$ , sooner the all  $\phi_n$ 's start following uniform distribution. In uniform distribution, the probability of having a larger phase (closer to  $180^\circ$ ) is equal to the probability of having a  $0^\circ$  phase which would affect the transmitted signal PAPR and the obtained PCE at the output as discussed further.

PAPR for  $x(t)$  can be obtained from

$$\text{PAPR} = \frac{\max\{|x(t)|^2\}}{\frac{1}{T} \int_{-T/2}^{T/2} x^2(t) dt}, \quad (3.16)$$

where  $T$  is time-period of waveform  $x(t)$ . For an  $N$ -tone multitone signal, a maximum PAPR of  $2N$  can be attained by aligning all the phases [78]. However, phases are not aligned for the multitone PSK signal as information is needed to be passed in multitone phases. The PAPR for multitone PSK with varying  $N$  is shown in Fig. 3.14. PAPR for each point, for example PAPR for  $N = 6$ ,  $M = 4$ ,  $\delta = [-90^\circ, 90^\circ]$ , is obtained by analysing 1000 transmitted multitone waveforms  $x(t)$ . Firstly, for each transmitted waveform  $x(t)$ , random binary information data are encoded according to the available symbol set  $\mathbf{S}$  from (3.9). Then,  $x(t)$  tones' phases are modified accordingly from (3.7). The average input power level is set at  $-10$  dBm for all the transmitted waveforms so that only the effect of the tones' phases can be observed. The average of these 1000 obtained PAPR levels is considered to provide a PAPR value for a single case. Three cases of phase range  $\delta$  are considered to analyze the phase distribution effect over the multitone signal PAPR with an increasing number of tones.

It can be seen that multitone PSK input PAPR is lower compared to multitone having all  $\phi_n = 0$ , as expected. Further, as  $N$  is increased for the multitone waveform, the PAPR for a phase range gets saturated to the maximum obtained PAPR. As  $N$  for multitone PSK is increased, uniform distribution starts dominating for most of the  $\phi_n$ , i.e., all phase combinations having equal probability. This means that now, even phases that are closer to  $180^\circ$  have the same probability of occurrence as

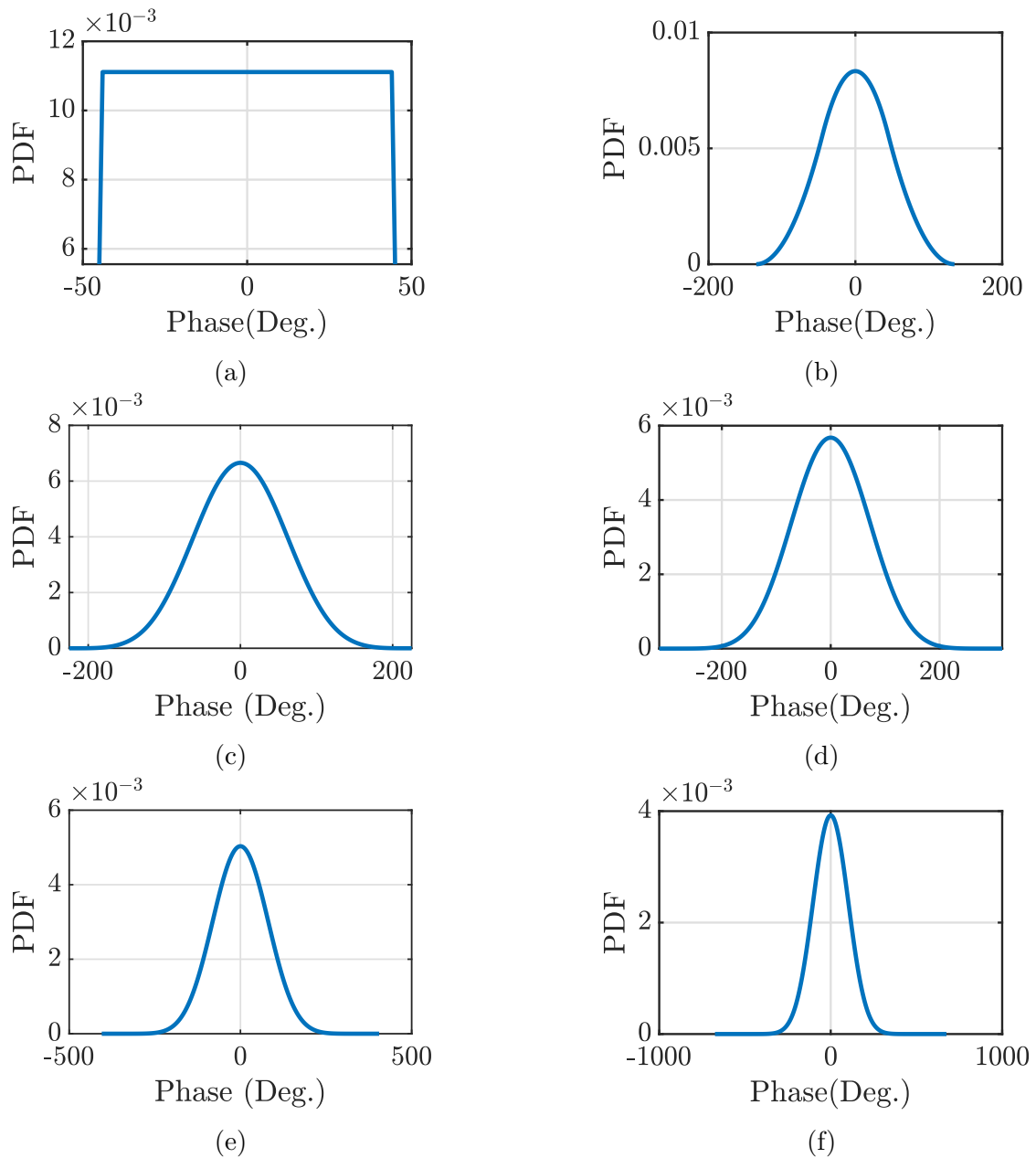


Fig. 3.8. Irwin-Hall Probability density function (PDF) for  $n^{th}$  tone of multitone PSK for (a)  $n = 2$ , (b)  $n = 4$ , (c)  $n = 6$ , (d)  $n = 8$ , (e)  $n = 10$ , and (f)  $n = 16$  for  $\delta = [-45^\circ, 45^\circ]$ .

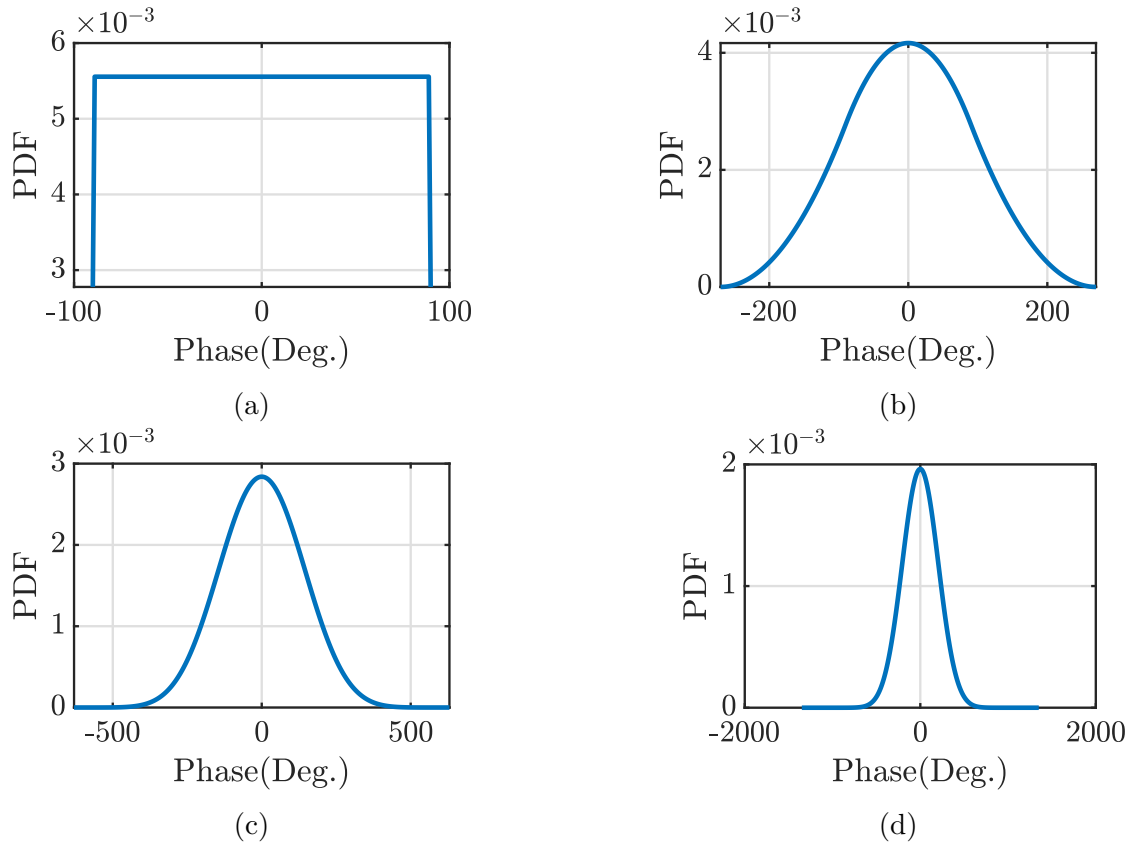


Fig. 3.9. Irwin-Hall Probability density function (PDF) for  $n^{th}$  tone of multitone PSK for (a)  $n = 2$ , (b)  $n = 4$ , (c)  $n = 8$ , and (d)  $n = 16$  for  $\delta = [-90^\circ, 90^\circ]$ .

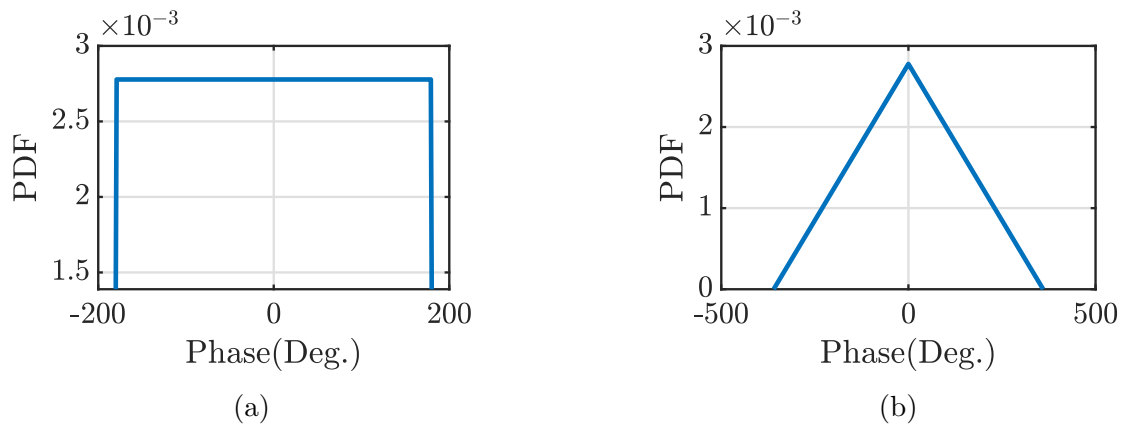


Fig. 3.10. Irwin-Hall Probability density function (PDF) for  $n^{th}$  tone of multitone PSK for (a)  $n = 2$  and (b)  $n = 3$  for  $\delta = [-180^\circ, 180^\circ]$ .

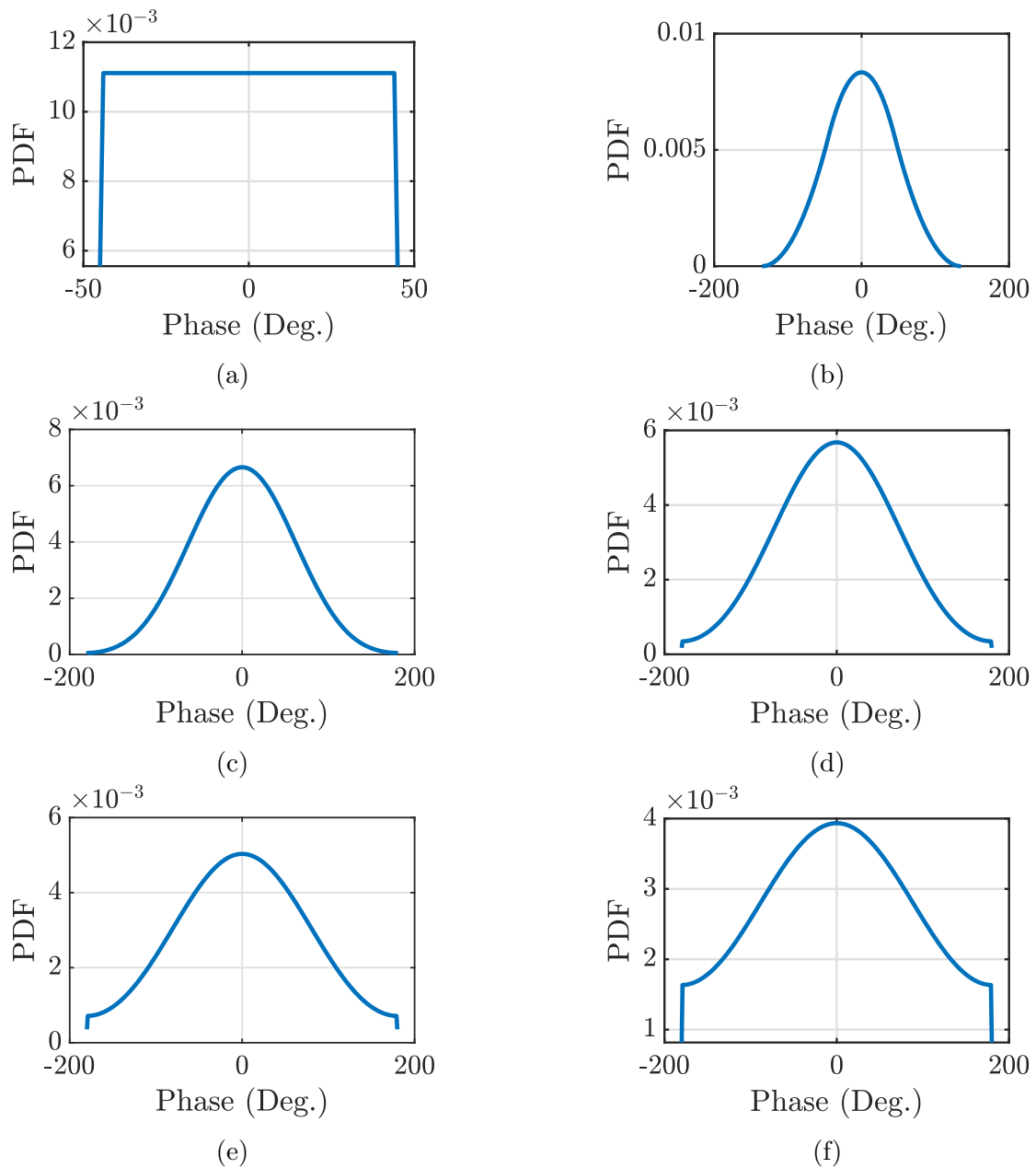


Fig. 3.11. Probability density function (PDF) for  $n^{\text{th}}$  tone of multitone PSK for (a)  $n = 2$ , (b)  $n = 4$ , (c)  $n = 6$ , (d)  $n = 8$ , (e)  $n = 10$ , and (f)  $n = 16$  for  $\delta = [-45^\circ, 45^\circ]$ .

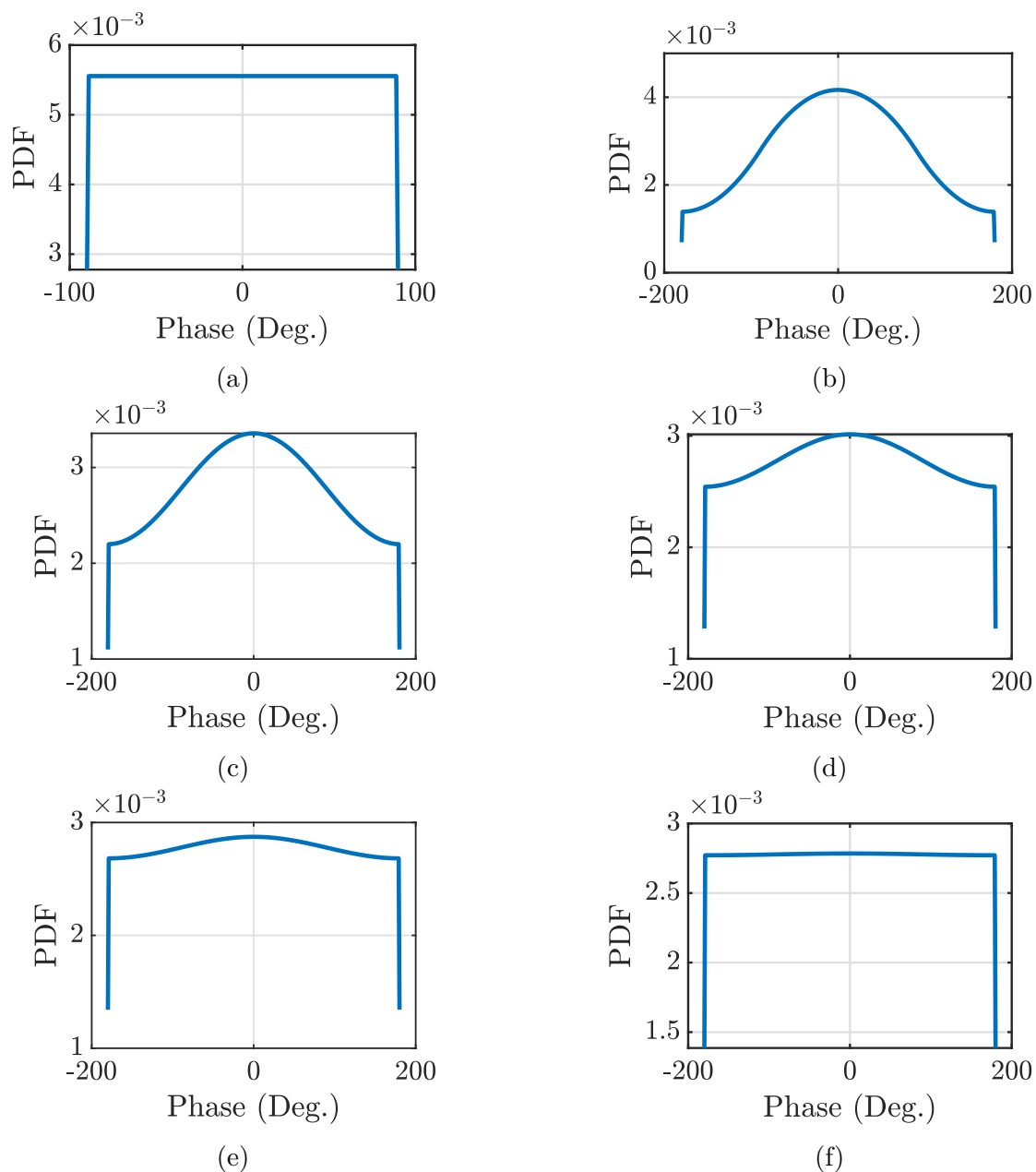


Fig. 3.12. Probability density function (PDF) for  $n^{\text{th}}$  tone of multitone PSK for (a)  $n = 2$ , (b)  $n = 4$ , (c)  $n = 6$ , (d)  $n = 8$ , (e)  $n = 10$ , and (f)  $n = 16$  for  $\delta = [-90^\circ, 90^\circ]$ .

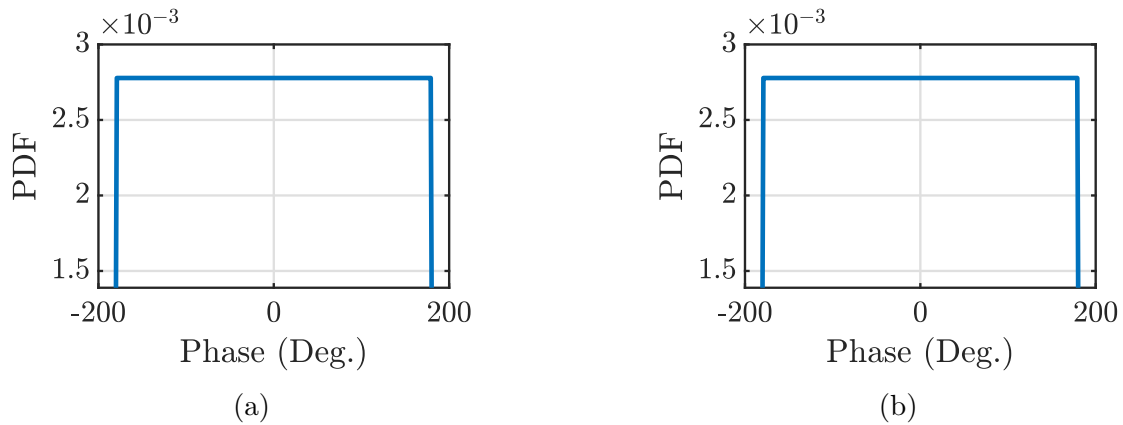


Fig. 3.13. Probability density function (PDF) for  $n^{\text{th}}$  tone of multitone PSK for (a)  $n = 2$  and (b)  $n = 3$  for  $\delta = [-180^\circ, 180^\circ]$ .

phases closer to  $0^\circ$ . Therefore, the overall PAPR reduces and saturates to a maximum upper value for a particular  $M$  and  $\delta$ . It can also be seen that multitone PSK PAPR saturates earlier for larger  $\delta$ , i.e.,  $\delta = [-180^\circ, 180^\circ]$ , resulting in the lowest PAPR, because  $\phi_n$  starts following uniform distribution for all  $n \geq 2$  for the case of maximum  $\delta = [-180^\circ, 180^\circ]$ .

Multitone signals are already being used for WPT transfer for quite some time. However, high PAPR signals deteriorate the overall end-to-end practical system performance as these signals may drive the transmitter amplifier into saturation. However, the PAPR of the transmitted multitone PSK signal is not increasing linearly with  $N$ . Therefore, the transmission of information in terms of tones' phases offers an additional advantage of improving the overall SWIPT system performance.

### 3.4 Receiver Model

The simple rectifier model consisting of a matching network and diode circuitry followed by an LPF is designed. Further, the rectifier is fabricated and all multitone PSK simulation results are verified by the measurement results.

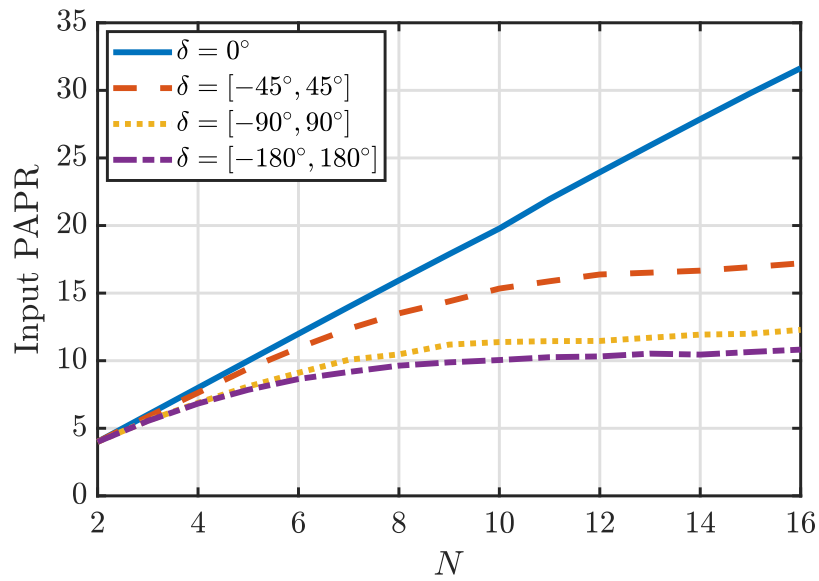


Fig. 3.14. Multitone PSK PAPR with varying  $N$  for  $M = 4$ , GCD = 1 MHz and 1000 multitone streams for each  $N$  and  $\delta$ .

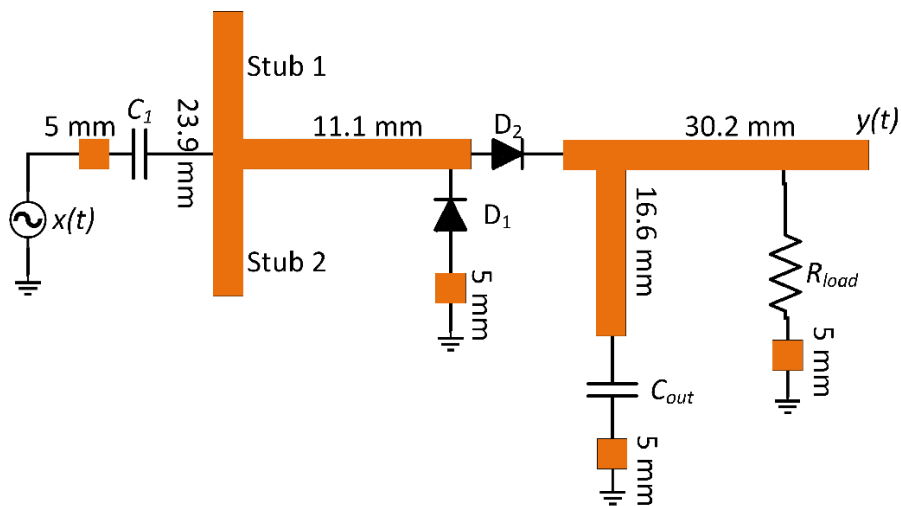


Fig. 3.15. Rectifier simulation model for SWIPT for a matched BW of 100 MHz with  $C_1 = 1$  pF, two Schottky diodes (Skyworks SMS7630-079LF), and a LPF ( $C_{out} = 0.1$  pF and  $R_{load} = 4.4$  k $\Omega$ ).

### 3.4.1 Rectifier Design

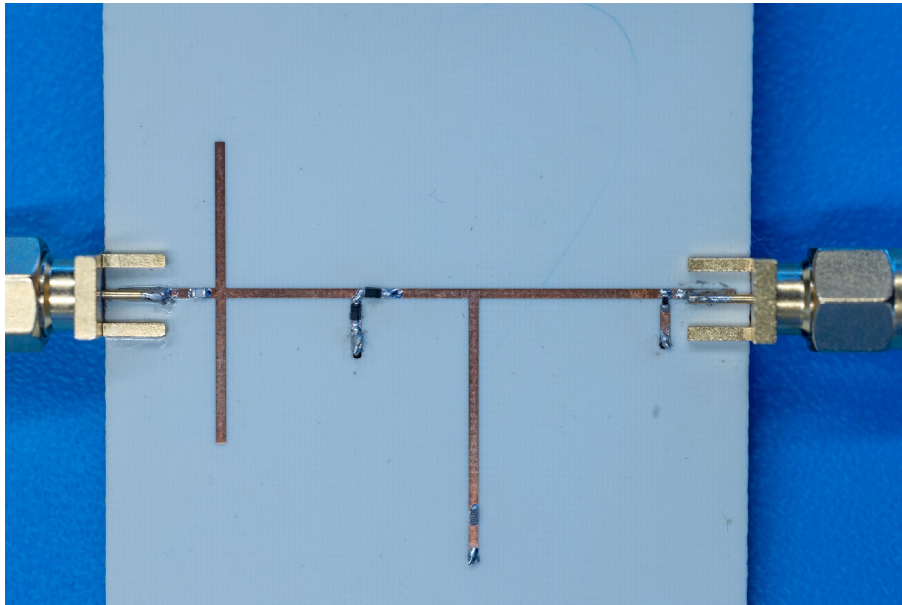
A rectifier model depicted in Fig. 3.15 is designed solely to demonstrate the feasibility of the proposed multitone PSK for SWIPT operation and the topology is inspired from [122]. The topology consists of an input matching network with  $C_1 = 1$  pF, two Schottky diodes (Skyworks SMS7630-079LF), and a LPF ( $C_{\text{out}} = 0.1$  pF and  $R_{\text{load}} = 4.4$  k $\Omega$ ). The rectifier has been designed to maximize the PCE for comparatively larger matched BW of around 100 MHz centered on 2.45 GHz in terms of reflection coefficient ( $S_{11}$ ) by the use of  $C_1$ , stub lengths, transmission lines lengths, and,  $R_{\text{load}}$ . This is required to make multitone PSK possible with larger  $N$  to increase the throughput, i.e., for the WIT performance of the SWIPT system. In short, the rectifier model has been designed keeping in mind WPT as well as WIT.

In the rectifier design, the LPF cut-off frequency is selected in such a way that all the harmonics are filtered out by the LPF, while simultaneously it should have sufficient BW to pass the relevant IM<sub>2</sub> baseband information tones. Therefore, the rectifier is designed to have a larger LPF BW than the highest relevant IM<sub>2</sub> frequency component, but smaller than the RF fundamental tones. For all the simulation and measurement results, GCD and  $N$  for the multitone PSK signal are selected in such a way that the resulting signal would have a BW smaller than the RF BW.

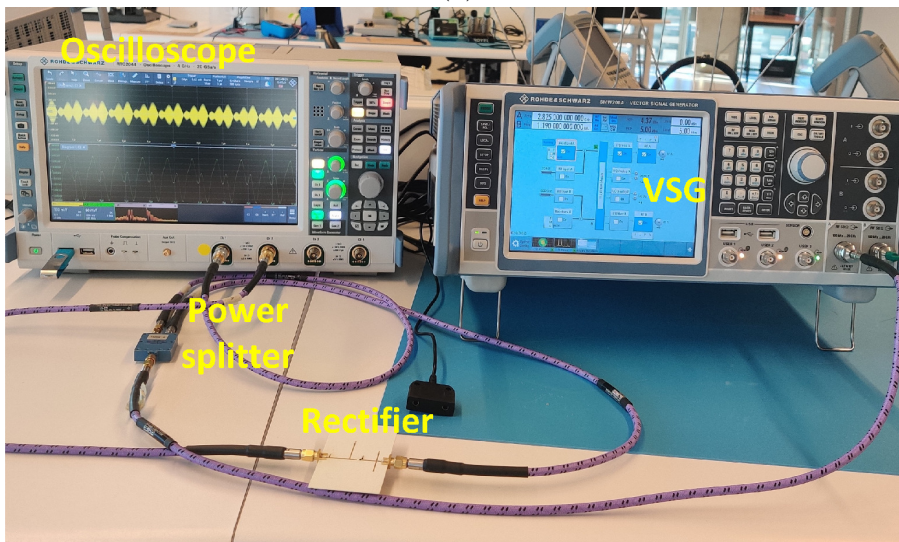
The WIT and WPT performances of the multitone PSK signals have been measured in terms of achievable PCE and BER, respectively, in order to analyze the overall SWIPT performance. The PCE at the output can be defined as

$$\text{PCE} = \frac{|y_{\text{dc}}|^2/R_{\text{load}}}{P_{\text{in}}} \times 100, \quad (3.17)$$

in terms of the transmitted average power  $P_{\text{in}}$  of  $x(t)$  and dc voltage  $y_{\text{dc}}$  of the received signal  $y(t)$ . The PCE at the rectifier output varies according to the multitone PSK signal PAPR.



(a)



(b)

Fig. 3.16. (a) Fabricated integrated receiver rectifier and (b) Measurement setup with VSG R&S SMW200A, power splitter, rectifier, and oscilloscope R&S RTO2044.

### 3.4.2 Measurement Setup

The designed rectifier is fabricated on RO4350B substrate having dielectric constant as 3.66, loss tangent as 0.0031, and thickness of 0.762 mm and is shown in Fig. 3.16(a). The measurements are performed using the setup shown in Fig. 3.16(b). The transmitter and receiver are connected through the cabled connections. The modulated multitone PSK signals are generated using a vector signal generator (VSG) (R&S SMW200A). Further, the signal is divided into two streams using a power splitter. One stream is directly fed to the Oscilloscope (R&S RTO2044 Channel 1), which is considered as the transmitted multitone signal reference from VSG as the multitone PSK signal power has been reduced after passing through the power splitter. The other stream is passed through the rectifier and fed to the Oscilloscope Channel 2. Calibration for different cable lengths is performed before comparing the transmitted and the received signal from the oscilloscope for power and information analysis. As the information is in the phases of spectral components, a spectrum analyzer does not meet the requirement for information decoding. Therefore, an oscilloscope is used for the measurements. For the received signal, the input impedance of the oscilloscope has been set at a 1 M $\Omega$  value to minimize its effect over the rectifier's output impedance. This is performed to keep the measured performance similar to the simulated performance.

The Multitone PSK signals  $x(t)$  with varying parameters  $P_{in}$ ,  $M$ ,  $N$ ,  $\delta$ , and GCD are generated, and the demodulated signals  $y(t)$  are analyzed for the SWIPT performance in terms of attained PCE and BER. The effect of  $\delta$  over the transmitted signal PAPR as discussed in Section 3.3 is verified by the measured PAPR over the Oscilloscope Channel 1 output and illustrated in Fig. 3.17. The Multitone PSK signal streams are generated for each  $N$  for each different allocated symbol phase range, similar to the simulation analysis in Section 3.3. It can be seen that the narrower the transmitted symbols' phase range, the better would be the WPT performance of the designed scheme as observed in simulated results in Fig. 3.14. It can be seen that the curves in Fig. 3.17 are not smooth as are in Fig. 3.14. The

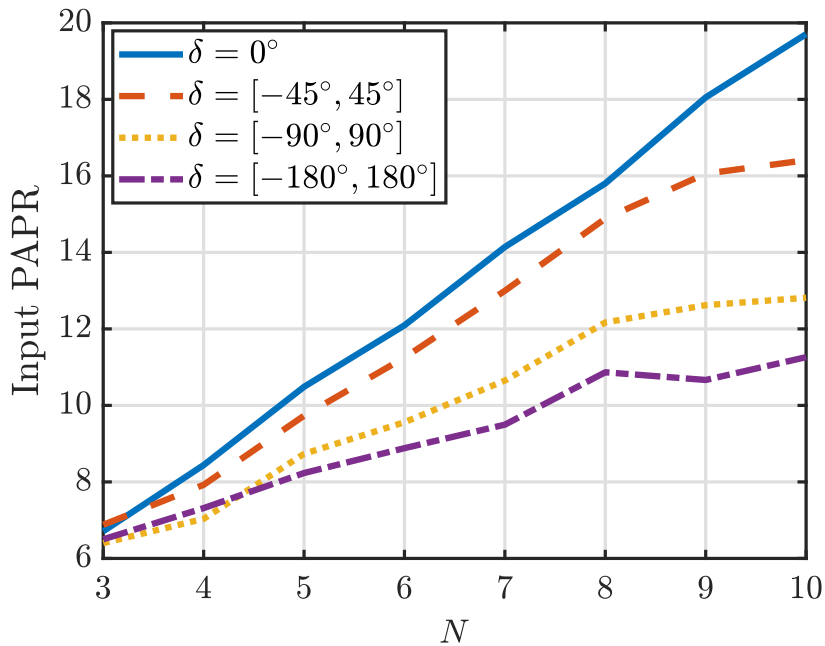
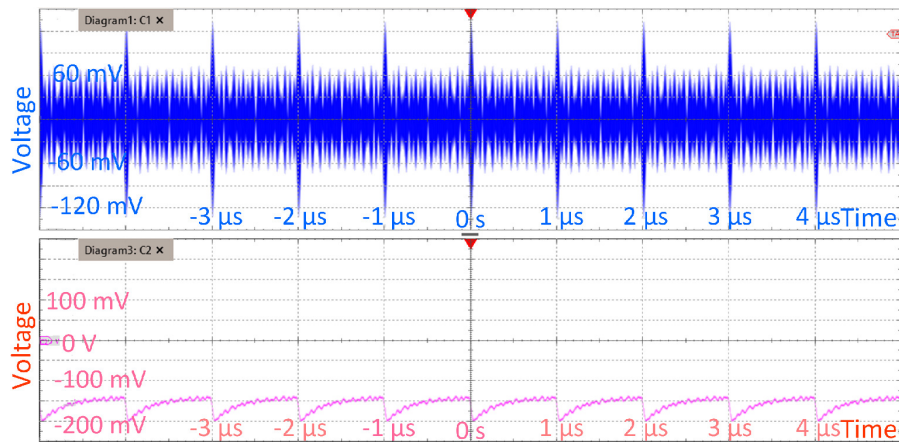


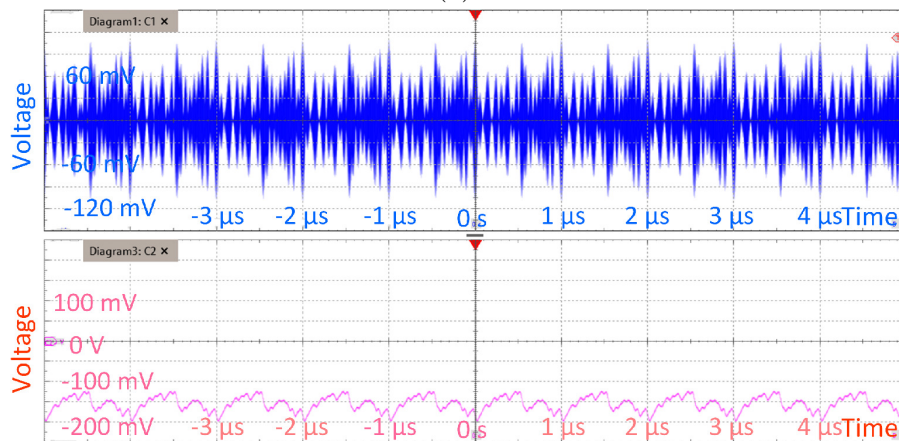
Fig. 3.17. Measured multitone PSK PAPR with varying  $N$  for  $M = 4$ , GCD = 1 MHz, and 50 multitone streams for each  $N$  and  $\delta$ .

reason for this is that measured PAPR is evaluated for 50 multitone streams whereas simulated PAPR is evaluated for 1000 multitone streams. Due to the time taken in transmission of multiple information-encoded waveforms, fewer waveforms are considered for measurements. However, measured PAPR would be similar to Fig. 3.14 when evaluated for a large number of multitone streams.

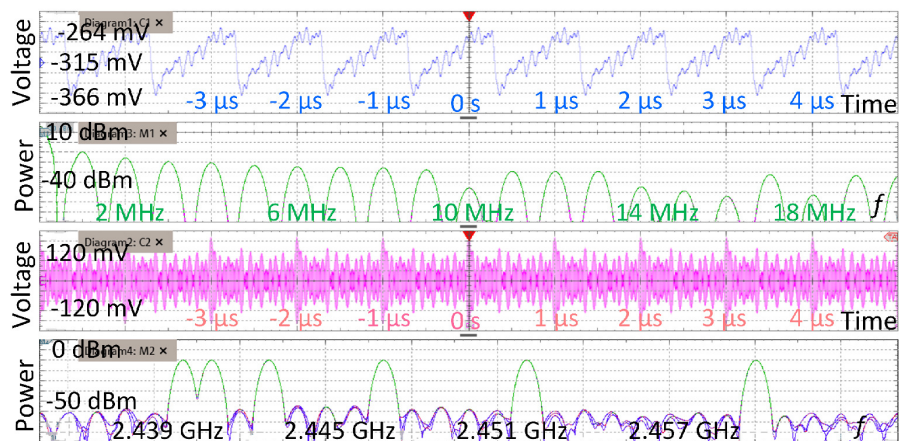
Here, over-the-air measurements with a receiving antenna are not considered. Indeed, the received input power decreases with the transmission distance, which would affect the end-to-end power efficiency. To evaluate the over-the-air performance of the proposed scheme with distance, the effect of the channel would be required to be modeled and investigated. Accordingly, appropriate coding schemes would be utilized for performance enhancement. The focus of this thesis has been to show the feasibility of the proposed transmission scheme and over-the-air measurements are considered as a part of future work.



(a)



(b)



(c)

Fig. 3.18. Oscilloscope measured transmitted  $x(t)$  and received  $y(t)$  waveforms with (a) all phases aligned (b) with information symbol transmission, and (c) frequency spectra.

### 3.5 Performance Analysis of Multitone PSK

To analyze the SWIPT performance of the multitone PSK, PCE, and BER are used as figures of merit for WPT and WIT performances, respectively. Multitone stream frequencies and phases are designed as discussed in Section 3.2.1 and Section 3.2.2. For example, for  $N = 6$ ,  $\text{GCD} = 1$  MHz, frequency spacings between consecutive tones are obtained as 1 MHz, 2 MHz, 4 MHz, 5 MHz, and 8 MHz from Algorithm 1.  $x(t)$  would result into multitones having tones at 2.44 GHz, 2.441 GHz, 2.443 GHz, 2.447 GHz, 2.452 GHz, and 2.46 GHz. The time-domain transmitted waveform  $x(t)$  and the corresponding received waveform  $y(t)$  measured by the oscilloscope for the case of all tones' phases aligned and  $P_{\text{in}} = -16$  dBm, are illustrated in Fig. 3.18(a).

The phases of these tones would get modified according to the transmitted bit patterns in each multitone stream. For example, for  $M = 4$  and  $\delta = [-180^\circ, 180^\circ]$  in the above case with a transmitted bit stream of 1 0 0 1 0 1 0 1 0 0, the 6 tones phases would be  $0^\circ$ ,  $-45^\circ$ ,  $90^\circ$ ,  $-135^\circ$ ,  $0^\circ$ , and  $45^\circ$  by utilizing Fig. 3.5(a), (3.7), and (3.9). The symbols are encoded using the gray coding scheme to minimize the BER [121] as shown in Fig. 3.5(a). The corresponding transmitted waveform  $x(t)$  and received waveform  $y(t)$  measured by the oscilloscope are shown in Fig. 3.18(b). Another example of measured  $x(t)$  and  $y(t)$  with their respective frequency spectrum  $X(f)$  and  $Y(f)$  with random bit stream pattern, is illustrated in Fig. 3.18(c).

PCE and BER are analyzed by obtaining the rectifier output time-domain waveform  $y(t)$ . Fig. 3.19 shows the obtained simulated PCE for a multitone PSK with  $N = 6$ ,  $M = 4$ ,  $\text{GCD} = 1$  MHz,  $r = 0$  for 100 transmitted multitone streams, i.e., 1000 bits. From Algorithm 1, BW of such signal is 20 MHz which is under the designed rectifier BW range. Hundreds of multitone streams for each scenario are transmitted where each time their phases are encoded according to a random information bit pattern. It can be seen that the PCE is maximum for the aligned phases and decreases with increased  $\delta$ , as observed in the case of PAPR as well. Maximum attained PCE at  $P_{\text{in}} = 0$  dBm, falls by around 3% when  $\delta$  is increased from  $0^\circ$  to  $[-180^\circ, 180^\circ]$ ,

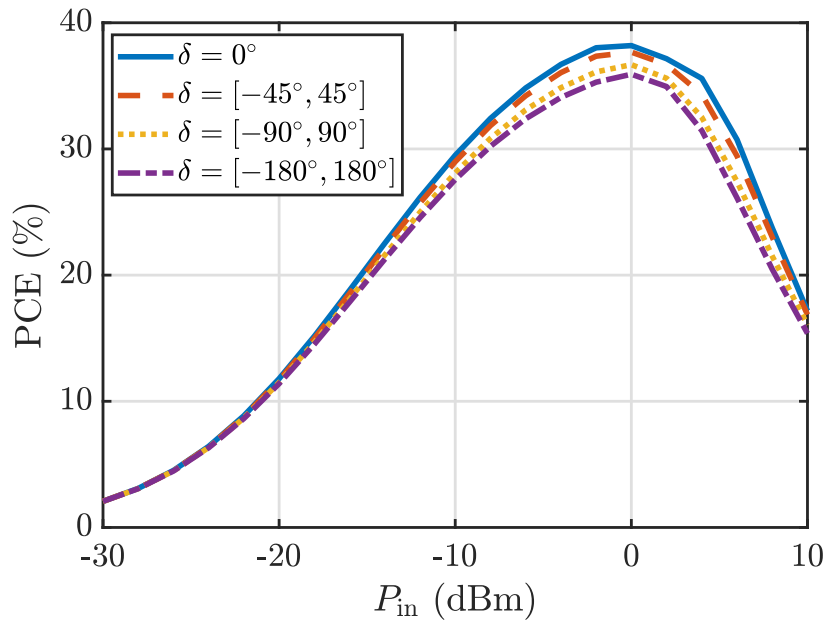


Fig. 3.19. Simulated PCE for multitone PSK centred around 2.45 GHz with  $N = 5$ , GCD = 1 MHz, and  $M = 4$  for 100 multitone streams, i.e., 1000 bits.

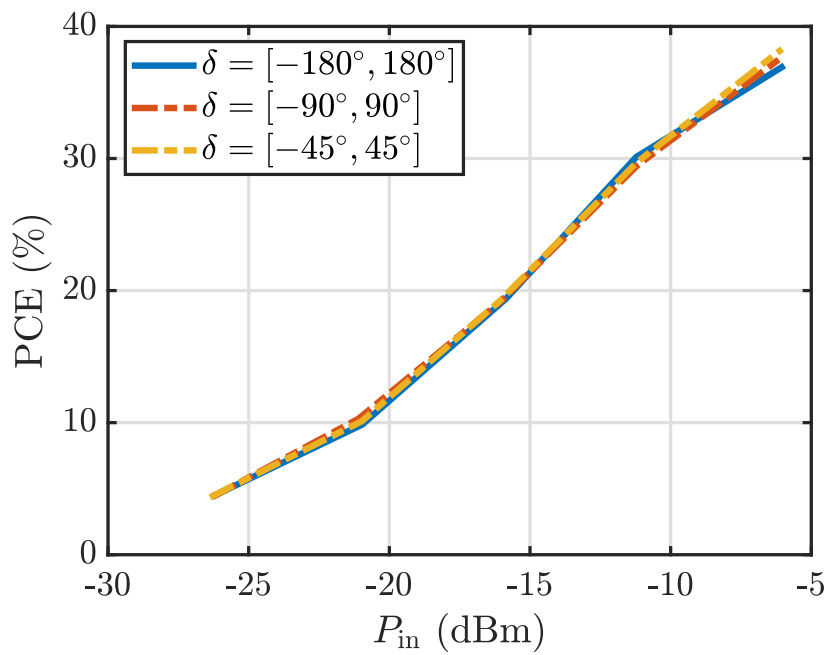


Fig. 3.20. Measured PCE for multitone PSK with  $N = 6$ , GCD = 1 MHz, and  $M = 4$  for 100 multitone streams, i.e., 1000 bits.

implying that simultaneous transmission of information in terms of multitone phases with the help of multitone PSK costs only around 3% of WPT performance when a WPT multitone signal is replaced by a multitone PSK signal for SWIPT transfer.

Here, the peak PCE of the rectifier has been reduced somewhat to have a larger low-pass filter BW to simultaneously receive the DC signal for WPT as well as the baseband signal which contains the information, compared to conventional rectifiers that are utilized solely for WPT path (for separated information and energy receiver architecture). It is possible to design a rectifier to have 60% PCE but with only 0.5 MHz LPF BW [122]. On the other hand, a larger LPF BW is required to accommodate baseband tones carrying the information. Therefore, enabling the transmission of information is at the cost of some reduction in power conversion efficiency. Overall, it is well known that a trade-off exists between WPT performance and WIT performance in the case of an integrated information and energy receiver architecture [12]. However, the overall system efficiency is increased as we are able to receive power while decoding information using the same rectifier, hence removing the need for additional downconversion electronics at the receiver. It is undoubtedly a low-cost solution, compared to others considered, without affecting the correct demodulation of the data.

The simulated results are further verified through measurements over the designed rectifier from Oscilloscope Channel 2 (measured  $y(t)$ ). Measurements are performed till the highest average power of  $-6$  dBm. The reason for this is to keep the working of diode safe and accurate as with higher average power signals, diode may go into breakdown region. Fig. 3.20 illustrates PCE for  $N = 6$ ,  $M = 4$ , GCD = 1 MHz,  $r = 0$ , and BW = 20 MHz for 100 transmitted multitone streams, i.e., 1000 bits stream over an input power range of around  $-27$  dBm to  $-6$  dBm. For the case of  $-6$  dBm transmitted power, it is possible to receive  $-10$  dBm power which results in PCE of 38%. Less variation in PCE in accordance with  $\delta$  is an advantage of the proposed multitone PSK scheme. In the earlier amplitude-based modulation schemes, information transfer through amplitudes results in varying ripple voltage

at the output with varying symbol patterns. As the information is in phases for multitone PSK, only the tones' phases change for different transmitted bit stream patterns, while keeping their amplitudes constant. Therefore, the output voltage does not change much with the information transfer which is a beneficial point from the WPT perspective making power transfer performance less dependent upon information transfer for SWIPT systems.

To analyze the BER of multitone PSK, the time-domain output waveform  $y(t)$  of the rectifier is further processed in MATLAB in the frequency-domain, to extract the phase information from the relevant baseband tones. For BER calculation of one scenario, hundreds of such multitone streams are transmitted where each time their phases are encoded according to a random information bit pattern as discussed above. From the rectified waveforms, phases of relevant baseband tones are obtained. For example, in the above-mentioned case, phases of baseband tones present at 1 MHz, 2 MHz, 4 MHz, 5 MHz, and 8 MHz in the rectified  $y(t)$  are extracted. Further, these extracted phases are decoded into a bit pattern according to an assigned phase margin for the symbols as

$$\text{Phase margin} = \pm \frac{\delta}{2M}. \quad (3.18)$$

Then, the obtained bit patterns for hundreds of waveforms are compared with the transmitted bit patterns for BER calculation.

Simulated BER for multitone PSK signal transmission of 1000 bits with  $N = 6$ ,  $M = 4$ , GCD = 1 MHz,  $r = 0$  is shown in Fig. 3.21. As the same baseband signal which is obtained from AC-DC conversion circuitry, is being used for information as well as power, the rectifier's non-linearity introduces phase distortion in information detection.

It can be seen that the BER is lowest for  $\delta = [-180^\circ, 180^\circ]$  and it is possible to have 0 BER using multitone PSK for power levels lower than  $-15$  dBm. BER increases with the decrease in  $\delta$ , and it is the highest for  $\delta = [-45^\circ, 45^\circ]$  as allowable

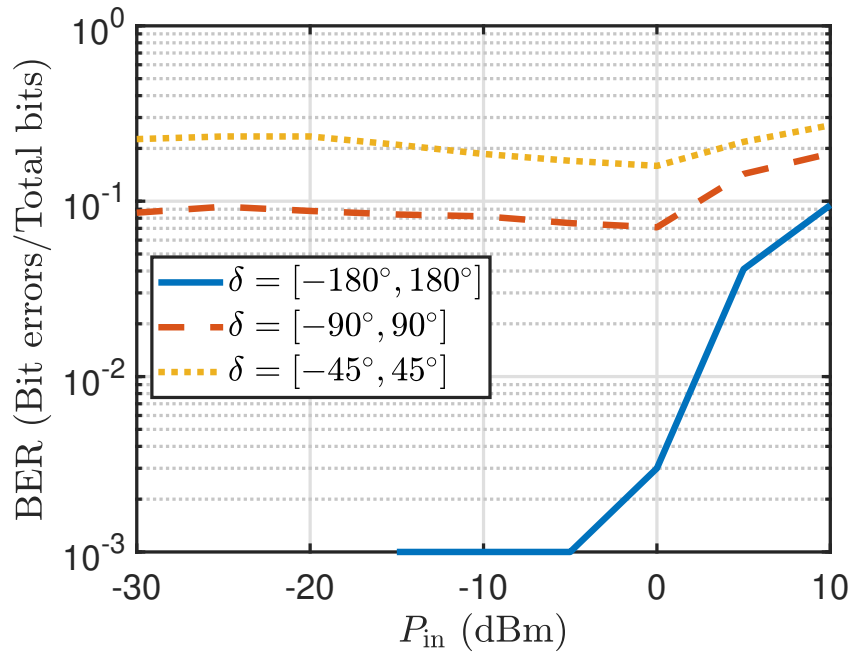


Fig. 3.21. Simulated BER using multitone PSK with  $N = 6$ ,  $M = 4$ , GCD = 1 MHz,  $r = 0$ , and for 100 multitone streams, i.e., 1000 bits.

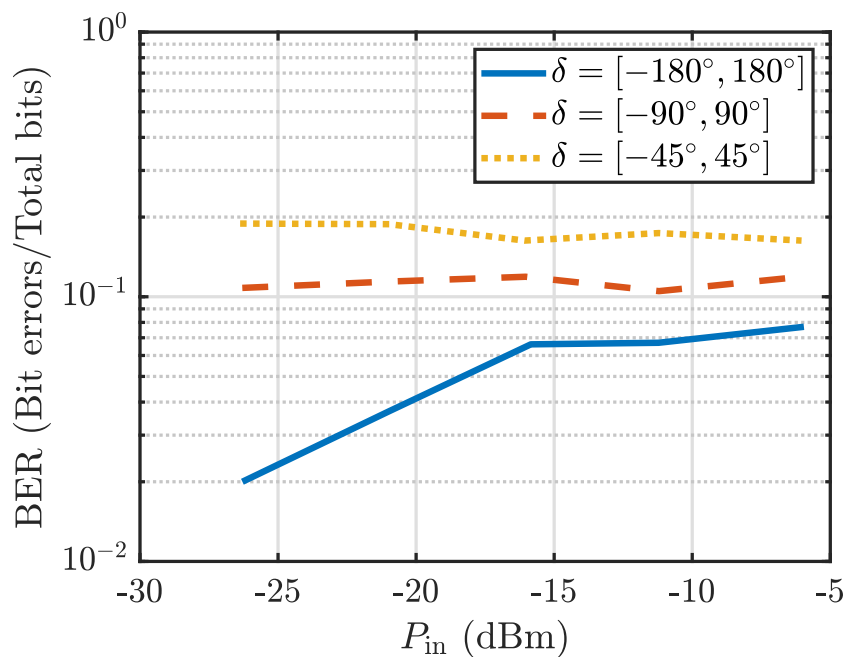


Fig. 3.22. Measured BER using multitone PSK with  $N = 6$ ,  $M = 4$ , GCD = 1 MHz,  $r = 0$ , and for 100 multitone streams, i.e., 1000 bits.

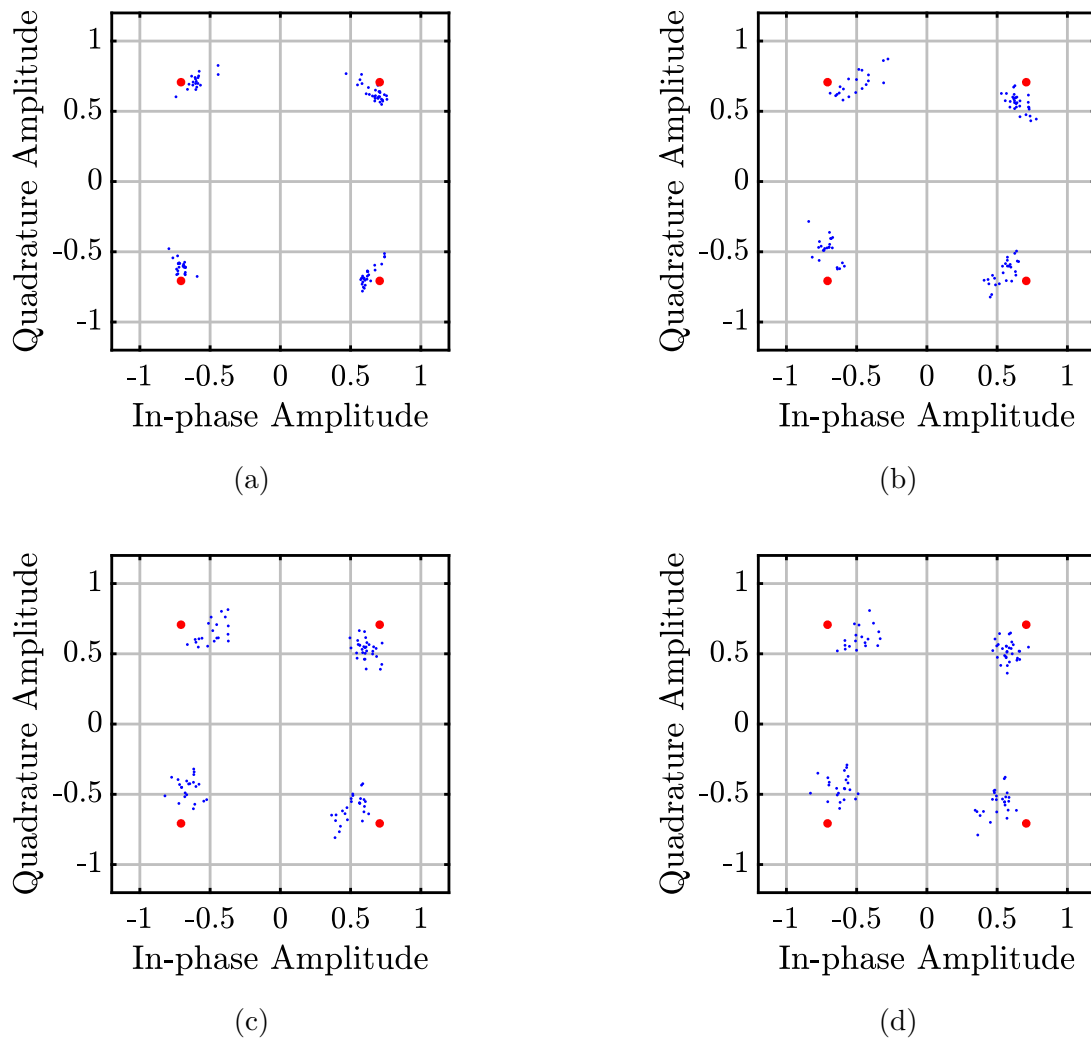


Fig. 3.23. Symbols constellations at baseband tone of 1 MHz for  $N = 6$ ,  $M = 4$ ,  $\delta = [-180^\circ, 180^\circ]$ , received input power (a)  $P_{\text{in}} = -21$  dBm, (b)  $P_{\text{in}} = -16$  dBm, (c)  $P_{\text{in}} = -11$  dBm, and (d)  $P_{\text{in}} = -6$  dBm for 100 multitone streams, i.e., 500 symbols.

phase margin for correct symbol detection reduces to a narrower  $\pm 11.25^\circ$  with the decreasing  $\delta = [-45^\circ, 45^\circ]$  compared to a phase margin of  $\pm 45^\circ$  for  $\delta = [-180^\circ, 180^\circ]$ . Furthermore, BER increases with increasing input power above a certain power level due to the presence of nonlinearities (diodes) in the circuit, causing AM-PM distortion and thus negatively impacting the BER [51].

The simulated results are verified by the performed measurements shown in Fig 3.22. The increase in the BER with the decreasing  $\delta$  is clearly visible in the measured results. However, the measured BER is slightly higher than the simulated results.

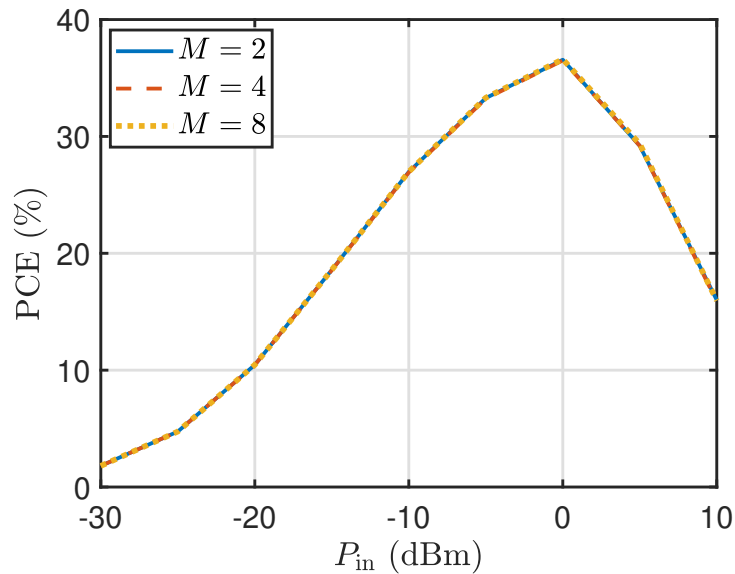


Fig. 3.24. Simulated PCE using multitone PSK with  $N = 3$ , GCD = 1 MHz,  $\delta = [-180^\circ, 180^\circ]$ ,  $r = 0$ , and 100 multitone streams for different  $M$ .

Harmonics can reflect back to the diode, and this can influence the BER. The impact of these reflected harmonics and the inter-frequency interference that may lie on desired information symbols increases with increasing input power. Therefore, the BER increases with increasing input power. Measured symbol constellations for  $N = 6$ ,  $M = 4$ ,  $\delta = [-180^\circ, 180^\circ]$ , and 1 MHz baseband tone, for different received input power levels (a)  $P_{in} = -21$  dBm, (b)  $P_{in} = -16$  dBm, (c)  $P_{in} = -11$  dBm, and (d)  $P_{in} = -6$  dBm are illustrated in Fig. 3.23 for 100 multitone streams, i.e., 500 symbols. The ideal normalized symbol constellation is depicted in orange, and the normalized measured symbol constellations are illustrated in blue. It can be observed that phase distortion increases as input power increases. However, a low power range (below 0 dBm) is of main interest for SWIPT applications, and the effect of these factors on BER is limited at low power levels. Compensation techniques such as pre-compensation at the transmitter or post-compensation at the receiver can be introduced to reduce the AM-PM distortion.

Further, the effect of various  $M$  over the PCE and BER performances is analyzed. Fig. 3.24 shows PCE for  $N = 3$ , GCD = 1 MHz,  $r = 0$ ,  $\delta = [-180^\circ, 180^\circ]$ , and 100 multitone streams for  $M = 2$ , 4, and 8. It is observed that the PCE does not change

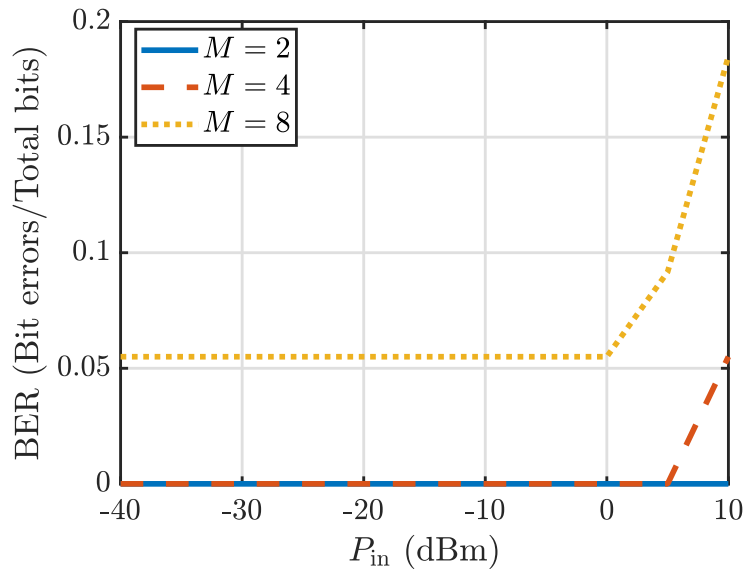


Fig. 3.25. Simulated BER using multitone PSK with  $N = 3$ ,  $\text{GCD} = 1$  MHz,  $\delta = [-180^\circ, 180^\circ]$ ,  $r = 0$ , and 100 multitone streams for different  $M$ .

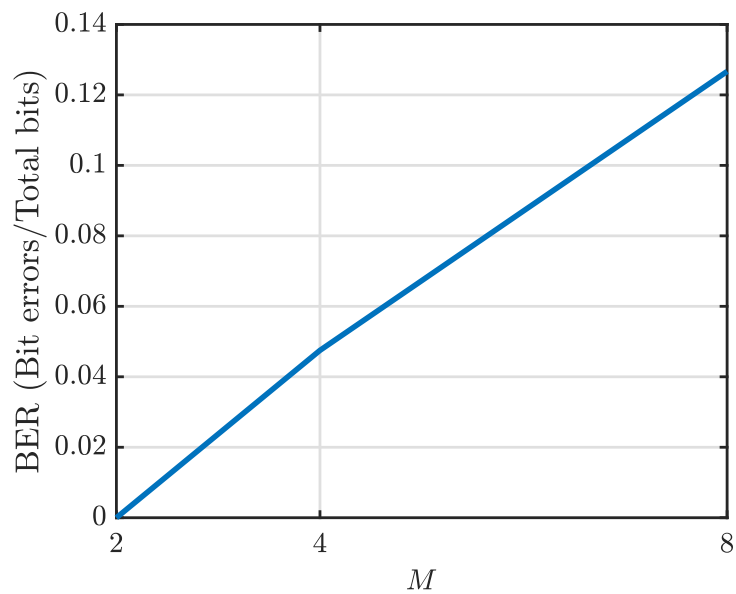


Fig. 3.26. Measured BER using multitone PSK with  $N = 3$ ,  $\text{GCD} = 1$  MHz,  $\delta = [-180^\circ, 180^\circ]$ ,  $P_{in} = -6$  dBm,  $r = 0$ , and 100 multitone streams for  $M = 2$ ,  $M = 4$ , and  $M = 8$ .

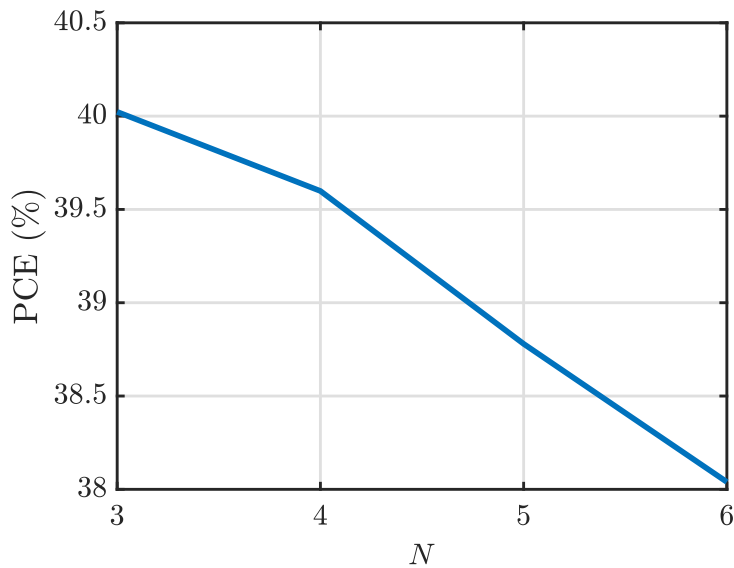


Fig. 3.27. Measured PCE using multitone PSK with  $M = 4$ ,  $\text{GCD} = 1$  MHz,  $\delta = [-180^\circ, 180^\circ]$ ,  $P_{\text{in}} = -6$  dBm,  $r = 0$ , and 100 multitone streams for  $N = 3$ ,  $N = 4$ ,  $N = 5$ , and  $N = 6$ .

significantly with the increased modulation order  $M$  for  $N = 3$ . As  $M$  increases from  $M = 2$  to  $M = 8$ , PCE increases only slightly. The reason is that now, the same symbol phase range is divided among a larger number of available symbols for the case of  $M = 8$  and the tone phases would be closer to zero. Although this effect would be more visible for a larger  $N$ , the PCE does not vary much with  $M$  compared to WIT performance.

Fig. 3.25 represents the simulated BER for  $N = 3$ ,  $\text{GCD} = 1$  MHz,  $r = 0$ ,  $\delta = [-180^\circ, 180^\circ]$ , and 100 multitone streams for each  $M = 2, 4$ , and 8. The corresponding measured BER performance for  $N = 3$ ,  $\text{GCD} = 1$  MHz,  $\delta = [-180^\circ, 180^\circ]$ , and  $P_{\text{in}} = -6$  dBm at the rectifier input with 100 multitone PSK streams for various  $M$  is shown in Fig. 3.26. It can be observed that it is possible to attain 0 BER with the lowest  $M = 2$ . However, the BER increases from 0 to around 0.05 for  $M = 4$  with the increase of just 1 bit/symbol as now, we are dividing the same  $\delta$  region within the increased  $M$  symbol constellation points (each with  $\log_2 M$  bits). Therefore, the phase margin per individual symbol from (3.18) reduces from  $\pm 90^\circ$  for  $M = 2$  to  $\pm 45^\circ$   $M = 4$  for the correct detection at the output.

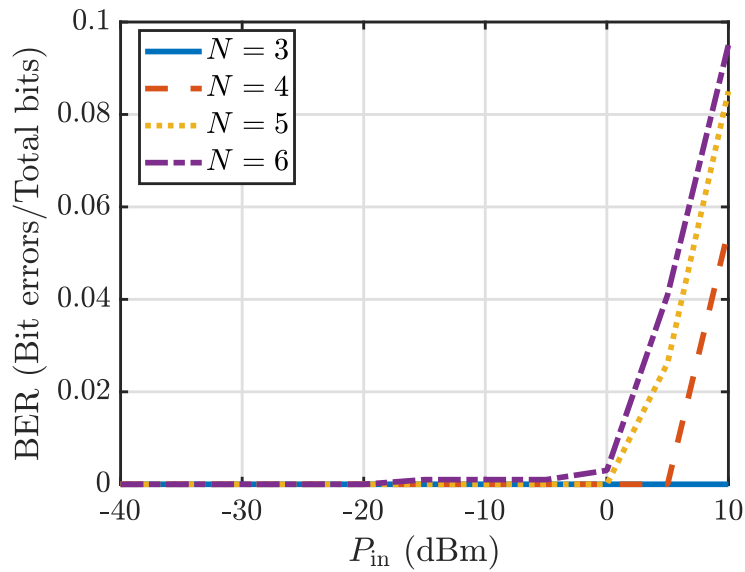


Fig. 3.28. Simulated BER using multitone PSK with  $M = 4$ , GCD = 1 MHz,  $\delta = [-180^\circ, 180^\circ]$ ,  $P_{in} = -6$  dBm,  $r = 0$ , and 100 multitone streams for  $N = 3$ ,  $N = 4$ ,  $N = 5$ , and  $N = 6$ .

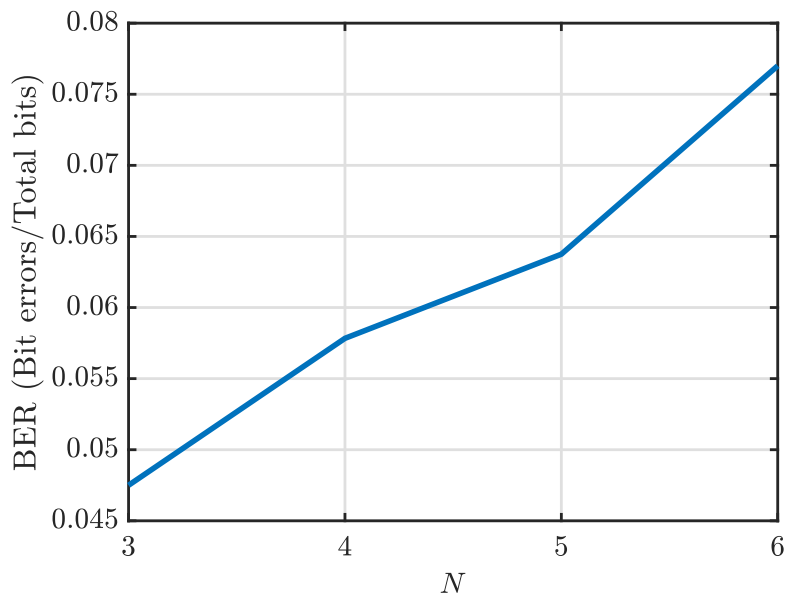


Fig. 3.29. Measured BER using multitone PSK with  $M = 4$ , GCD = 1 MHz,  $\delta = [-180^\circ, 180^\circ]$ ,  $P_{in} = -6$  dBm,  $r = 0$ , and 100 multitone streams for  $N = 3$ ,  $N = 4$ ,  $N = 5$ , and  $N = 6$ .

Table. 3.1 compares the proposed multitone PSK with the existing transmission schemes for an integrated information and energy receiver architecture. Further, to analyse PCE and BER performances with varying  $N$ , 100 multitone PSK streams with  $M = 4$ ,  $\text{GCD} = 1$  MHz,  $\delta = [-180^\circ, 180^\circ]$  for each case of  $N = 3$ ,  $N = 4$ ,  $N = 5$ , and  $N = 6$  are recorded. Fig. 3.27 illustrates the PCE behaviour with varying  $N$  for  $P_{\text{in}} = -6$  dBm. It is observed that the PCE reduces slightly with increasing  $N$ . The reason for this is that now, more tones with misaligned phases have been included. Also, now, the multitone PSK signal BW increases with the increased  $N$ . For example, a 6-tone multitone PSK signal has a BW of 20 MHz, whereas a 5-tone signal has 12 MHz. Therefore, now for  $N = 6$ , the required 5<sup>th</sup> intermodulation tone at 8 MHz has lower amplitude due to the effect of LPF. Here, the impact of  $N$  on PCE is evaluated for  $P_{\text{in}} = -6$  dBm as measurements are performed to the highest power level of  $-6$  dBm to keep the operation of the diode safe. Also, as the output PCE is maximum for  $-6$  dBm, this region is of main interest for the SWIPT applications.

Table 3.1: Transmission strategies for integrated information and energy receiver architecture.

Transmission Approach	Advantages	Limitations	Power Performance	Information Performance
PAPR based [78, 82]	- High PAPR.	<ul style="list-style-type: none"> <li>- Rectifier's RF BW and output filter BW increase with increasing modulation order.</li> <li>- 1 information symbol per a single multitone signal.</li> </ul>	<ul style="list-style-type: none"> <li>- DC of 3.5 times higher compared to the single carrier input signal for 30 dB average received SNR [78].</li> <li>- 0.5 <math>\mu</math>A for <math>-10</math> dB input power [82].</li> <li>- Measurements are not performed.</li> </ul>	<ul style="list-style-type: none"> <li>- BER = <math>10^{-2}</math> for 30 dB average received SNR [78].</li> <li>- BER = <math>10^{-1}</math> for <math>-10</math> dB input power [82].</li> <li>- Measurements are not performed.</li> </ul>

Biased-ASK [84]	- Each symbol has some minimum energy.	<ul style="list-style-type: none"> <li>- Single tone is used instead of a multitone signal.</li> <li>- 1 information symbol per a single multitone signal.</li> <li>- Modulation order limited by ripple voltage.</li> </ul>	- 0.13 V for $M = 2$ , $A_{ratio} = 0.5$ , and 20 dB SNR.	- $10^{-2}$ BER for $M = 2$ , $A_{ratio} = 0.5$ , and SNR = 20 dB.
Amplitude ratio [88]	- Independent of transmission distance.	<ul style="list-style-type: none"> <li>- Information detection is possible only for the multitone with a small number of tones.</li> <li>- Modulation order limited by ripple voltage.</li> <li>- 1 information symbol per a single multitone signal.</li> </ul>	- 48% PCE for total input power of $-10$ dBm for tones power ratio $r = 1/6$ .	- WIT performance such as EVM or BER is not analyzed.

ADSK, ARSK [89]	- Increased operational constellation range.	- Modulation order limited by ripple voltage. - 1 information symbol per a single multitone signal.	- 0.1 $\mu$ W at $-15$ dBm input power. - Measurements are not performed.	- $10^{-1}$ BER for $M = 4$ , and SNR = 20 dB. - Measurements are not performed.
Multitone- FSK [90]	- Lessened envelope variations. - Reduced impact of WIT on WPT.	- Rectifier's RF BW and output filter BW increase with increasing modulation order. - 1 information symbol per a single multitone signal.	- 0.3 V for input power of $-5$ dBm.	- SER = 0.05 for $M = 4$ , $r = 0.5$ , and input power of 0 dBm.

<p>Proposed multitone PSK in this work</p>	<ul style="list-style-type: none"> <li>- Transmission of <math>(N - 1)</math> symbols over an <math>N</math>-tone multitone signal.</li> <li>- OFDM-type communication for WIT.</li> <li>- Lower ripples with information embedding in tones' phases.</li> <li>- Modulation order independent of ripple voltage.</li> <li>- RF matched BW and output filter BW independent of modulation order.</li> <li>- Avoid saturation of the transmitter power amplifier for end-to-end SWIPT performance.</li> </ul>	<ul style="list-style-type: none"> <li>- RF matched BW and output filter BW increases with an increasing number of tones <math>N</math>.</li> </ul>	<ul style="list-style-type: none"> <li>- 38% PCE for <math>N = 3</math>, <math>M = 4</math>, <math>\delta = [-180^\circ, 180^\circ]</math>, and <math>P_{in} = -6</math> dBm.</li> </ul>	<ul style="list-style-type: none"> <li>- BER of 0 for <math>M = 2</math>, and BER = 0.047 for <math>M = 4</math> with <math>N = 3</math>, <math>\delta = [-180^\circ, 180^\circ]</math>, and <math>P_{in} = -6</math> dBm.</li> </ul>
--	---	---	--	---

Table 3.2: SWIPT performance for Multitone PSK with various parameters.

Performance Parameters	PCE	BER
Phase range, $\delta$	Decreases slightly ( $\sim 3\%$ when $\delta$ is increased from $0^\circ$ to $[-180^\circ, 180^\circ]$ ).	Decreases ( $10^{-1}$ for $\delta = [-90^\circ, 90^\circ]$ to $10^{-3}$ for $[-180^\circ, 180^\circ]$ ).
Modulation order, $M$	does not change much.	Increases (0 for $M = 2$ to 0.05 for $M = 4$ ).
Number of Tones, $N$	Decreases slightly ( $\sim 2\%$ from $N = 3$ to $N = 6$ ).	Increases (0.047 for $N = 3$ to 0.075 for $N = 6$ ).

Fig. 3.28 shows the simulated BER behavior with the varying  $N$  and the corresponding measurement results for  $P_{\text{in}} = -6$  dBm are shown in Fig. 3.29. BER increases with the increased  $N$ . This is due to the increased signal BW as now, there is more probability of having phase error with the lower amplitudes of the desired baseband tones. The effect of an increase in the above-discussed parameters such as  $\delta$ ,  $M$ , and  $N$  over WIT and WPT performances is listed in Table 3.2.

Here, in this scheme, we can transmit  $(N - 1)$  symbols over an  $N$ -tone signal. Therefore, the throughput can be defined by

$$T_p = \frac{(N - 1) \cdot \log_2 M}{T_{\text{PSK}}}, \quad (3.19)$$

where  $T_{\text{PSK}}$  is the time period of the multitone PSK signal. From (3.19), it can be seen that the chosen  $\delta$  does not affect the system throughput. However, an appropriate GCD would be needed for the required throughput as it affects  $T_{\text{PSK}}$ . The larger the GCD, the smaller would be the  $T_{\text{PSK}}$ , and in turn, the higher would be the throughput. However, BER increases with the increase in GCD because now, the multitone PSK signal has a larger BW, and matched circuit BW limits the BER performance.

Multitone PSK signal is designed for information detection using only one rectifier while simultaneously utilizing the signal power. Multitone PSK signal can also be used for low-power signal communications as an information transmission scheme, but with low PCE. However, it still helps with improving end-to-end power efficiency as information reception is performed by only one rectifier. This can be a potential application in heterogeneous networks where nearby users utilize the signal for wireless power transmission and far-away users utilize it for wireless information transmission.

## 3.6 Conclusion

In this chapter, a novel multitone PSK transmission scheme for integrated receiver SWIPT architecture with low power consumption is proposed. Information is encoded in terms of phase differences of consecutive tones of the multitone signal.  $(N - 1)$  symbols are transmitted over a single stream of  $N$ -tone multitone PSK signal. The WPT and WIT performances of the proposed transmission scheme are analyzed in terms of PCE and BER, respectively. The main advantage of encoding the information in tone phases instead of tone amplitudes is the lesser variation in the output ripple voltage. Therefore, increasing the modulation order mainly affects WIT performance only while keeping the WPT performance approximately the same, which is a benefit from the SWIPT perspective. A suitable rectifier circuitry is fabricated and all the simulation results are verified with the measurements. The effect of various signal designing parameters, such as allocated phase range, modulation order, and the number of tones, is analyzed from both WIT and WPT perspectives for the overall SWIPT performance of a system.

Transmitting information in tones' phases requires a relatively complex transmitter and proper phase synchronization. In the case of practical and time-varying scenarios, phase distortion would be significant. Therefore, additional algorithms would be required for managing the distortion. Amplitude-based SWIPT transmission

schemes result in larger ripples in WPT performance while simultaneously offering the benefit of better performance in noisy atmospheres.

# Chapter 4

## Multitone ASK

This chapter contributes to the design of a Multitone ASK transmission signal scheme for an integrated information-energy receiver where information is transmitted using the tones' amplitudes. WIT and WPT performances at the receiver are evaluated. The contributions in this chapter are based on the author's paper [16]:

- **Prerna Dhull**, Dominique Schreurs, Sofie Pollin, Mehran Abolhasan and Negin Shariati, "Multitone ASK Waveform Design for Simultaneous Wireless Information and Power Transfer," *IEEE Access*, 2024, doi: [10.1109/ACCESS.2024.3519316](https://doi.org/10.1109/ACCESS.2024.3519316) (early access).

### 4.1 Introduction

Internet of Things (IoT) envisions a global wireless network where trillions of wireless sensors are connected via the Internet and generate data from a diverse range of applications in biomedical implants, vehicular communications, home automation, etc. Wireless standards such as 5G and beyond will underpin the growth in the ubiquitous deployment of IoT devices [4]. To make such deployments feasible, there is a need for sustainable batteryless energy sources. One promising technology aiming to provide both power and data transfer is Simultaneous Wireless Information and Power Transfer (SWIPT). SWIPT provides an energy-efficient green solution

by exploiting the same communication signal for data transfer as well as Wireless Power Transfer (WPT) [110].

At the receiver, SWIPT operation can be achieved by two types of receiver architectures: separated information-energy receiver architecture with two separate paths for information detection and power extraction and integrated information-energy receiver architecture utilizing a rectifier circuitry for power transfer as well as information detection [38, 118, 123, 124]. In the separated information-energy receiver architecture, information demodulation is performed using conventional techniques with a local oscillator and mixer. High-frequency RF components consume a high amount of power. For example, the power consumption of a full ultra-low-power receiver is 3.8 mW, out of which the local oscillator consumes 28% of the total power consumption, and 9% is consumed by the mixer [125–127].

The latter integrated information-energy receiver architecture offers the advantage of removing the local oscillator for information detection from the receiver circuitry and reduces the overall power consumption for signal processing [12, 18, 89]. However, conventional communication signals cannot be used for information detection at the rectifier output. Therefore, new communication signals are required to be designed for such an integrated information-energy receiver architecture.

Initially, for an integrated information-energy receiver architecture, a simple energy modulation scheme using a single-tone waveform, transmitting information symbols by varying the energy levels of the waveform, is introduced [12]. In [89], a double half-wave rectifier is utilized to extend the voltage region for amplitude symbols. A biased amplitude-shift-keying (ASK) transmission scheme has been introduced where each symbol carries some minimum energy to attain a continuous minimum power transfer with the information transfer [84]. However, in all these transmission schemes for integrated information-energy receiver architecture, only a single-tone signal is utilized, and a complex case of OFDM, where multiple symbols over multiple tones are transmitted, is not considered.

From the WPT perspective, higher peak-to-average-power ratio (PAPR) waveforms such as multitone signals perform better than a single-tone waveform, delivering higher power conversion efficiency (PCE) at the rectifier output [56, 62, 113–116, 128, 129]. Utilizing the PAPR of the multitone signal by varying the number of tones according to the transmitted information has been proposed in [78]. Further, a non-uniformly spaced multitone waveform utilizing PAPR has also been shown to perform better in the case of low signal-to-noise ratio scenarios [82]. A multitone transmission method by transmitting information in the ratios of tones' amplitudes has been introduced in [88], which helps make the communication signal immune to the transmission distance. However, information detection at the receiver is feasible for only two or three tones and becomes complicated and impractical for more than the 3-tone multitone signal.

A frequency-based information detection has been introduced in [90] to minimize the ripples at the rectifier output. Information is transferred by varying the frequency spacing between the tones of the multitone frequency-shift-keying (FSK) signal according to transmitted symbols. Another way of information detection for the multitone FSK has also been proposed by measuring the output PAPR levels [92]. A Multitone phase-shift-keying (PSK) waveform scheme utilizing the tones' phases for information transmission with the higher transmission output data rate has been introduced in [15]. Ripples in the output voltage have been reduced by utilizing the phases for information symbols transmission. However, complex transmitters would be required to modify multiple-tone phases for information transmission. Also, phase-based information transmission is more susceptible to noisy and fading environments compared to amplitude-based modulations [130–132]. Therefore, it is necessary to develop amplitude-based transmission schemes for the SWIPT integrated receiver architecture shown in Fig. 4.1.

In this chapter, a novel Multitone ASK transmission scheme for an integrated information-energy receiver architecture is proposed. The signal is designed in such a way that the non-linearity of the rectifier is utilized for information detection.

The information detection and power transfer are performed from the same rectified signal. Information is transmitted by varying the amplitudes of tones at the transmitter, and the information detection is performed by analyzing the magnitudes of the corresponding relevant baseband tones at the rectifier output. PCE and bit-error-rate (BER) are used to investigate WPT and wireless information transfer (WIT) performances, respectively. The effect of the chosen minimum energy level of the symbols, number of tones, and symbols' amplitude distribution over signal PAPR, output PCE, and BER is analyzed.

The advantage of the proposed Multitone ASK transmission scheme is its information detection via exploiting the intermodulation process of the same rectifier circuitry, which eliminates the need for a local oscillator and reduces the overall power consumption of the SWIPT system. In this work, it is possible to transmit  $(N - 1)$  symbols over an  $N$ -tone multitone signal, providing a conventional OFDM-type communication for the integrated information-energy receiver architecture. Therefore, a higher data rate is achieved without increasing the bandwidth by using the same multitone signal earlier used for WPT solely. In this work, only the individual tones' power level would be modified according to the transmitted data stream, resulting in a simple transmitter.

This chapter is organized as follows. Section 4.2 introduces the theoretical model of designing a Multitone ASK signal and analyses the effect of different information streams versus varying average signal power with the non-linearity of the rectifier. Next, Section 4.3 discusses the effect of the symbol levels' distribution over the PCE in terms of achievable signal PAPR. Then, the WPT and WIT performances of the SWIPT system with the Multitone ASK transmission scheme are analyzed in Section 4.4. In the end, a conclusion is drawn in Section 4.5.

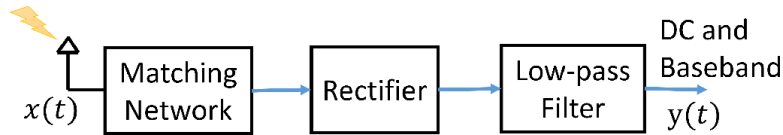


Fig. 4.1. Integrated receiver rectifier for SWIPT.

## 4.2 Signal Model

An integrated information-energy rectifier receiver is illustrated in Fig. 4.1 consisting of an input matching network, diodes rectifier, and a resistor-capacitance low-pass-filter (RC-LPF). Here, the same rectifier receiver is used for both WPT and WIT. Received Multitone ASK signal  $x(t)$  centered around frequency  $f_c = 2.45$  GHz is passed through the rectifier receiver, resulting in a baseband signal  $y(t)$  which is utilized not only for power transfer but also for decoding the transmitted information.

The transmitted Multitone ASK signal spectrum  $X(f)$  and the corresponding rectified baseband output signal spectrum  $Y(f)$  are shown in Fig. 4.2. The information is embedded in the amplitudes of tones of the  $N$ -tone multitone RF signal. Information is encoded in the multitone RF signal in such a way that the non-linearity of the rectifier is utilized to extract the information from the baseband signal  $y(t)$  at the output. The  $N$ -tones multitone signal, after passing through the rectifier, results in a baseband signal consisting of various intermodulation (IM) frequency components of various orders as a result of mixing between various tones of the multitone signal. However,  $2^{nd}$  order intermodulation frequency components (IM<sub>2</sub>) dominates at the receiver output [51].

Here, information is transmitted as amplitudes of tones of a multitone signal, and after rectification, information is decoded from the second-order intermodulation frequency components, IM<sub>2</sub>s between consecutive tones. A reference  $N$ -tone multitone signal  $r(t)$  with an average signal power of  $P_{in}$  is considered as

$$r(t) = \text{Re} \left\{ \sum_{n=1}^N \sqrt{\frac{2P_{in}}{N}} e^{j(2\pi f_n t)} \right\}. \quad (4.1)$$

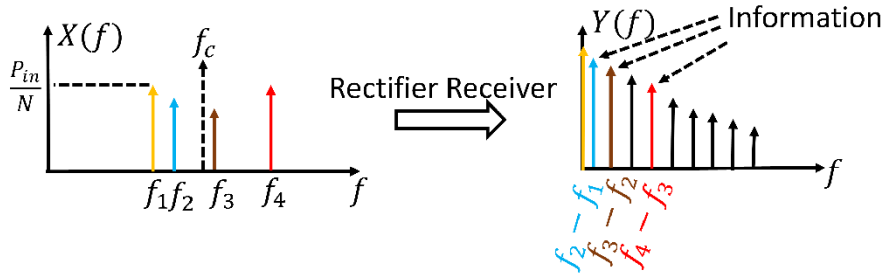


Fig. 4.2. Four-tone Multitone ASK RF signal spectrum  $X(f)$  centered around frequency  $f_c$  and rectified baseband output spectrum  $Y(f)$  consisting of intermodulations frequency tones (in MHz) carrying information (colored) and extra intermodulations components (black).

The transmitted Multitone ASK signal  $x(t)$  is generated by embedding the information symbols over the reference signal  $r(t)$  and can be considered as

$$x(t) = \text{Re} \left\{ \sum_{n=1}^N \sqrt{\frac{2l_{s_{n-1}} P_{\text{in}}}{N}} e^{j(2\pi f_n t)} \right\} \quad (4.2)$$

where  $l_{s_{n-1}}$  denotes the transmitted information level over the  $n^{\text{th}}$  tone frequency  $f_n$ . Here,  $n^{\text{th}}$  tone of  $r(t)$  are modified by the transmitted information symbol level  $l_{s_{n-1}}$ . For an amplitude modulation order of  $L$ ,  $l_{s_{n-1}}$  is chosen from the available information symbol set ( $\mathcal{S}$ ) consisting of  $L$  levels  $l_1, l_2, \dots, l_L$ . Here, phases of the transmitted tones are considered zero.

At the rectifier output, the information is decoded from the amplitudes of the relevant baseband tones in the MHz frequency range, as shown in Fig. 4.2. The filtered baseband output consists of dc and the accumulation of several intermodulation frequency components. However, the filtered output  $y(t)$  consists of only dc and even order  $4^{\text{th}}$  order,  $6^{\text{th}}$  order,  $\dots$ , etc., frequency components. All the odd-order intermodulation components  $3^{\text{rd}}$  order,  $5^{\text{th}}$  order,  $\dots$ , etc., are filtered out by LPF as all these IM frequency components lie in the RF frequency range. Among even order frequency components,  $\text{IM}_2$  would be dominating compared to  $4^{\text{th}}$  order,  $6^{\text{th}}$  order,  $\dots$ , etc., frequency components [51].

For example, after passing a 3-tone Multitone ASK signal  $x(t)$  from (4.2) through the rectifier receiver model depicted in Fig. 4.1, the obtained baseband rectifier

output  $y(t)$  can be represented as a combination of dc and the dominant IM<sub>2</sub>s as

$$y(t) = \text{dc} + A_1 \cos(2\pi(f_2 - f_1)t) + A_2 \cos(2\pi(f_3 - f_2)t) + A_3 \cos(2\pi(f_3 - f_1)t), \quad (4.3)$$

where  $A_1$ ,  $A_2$ , and  $A_3$  represent the amplitudes of IM<sub>2</sub> at  $(f_2 - f_1)$ ,  $(f_3 - f_2)$ , and  $(f_3 - f_1)$ , respectively. Here, the baseband tones amplitudes are related to the corresponding intermodulating tones' amplitudes of multitone RF signal. The baseband tone amplitude corresponds to the product of the intermodulating tones, i.e.,  $A_1 \propto l_{s_0}l_{s_1}$ ,  $A_2 \propto l_{s_1}l_{s_2}$ , and  $A_3 \propto l_{s_1}l_{s_3}$  as  $A_1$ ,  $A_2$ , and  $A_3$  are amplitudes of intermodulation frequency component between  $f_1$  and  $f_2$ ,  $f_2$  and  $f_3$ , and  $f_1$  and  $f_3$ , respectively.

In this chapter,  $(N - 1)$  information symbols are transmitted over a single  $N$ -tone multitone signal. The Multitone ASK signal is designed in such a way that the information is in amplitude levels of IM<sub>2</sub> between consecutive tones only, i.e.,  $(f_2 - f_1)$ ,  $(f_3 - f_2)$ ,  $\dots$ ,  $(f_N - f_{N-1})$  tones amplitudes would carry the information as shown in Fig. 4.2. In Fig. 4.2, 4-tone signal is depicted where the first tone is kept constant, and the other three tones' amplitudes are modified according to the transmitted information symbols from the available symbol set  $\mathcal{S}$ . The baseband output signal spectrum  $Y(f)$  contains various intermodulation frequency components. However, the three information symbols are decoded from the corresponding intermodulation frequency components,  $(f_2 - f_1)$ ,  $(f_3 - f_2)$ , and  $(f_4 - f_3)$  as depicted in colour in Fig. 4.2.

To make a simultaneous transmission of these  $(N - 1)$  information symbols possible over a single  $N$ -tone multitone signal,  $f_n$ 's are chosen in a particular way such that  $(N - 1)$  IM<sub>2</sub>s between consecutive frequencies do not overlap each other and also do not coincide with other non-consecutive IM<sub>2</sub>s. This is done to obtain a unique  $(N - 1)$  desired baseband frequencies at the output. This results in asymmetrically spaced tones around the center frequency of 2.45 GHz instead of general equally

spaced tones of a multitone signal. Here, these frequencies  $f_n$ s are obtained using the algorithm used in [15].

For an  $N$ -tone Multitone ASK signal from (4.2), average power of the transmitted signal after embedding  $(N - 1)$  information symbols would be

$$P_{\text{avg}} = \frac{P_{\text{in}}}{N}(l_{s_0} + l_{s_1} + l_{s_2} + \cdots + l_{s_{N-1}}), \quad (4.4)$$

and should satisfy

$$\frac{P_{\text{in}}}{N}(l_{s_0} + l_{s_1} + l_{s_2} + \cdots + l_{s_{N-1}}) \leq P_{\text{in}}. \quad (4.5)$$

Assuming the first tone amplitude is constant equal to  $P_{\text{in}}/N$ , i.e.,  $l_{s_0}$  be equal to 1, (4.4) results into

$$l_{s_1} + l_{s_2} + \cdots + l_{s_{N-1}} \leq N - 1. \quad (4.6)$$

There exists a condition over the possible maximum information symbol level  $l_L$  so that it is feasible to transmit all  $(N - 1)$  symbols to be the maximum  $l_L$  simultaneously. Therefore, from (4.6),  $l_L$  must satisfy

$$(N - 1)l_L \leq N - 1, \quad (4.7)$$

$$l_L \leq 1. \quad (4.8)$$

As the information is being transmitted through the tones' amplitudes, the average power of the transmitted multitone signal keeps changing with the transmitted information patterns. For a particular available average power  $P_{\text{in}}$  at the transmitter, the maximum average power of the transmitted signal after embedding information in multitone signal's tones is  $P_{\text{avg,max}} = P_{\text{in}}$  when all the transmitted information symbols are chosen to be the maximum levels  $l_L = 1$ . Similarly, the average power of the transmitted signal would be minimal when all the transmitted information

levels are chosen to be the lowest information level  $l_1$ ,

$$P_{\text{avg,min}} = (1 + (N - 1)l_1) \frac{P_{\text{in}}}{N}. \quad (4.9)$$

For the  $L$  information symbols, the average symbol power would be

$$P_{\text{sym\_avg}} = \frac{1}{L} \sum_{i=1}^L l_i. \quad (4.10)$$

Let the information levels be linearly distributed between  $l_{\min}$  and  $l_{\max}$  for a modulation order  $L$ . Thus, the available  $L$  information symbol levels can be defined as

$$l_i = l_{\min} + (i - 1) \frac{l_{\max} - l_{\min}}{L - 1}, \quad \forall i = 1, 2, \dots, L. \quad (4.11)$$

For example, for  $L = 4$ ,  $l_{\min} = 0.1$ , and  $l_{\max} = 1$ , available symbol levels set  $\mathbf{S}$  would be having information levels as 0.1, 0.4, 0.7, and 1.

For an  $N$ -tone multitone signal carrying  $(N - 1)$  information symbols with a modulation order  $L$ ,  $L^{N-1}$  different patterns of the transmitted symbols are possible, which is also similar to different possible patterns of  $(N - 1) \log_2 L$  bits over the  $N$ -tone multitone signal, and can also be represented by  $2^{(N-1) \log_2 L}$  different information bits patterns. Different information patterns over the multitone signal may still result in the same average signal power of the transmitted stream. For example, from (4.4), the multitone signal average power for a 4-tone signal with [0.1 0.4 0.7] information stream is similar to a signal having [0.4 0.7 0.1] information stream. Therefore, out of these  $L^{N-1}$  different multitone streams information patterns, the total possible different transmitted power levels would be  $\binom{N+L-2}{N-1}$ . The mean of these different average powers of the transmitted multitone streams,  $P_{\text{avg}}|_{\text{mean}}$  as a result of different information symbol combinations and from (4.4)

can be represented as

$$P_{\text{avg}}|_{\text{mean}} = \frac{P_{\text{in}}}{N} + \frac{1}{\binom{N+L-2}{N-1}} \sum_{j=1}^{\binom{N+L-2}{N-1}} \left( \sum_{i=1}^{N-1} l_{s_{j,i}} \frac{P_{\text{in}}}{N} \right) \quad (4.12)$$

where  $l_{s_{j,i}}$  represents  $i^{\text{th}}$  symbol  $l_{s_i}$  in the  $j^{\text{th}}$  possible combination of transmitted power levels. These  $\binom{N+L-2}{N-1}$  different combinations of information sequence over a single multitone stream can further be reduced depending upon  $L$  and the amplitude distribution between  $l_{\text{min}}$  and  $l_{\text{max}}$  due to further overlapping among the average signal power.

For linearly distributed information symbol levels, the average signal power of a single  $N$ -tone signal can be rewritten from (4.4) and (4.11) as

$$P_{\text{avg}} = \frac{P_{\text{in}}}{N} \left[ 1 + (N-1)l_{\text{min}} + \left\{ \sum_{n=1}^{N-1} i_n - (N-1) \right\} \frac{l_{\text{max}} - l_{\text{min}}}{L-1} \right], i_n \in \{1, 2, \dots, L\}. \quad (4.13)$$

For a 3-tone signal, the average signal power  $P_{\text{avg}}$  of the transmitted signal from (4.4) and (4.13) is  $P_{\text{avg}} = (1 + l_{s_1} + l_{s_2}) P_{\text{in}}/N$  with first tone power to be constant as  $P_{\text{in}}/N$  and  $l_{s_0}$  to be 1, and can also be represented as

$$P_{\text{avg}}|_{N=3} = \frac{P_{\text{in}}}{N} \left\{ 1 + 2l_{\text{min}} + (i+j-2) \frac{l_{\text{max}} - l_{\text{min}}}{L-1} \right\}, \quad i, j \in \{1, 2, \dots, L\}. \quad (4.14)$$

In (4.14),  $(i+j)$  for  $i, j \in \{1, 2, \dots, L\}$  results in  $(2L-1)$  different mutually exclusive values. Table 4.1 represents the  $L^{(N-1)} = 16$  different patterns of transmitted information symbols  $l_{s_1}$  and  $l_{s_2}$  for  $N = 3$ ,  $L = 4$ ,  $l_{\text{min}} = 0.1$ , and  $l_{\text{max}} = 1$ . However, it can be seen that for these 16 different patterns, the factor  $(l_{s_1} + l_{s_2})$  affecting average signal power  $P_{\text{avg}}$  results in a set of only seven different values  $\{0.2, 0.5, 0.8, 1.1, 1.4, 1.7, 2\}$  from (4.14), for information embedded multitone stream. Table 4.2 represents a few of 64 possible combinations for  $N = 4$  with  $L = 4$ ,  $l_{\text{min}} = 0.1$ , and  $l_{\text{max}} = 1$ . Here in Table 4.1 and Table 4.2, transmitted

Table 4.1: Different patterns of  $(N - 1)$  transmitted symbols for Multitone ASK with  $N = 3$ ,  $L = 4$ , and  $l_{\min} = 0.1$ .

$l_{s_1}$	$l_{s_2}$	$(l_{s_1} + l_{s_2})$	$l_{s_0}l_{s_1}$	$l_{s_1}l_{s_2}$
0.1	0.1	0.2	0.1	0.01
0.4	0.1	0.5	0.4	0.04
0.1	0.4	0.5	0.1	0.04
0.7	0.1	0.8	0.7	0.07
0.1	0.7	0.8	0.1	0.07
0.4	0.4	0.8	0.4	0.16
1	0.1	1.1	1	0.1
0.7	0.4	1.1	0.7	0.28
0.1	1	1.1	0.1	0.1
0.4	0.7	1.1	0.4	0.28
1	0.4	1.4	1	0.4
0.4	1	1.4	0.4	0.4
0.7	0.7	1.4	0.7	0.49
0.7	1	1.7	0.7	0.7
1	0.7	1.7	1	0.7
1	1	2	1	1

symbol sequences are arranged in such a way that symbol sequence patterns resulting in the same average power of the transmitted multitone stream are being put together. The resulting same average signal power for different symbol patterns is highlighted by grouping these in red. By generalizing for an  $N$ -tone multitone signal, there exist  $(N - 1)L - (N - 2)$  different transmitted average signal powers for the different patterns of  $(N - 1)$  transmitted symbols  $l_{s_1}, l_{s_2}, \dots, l_{s_{N-1}}$  with the factor of  $(l_{s_1} + l_{s_2} + \dots + l_{s_{N-1}})$  from (4.4), lying between  $[(N - 1)l_{\min}, (N - 1)l_{\max}]$ .

From (4.3), it can be seen that relevant baseband intermodulation tones amplitudes at  $\Delta f_n$  are proportional to the product of transmitted symbols at  $n^{\text{th}}$  and  $(n + 1)^{\text{th}}$  tone. For example, amplitudes of relevant baseband intermodulation tones at  $\Delta f_1$  and  $\Delta f_2$  are proportional to  $l_{s_0}l_{s_1}$  and  $l_{s_1}l_{s_2}$ , respectively. Table 4.1 highlights relevant information carrying products  $l_{s_0}l_{s_1}$  for  $\Delta f_1$  and  $l_{s_1}l_{s_2}$  for  $\Delta f_2$  for  $N = 3$  with 16 possible different transmitted symbols patterns. Table 4.2 highlights relevant information carrying products  $l_{s_0}l_{s_1}$  for  $\Delta f_1$ ,  $l_{s_1}l_{s_2}$  for  $\Delta f_2$ ,  $l_{s_2}l_{s_3}$  for  $\Delta f_3$  for  $N = 4$  with a few of 64 possible different transmitted symbols patterns. It can be seen that the signals with the same average transmitted signal power but having a

Table 4.2: Different patterns of  $(N - 1)$  transmitted symbols for Multitone ASK with  $N = 4$ ,  $L = 4$ , and  $l_{\min} = 0.1$ .

$l_{s_1}$	$l_{s_2}$	$l_{s_3}$	$(l_{s_1} + l_{s_2} + l_{s_3})$	$l_{s_0} l_{s_1}$	$l_{s_1} l_{s_2}$	$l_{s_2} l_{s_3}$
0.1	0.1	0.1	0.3	0.1	0.01	0.01
0.4	0.1	0.1	0.6	0.4	0.04	0.01
0.1	0.4	0.1	0.6	0.1	0.04	0.04
0.1	0.1	0.4	0.6	0.1	0.01	0.04
0.7	0.1	0.1	0.9	0.7	0.07	0.01
0.4	0.4	0.1	0.9	0.4	0.16	0.04
0.1	0.7	0.1	0.9	0.1	0.07	0.07
0.4	0.1	0.4	0.9	0.4	0.04	0.04
0.1	0.4	0.4	0.9	0.1	0.04	0.16
0.1	0.1	0.7	0.9	0.1	0.01	0.07

different sequence of symbol streams result in different variations in output baseband amplitudes. The reason for this is the non-linearity of the rectifier circuitry, where the baseband output tones magnitudes are a result of intermodulations among tones.

Due to the non-linearity of the rectifier, all baseband tones do not reflect the changes according to the varying signal average power  $P_{\text{avg}}$  while changing the symbol stream. For example, Fig. 4.3 shows the magnitude behavior of the first baseband output tone ( $\Delta f_1$ ) at 1 MHz for varying information symbols pattern for a 3-tone Multitone ASK centred around 2.45 GHz with  $L = 2$  and  $l_{\min} = 0.1$ . Multitone ASK signal frequencies are selected using the Algorithm 1 of [15]. As the modulation order  $L$  is 2, the transmitted symbols can be either 0.1 or 1, and four different symbol patterns are possible over a 3-tone Multitone ASK signal. These different patterns are divided between two cases of symbol streams,  $[0.1 \ l_{s_2}]$  and  $[1 \ l_{s_2}]$ . The symbol  $l_{s_2}$  transmitted over the third tone  $f_3$  can switch between 0.1 and 1. It can be seen that although the transmitted signal average power,  $P_{\text{avg}}$  increases with the changing symbol  $l_{s_2}$  from 0.1 to 1, the magnitude of the first baseband tone reduces.

Fig. 4.4 and Fig. 4.5 illustrate the magnitude behavior of the relevant two baseband tones carrying information at  $\Delta f_1 = 1$  MHz and  $\Delta f_2 = 2$  MHz, respectively, for a 3-tone Multitone ASK signal with a modulation order of  $L = 4$  and  $l_{\min} = 0.1$ . Here, the 16 possible symbol patterns are divided among four cases. For example, the blue

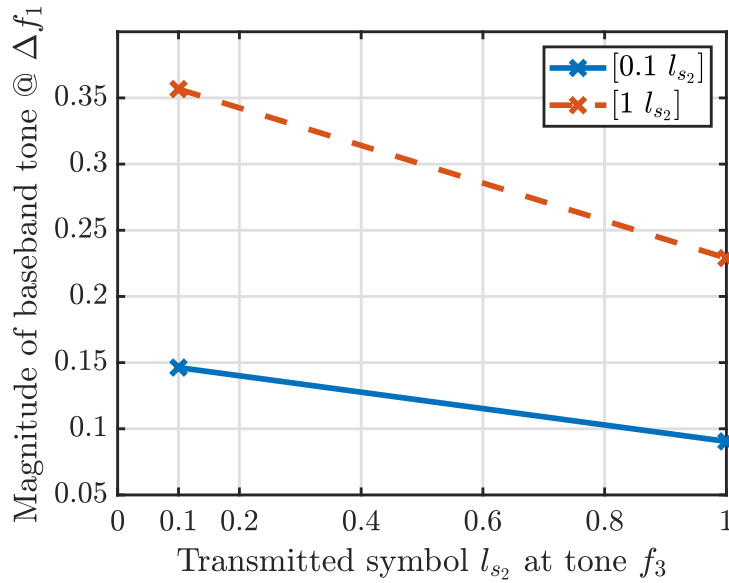


Fig. 4.3. Magnitude variation of first baseband tone ( $\Delta f_1 = 1$  MHz) for Multitone ASK centered around 2.45 GHz with  $N = 3$ ,  $L = 2$ , and  $l_{\min} = 0.1$  for different information symbol patterns over multitone streams by varying symbol  $l_{s_2}$ .

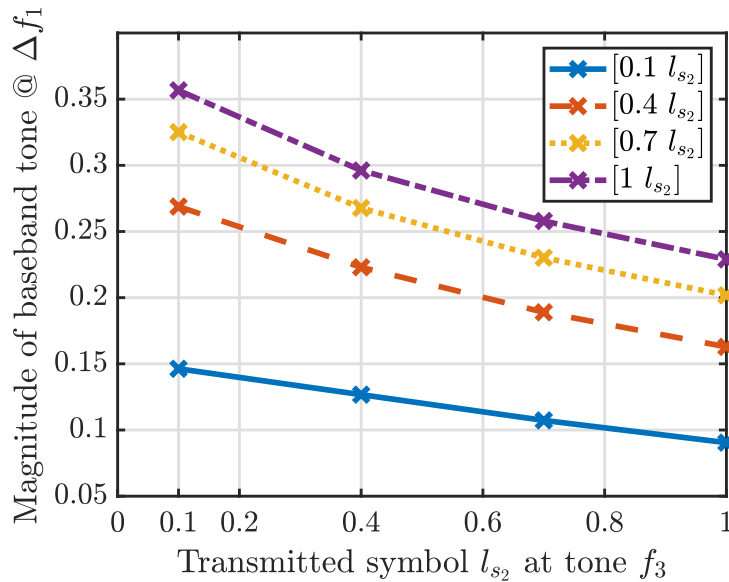


Fig. 4.4. Magnitude variation of first baseband tone ( $\Delta f_1 = 1$  MHz) for Multitone ASK centered around 2.45 GHz with  $N = 3$ ,  $L = 4$ , and  $l_{\min} = 0.1$  for different information symbol patterns over multitone streams by varying symbol  $l_{s_2}$ .

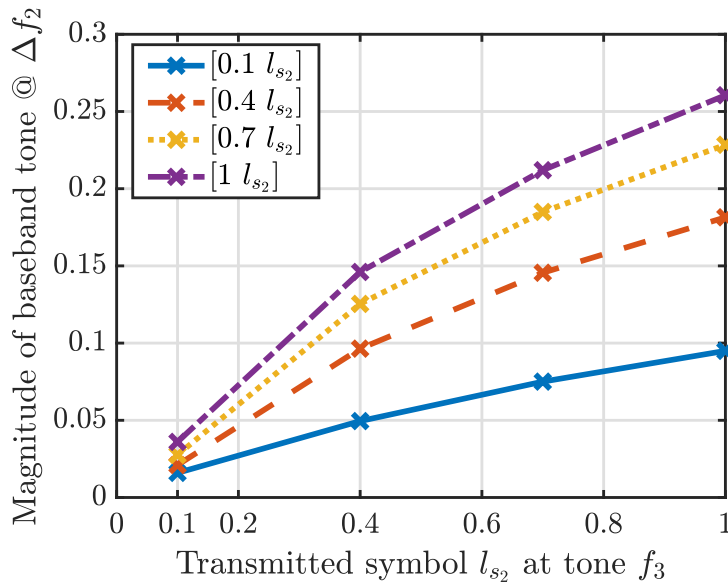


Fig. 4.5. Magnitude variation of second baseband tone ( $\Delta f_2 = 2$  MHz) for Multitone ASK centered around 2.45 GHz with  $N = 3$ ,  $L = 4$ , and  $l_{\min} = 0.1$  for different information symbol patterns over multitone streams by varying symbol  $l_{s_2}$ .

curve  $[0.1 l_{s_2}]$  represents the multitone streams with a constant transmitted symbol  $l_{s_1}$  as 0.1 over  $f_2$  and varying the transmitted symbol level  $l_{s_2}$  over  $f_3$  among 0.1, 0.4, 0.7, and 1. Similarly, other cases are simulated where  $l_{s_1}$  are considered constant as  $[0.4]$ ,  $[0.7]$ , and  $[1]$  and only  $l_{s_2}$  is varied. From Fig. 4.4, it can be seen that the magnitude of the baseband tone at 1 MHz ( $\Delta f_1$ ) reduces for the multitone streams when the symbol  $l_{s_2}$  over the third transmitted tone  $f_3$  increases in the order of 0.1, 0.4, 0.7, and 1 despite the increase in transmitted signal average power from (4.4).

However, the magnitude of the baseband tone  $\Delta f_2$  at 2 MHz increases with the increasing symbol level of  $l_{s_2}$  as seen in Fig. 4.5 for all cases of transmitted multitone streams. It shows that the different baseband tones undergo different variations when the overall average power of the transmitted signal changes while the transmitted symbols change. Therefore, a comparison among the obtained magnitude levels of the baseband tones at the rectifier output for the different cases of transmitted symbol streams having different transmitted average power is not feasible due to the non-linearity of the rectifier. The baseband tones at the output reflect the changes in the symbol amplitudes only when the transmitted symbols result in the multitone streams having the same average signal power,  $P_{\text{avg}}$ .

### 4.3 Amplitude Levels Distribution and PAPR

In the proposed Multitone ASK transmission scheme, the information is being transmitted through the varying amplitudes of tones. The reference multitone signal  $r(t)$  is changed to Multitone ASK signal  $x(t)$  by varying the amplitudes as in (4.2) to make the SWIPT transfer feasible. The average power  $P_{\text{in}}$  of the reference signal  $r(t)$  is reduced to average signal power  $P_{\text{avg}}$  for  $x(t)$ .  $P_{\text{avg}}$  depends upon the magnitudes of the transmitted information symbols from (4.4). Therefore, it is important to analyze the effect of tones's varying amplitudes on the WIT and WPT performances of the SWIPT system. PAPR is one such merit to analyze the signal's WPT performance. From the WPT perspective, a multitone without the information would result in the highest PAPR. However, varying tones' amplitudes provide the benefit of WIT in addition to WPT.

PAPR for a signal  $x(t)$  can be represented by

$$\text{PAPR} = \frac{P_{\text{peak}}}{P_{\text{avg}}} = \frac{\max\{|x(t)|^2\}}{\frac{1}{T} \int_{-T/2}^{T/2} x^2(t) dt}, \quad (4.15)$$

where  $T$  denotes the time-period of waveform  $x(t)$ . The peak power of the Multitone ASK signal in (4.2) can be represented as

$$P_{\text{peak}} = \frac{2P_{\text{in}}}{N} \left| \sqrt{l_{s_0}} + \sqrt{l_{s_1}} + \sqrt{l_{s_2}} + \cdots + \sqrt{l_{s_{N-1}}} \right|^2. \quad (4.16)$$

From (4.15), (4.16), and (4.4), PAPR of a Multitone ASK signal can be represented in terms of transmitted information symbols levels  $l_{s_i}$ s as

$$\text{PAPR} = \frac{2 \left| \sum_{i=1}^N \sqrt{l_{s_{i-1}}} \right|^2}{\sum_{i=1}^N l_{s_{i-1}}}. \quad (4.17)$$

By keeping the first tone's power level constant, i.e.,  $l_{s_0} = 1$ , the PAPR of a Multi-

tone ASK signal would be

$$\text{PAPR} = \frac{2 \left| 1 + \sqrt{l_{s_1}} + \sqrt{l_{s_2}} + \cdots + \sqrt{l_{s_{N-1}}} \right|^2}{1 + l_{s_1} + l_{s_2} + \cdots + l_{s_{N-1}}}. \quad (4.18)$$

For all symbols having equal probability of transmission, the mean PAPR across multitone streams,  $\text{PAPR}|_{\text{mean}}$ , having transmission of different combinations of information symbols can be represented by

$$\text{PAPR}|_{\text{mean}} = \frac{2 \left| 1 + (N-1) \frac{1}{L} \sum_{i=1}^L \sqrt{l_i} \right|^2}{1 + (N-1) \frac{1}{L} \sum_{i=1}^L l_i}. \quad (4.19)$$

From (4.19), it can be seen that a maximum PAPR of  $2N$  can be achieved when all the transmitted symbols are chosen as the highest available information level,

$$\text{PAPR}|_{\text{max}} = \text{PAPR}|_{l_i=1} = 2N. \quad (4.20)$$

Similarly, signal PAPR would be lowest when the transmitted symbols are chosen as the lowest available information level,  $l_{\min}$ ,

$$\text{PAPR}|_{\text{min}} = \frac{2 \left| 1 + (N-1) \sqrt{l_{\min}} \right|^2}{1 + (N-1) l_{\min}}. \quad (4.21)$$

Symbol levels are distributed between  $l_{\min}$  and  $l_{\max} = 1$ . Therefore, it is important to analyze the effect of the chosen  $l_{\min}$  over the WPT and WIT performance. For linearly distributed information symbols defined in (4.11), (4.19) can be approximated as

$$\text{PAPR} = \frac{\left| 1 + \frac{2(N-1)(L-1)}{3L(1-l_{\min})} \left\{ 1 + \left( \frac{L-l_{\min}}{L-1} \right)^{3/2} \right\} \right|^2}{1 + (N-1) \left( \frac{1+l_{\min}}{2} \right)}. \quad (4.22)$$

Fig. 4.6 illustrates the analytical mean PAPR variation of 100 streams of 6-tone Multitone ASK signal with increasing  $l_{\min}$  by (4.22) for multiple modulation orders. It can be seen that as the minimum assigned level to a symbol is increased, PAPR

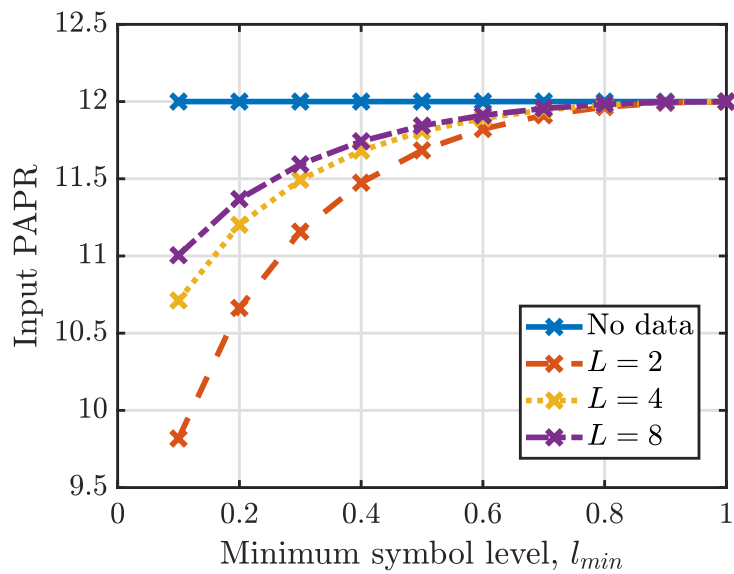


Fig. 4.6. Analytical PAPR for Multitone ASK centred around 2.45 GHz with  $N = 6$  and linearly distributed amplitudes with variation in  $l_{\min}$ .

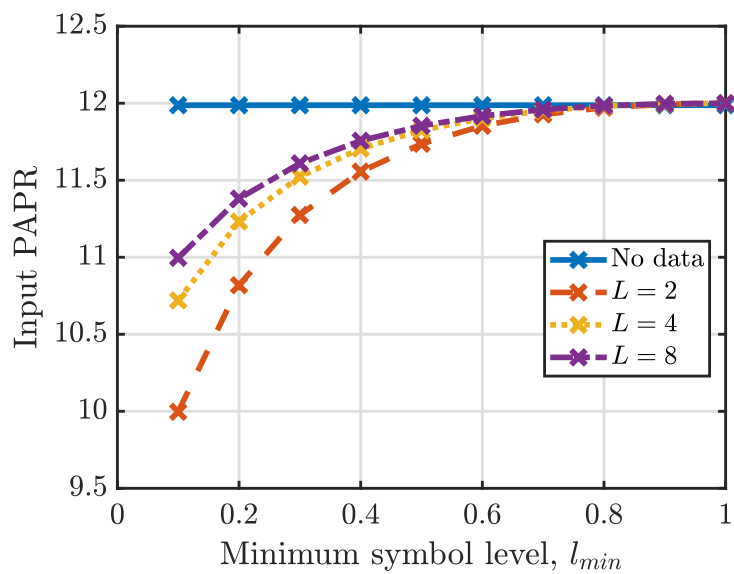


Fig. 4.7. Simulated PAPR for Multitone ASK centred around 2.45 GHz with  $N = 6$  and linearly distributed amplitudes with variation in  $l_{\min}$  for 100 multitone streams.

increases, and after a certain level, PAPR converges to the maximum attained value of  $2N$ , similar to the case of a signal having all tones of equal power with the average signal power of  $P_{\text{in}}$  [13, 78]. Further, simulated PAPR variation of 6-tone Multitone ASK with  $l_{\text{min}}$  for 100 multitone streams is shown in Fig. 4.7. Fig. 4.7 illustrates that as  $l_{\text{min}}$  is increased, the PAPR is also increased, which indicates that the WPT performance of the signal is also improved. However, from a WIT perspective, this would minimize the difference between the received symbols' magnitude over the output baseband tones worsening the WIT performance.

Also, it can be seen from Fig. 4.6 and Fig. 4.7 that as the modulation order  $L$  is increased, PAPR increases which implies that having a larger modulation order benefits the WPT performance. However, with the larger modulation order,  $L$ , it would be difficult to distinguish the different symbol levels. Therefore, there exists a trade-off for  $l_{\text{min}}$  selection as well as  $L$  selection for designing a Multitone ASK signal from WPT and WIT perspective for SWIPT operation.

Due to the presence of non-linearity in the rectifier, it is important to analyze the effect of non-linearly distributed amplitudes between  $l_{\text{min}}$  and  $l_{\text{max}}$  on the WPT and WIT performances. Let  $gf_{\text{exp}}$  be the growth factor for exponentially distributed amplitude levels for a modulation order of  $L$ , which can be represented as

$$gf_{\text{exp}} = (l_{\text{max}}/l_{\text{min}})^{1/(L-1)}. \quad (4.23)$$

Therefore, exponentially distributed amplitude levels  $l_i|_{\text{exp}}$  can be defined as

$$l_i|_{\text{exp}} = l_{\text{min}}gf_{\text{exp}}^{(i-1)}, \quad \forall \quad i = 1, 2, \dots, L. \quad (4.24)$$

Similarly, for a logarithmic growth factor  $gf_{\text{log}}$ , logarithmically distributed ampli-

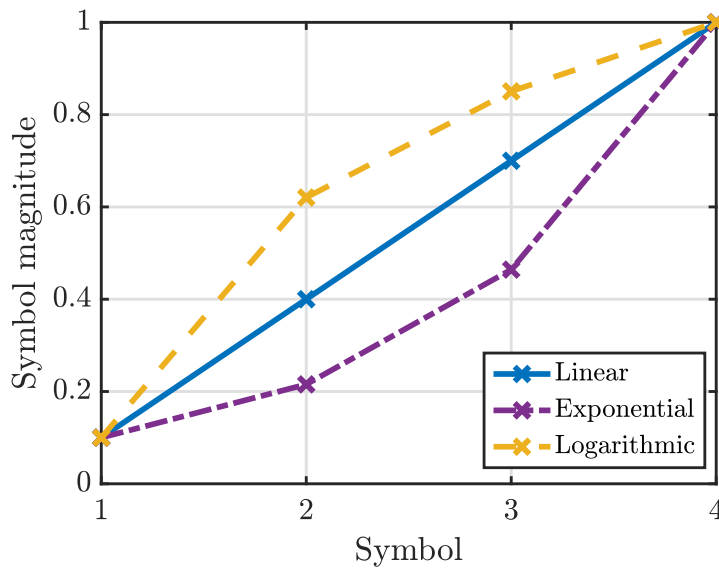


Fig. 4.8. Linearly distributed, exponentially distributed, and logarithmically distributed symbols with  $gf = 10$  for  $l_{\min} = 0.1$  and  $L = 4$ .

tude levels  $l_i|_{\log}$  can be defined as

$$l_i|_{\log} = \log_{gf|_{\log}} \left\{ gf_{\log}^{l_{\min}} + (i - 1) \left( \frac{gf_{\log}^{l_{\max}} - gf_{\log}^{l_{\min}}}{L - 1} \right) \right\}, \quad \forall \quad i = 1, 2, \dots, L. \quad (4.25)$$

Linearly distributed, exponentially distributed, and logarithmically distributed symbol levels between  $l_{\min} = 0.1$  and  $l_{\max} = 1$  for  $L = 4$  are shown in Fig. 4.8. PAPR for exponential and logarithmically distributed amplitude levels,  $\text{PAPR}_{\text{exp}}$  and  $\text{PAPR}_{\log}$  are shown in Fig. 4.9 and Fig. 4.10, respectively. It can be observed that exponentially distributed amplitude levels result in the lowest PAPR whereas logarithmically distributed amplitude levels result in the highest PAPR for a particular  $l_{\min}$ .

$$\text{PAPR}_{\text{exp}} < \text{PAPR}_{\text{linear}} < \text{PAPR}_{\log} \quad (4.26)$$

The reason for this is the resulting average Multitone ASK signal average power which is higher for the logarithmic distributed levels compared to linearly distributed levels whereas exponential distributed symbol levels result in the Multitone ASK signals with a lower average power. A comparison of 6-tone Multitone ASK signal PAPR for different distributions of information symbol levels with  $L = 4$  are shown

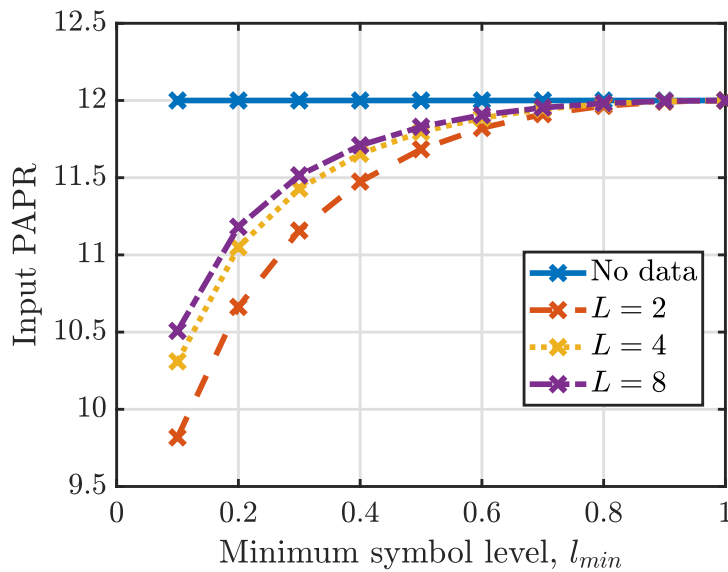


Fig. 4.9. PAPR for Multitone ASK centred around 2.45 GHz with  $N = 6$  and exponentially distributed amplitudes with variation in  $l_{min}$  for 100 multitone streams.

in Fig. 4.11. It can be seen that logarithmic amplitude level distribution is beneficial compared to linearly distributed amplitudes from WPT perspective.

However, WIT performance will be worse for logarithmically distributed levels compared to linearly distributed levels. This can be observed from the analysis of the magnitude of the obtained baseband output tones at the rectifier output when transmitted symbols levels are logarithmically distributed in Fig. 4.12, Fig. 4.13, and Fig. 4.14. Fig. 4.12 illustrates the behavior of output baseband tone  $\Delta f_1$  for the 3-tone Multitone ASK signal for  $L = 2$  and  $l_{min} = 0.1$ . As  $L = 2$ , there are only two possible symbols 0.1 and 1 which is similar to the case of linear distribution in Fig. 4.3. Therefore, for the modulation order  $L$  of 2, symbol distribution does not provide any advantage and the only way to increase the WPT performance is to increase  $l_{min}$ .

Fig. 4.13 and Fig. 4.14 shows the magnitudes of  $\Delta f_1$  and  $\Delta f_2$ , respectively, for the 3-tone Multitone ASK signal for  $L = 4$  and  $l_{min} = 0.1$ . It can be seen that the magnitude of output baseband tones gets compressed when higher symbol levels are transmitted, compared to the linear distribution case of Fig. 4.4 and Fig. 4.5. This results in lower WIT performance compared to the case of symbols' linear

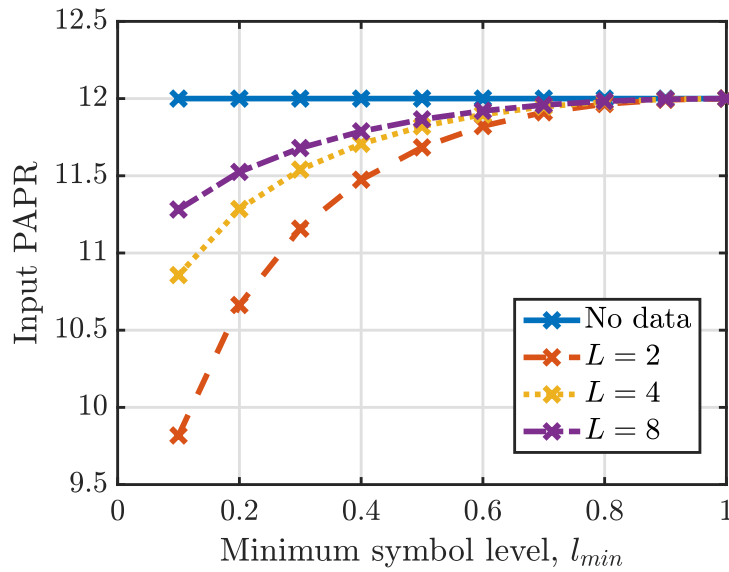


Fig. 4.10. PAPR for 6-tone Multitone ASK centred around 2.45 GHz with logarithmic amplitudes ( $gf = 10$ ) with variation in  $l_{min}$  for 100 multitone streams.

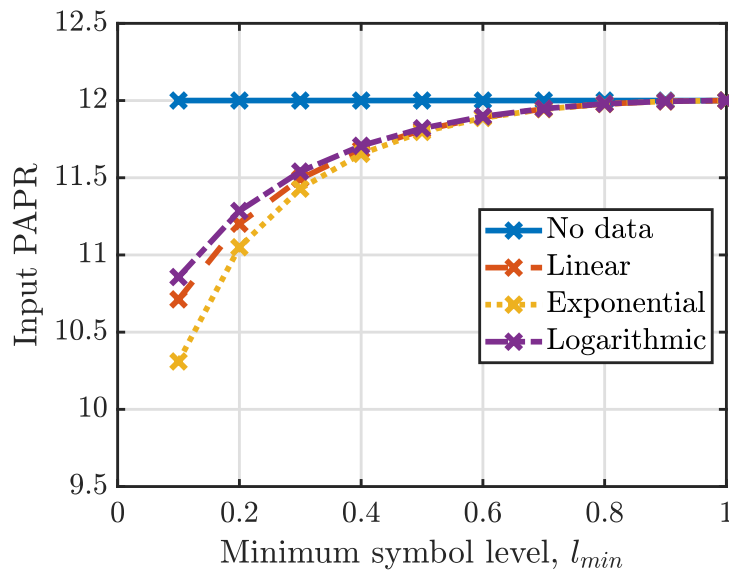


Fig. 4.11. PAPR for 6-tone Multitone ASK centered around 2.45 GHz with linearly distributed, exponentially distributed, and logarithmically distributed levels ( $gf = 10$ ) with variation in  $l_{min}$  and  $L = 4$  for 100 multitone streams.

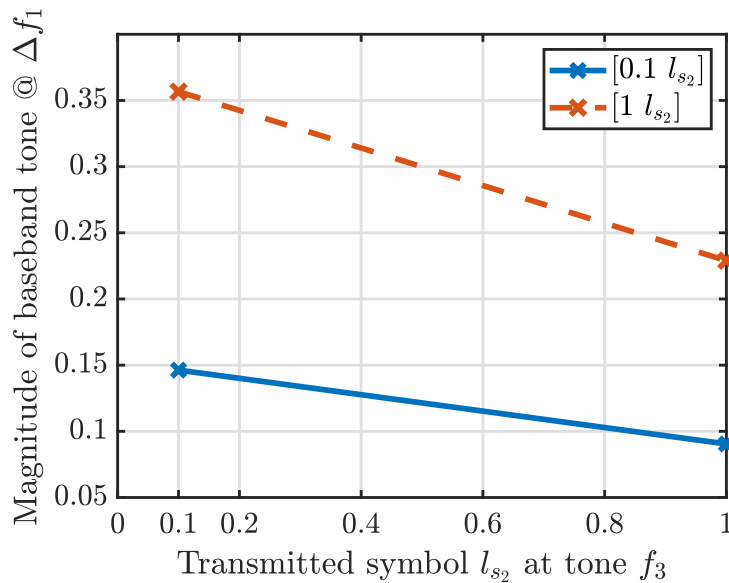


Fig. 4.12. Magnitude variation of first baseband tone ( $\Delta f_1 = 1$  MHz) for Multitone ASK centred around 2.45 GHz with  $N = 3$ ,  $L = 2$ , and  $l_{\min} = 0.1$  for different patterns of logarithmically distributed information symbol over multitone streams by varying symbol  $l_{s_2}$ .

distribution. Therefore, there exists a trade-off between WIT performance and WPT performance for the selection of the transmitted symbol distribution.

SWIPT system with desired WIT and WPT performances can be designed by an appropriate selection of minimum symbol level  $l_{\min}$  and symbol distribution. If WIT performance is of more importance, lower  $l_{\min}$  can be chosen while optimizing the symbol distribution for the required WPT performance. On the other hand, if WPT performance is of more importance, higher  $l_{\min}$  can be chosen to the maximum WPT performance of the receiver.

## 4.4 Performance Analysis of Multitone ASK

This section investigates the SWIPT performance of the designed Multitone ASK transmission scheme. To do this, the WPT and WIT performances are investigated using PCE and BER performance metrics. WPT and WIT performances of the designed Multitone ASK signal are evaluated on an information-energy rectifier-receiver model. The rectifier-receiver model consists of the input matching network

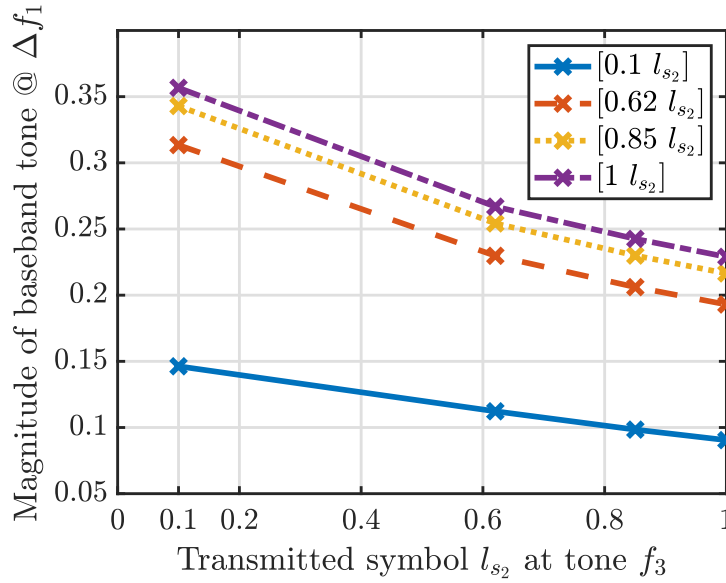


Fig. 4.13. Magnitude variation of first baseband tone ( $\Delta f_1 = 1$  MHz) for Multitone ASK centred around 2.45 GHz with  $N = 3$ ,  $L = 4$ , and  $l_{\min} = 0.1$  for different patterns of logarithmically distributed information symbol over multitone streams by varying symbol  $l_{s_2}$ .

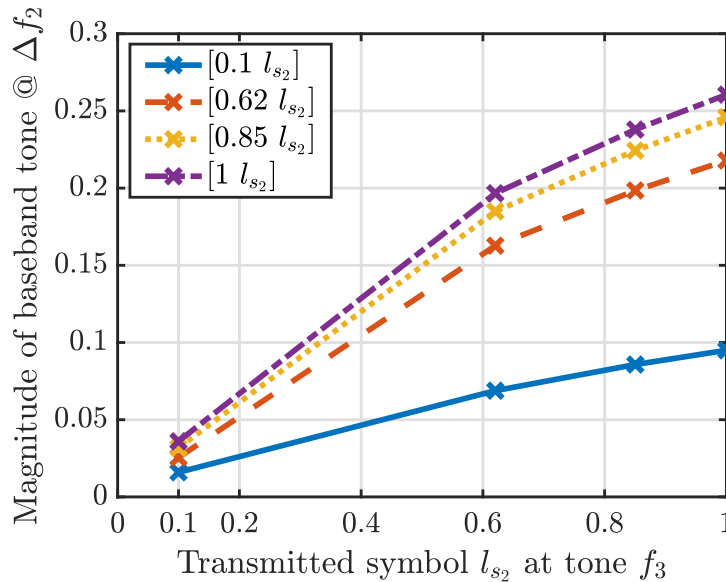


Fig. 4.14. Magnitude variation of second baseband tone ( $\Delta f_2 = 2$  MHz) for Multitone ASK centred around 2.45 GHz with  $N = 3$ ,  $L = 4$ , and  $l_{\min} = 0.1$  for different patterns of logarithmically distributed information symbol over multitone streams by varying symbol  $l_{s_2}$ .

with stubs and an input capacitance, a voltage doubler with two Skyworks SMS7630-079LF Schottky diodes, and an RC-LPF with an output capacitance and output load  $R_{\text{load}}$ . The model, implemented in Keysight ADS, corresponds to the physical design reported in [15], in which this rectifier model has been verified with measurements. In this chapter, all Multitone ASK results are obtained by interfacing MATLAB with this Keysight ADS rectifier receiver model to have simulation results close to measurements.

Multitone ASK tone frequencies are selected as discussed in [15]. For example, tone frequencies for a multitone signal centered around 2.45 GHz results in 2.446 GHz, 2.447 GHz, 2.449 GHz, and 2.453 GHz for  $N = 4$  and greatest-common-divisor  $\text{GCD} = 1$  MHz from [15]. Figure 4.15 illustrates the 4-tone Multitone ASK waveform  $x(t)$  centered around 2.45 GHz having all tones power equal and maximum for a data transfer of [1 0 1 0 1 0] at  $P_{\text{in}} = 0$  dBm. The symbol encoding is performed by gray coding for a minimal bit error [121]. Therefore, tones carry the information symbols  $l_{s_1}$ ,  $l_{s_2}$ , and  $l_{s_3}$  as the maximum [1 1 1]. In such a case, Multitone ASK carries a maximum transmitted average signal power of  $P_{\text{in}}$ . Multitone ASK waveform with transmitted symbols of maximum level  $l_{\text{max}}$  result in Fig. 4.15 regardless of the symbol distribution.

Fig. 4.16 illustrates the 4-tone Multitone ASK waveform when six information bits [0 0 0 0 0 0] are transferred over the multitone stream with  $l_{\text{min}} = 0.1$  and  $L = 4$ . As the transmitted symbols for this case are [0.1 0.1 0.1], i.e., three transmitted symbols are lowest amplitude level  $l_1 = 0.1$ , the transmitted average signal power  $P_{\text{avg}}$  is the lowest, which is also represented in (4.9) by  $P_{\text{avg,min}}$ . Fig 4.17 shows the Multitone ASK for the same [0 0 0 0 0 0] information stream with the increased minimum symbol level  $l_{\text{min}} = 0.5$ . As can be seen, it carries a higher average signal power in comparison to Fig. 4.16, which would be helpful from WPT perspective.

Further, transmitted 4-tone Multitone ASK waveform  $x(t)$  for a data transfer of [0 0 1 1 0 1] is shown in Fig. 4.18 with the corresponding  $l_{s_i}$ s as [0.1 0.7 0.4] with

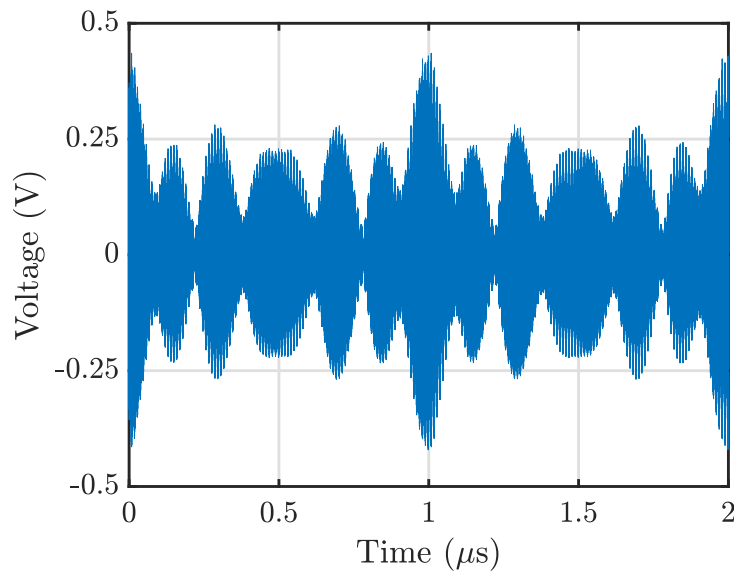


Fig. 4.15. 4-tone Multitone ASK waveform  $x(t)$  centred around 2.45 GHz having all tones power equal and maximum for a data transfer of [1 0 1 0 1 0].

$L = 4$ ,  $l_{\min} = 0.1$ , and  $P_{\text{in}} = 0$  dBm. Similarly, a Multitone ASK waveform with a larger number of tones  $N = 6$  carrying a higher number of 10 information bits [0 1 1 1 1 0 1 0 1 0] is shown in Fig. 4.19 for  $L = 4$ ,  $l_{\min} = 0.3$ , and  $P_{\text{in}} = 0$  dBm. Hundreds of such multitone streams are transmitted to evaluate WPT and WIT performances for a particular minimum symbol level  $l_{\min}$ , the number of tones  $N$ , and input power  $P_{\text{in}}$  by varying the tones' amplitudes according to the transmitted information patterns.

PCE of the obtained time-domain output waveform  $y(t)$  in terms of  $P_{\text{avg}}$ , received output dc power  $y_{\text{dc}}$ , and output load  $R_{\text{load}}$  of RC-LPF can be represented as

$$\text{PCE} = \frac{|y_{\text{dc}}|^2/R_{\text{load}}}{P_{\text{avg}}} \times 100. \quad (4.27)$$

Fig. 4.20 shows the achieved simulated PCE for 4-tone Multitone ASK transmission signals with  $L = 4$  and multiple cases of the minimum information level  $l_{\min}$  of 0.1, 0.3, 0.5, and 0.7. Here, the PCE is analyzed for 600 Multitone ASK streams, i.e., for a data transfer of 3600 bits. It can be observed that the PCE is maximum when no information is being transferred over a multitone signal, i.e., when the signal

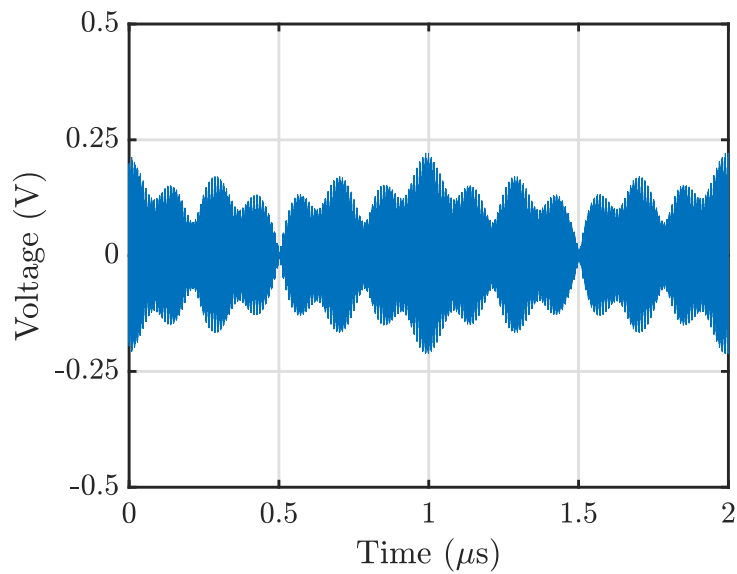


Fig. 4.16. 4-tone Multitone ASK waveform  $x(t)$  centred around 2.45 GHz for  $l_{\min} = 0.1$  and  $L = 4$  for a data transfer of  $[0\ 0\ 0\ 0\ 0\ 0]$ .

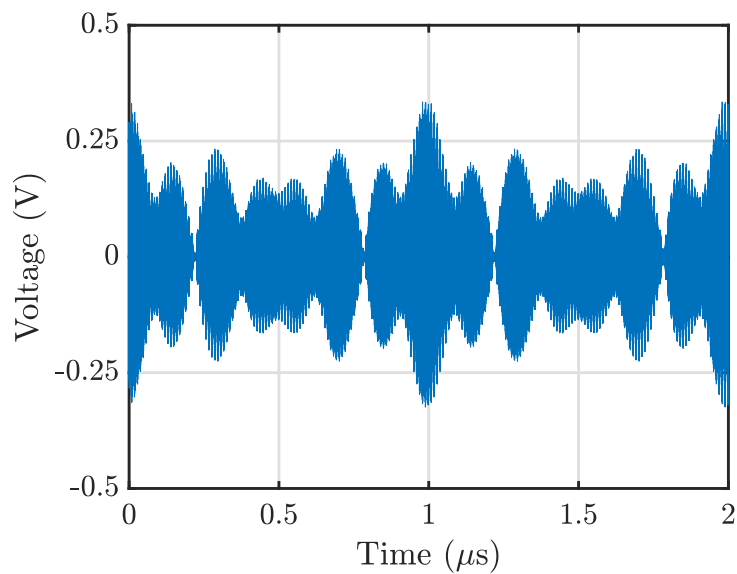


Fig. 4.17. 4-tone Multitone ASK waveform  $x(t)$  centred around 2.45 GHz for  $l_{\min} = 0.5$  and  $L = 4$  for a data transfer of  $[0\ 0\ 0\ 0\ 0\ 0]$ .

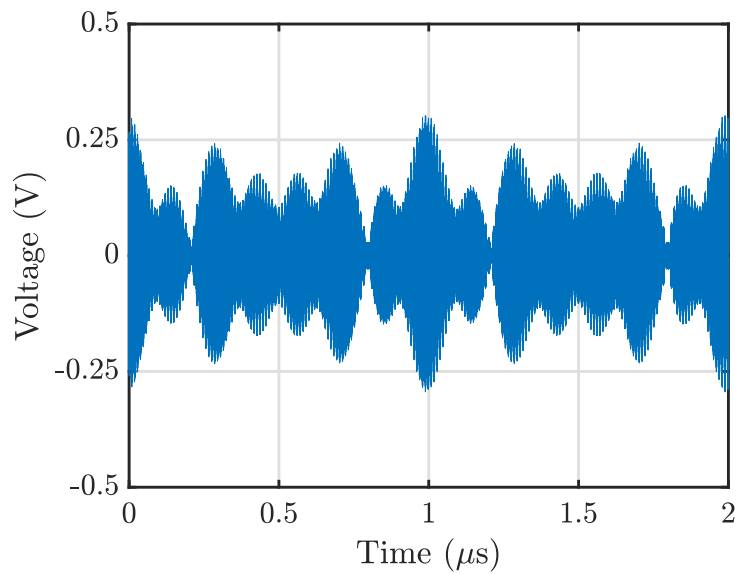


Fig. 4.18. 4-tone Multitone ASK waveform  $x(t)$  centred around 2.45 GHz for  $l_{\min} = 0.1$  and  $L = 4$  for a data transfer of  $[0\ 0\ 1\ 1\ 0\ 1]$ .

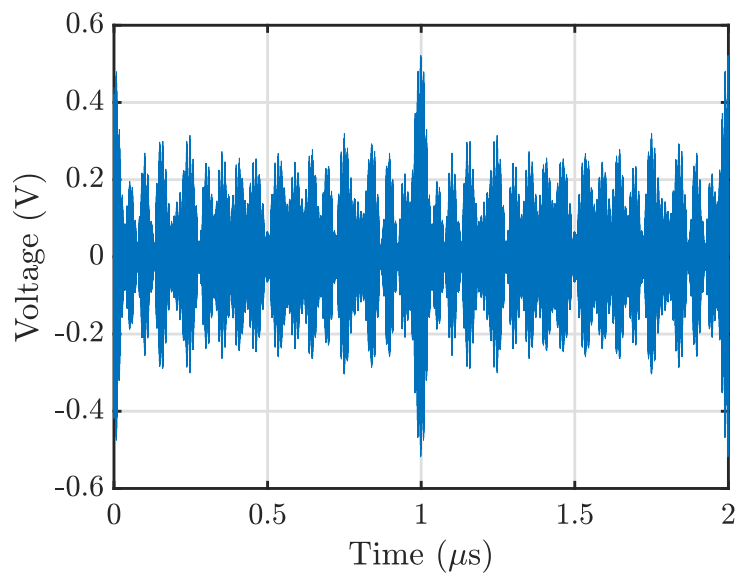


Fig. 4.19. 6-tone Multitone ASK waveform  $x(t)$  centred around 2.45 GHz for  $l_{\min} = 0.3$  and  $L = 4$  for a data transfer of  $[0\ 1\ 1\ 1\ 1\ 0\ 1\ 0\ 1\ 0]$ .

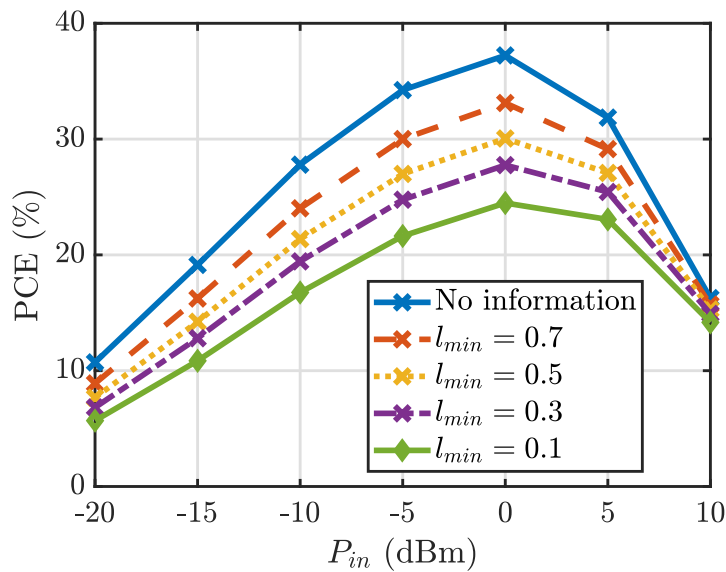


Fig. 4.20. PCE for 4-tone Multitone ASK centred around 2.45 GHz with  $L = 4$  for 600 multitone streams, i.e., 3600 bits data transfer for  $l_{min} = 0.1$ ,  $l_{min} = 0.3$ ,  $l_{min} = 0.5$ , and  $l_{min} = 0.7$ .

is solely being used for WPT transfer. The input power levels  $P_{in}$  are considered to be in the range of  $-20$  dBm to  $10$  dBm. For a 4-tone Multitone ASK with  $P_{in} = 0$  dBm, an output power of  $-4$  dBm is received when no information is being transferred. PCE further reduces with the inclusion of WIT transmission according to the selected  $l_{min}$  level. For  $P_{in} = 0$  dBm and  $l_{min} = 0.5$ , an output power of  $-4.33$  dBm is received. Therefore, a full SWIPT operation with the inclusion of WIT transfer in addition to WPT transfer reduces the overall system PCE. However, a full SWIPT communication provides an additional advantage of data transfer over the same transmitted communication signal while extracting the signal power for signal processing usages at the receiver.

From Fig. 4.20, it can be seen that as  $l_{min}$  increases from  $0.1$  to  $0.7$ , PCE increases towards the maximum attainable levels. This is due to the increment of the average signal power of the Multitone ASK signal as well as the increment in PAPR levels as discussed in Section 4.2 and Section 4.3. PCE variation for 4-tone Multitone ASK for  $L = 4$  and  $P_{in} = 0$  dBm with the increase in minimum symbol level  $l_{min}$  is also shown in Fig. 4.21 where the PCE is increasing linearly with the increase in the minimum symbol level. Therefore, the system WPT performance can be increased

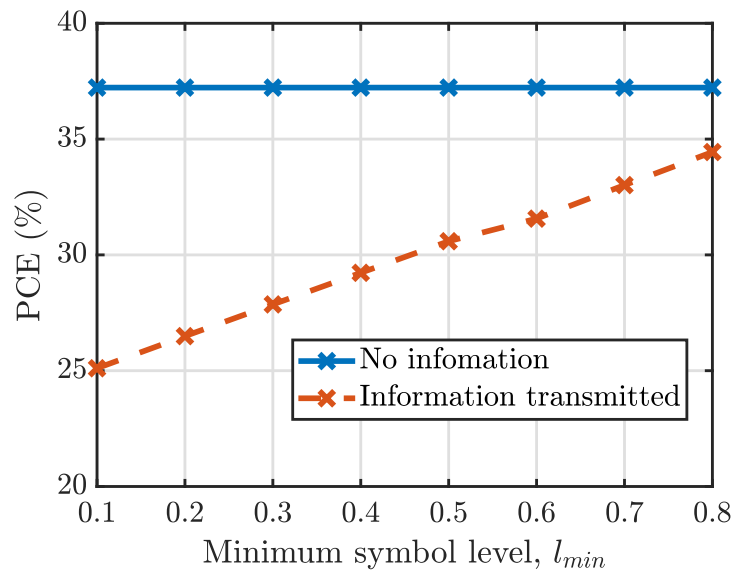


Fig. 4.21. PCE for 4-tone Multitone ASK centred around 2.45 GHz with  $L = 4$  and  $P_{in} = 0$  dBm for 600 multitone streams, i.e., 1800 symbols with the variation in  $l_{min}$ .

by choosing an increased minimum symbol level  $l_{min}$ .

The PCE for a Multitone ASK signal consisting of different numbers of tones is shown in Fig. 4.22. Multitone ASK signals with minimum symbol levels of  $l_{min} = 0.1$  and  $L = 4$  with the 600 multitone streams transmission of 3-tones, 4-tones, and 6-tones are compared. It can be observed that the PCE reduces slightly with the increase in the number of tones. This is due to the LPF at the rectifier output. With the increase in the number of tones, now the relevant baseband tones at the output lie in a wider band. Therefore, the relevant tones for Multitone ASK having a higher number of tones face higher attenuation due to the output bandwidth. PCE reduces slightly by around 2.5% from  $N = 3$  to  $N = 6$ . Therefore, to operate a Multitone ASK signal with a larger number of tones for higher throughput, it is required to design the rectifier with a larger output bandwidth.

To analyze WIT performance, the BER is calculated from the rectified output  $y(t)$ . Obtained magnitudes of relevant baseband tones are analyzed. For example, for a 4-tone Multitone ASK signal having tones at 2.446 GHz, 2.447 GHz, 2.449 GHz, and 2.453 GHz centred around 2.45 GHz, the relevant baseband tones containing the transmitted information will be present at 1 MHz, 2 MHz, and 4 MHz and for a 6-

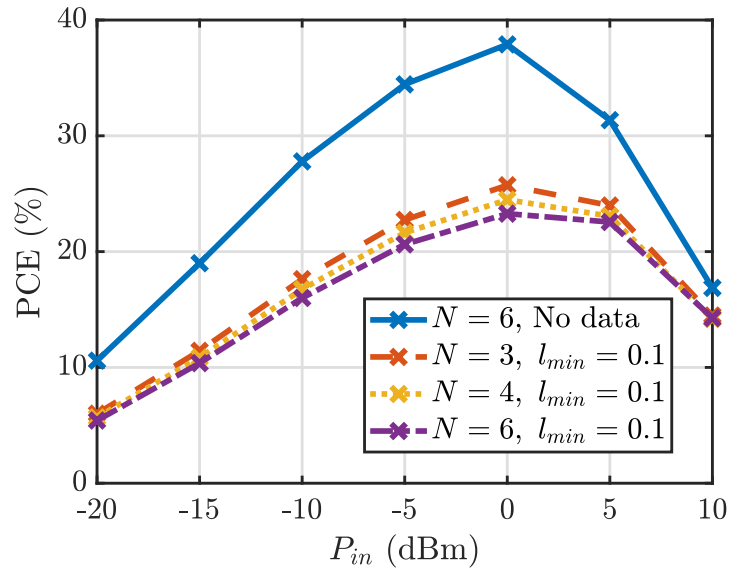


Fig. 4.22. PCE for Multitone ASK centred around 2.45 GHz with  $l_{min} = 0.1$  and  $L = 4$  for 600 multitone streams for  $N = 3$ ,  $N = 4$ , and  $N = 6$ .

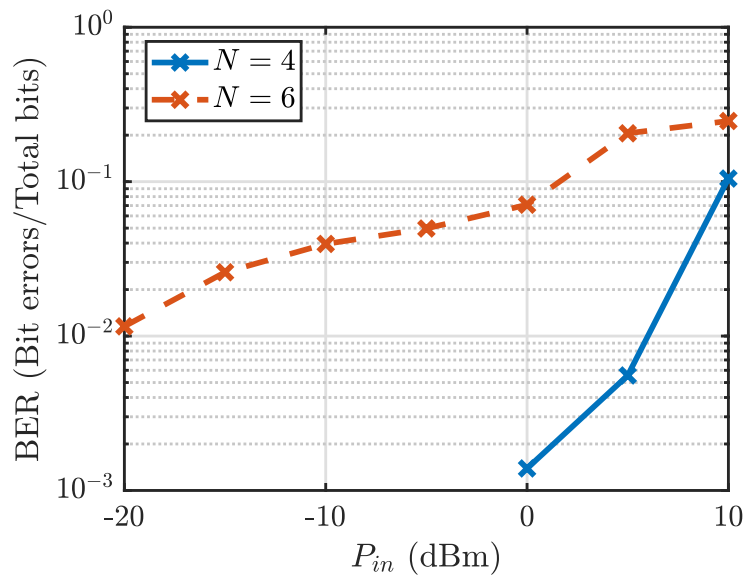


Fig. 4.23. BER for Multitone ASK centred around 2.45 GHz with  $N = 6$ ,  $l_{min} = 0.1$ , and  $L = 4$  for 600 multitone streams, i.e., 3000 symbols.

tone Multitone ASK signal, the relevant baseband tones containing the transmitted information will be present at 1 MHz, 2 MHz, 4 MHz, 5 MHz, and 8 MHz.

Fig. 4.23 illustrates the BER for a 4-tone and 6-tone Multitone ASK signals with a modulation order of  $L = 4$  and minimum symbol level  $l_{\min} = 0.1$  by transmitting hundreds of information streams. It can be seen that the BER increases with an increase in input power, and the increase in BER becomes significantly higher for power levels larger than 0 dBm. The reason for this is amplitude-to-amplitude (AM-AM) distortion due to the nonlinearity of the rectifier circuitry. However, the focus of SWIPT applications is more on lower-power regions for low-power IoT devices for which our transmission scheme works properly. To further enhance the performance, encoding schemes and pre-compensation techniques at the transmitter can be utilized.

From Fig. 4.23, it can also be observed that BER increases significantly from 4-tone Multitone ASK to 6-tone Multitone ASK. For a 4-tone signal, it is possible to have a good WIT performance with a negligible BER in the desired power region ( $P_{\text{in}} < 0$  dBm), and it increases significantly above 0 dBm. For  $N = 6$ , larger BER is observed even for lower input power regions. The reason for this is the output bandwidth of the rectifier, which distorts the now wider desired baseband tones compared to a few narrower baseband tones for Multitone ASK with a smaller number of tones.

In the chapter, the trade-off between WPT and WIT performances is discussed in terms of various parameters, such as allocated minimum symbol level  $l_{\min}$ , symbol distribution, modulation order  $L$ , number of tones  $N$ . This trade-off can be utilized according to the low-power sensor application being used. For example, if the low-power sensor is not communicating the data and is sitting idle, this time can be utilized to charge the sensor fully. In the case of Multitone ASK, this can be done by raising the minimum symbol level  $l_{\min}$ . On the other hand, if the low-power sensor is transmitting crucial data, then WIT performance is of main concern. In this case,

a lower level of  $l_{\min}$  is used. Both WPT and WIT can be achieved simultaneously. However, boundary conditions for the operation would depend upon the low-power sensor application requirements.

## 4.5 Conclusion

In this chapter, a novel Multitone ASK transmission scheme for an integrated information and energy receiver SWIPT architecture has been proposed. The main advantage is the reduction in power consumption at the receiver by removing the local oscillator, which results in overall increased power performance. Information is embedded by varying the tones' power levels of the multitone signal. The data rate is increased by transmitting  $(N - 1)$  symbols over a single  $N$ -tone Multitone ASK signal stream. The effect of varying average power of the transmitted signal with the varying information patterns is evaluated. The WPT and WIT performances of the proposed transmission scheme are analyzed in terms of PCE and BER, respectively, and a trade-off between WPT and WIT performances is discussed. WPT performance of the designed transmitted signal has been shown to improve with increasing the minimum level of the symbols, which has approached the maximum power efficiency of the designed rectifier. Although logarithmically distributed symbols have been shown to improve WPT compared to linearly distributed symbols in terms of signal PAPR due to the non-linearity of the rectifier circuitry, linearly distributed symbols result in better WIT performance. It is possible to attain a very low bit error rate with a low transmitted signal power.

Transmitting information in tones' amplitude levels offers the benefit of a simpler transmitter circuitry compared to the one required for transmitting information in tones' phases, as in the latter case, phase synchronization is more critical. Therefore, the SWIPT transmission signal scheme should be chosen depending on the present environmental conditions. In Chapter 5, a hybrid of multitone ASK and multitone PSK is utilized to further increase the information data rate.

# Chapter 5

## Multitone QAM

This chapter contributes to the design of a Multitone QAM transmission scheme for an integrated information-energy receiver, by utilizing both the amplitudes and phases of a multitone signal for carrying the information. WPT performance of the scheme is studied, and the effect of QAM constellation design on SWIPT performance is analyzed. The contributions in this chapter are based on the author’s paper [17]:

- **Perna Dhull**, Negin Shariati, Sofie Pollin, Mehran Abolhasan and Dominique Schreurs, “Multitone QAM Modulation Design for Simultaneous Wireless Information and Power Transfer,” *IEEE Access*, 2024, doi: [10.1109/ACCESS.2024.3520104](https://doi.org/10.1109/ACCESS.2024.3520104) (early access).

### 5.1 Introduction

The applications of the Internet of Things (IoT) with enhanced sensing capabilities have been expanding to a diverse range of domains such as agriculture, smart cities, transportation, wearable devices, and homes [4]. The rapid surge of IoT devices has raised the challenge of periodically charging/replacing batteries. Far-field radio-frequency (RF) wireless power transfer (WPT) offers a promising solution for reducing the reliance of sensors on batteries [133]. Simultaneous wireless informa-

tion and power transfer (SWIPT) integrates far-field WPT with wireless information transfer (WIT) and provides an energy-efficient solution by exploiting the same communication signal for power transfer earlier used for data transfer solely [18, 110].

In the integrated SWIPT architecture, conventional communication signals are not possible to be used for information decoding after rectification through diodes. Therefore, new communication signals need to be proposed for an integrated reception of power and information at the rectifier output. Research has been conducted to improve the rectifier's power conversion efficiency (PCE) [21, 115]. It has been shown that due to the non-linearity introduced by the rectifier, the rectifier output DC power is not only a function of received signal power and rectenna design but also is a function of the received signal's shape [38, 42, 120]. High peak-to-average-power ratio (PAPR) waveforms have been shown to exploit this non-linearity to improve the harvested DC power [37, 134].

A single-tone modulation signal for integrated architecture is introduced in [12], where information symbols are transmitted with different energy levels through a rectifier. Pulse-position modulation for integrated receivers has been introduced in [120]. In [78, 82], the authors present methods which utilize multitone signals for higher PAPR. Information symbols are transmitted by varying the number of tones and frequency spacing between tones based on the transmitted information, which results in varying signal PAPR. A two-dimensional signaling scheme with subcarrier number component and amplitude component is introduced in [86], where information is transmitted in signal PAPR variation due to varying numbers of subcarriers and amplitudes of subcarriers.

An amplitude-based biased-ASK is introduced where a minimum non-zero amplitude is transmitted to avoid periods of zero energy harvesting [84]. A dual ASK scheme for a double half-wave rectifier is proposed, having a higher degree of freedom for signal amplitudes' constellation range, increasing the information rate [89]. Recently, a customized on-off keying scheme for Terahertz imaging with simultane-

ous information and power transfer with the help of an integrated receiver has been proposed in [135]. However, a single-tone communication signal does not benefit the high PAPR signals for improved energy harvesting. A modulation technique that uses a multitone signal is introduced in [88] where a model of embedding information in the ratios of the amplitudes of the different tones is proposed rather than in the amplitudes directly. Although it offers the advantage of making the system less dependent on transmission distance, the drawback of this technique is that it is not suitable for more than a three-tone signal.

Amplitude variations impose a limit on achievable WPT due to the presence of ripples in the output voltage that degrade the WPT performance [84, 88, 136]. Multitone FSK has been introduced in [90, 92] where information symbols are transmitted through rectifier by varying frequency spacings among tones, and a Fast Fourier transform (FFT) is used for information decoding. A Multitone PSK modulation technique is introduced in [15] where tones's phases are used for transmitting multiple symbols over a single multitone transmission. It is shown that for Multitone PSK, the output PCE does not vary much with information transmission as was the case with amplitude-based schemes.

Although Multitone PSK offers the advantage of minimizing the effect of information transfer over the SWIPT system's power performance compared to amplitude-based schemes, amplitude-based schemes are beneficial in the case of a noisy channel [130–132]. Till now, either the multitone signal amplitudes or only the multitone signal phases have been exploited for information transfer through integrated receiver architecture. An ideal waveform for a SWIPT system would entail minimal variations in the envelope, with the stream of information symbols having an approximately stable WPT while also having a good data transfer rate. Therefore, a higher data rate can be achieved by the simultaneous usage of both amplitudes and phases of the multitone signal for information transfer.

This chapter presents the design of a novel multitone quadrature amplitude modu-

lation (QAM) transmission scheme utilizing multitone signal's amplitudes, phases, and number of tones for the integrated information-energy SWIPT receiver architecture. Both amplitudes and phases of tones are utilized for information transmission. Power transfer and data reception are performed from the same rectified output signal. The impact of QAM symbol constellation on the PAPR of the designed multitone waveform is studied. Further, a redesign of QAM symbol constellations for a more stable output PCE is proposed to minimize the difference between the achievable PCE of the rectifier for different transferred symbols. In particular, asymmetric expanded QAM constellation and asymmetric compressed QAM constellation are proposed to allow trade-offs of application-specific demands such as power demands, symbol error rate, and data rate. Further, probabilities of transmission probabilities of inner symbols and outer symbols can be varied to enhance the performance.

Multitone QAM offers the advantage of a higher degree of freedom to optimize PCE, information rate, and symbol error rate by utilizing amplitudes, phases, and number of tones. It is possible to transmit  $(N - 1)$  symbols over a single stream of an  $N$ -tone Multitone QAM signal resulting in an OFDM-type communication with non-uniform frequency spacings for the integrated information-energy receiver where RF to baseband conversion is performed with a simple rectifier circuitry, removing the need for a local oscillator at the receiver. It is shown that due to the non-linearity of the rectifier, it is important to redesign the QAM constellation according to the application-specific requirements, such as whether a higher level of minimum continuous power transfer is critical or if a high-power transfer in short bursts is preferred for the SWIPT's operation.

This chapter is organized as follows. Section 5.2 introduces the theoretical design of a multitone QAM signal and analyses the effect of symbol constellation over the resulting PAPR of the designed waveform. Next, section 5.3.1 discusses the proposed redesigned asymmetric QAM constellations. Then, the performance of the proposed multitone QAM signal and proposed asymmetric QAM constellation designs are analysed in Section 5.4. In the end, a conclusion is drawn in Section 5.5.

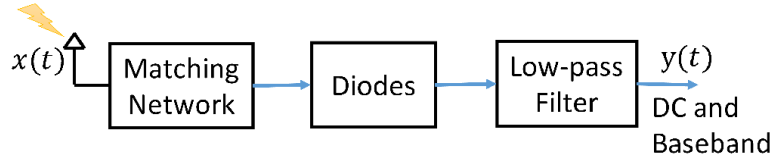


Fig. 5.1. Integrated information-energy receiver rectifier for SWIPT.

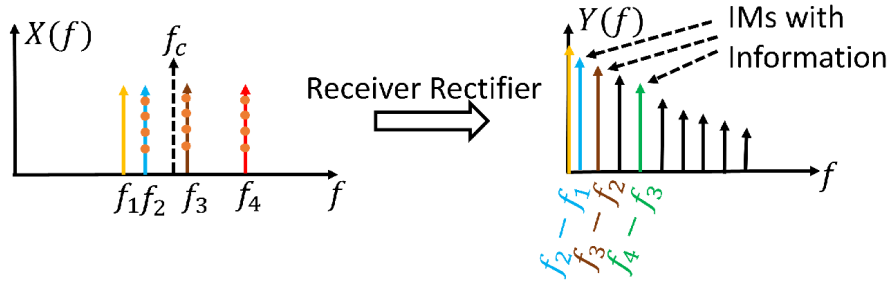


Fig. 5.2. Four-tone multitone QAM RF signal frequency spectrum  $X(f)$  centered around frequency  $f_c = 2.45$  GHz and rectified baseband output spectrum  $Y(f)$  consisting of dc, IM frequency tones used for information decoding (colored), and extra IM components (black).

## 5.2 Signal Model

The integrated rectifier-receiver illustrated in Fig. 5.1 consisting of an input matching network, rectifier diodes, and a resistance-capacitance (RC)-low-pass filter (LPF) is utilized for both WPT and WIT simultaneously. Multitone QAM signal  $x(t)$  is designed using an  $N$ -tone multitone signal and modifying the tones' amplitudes and phases according to the transmitted QAM information symbols.  $x(t)$  is designed around the center frequency  $f_c$  of 2.45 GHz. The received signal  $x(t)$  is passed through the rectifier, and subsequently, the baseband rectified signal output  $y(t)$  is used for both power transfer and information decoding.

### 5.2.1 Signal Design

An  $N$ -tone reference signal  $r(t)$  with an average power of  $P_{\text{in}}$  is considered as

$$r(t) = \text{Re} \left\{ \sum_{n=1}^N \sqrt{\frac{2P_{\text{in}}}{N}} e^{j(2\pi f_n t)} \right\}. \quad (5.1)$$

$(N - 1)$  information symbols are transmitted over an  $N$ -tone multitone QAM signal. The  $N$ -tones multitone signal with non-uniform frequency spacings is used to utilize the non-linearity of the rectifier. QAM information is transmitted in amplitudes and phases of the tones of the multitone signal  $r(t)$ . The transmitted multitone QAM signal  $x(t)$  after modifying the tones' amplitudes and phases of  $r(t)$  in (5.1) according to the transmitted information, can be represented as

$$x(t) = \text{Re} \left\{ \sum_{n=1}^N \sqrt{\frac{2|s_{n-1}|P_{\text{in}}}{N|s|_{\text{max}}}} e^{j(2\pi f_n t + \phi_n)} \right\} \quad (5.2)$$

where each  $n^{\text{th}}$  tone of  $r(t)$  has been modified to include the transmitted information symbol  $s_{n-1}$ .  $|s|_{\text{max}}$  represents the maximum available magnitude among  $M$  information symbols, i.e.,  $|s_{\sqrt{M}, \sqrt{M}}|$ . The first tone is considered constant, with  $s_0$  being 1. In this way,  $(N - 1)$  symbols are transmitted over a single multitone transmission. Information symbols  $s_n$  are selected from the available information set  $\mathbf{S}$  of  $M$  QAM symbols for the modulation order of  $M$ . The  $M$  information symbols can be represented as

$$s_{i,k} = |s_{i,k}| e^{j\phi_{i,k}}, \quad \forall i, k = \{1, 2, \dots, \sqrt{M}\}. \quad (5.3)$$

Information is transmitted through the amplitudes and phases of the tones of the multitone QAM signal as represented in (5.2).  $(N - 1)$  information symbols are transmitted with a single stream of  $N$ -tone multitone QAM signal. For each  $n^{\text{th}}$  tone,  $s_{n-1}$  and  $\phi_n$  of (5.2) are modified according to the chosen transmitted information symbol  $s_{i,k}$  from set  $\mathbf{S}$  of (5.3).

The spectra of the multitone QAM signal  $X(f)$  and the rectified baseband output signal  $Y(f)$  are shown in Fig. 5.2. The essence is a block of  $N$  tones with non-uniform frequency spacing so that the intermodulation frequencies of the different tones can be found at different frequencies.  $N$ -tones multitone QAM signal is designed to carry  $(N - 1)$  information symbols. The information is transmitted through both the tones' amplitudes and phases. The non-linearity of the rectifier is utilized to extract

the transmitted information from the baseband signal  $y(t)$  at the rectifier output. Due to the non-linearity of the rectifier, an  $N$ -tone multitone signal, after passing through the rectifier, produces a baseband signal that includes intermodulation (IM) frequency components of various orders, resulting from the mixing of the different tones in the multitone QAM signal [137]. These IM frequency components result in ripple voltage at the rectifier output in addition to the required output DC.

Although the presence of ripple voltage is not efficient for wireless power transfer, these ripples can be used for wireless information transfer and decoding through the same rectifier-receiver, lowering the power consumption for signal processing at the receiver. Therefore, the rectifier's non-linearity is exploited to bring the information down to the baseband at the receiver. The signal is designed so that the information resides in the intermodulation products present at baseband frequencies in the output of the integrated rectifier-receiver.

Among IM frequency components of various orders produced at the rectifier output due to mixing among the tones of the multitone QAM signal, the second-order intermodulation ( $IM_2$ ) frequency components dominate at the receiver output compared to higher-order IM components [51]. The second-order IM frequency components are the result of mixing between two tones of a multitone QAM signal. In our work, we encode information in a multitone QAM signal in such a way that information at the rectifier output would be extracted from the  $IM_2$  frequency components between consecutive frequency tones. For this, multitone QAM signal tones' frequencies are designed in such a way that these desired  $IM_2$  do not overlap with each other. Hence, Algorithm 1 of [15] is used to design such an unequal-spaced multitone signal.

The rectified baseband output  $y(t)$  consists of dc and several intermodulation frequency components due to the rectifier's non-linearity. However, all the odd order  $3^{rd}$  order,  $5^{th}$  order,  $\dots$ , etc., intermodulation frequency components lie in the GHz frequency range, and all the even order  $4^{th}$  order,  $6^{th}$  order,  $\dots$ , etc., intermodulation frequency components lie in the baseband frequency range. All the odd-order

intermodulation frequency components are filtered out by the LPF, and  $y(t)$  consists of only dc and even-order intermodulation frequency components. Therefore, as a result of LPF after diodes at the output,  $y(t)$  results in a baseband signal consisting of only dc and intermodulation frequency components in the MHz frequency range. Furthermore, second-order IM frequency components dominate among these even-order intermodulation frequency components [51].

For example, from (5.2),  $x(t)$  for a three-tone signal can be represented by

$$x(t) = \sqrt{\frac{2|s_0|P_{\text{in}}}{N|s|_{\text{max}}}} \cos(2\pi f_1 t + \phi_0) + \sqrt{\frac{2|s_1|P_{\text{in}}}{N|s|_{\text{max}}}} \cos(2\pi f_2 t + \phi_1) + \sqrt{\frac{2|s_2|P_{\text{in}}}{N|s|_{\text{max}}}} \cos(2\pi f_3 t + \phi_2) \quad (5.4)$$

The signal (5.4) after passing through the rectifier results in rectified baseband signal  $y(t)$  consisting of dc and three second-order IM frequency components among tones as

$$y(t) \propto \text{dc} + \sqrt{|s_0||s_1|} \frac{2P_{\text{in}}}{N|s|_{\text{max}}} \cos(2\pi(f_2 - f_1)t + \phi_1 - \phi_0) + \sqrt{|s_1||s_2|} \frac{2P_{\text{in}}}{N|s|_{\text{max}}} \cos(2\pi(f_3 - f_2)t + \phi_2 - \phi_1) + \sqrt{|s_0||s_2|} \frac{2P_{\text{in}}}{N|s|_{\text{max}}} \cos(2\pi(f_3 - f_1)t + \phi_2 - \phi_0) \quad (5.5)$$

Here,  $(N - 1)$  information symbols are considered to be transmitted over an  $N$ -tone multitone signal. The first tone  $f_1$  is assumed to be transmitted with a constant amplitude of  $\sqrt{2P_{\text{in}}/N}$  and phase  $0^\circ$ , i.e.,  $|s_0| = 1$  and  $\phi_0 = 0^\circ$ . The multitone signal is designed in such a way that  $(N - 1)$  intermodulation baseband tones as a result of consecutive frequency tones would consist of  $(N - 1)$  information symbols at the rectifier output, i.e.,  $(f_2 - f_1)$ ,  $(f_3 - f_2)$ ,  $\dots$ ,  $(f_N - f_{N-1})$  baseband tones amplitudes would carry the information as shown in Fig. 5.2. A 4-tone multitone signal is depicted in Fig. 5.2 with the first tone having constant amplitude and phase, and three information symbols from the available symbol set  $\mathbf{S}$  are transmitted over

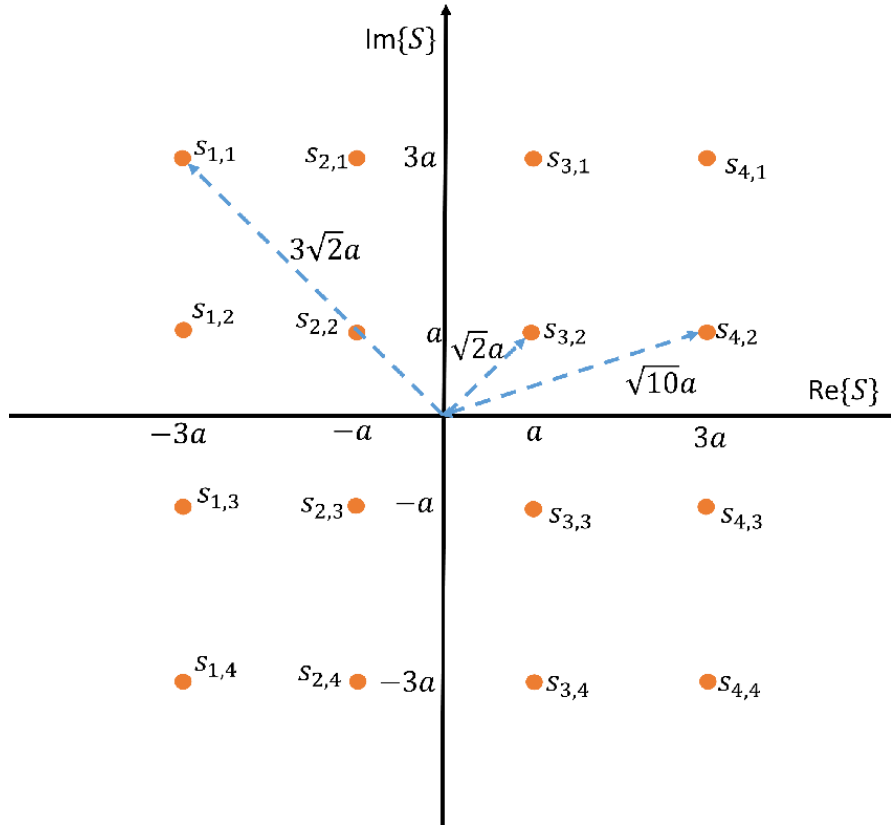


Fig. 5.3. Symbol constellation for multitone QAM with modulation order of  $M = 16$ .

the other three tones of  $x(t)$ . SWIPT is achieved at the output by both WIT and WPT from the same rectified signal. The whole output baseband signal is utilized for power transfer, whereas three information symbols are decoded by analysing the three relevant baseband tones  $(f_2 - f_1)$ ,  $(f_3 - f_2)$ , and  $(f_4 - f_3)$ ' magnitudes and phases as shown in Fig. 5.2.

To ensure that the  $(N - 1)$  desired baseband tones at the rectifier output are distinct, the  $N$ -tone multitone signal is designed so that the second-order intermodulation  $\text{IM}_2$  frequency components between consecutive tones do not overlap. Specifically, the baseband tones  $(f_2 - f_1)$ ,  $(f_3 - f_2)$ ,  $\dots$   $(f_N - f_{N-1})$  should be distinct from one another and also these  $(N - 1)$  baseband tones should not coincide with any other non-consecutive  $\text{IM}_2$ s. Therefore, to make SWIPT feasible with only a rectifier-receiver, the  $N$ -tone multitone signal does not consist of equally spaced tones around the central frequency of 2.45 GHz and needs to have unequal frequency spacings between tones. We proposed an algorithm to design this frequency spacing in [15].

Here, Algorithm 1 from [15] is used to define the tone frequencies of the multitone QAM signal.

QAM constellation for a modulation order of  $M = 16$  is shown in Fig. 5.3.  $M$ -ary QAM can be considered as a combination of two  $\sqrt{M}$ -ary Pulse Amplitude Modulation (PAM) with a quadrature phase difference between them [121]. Let  $b_i$  denote the PAM constellation with  $\sqrt{M}$  symbols represented as

$$b_i = -(\sqrt{M} - 1) + (i - 1)\frac{\sqrt{M}}{2}, \quad \forall i = \{1, 2, \dots, \sqrt{M}\}. \quad (5.6)$$

Then, the QAM symbols can be represented as a combination of two PAM symbols constellations as

$$s_{i,k} = b_i + jb_k, \quad \forall i, k = \{1, 2, \dots, \sqrt{M}\} \quad (5.7)$$

resulting in  $M$  symbols and depicted in Fig. 5.3. Further, QAM symbols are normalized with respect to the maximum available magnitude of symbols  $|s_{\sqrt{M},\sqrt{M}}|$  and can be represented as

$$s_{i,k} = \frac{b_i + jb_k}{|s_{\sqrt{M},\sqrt{M}}|} = \frac{b_i + jb_k}{\sqrt{b_{\sqrt{M}}^2 + j^2 b_{\sqrt{M}}^2}}, \quad \forall i, k = \{1, 2, \dots, \sqrt{M}\}. \quad (5.8)$$

After normalization, the maximum available magnitude among  $M$  information symbols  $s_{\sqrt{M},\sqrt{M}}$  would be 1 in all symbol constellations.  $(N - 1)$  symbols in (5.2) are chosen from the available normalized information symbol set ( $\mathcal{S}$ ) in (5.8) consisting of  $M$  symbols  $s_{1,1}, s_{1,2}, \dots, s_{\sqrt{M},\sqrt{M}}$ .

### 5.2.2 PAPR Analysis

In the proposed multitone QAM transmission scheme, the reference multitone signal  $r(t)$  is modified to multitone QAM signal  $x(t)$  by varying the tones' amplitudes and phases as in (5.2) to make the WIT possible in addition to WPT. The resulting average power of the transmitted SWIPT signal,  $P_{\text{avg}}$ , after embedding information becomes lower than  $P_{\text{in}}$ , i.e.,  $P_{\text{avg}} \leq P_{\text{in}}$ . Therefore, it is important to analyze the

effect of WIT with QAM symbols on the WPT performance of the SWIPT system. Here, PAPR is considered as a figure of merit for evaluating WPT performance as high PAPR waveforms result in higher harvested energy [42]. For electronics systems designed only for WPT,  $r(t)$  would achieve maximum PAPR and the corresponding maximum PCE as no information is being transmitted. However, it is necessary to compromise a little with the WPT performance to design signals for SWIPT systems for additional usage of resources. The channel is considered ideal, i.e., there is no signal distortion between transmitter and receiver, and the performance of the designed signal  $x(t)$  is analysed.

PAPR for a signal  $x(t)$  can be represented by

$$\text{PAPR} = \frac{P_{\text{peak}}}{P_{\text{avg}}} = \frac{\max\{|x(t)|^2\}}{\frac{1}{T} \int_{-T/2}^{T/2} x^2(t) dt}, \quad (5.9)$$

where  $T$  denotes the time-period of waveform  $x(t)$ . The peak power of a multitone QAM signal in (5.2) can be represented as

$$P_{\text{peak}} = \frac{2P_{\text{in}}}{N} \left| 1 + \sqrt{\frac{|s_1|}{|s_{\sqrt{M},\sqrt{M}}|}} \cos \phi_1 + \cdots + \sqrt{\frac{|s_{N-1}|}{|s_{\sqrt{M},\sqrt{M}}|}} \cos \phi_{N-1} \right|^2. \quad (5.10)$$

The average power of multitone QAM signal,  $P_{\text{avg}}$ , can be represented as

$$P_{\text{avg}} = \frac{P_{\text{in}}}{N} \left( 1 + \frac{|s_1|}{|s_{\sqrt{M},\sqrt{M}}|} + \cdots + \frac{|s_{N-1}|}{|s_{\sqrt{M},\sqrt{M}}|} \right). \quad (5.11)$$

Therefore, from (5.9), (5.10), and (5.11), the PAPR for the multitone QAM signal  $x(t)$  in terms of  $(N - 1)$  transmitted symbols can be represented as

$$\text{PAPR} = \frac{2 \left| \sqrt{|s_{\sqrt{M},\sqrt{M}}|} + \sqrt{|s_1|} \cos \phi_1 + \cdots + \sqrt{|s_{N-1}|} \cos \phi_{N-1} \right|^2}{|s_{\sqrt{M},\sqrt{M}}| + |s_1| + |s_2| + \cdots + |s_{N-1}|}. \quad (5.12)$$

The mean PAPR across the multitone signal streams with QAM streams can be

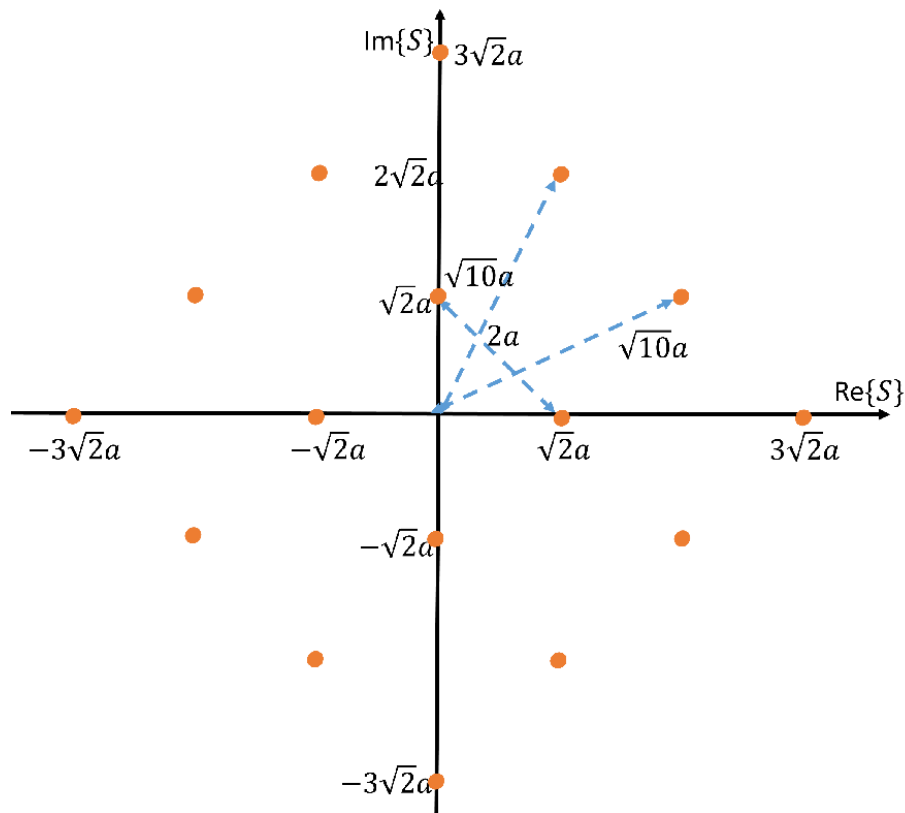


Fig. 5.4. Rotated symbols constellations for QAM multitone for a modulation order of  $M = 16$  with a phase shift of  $45^\circ$ .

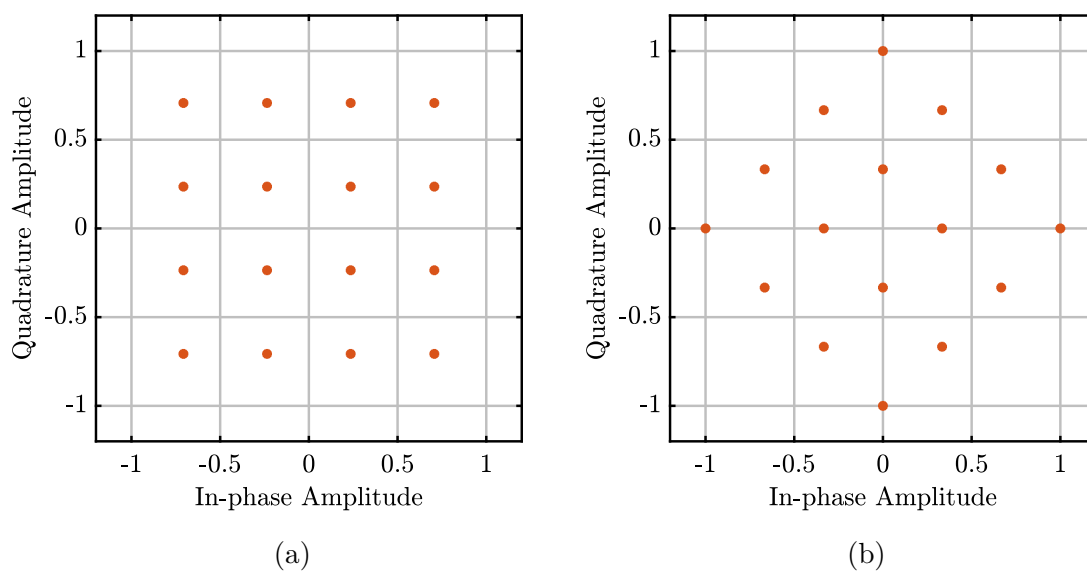


Fig. 5.5. Normalized symbols constellations for  $M = 16$  QAM (a) conventional and (b) with phase rotation of  $45^\circ$ .

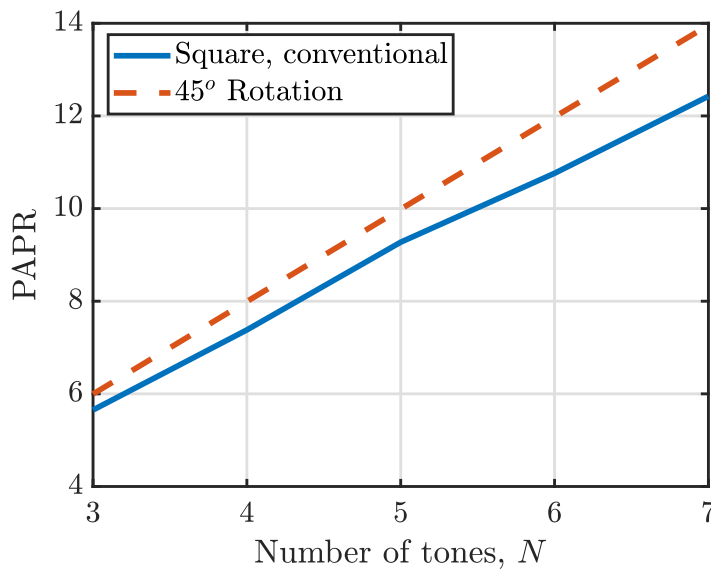


Fig. 5.6. Multitone QAM signal PAPR with conventional QAM symbols constellation and the QAM symbols constellation rotated with  $45^\circ$ .

represented as

$$\text{PAPR}|_{\text{mean}} = \frac{2 \left| \sqrt{|s|_{\max}} \cos \phi_1 + \left( \frac{N-1}{M} \right) \sum_{i=1}^M \sqrt{|s_i|} \cos \phi_i \right|^2}{|s|_{\max} + \left( \frac{N-1}{M} \right) \sum_{i=1}^M |s_i|}. \quad (5.13)$$

It can be seen that the effect of symbol phases, in addition to symbol magnitudes, also plays a role in determining the signal PAPR. It is well known that multitone signals with tones' phases zero result in the highest PAPR [13]. Therefore, symbol constellations can be modified to maximize the multitone QAM signal PAPR. Fig. 5.4 illustrates a rotated symbol constellation for the 16-QAM symbol in Fig. 5.3 such that now, symbols with maximum magnitudes have zero phases. The average symbol energy remains the same as the rotation of symbols does not change the overall average symbols energy [121]. Fig. 5.5(a) and Fig. 5.5(b) illustrate the normalized 16-QAM constellation without and with phase rotation, respectively.

Variation in PAPR of transmitted waveform  $x(t)$  with the number of tones  $N$  is illustrated in Fig. 5.6. It can be seen that with the phase shifting of the symbols' constellation, it is possible to achieve the maximum possible PAPR of  $2N$  for the transmission of symbols carrying the highest energy. Therefore, by modifying only

the phases of the symbols constellation, PAPR improves. However, the magnitudes of individual symbols remain the same. For further improvement in signal PAPR and in-turn output PCE, it is necessary to observe the effect of variations in symbols' magnitudes.

### 5.3 Asymmetric QAM Constellation

In SWIPT communication, WPT performance is reduced because of the simultaneous WIT transfer. Due to information transfer over the same signal for SWIPT, the overall average power of the signal stream varies and the PCE at the output is lower compared to the achievable PCE for the case of a solely WPT. Therefore, it becomes important to look for ways to maximize the output PCE while having simultaneous information symbols transmission.

Conventional QAM symbols constellation and the rotated QAM constellation discussed in the previous section, are symmetric in magnitude and do not consider the non-linearity of the rectifier. Such symmetric symbol constellations do not perform efficiently for power delivery at the rectifier output due to the non-linearity of the rectifier. Therefore, asymmetric QAM constellations need to be designed to achieve maximum PCE while simultaneously having good information detection at the rectifier output.

#### 5.3.1 QAM Constellation Redesign

To design an asymmetric  $\sqrt{M}$ -PAM constellation  $\mathbf{B}_{\text{asym},\sqrt{M}}$  from a symmetric  $\sqrt{M}$ -PAM constellation  $\mathbf{B}_{\sqrt{M}}$ , a multiplication factor  $\Delta\mathbf{B}_{\sqrt{M}}$  is evaluated. Let  $\mathbf{B}_{\sqrt{M}}$  be a square  $\sqrt{M} \times \sqrt{M}$  matrix having the symmetric  $\sqrt{M}$ -PAM constellation symbols

from (5.6) and  $\mathbf{B}_{\sqrt{M}}$  can be represented as

$$\mathbf{B}_{\sqrt{M}} = \begin{bmatrix} b_1 & 0 & 0 & \cdots & 0 \\ 0 & b_2 & 0 & \cdots & 0 \\ 0 & 0 & b_3 & \cdots & 0 \\ \vdots & \vdots & \vdots & \ddots & \vdots \\ 0 & 0 & 0 & \cdots & b_{\sqrt{M}} \end{bmatrix}. \quad (5.14)$$

Let  $\alpha$  and  $\beta$  be considered as parameters to convert the symmetric symbol constellation to an asymmetric constellation.  $\alpha$  is considered to redesign the  $M/4$  inner constellation points for QAM, i.e.,  $s_{2,2}$ ,  $s_{2,3}$ ,  $s_{3,2}$ , and  $s_{3,3}$  for  $M = 16$  whereas  $\beta$  is considered to redesign the remaining  $3M/4$  outer constellation points to result in an overall asymmetric QAM symbol constellation. Let  $\alpha_{\sqrt{M}}$  be a  $\frac{\sqrt{M}}{2} \times 1$  column vector consisting of the parameter  $\alpha$  as

$$\alpha_{\sqrt{M}} = \begin{bmatrix} \alpha \\ \alpha \\ \vdots \\ \alpha \end{bmatrix} \quad (5.15)$$

and  $\beta_{\sqrt{M}}$  be a  $\frac{\sqrt{M}}{4} \times 1$  column vector consisting of the parameter  $\beta$  as

$$\beta_{\sqrt{M}} = \begin{bmatrix} \beta \\ \beta \\ \vdots \\ \beta \end{bmatrix}. \quad (5.16)$$

Then the  $\sqrt{M} \times 1$  column vector  $\Delta \mathbf{B}_{\sqrt{M}}$  can be used for designing asymmetric  $\sqrt{M}$ -PAM constellation and by (5.15) and (5.16), can be defined as

$$\Delta \mathbf{B}_{\sqrt{M}} = \begin{bmatrix} \beta_{\sqrt{M}} \\ \alpha_{\sqrt{M}} \\ \beta_{\sqrt{M}} \end{bmatrix}. \quad (5.17)$$

From (5.14) and (5.17), the redesigned asymmetric  $\sqrt{M}$ -PAM constellation can be obtained as

$$\mathbf{B}_{\text{asym}, \sqrt{M}} = \mathbf{B}_{\sqrt{M}} \times \Delta \mathbf{B}_{\sqrt{M}}. \quad (5.18)$$

Further,  $\sqrt{M}$ -PAM constellation in (5.18) can be used to design asymmetric QAM symbol constellation.

### 5.3.2 Expanded Multitone QAM symbols constellations

$\alpha$  modifies the  $M/4$  inner symbols and  $\beta$  modifies the  $3M/4$  outer symbols. In the case of the increased symbol energy for outer symbols,  $\beta$  needs to be greater than 1. For this,  $\alpha$  would be lower than 1 considering the same overall average symbol energy. The resulting modified symbol constellation would be expanded compared to the conventional QAM constellation. Here, all symbol phases are considered the same as the conventional constellation without redesign.

Let  $\alpha_e$  and  $\beta_e$  be the modified parameters for expanded constellation symbols i.e., the increased maximum available energy of the outer symbols. For  $\alpha_e \leq 1$ ,  $\beta_e$  for a modified symbol constellation with the same average symbol energy can be represented as

$$\beta_e = \frac{4 + 2\sqrt{5} + \alpha_e}{3 + 2\sqrt{5}}. \quad (5.19)$$

Fig. 5.7(a) illustrates a modified expanded constellation where inner  $M/4$  symbols are compressed and outer  $3M/4$  outer symbols are expanded.

Multitone QAM symbol constellations with  $M = 16$  for different cases of  $\alpha_e = 0.9$ ,

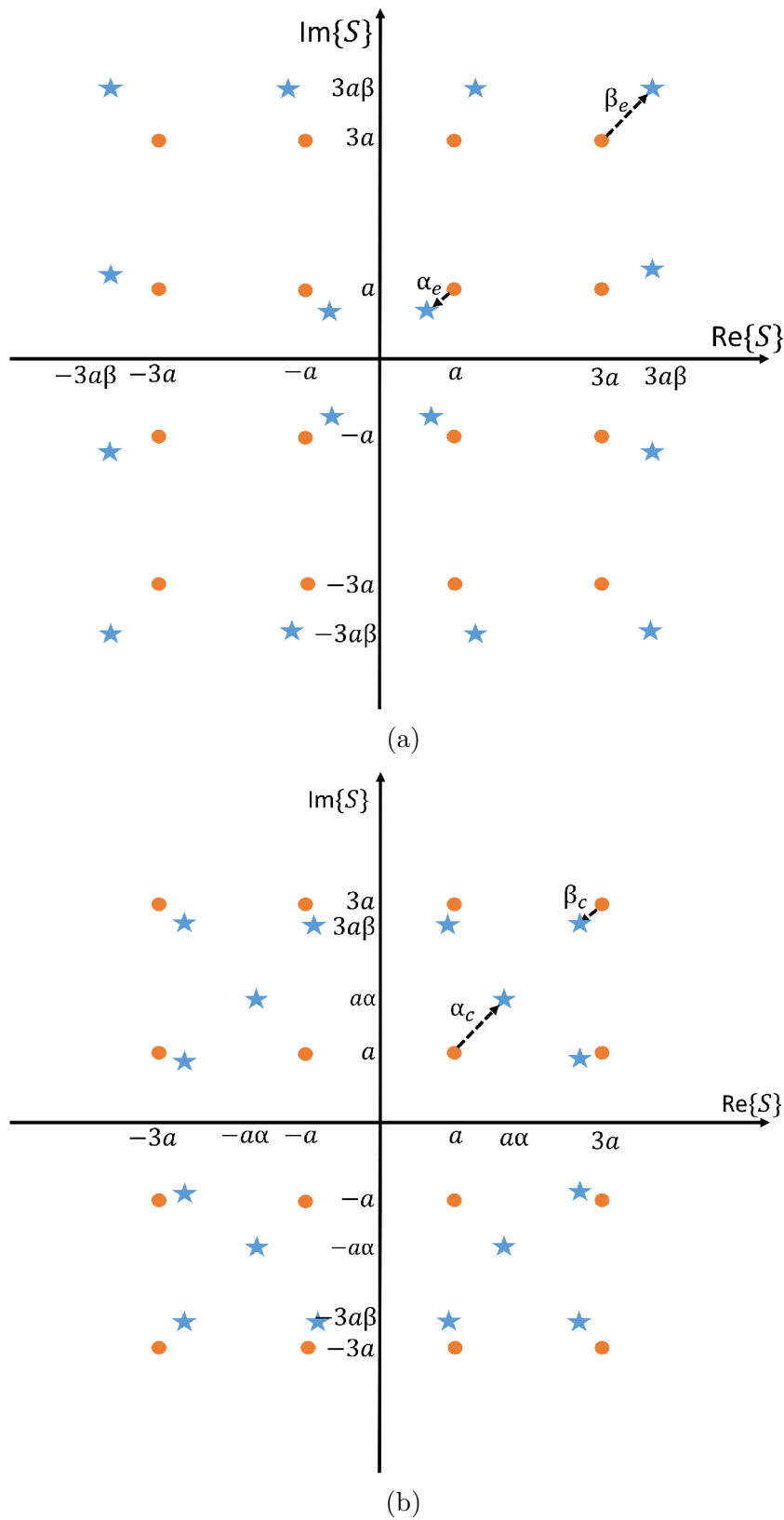


Fig. 5.7. (a) Modified expanded Multitone QAM symbols constellations with  $\alpha_e \leq 1$  (blue starred) and (b) Modified compressed Multitone QAM symbols constellations with  $\beta_c \leq 1$  (blue starred) with respect to conventional Multitone QAM symbols constellations (orange dots) for  $M = 16$ .

$\alpha_e = 0.7$ ,  $\alpha_e = 0.5$ , and  $\alpha_e = 0.3$  using (5.17) and (5.18) are shown in Fig. 5.8. It can be seen that as the  $\alpha_e$  is reduced  $\beta_e$  increases. The amount with which the inner symbols are compressed is higher than the amount with which outer symbols are expanded as  $M/4$  symbols compression is balanced by the expansion of  $3M/4$  symbols for the same average symbol constellation energy. The proposed expanded QAM constellation design is applicable for all modulation orders, for example, Fig. 5.9(a) illustrates a modified expanded constellation for  $M = 64$  where inner  $M/4$  symbols, i.e., 16 symbols are compressed, and the outer  $3M/4$  symbols, i.e., 48 symbols are expanded.

### 5.3.3 Compressed Multitone QAM symbols constellations

If the minimum available symbol energy is increased, the outer symbols' energy would be decreased for the same average symbol energy of the constellation, resulting in an overall compressed symbol constellation. Let  $\beta_c$  be the compression factor for outer  $3M/4$  symbols, then  $\alpha_c$  be the factor for inner  $M/4$  symbols can be represented by

$$\alpha_c = (4 + 2\sqrt{5}) - (2 + \sqrt{5})\beta_c. \quad (5.20)$$

Fig. 5.7(b) illustrates a modified compressed constellation where inner  $M/4$  symbols are expanded, i.e., minimum symbol magnitude increased and outer  $3M/4$  symbols are compressed, i.e., maximum available symbol magnitude decreased. As the outer symbols are compressed resulting in the expanded inner symbols for the same average symbol constellation energy, there must be a compression limit so that the inner symbols' magnitudes do not replace the outer symbols and the limit over  $\beta_c$  can be represented as

$$\frac{\alpha_c}{3} < \beta_c \leq 1. \quad (5.21)$$

Multitone QAM symbol constellations with  $M = 16$  for different cases of  $\beta_c = 0.88$ ,  $\beta_c = 0.9$ ,  $\beta_c = 0.92$ , and  $\beta_c = 0.96$  using (5.17) and (5.18) are shown in Fig. 5.10. It can be seen that as the  $\beta_c$  is reduced,  $\alpha_c$  increases, resulting in a higher minimum

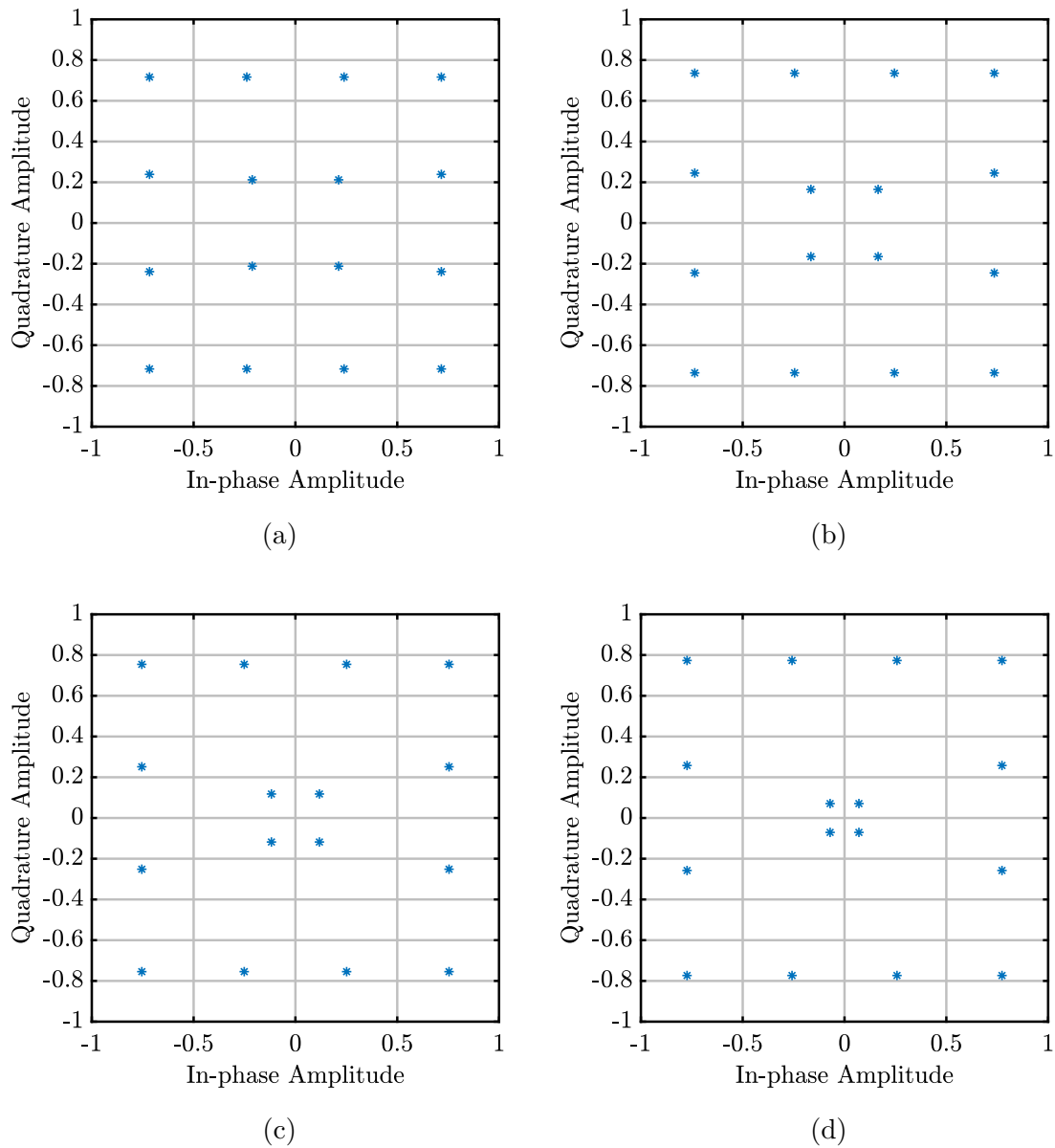


Fig. 5.8. Multitone QAM expanded symbols constellations for (a)  $\alpha_e = 0.9$ , (b)  $\alpha_e = 0.7$ , (c)  $\alpha_e = 0.5$ , and (d)  $\alpha_e = 0.3$ , for  $M = 16$ .

available symbol energy. As  $3M/4$  outer symbols compression is balanced by the expansion of  $M/4$  inner symbols for the same average symbol constellation energy, inner symbols energy increases with a larger amount compared to the decrease in the outer symbol energy and can be observed by Fig. 5.10(d) for  $\beta_c = 0.88$ . The proposed compressed QAM constellation design is applicable for all modulation orders, for example, Fig. 5.9(b) illustrates a modified compressed constellation for  $M = 64$  where inner  $M/4$  symbols, i.e., 16 symbols are expanded, and the outer  $3M/4$  symbols, i.e., 48 symbols are compressed.

## 5.4 Performance Analysis of Multitone QAM

Utilization of the same RF signal for information transfer, in addition to the power transfer, somewhat reduces the transferred power at the rectifier output. However, it offers an additional benefit of transferring the data as well as power simultaneously. Here, power conversion efficiency is considered as a metric for measuring the WPT performance of the designed Multitone QAM signal. Performance of the designed Multitone QAM signal is evaluated over an information-energy rectifier receiver model depicted in Fig. 5.1. The rectifier model is implemented in Keysight ADS and was experimentally validated by measurements in the paper [15].

The rectifier-receiver model consists of the input matching network with stubs and an input capacitance of 0.1 pF, two Skyworks SMS7630-079LF Schottky diodes, and an RC-LPF with an output capacitance of 0.1 pF and output load of  $R_{\text{load}} = 4.4 \text{ k}\Omega$ . For SWIPT, the rectifier-receiver model needs to be designed from both wireless power transfer and wireless information transfer perspectives. The rectifier is required to have maximum PCE over a large bandwidth to make the transmission of multitone signal with a large number of tones feasible for an increased throughput for wireless information transfer performance of the SWIPT system. Here, the rectifier is designed to maximize PCE over a large matched bandwidth of around 100 MHz. This is achieved by optimizing PCE and reflection coefficient with the

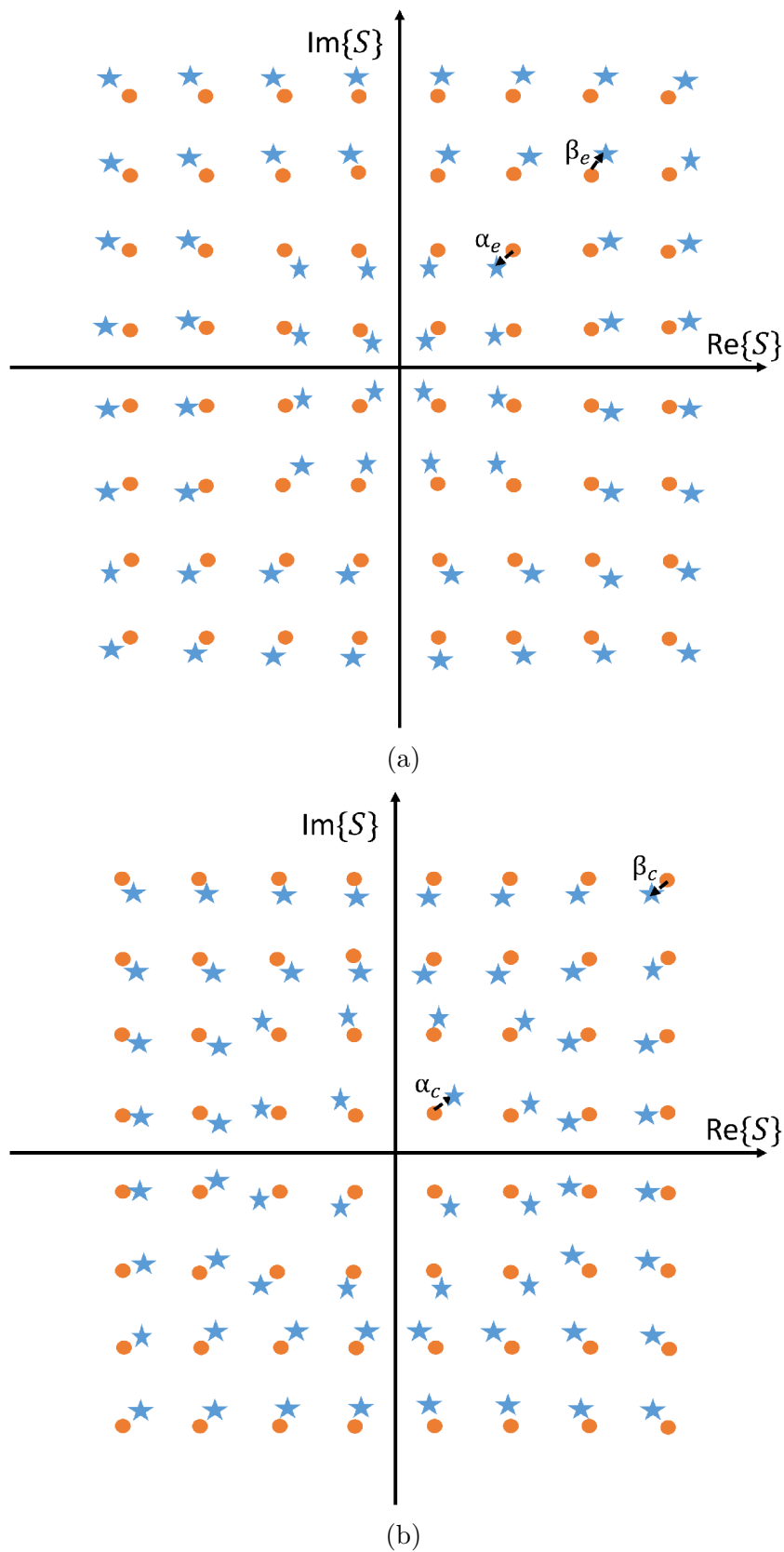


Fig. 5.9. (a) Modified expanded Multitone QAM symbols constellations with  $\alpha_e \leq 1$  (blue starred) and (b) Modified compressed Multitone QAM symbols constellations with  $\beta_c \leq 1$  (blue starred) with respect to conventional Multitone QAM symbols constellations (orange dots) for  $M = 64$ .

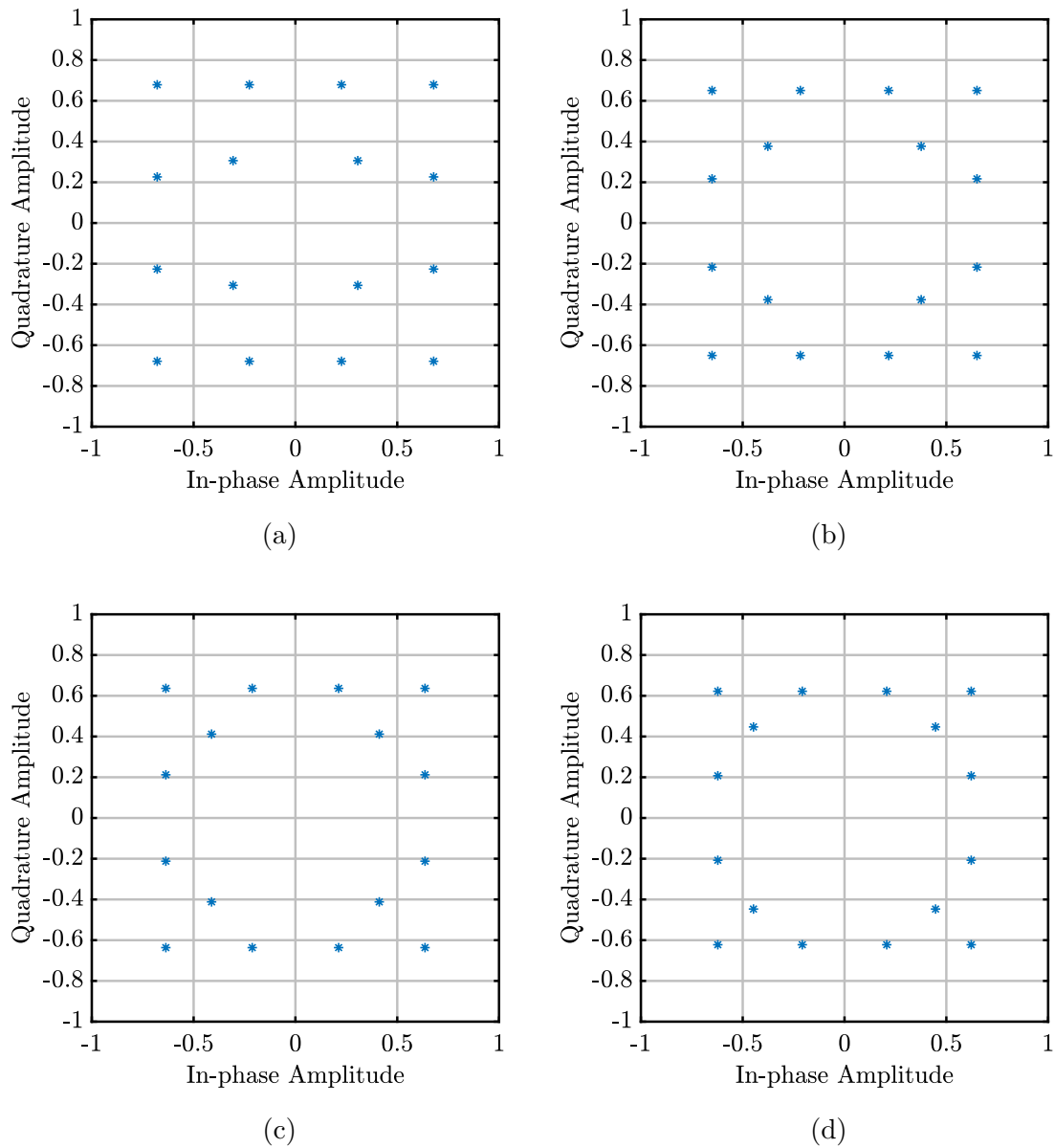


Fig. 5.10. Multitone QAM symbols constellations for (a)  $\beta_c = 0.96$ , (b)  $\beta_c = 0.92$ , (c)  $\beta_c = 0.9$ , and (d)  $\beta_c = 0.88$ , for  $M = 16$ .

help of stub lengths, input capacitance, and output load  $R_{\text{load}}$ . Also, LPF is designed to filter out fundamental tones and all the harmonics while simultaneously having a sufficiently large bandwidth to pass the second-order baseband intermodulation frequency components  $\text{IM}_2\text{s}$  used for information decoding at the receiver. Load resistance is selected according to this, and it is considered to be a fixed value. WIT performance deteriorates if the LPF cutoff frequency is selected too narrow as now, relevant baseband tones carrying information would suffer attenuation.

Multitone QAM tone frequencies are selected as asymmetrically spaced tones as discussed in [15]. For example, tone frequencies for a 6-tone Multitone QAM signal centered around 2.45 GHz results in 2.440 GHz, 2.441 GHz, 2.443 GHz, 2.447 GHz, 2.452 GHz, and 2.460 GHz with a Greatest common divisor,  $\text{GCD} = 1$  MHz from Algorithm 1 of [15]. The PCE at the rectifier output from Fig. 5.1 in terms of rectified signal DC power  $y_{\text{dc}}$  of  $y(t)$ , output load  $R_{\text{load}}$  of RC-LPF, and resulting average power  $P_{\text{avg}}$  of transmitted signal can be represented by

$$\text{PCE} = \frac{|y_{\text{dc}}|^2/R_{\text{load}}}{P_{\text{avg}}} \times 100. \quad (5.22)$$

All multitone QAM results are obtained with the help of Keysight ADS rectifier receiver model and MATLAB. The multitone QAM signal is designed to have a bandwidth smaller than the RF matching bandwidth of the rectifier-receiver model. In this transmission scheme,  $(N - 1)$  information symbols are transmitted over a single  $N$ -tone multitone signal. Therefore, throughput can be represented as

$$\text{Throughput} = \frac{(N - 1) \times \log_2 M}{T_{\text{QAM}}}, \quad (5.23)$$

where  $T_{\text{QAM}}$  is the time period of the Multitone QAM signal. Here, the effect of transmission distance on transmission efficiency has not been considered. The focus of the work has been the proposal of a Multitone QAM transmission scheme for SWIPT where both wireless power transfer and wireless information transfer are

performed on the same rectified signal through the integrated information-energy rectifier receiver. To evaluate the over-the-air performance of the proposed scheme with distance, the effect of the channel would require to be considered. This can be investigated in future work for further performance evaluation. Accordingly, appropriate coding schemes can be utilized for performance enhancement.

Fig. 5.11 illustrates the output PCE variation with the average input power  $P_{\text{in}}$  for two cases: when the 6-tone multitone signal is solely used for power transfer and when the 16-QAM 6-tone multitone signal is used to carry the information data of 1750 information symbols, i.e., 7000 bits with a transmission rate of 20 Mbps in addition to power transfer simultaneously. The transmission rate of 20 Mbps is evaluated from (5.23) for  $N = 6$ ,  $M = 16$ , and  $\text{GCD} = 1$  MHz resulting in  $T_{\text{QAM}} = 1 \mu\text{sec}$ . The performance is evaluated for 350 multitone streams, i.e., 1750 information symbols, i.e., 7000 bits. For low-input power levels, the signal's power conversion efficiency is quite low as the signal is not able to cross the diode's threshold voltage. Subsequently, PCE further increases with increasing input power levels and starts decreasing after a certain input power level (in our case  $P_{\text{in}} = 0$  dBm). The output PCE performance is input power dependent, but the aim is to use the rectifier in the most optimal input power range to maximize PCE. Our modulated Multitone QAM waveform brings an additional degree of freedom to tailor PCE and BER. Multitone QAM allows the tuning of PCE and information rate as a function of the input power level to help overcome this fundamental limitation of WPT. For example, for low input powers, it is possible to select a waveform by varying different parameters that improve PCE more compared to the information transfer rate.

It can be seen that the maximum achievable PCE has been reduced for the Multitone QAM SWIPT signal compared to the obtained PCE for the RF signal for WPT transfer only. Therefore, the simultaneous flow of information over the multitone signal results in a slightly lower power efficiency, resulting in a trade-off between WPT performance and WIT performance for the overall SWIPT performance of the signal.

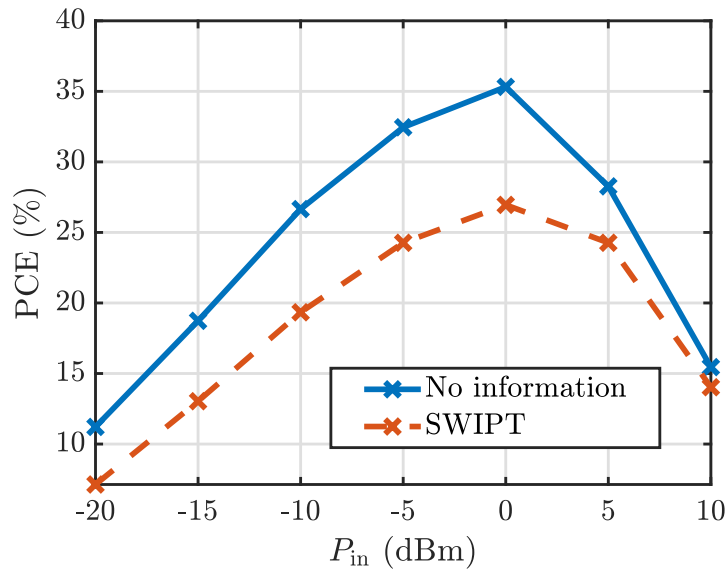


Fig. 5.11. PCE for a 6-tone multitone signal without information data and with a 16-QAM simultaneous information flow with a transmission rate of 20 Mbps varying with average input power  $P_{in}$ .

The attainable output PCE is affected by the transmitted information symbols magnitudes variations of different tones of the multitone signal. For  $M$ -QAM information transfer,  $M$  information symbols have different magnitudes. Consequently, the average power of the transmitted Multitone QAM signal depends upon the transmitted information symbols. The WPT performance of the system would be higher when the outer  $3M/4$  information symbols with higher magnitudes are transmitted compared to the cases where the inner  $M/4$  information symbols are transmitted. Therefore, it is necessary to minimize the difference between the achievable PCE of the rectifier for different transferred symbols. For this, a redesigning of QAM symbol constellations for a more stable output PCE is required, as discussed in Section 5.3.

Fig. 5.12 shows the achievable PCE for a 6-tone multitone signal at  $P_{in} = 0$  dBm when the outer  $3M/4$  information symbols are transmitted using asymmetric expanded 16-QAM symbol constellation with a transmission rate of 20 Mbps as discussed in Section 5.3.2. It can be seen that a PCE of a maximum of 37.7% can be achieved when no information is being transmitted over the RF multitone signal. This maximum possible efficiency of the rectifier depends upon the designed rectifier circuitry and may further be increased with an improved structure. With

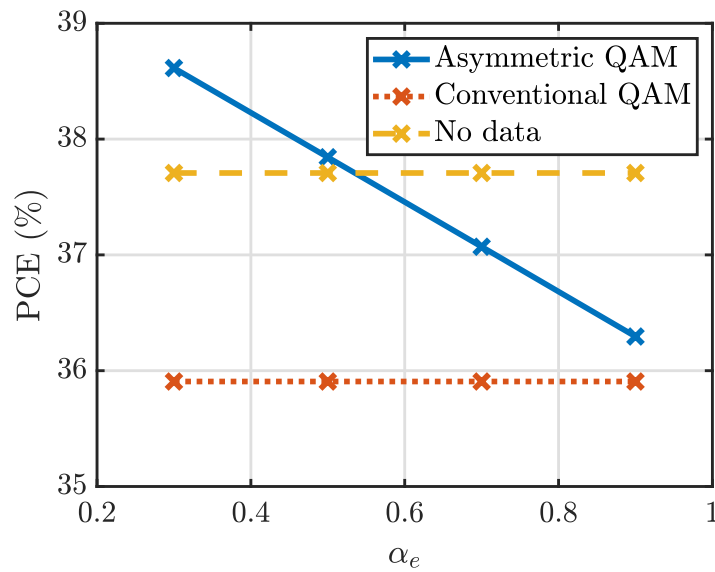


Fig. 5.12. PCE comparison for 6-tone multitone signal with no information flow, using conventional QAM, and the asymmetric expanded QAM symbols constellations for outer symbols with  $M = 16$  with a transmission rate of 20 Mbps and average input power  $P_{\text{in}} = 0$  dBm.

the transmission of the outer  $3M/4$  symbols of the conventional symmetric QAM symbols constellation, a maximum of 35.9% PCE can be achieved. This attainable power efficiency for the outer  $3M/4$  higher magnitudes can be increased by the asymmetric expanded 16-QAM symbol constellation of Fig. 5.7(a). In Fig. 5.12, it can be seen that PCE performance for outer symbols increases with the reduction in  $\alpha_e$ . The reason for this is the increased possible higher magnitudes for  $3M/4$  symbols with the reduction in  $\alpha_e$ . It can also be observed that with decreasing  $\alpha_e$ , obtained PCE can be higher compared to the case of multitone signal  $r(t)$  where no information is transmitted. This is due to the increased magnitude of outer symbols as  $\alpha_e$  decreases.

Similarly, Fig. 5.13 illustrates a comparison of achievable PCE for a 6-tone multitone signal at  $P_{\text{in}} = 0$  dBm where the inner  $M/4$  information symbols are transmitted using 16-QAM asymmetric symbol constellation with a transmission rate of 20 Mbps. It can be seen that WPT performance reduces from 37.7% to 15.31% when the inner information symbols of the conventional symmetric QAM symbol constellation of Fig. 5.5(a) are transmitted. The usage of asymmetric QAM constellation further

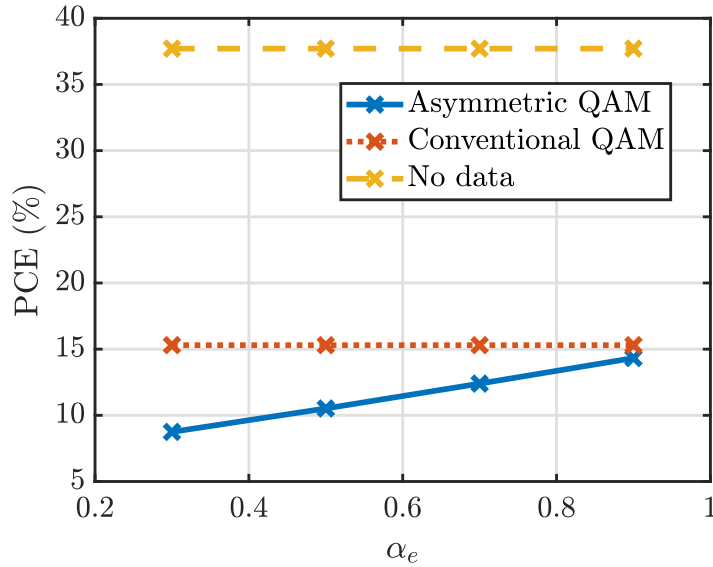


Fig. 5.13. PCE comparison for a 6-tone multitone signal with no information flow, using conventional QAM, and the asymmetric expanded QAM symbols constellations for inner symbols with  $M = 16$  with a transmission rate of 20 Mbps and average input power  $P_{\text{in}} = 0$  dBm.

reduces the WPT performance for the inner  $M/4$  symbols as transmitted magnitudes reduce with the reduced  $\alpha_e$  and are maximum when  $\alpha_e = 1$ , i.e., for conventional QAM. Therefore, SWIPT system performance can be improved with the help of an expanded symbols constellations when the outer  $3M/4$  symbols having larger magnitudes have a higher probability of transmission compared to the  $M/4$  inner symbols. From the WIT perspective, as  $\alpha_e$  reduces, the probability of detection error for the inner  $M/4$  symbols decreases due to the lower distance between inner symbols as shown in Fig. 5.8(c). However, for the outer  $3M/4$  symbols, the probability of error reduces with the reduction in  $\alpha_e$  because of the increased distance between outer symbols. For the case of a very low  $\alpha_e$ , increased detection error for inner symbols can be compensated with additional support vector machine (SVM) data classification and detection techniques [138].

Further, Fig. 5.14 compares the PCE performance of a 6-tone multitone QAM signal with a transmission rate of 20 Mbps using asymmetric compressed 16-QAM constellation (depicted in Fig. 5.7(b)) with conventional symmetric QAM constellation, and with no information flow at  $P_{\text{in}} = 0$  dBm. It can be seen that PCE performance for

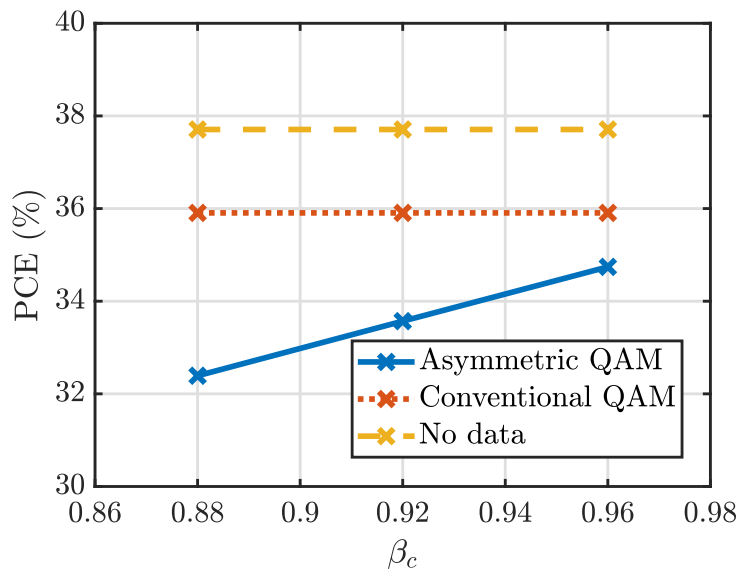


Fig. 5.14. PCE comparison for a 6-tone multitone signal with no information flow, using conventional QAM, and the asymmetric compressed QAM symbols constellations for outer symbols with  $M = 16$  with a transmission rate of 20 Mbps and average input power  $P_{\text{in}} = 0$  dBm.

outer  $3M/4$  symbols reduces slightly with the reduction in compression parameter  $\beta_c$  and is maximum  $\beta_c = 1$  for the conventional QAM constellation, i.e., from 36% for conventional 16-QAM to 32.4% for compressed 16-QAM for  $\beta_c = 0.88$ . However, PCE performance for inner  $M/4$  symbols improves to around 24.5% for  $\beta_c = 0.88$  compared to 15.31% for the conventional QAM as shown in Fig. 5.15. Therefore, for the case of the asymmetric compressed constellation, minimum power transfer using a multitone QAM signal can be increased with a small compromise in terms of maximal achievable PCE.  $\beta_c$  maybe selected close to the lowest possible values represented by (5.21) for the applications where minimum transferred power is of main concern. In such a case, WIT performance may get worse as symbols are now very close to each other, as shown in Fig. 5.10(d). Additional SVM-based classification and detection techniques can be utilized to improve the WIT performance [138].

From the WIT perspective, as  $\alpha_e$  reduces, the probability of detection error for the inner  $M/4$  symbols decreases due to the lower distance between inner symbols as shown in Fig. 5.8(c). However, for the outer  $3M/4$  symbols, the probability of error reduces with the reduction in  $\alpha_e$  because of the increased distance between outer

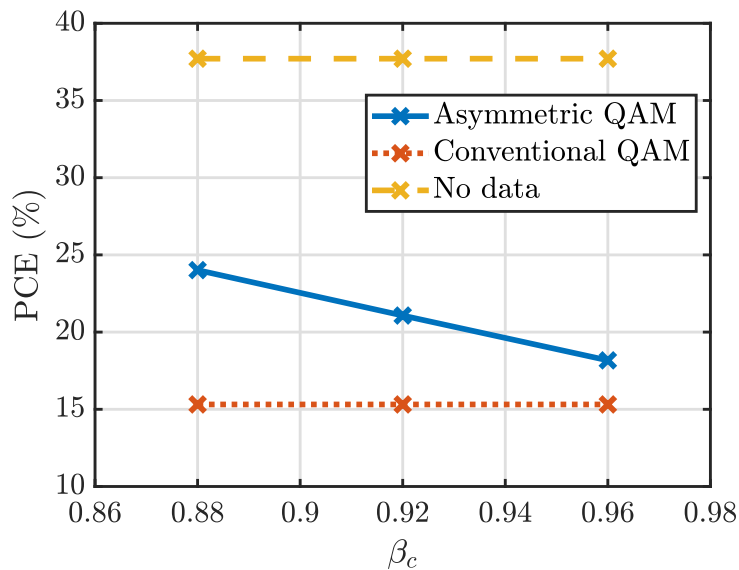


Fig. 5.15. PCE comparison for a 6-tone multitone signal with no information flow, using conventional QAM, and the asymmetric compressed QAM symbols constellations for inner symbols with  $M = 16$  with a transmission rate of 20 Mbps and average input power  $P_{\text{in}} = 0$  dBm.

symbols. For the case of a very low  $\alpha_e$ , increased detection error for inner symbols can be compensated with additional detection techniques such as support vector machine (SVM) detection. Therefore, the impact of information transfer on PCE can be reduced by using the asymmetric symbol constellation at the cost of a higher symbol error rate.

Further, an optimum value of  $\alpha_e$  or  $\beta_c$  can be selected depending on the probabilities of the transmission of the inner and outer symbols and depending upon the desired SWIPT performance. Till now, QAM constellations consist of symbols having equal probability. To observe the utilization of  $\alpha_e$  and  $\beta_c$ , a non-uniform probability distribution among inner and outer symbols is considered. Let inner  $M/4$  symbols have the probability of occurrence  $\Pr(s_{\text{inner}})$ . Then, the outer  $3M/4$  symbols probability  $\Pr(s_{\text{outer}})$  can be calculated as

$$\Pr(s_{\text{outer}}) = \frac{4 - M\Pr(s_{\text{inner}})}{3M}. \quad (5.24)$$

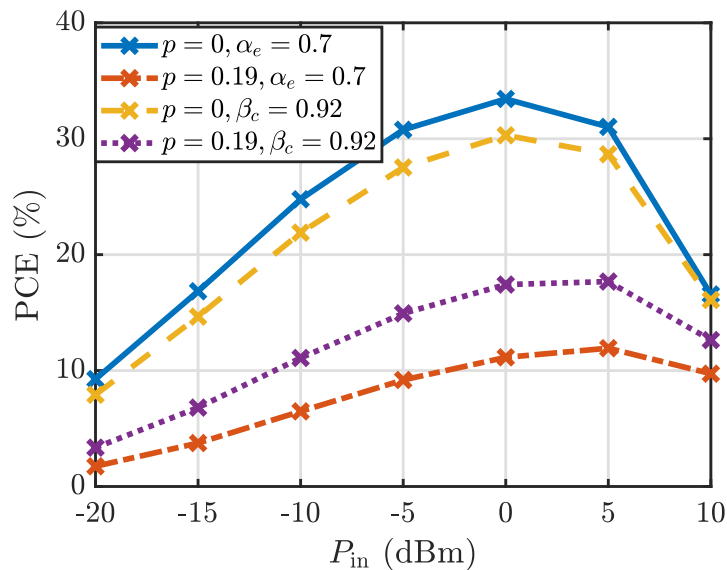


Fig. 5.16. PCE comparison for a 6-tone multitone signal with 16-QAM expanded constellation ( $\alpha_e = 0.7$ ) and compressed constellation ( $\beta_c = 0.92$ ) for  $\Pr(s_{\text{inner}}) = p$  for a transmission rate of 20 Mbps.

Fig. 5.16 illustrates the variation in the output PCE for 6-tone multitone QAM signal with the expanded QAM symbols as well as for the compressed QAM for unequal probabilities between inner and outer symbols. It can also be seen that the minimum level of power transfer can be increased by the usage of compressed QAM symbols. For example,  $\beta_c = 0.92$  performs better than  $\alpha_e = 0.7$  when inner symbols probability  $\Pr(s_{\text{inner}}) = p$  is also significant. Further, it can be observed that the maximum possible power transfer can be increased by the use of the expanded symbol constellation, i.e.,  $\alpha_e = 0.7$  performs better than the case of  $\beta_c = 0.92$  for the maximum possible power transfer.

Expanded asymmetric constellation provides enhanced WIT performance compared to compressed asymmetric constellations due to the increased distance between the symbols in the former case. Therefore, a compromise over system WPT performance is made with a multitone QAM signal. However, it provides an additional benefit of information transmission using the same resources. An expanded or compressed information symbols constellation can be utilized according to a desired WPT and WIT performance.

For different application demands, different transmission scenarios under these asymmetric constellations can be selected. For example, it is possible to have an output PCE close to the maximum possible PCE of the rectifier for the outer  $3M/4$  symbols with the help of an expanded symbol constellation which improves the information rate or number of bits per symbol (Fig. 5.12), i.e., it is possible to achieve maximum PCE while simultaneously transferring a data rate of 20 Mbps for a 6-tone multitone signal, but this is only possible with low symbol error rate at very high received signal powers. Asymmetric compressed QAM symbol constellation helps to increase the minimum transferred power level with the same data rate of 20 Mbps for a 6-tone multitone signal (Fig. 5.15) but would result in a higher symbol error rate. Therefore, the trade-off between the symbol error rate, modulation order (data rate), and power demands can be utilized according to the application's specific demands.

Furthermore, probabilities of symbol transmission (inner  $M/4$  symbols and outer  $3M/4$  symbols) can be varied to enhance the performance. Parameters can be selected based on the IoT device's operating conditions, such as whether consistent minimum power transfer is critical or if a high-power transfer in short bursts is preferred for the SWIPT's operation.

## 5.5 Conclusion

In this chapter, a novel Multitone QAM transmission scheme for an integrated information-energy SWIPT architecture has been proposed. Both amplitudes and phases of tones of the multitone signal are utilized for the information encoding, resulting in a higher data rate. Multiple symbols are transmitted simultaneously over a single stream of  $N$ -tone multitone QAM signal resulting in an OFDM-type communication. The effect of orientation of the QAM symbol constellation has been analyzed over the PAPR of the designed waveform. Further, varying magnitudes of the QAM symbols constellation have been shown to affect WPT performance significantly. Two asymmetric QAM constellation designs, expanded symbol constellation

and compressed symbol constellation, are proposed to enhance the power transfer performance according to the transmission probabilities of the inner symbols and outer symbols of the QAM constellation. It has been shown that it is important to design the QAM constellation properly according to the application-specific requirements of the IoT devices of the SWIPT system.

# Chapter 6

## Conclusions and Recommendations for Future Work

SWIPT is a promising future technology for charging sensors for self-sustainable networks. Replaceable batteries are not a feasible solution from the sensor's size perspective, sensor network size perspective, as well as from an environmentally friendly perspective. Therefore, exploiting available energy in RF signals can serve as a potential solution to meet the energy demands for the signal processing at the sensor nodes.

The existing transmission waveforms and the corresponding receiver architectures are still far from practical SWIPT systems. Some of the reasons are: (i) OFDM signal waveforms utilizing a separated receiver architecture consume significant power for signal processing at the receiver, (ii) the effect of WIT over WPT is still significant for the modulation methods used for an integrated information-energy architecture due to the presence of ripples at the output, (iii) moving toward more practical SWIPT systems, the constellation range needs to be increased so that the transmission can support higher modulation orders for increasing information rates,

and (iv) an end-to-end performance analysis including the transmitter performance for a particular waveform is required.

This Ph.D. thesis proposes novel modulated waveform designs to make simultaneous WIT and WPT operation possible at the sensor nodes. The transmission waveforms are designed in such a way that the overall power consumption is reduced at the sensor nodes by utilizing just a simple rectifier receiver circuitry not only for power transfer but also for information decoding purposes at the sensor node. Multiple transmission waveforms such as phase-based Multitone PSK, amplitude-based Multitone ASK, and a combination of amplitudes and phases Multitone QAM are proposed in this thesis.

## 6.1 Conclusions

A Multitone PSK transmission waveform has been designed to increase the data rate by transmitting  $(N - 1)$  symbols over an  $N$ -tone multitone signal which can be closely related to the non-uniformly spaced OFDM. It has been demonstrated that information transmission through phases does not reduce the overall PCE, and it is possible to have output power efficiency equivalent to the peak efficiency of the designed rectifier. Therefore, the effect of information transmission over the system WPT efficiency has been minimized with the Multitone PSK waveform. Information transmission with a wider phase range results in a lower signal PAPR, which is beneficial from the transmitter's perspective because it reduces the probability of saturating the power amplifier. From an information decoding perspective, a wider phase range with wider phase margins for information detection provides better BER performance at the sensor node, whereas a narrower phase range provides higher PCE. However, it has been shown that PCE reduces only about 3% with a wider phase range. Therefore, Multitone PSK has been shown to improve the end-to-end SWIPT performance by maximizing the rate-energy region.

Next, an  $N$ -tone Multitone ASK transmission signal scheme is proposed by utiliz-

ing the non-linearity of integrated information-energy rectifier receiver architecture. The data rate is increased by transmitting  $(N - 1)$  symbols over a single  $N$ -tone Multitone ASK signal stream. Information transmission results in a variation of the average power of the transmitted signal according to the transmitted information patterns affecting the attainable PCE. WPT performance of the designed transmitted signal has been shown to improve with increasing the minimum level of the symbols approaching the maximum possible power efficiency of the rectifier. However, BER increases with the decrease in amplitude margins. Logarithmically distributed symbols have been shown to improve WPT compared to linearly distributed symbols due to the non-linearity of the rectifier circuitry, whereas linearly distributed symbols result in better WIT performance. It is possible to attain a good WIT performance with a low transmitted signal power.

In the case of Multitone ASK, transmitting information in tones' amplitude levels offers the benefit of a simpler transmitter circuitry compared to the case of Multitone PSK, where information is transmitted through tones' phases, making phase synchronization more critical for WIT. Therefore, the desired SWIPT transmission signal scheme can be chosen depending on the requirements of the existing environmental conditions.

Then, an  $N$ -tone Multitone QAM transmission waveform carrying  $(N - 1)$  information symbols, is proposed for an integrated information-energy receiver. The multitone QAM signal is designed by exploiting the non-linearity of the receiver-rectifier, and both amplitudes and phases are used for information transfer offering an advantage of a higher degree of freedom to optimize WPT and WIT performances. It is shown that the power performance of the designed waveform varies with the orientation of the symbol constellation. Two asymmetric QAM constellation designs, expanded symbol constellation and compressed symbol constellation, are proposed to enhance WPT performance according to the application-specific requirement, such as whether a higher level of minimum continuous power transfer is critical or if a high-power transfer in short bursts is preferred for the SWIPT's

operation. It has been shown that WPT and WIT performances can be enhanced according to the IoT node's requirements by varying the transmission probabilities of inner symbols and outer symbols of the QAM constellation.

## 6.2 Recommendations & Future Works

This thesis proposes novel communication waveforms for SWIPT systems with integrated information-energy receiver rectifiers to minimize overall power consumption. However, the SWIPT performance of the above-proposed techniques can also be analyzed for other receiver architectures. The SWIPT research combining wireless communication and energy harvesting is a very vast area and an attractive research area for future wireless technologies. Some of the future research directions specifically for the research work presented in this Ph.D. thesis are highlighted as follows:

- **Multiuser SWIPT Design** In this Ph.D. thesis, waveforms are designed and their SWIPT performances are analyzed considering only single-user systems. However, practical WSNs are more complicated consisting of multiple sensor nodes. Therefore, the area of multiple access schemes for a multiuser SWIPT system still needs to be explored. Multiple access schemes utilizing the proposed transmission strategies would be needed to maximize the sum rate over all the users with a minimum energy constraint to optimize WIT performance and to maximize the PCE over all the users with a minimum information rate constraint to optimize WPT performance for overall SWIPT performance of IoT network.
- **Multiuser Heterogeneous SWIPT System** In a SWIPT-enabled WSN, different sensor nodes may be running different applications and now communication signals need to fulfill the different information and energy requirements of multiple sensors at the same time. Therefore, transmission strategies for multiple heterogeneous users need to be designed to maximize the information rate for data priority users and power transmission efficiency for energy-

harvesting priority users. An optimal resource management would require to be considered according to the available environmental conditions such as near-far scenarios. Beamforming techniques would be required to enhance the performance of the whole network.

- **Multi-mode SWIPT Receiver** Different SWIPT waveforms have different advantages and disadvantages in terms of transferred power and information rate and different sensor nodes have different data and energy requirements. A multi-mode receivers can be designed to receive different types of waveforms and the receiver would be able to switch between the modes according to the application. SWIPT system would further be optimized by combining these modes. The transmitter would need to be redesigned accordingly which would be able to switch between multiple waveforms.
- **High PAPR Waveforms** Multisine waveforms have been shown to perform better in terms of power transfer. In this thesis, high PAPR multisine waveforms are modulated to maximize the information rate as well as PCE. Designing and optimizing other high PAPR signals for a co-existence of energy harvesting and communication signals for SWIPT systems can be an interesting area of future research.
- **Channel Impact on Waveforms** The proposed modulated waveforms exploit amplitudes and phases of asymmetrically spaced multiple tones around a center frequency. For frequency selective channels and under multipath fading scenarios, phase distortion would occur and different tones would undergo different attenuation. Therefore, effect of channel over WPT and WIT performances need to be studied more on the designed SWIPT waveforms and further optimized according to the channel conditions.

# Bibliography

- [1] “Cisco annual internet report (2018–2023) white paper,” <https://www.cisco.com/c/en/us/solutions/collateral/executive-perspectives/annual-internet-report/white-paper-c11-741490.html>, accessed: 2021-06-27.
- [2] J. G. Andrews, S. Buzzi, W. Choi, S. V. Hanly, A. Lozano, A. C. K. Soong, and J. C. Zhang, “What will 5G be?” *IEEE Journal on Selected Areas in Communications*, vol. 32, no. 6, pp. 1065–1082, 2014.
- [3] A. Osseiran, F. Boccardi, V. Braun, K. Kusume, P. Marsch, M. Maternia, O. Queseth, M. Schellmann, H. Schotten, H. Taoka, H. Tullberg, M. A. Uusitalo, B. Timus, and M. Fallgren, “Scenarios for 5G mobile and wireless communications: the vision of the metis project,” *IEEE Communications Magazine*, vol. 52, no. 5, pp. 26–35, 2014.
- [4] I. Zhou, I. Makhdoom, N. Shariati, M. A. Raza, R. Keshavarz, J. Lipman, M. Abolhasan, and A. Jamalipour, “Internet of things 2.0: Concepts, applications, and future directions,” *IEEE Access*, vol. 9, pp. 70 961–71 012, 2021.
- [5] M. Agiwal, A. Roy, and N. Saxena, “Next generation 5G wireless networks: A comprehensive survey,” *IEEE Communications Surveys Tutorials*, vol. 18, no. 3, pp. 1617–1655, 2016.
- [6] D. Niyato, E. Hossain, M. M. Rashid, and V. K. Bhargava, “Wireless sensor networks with energy harvesting technologies: a game-theoretic approach to

- optimal energy management,” *IEEE Wireless Communications*, vol. 14, no. 4, pp. 90–96, 2007.
- [7] I. Krikidis, S. Timotheou, S. Nikolaou, G. Zheng, D. W. K. Ng, and R. Schober, “Simultaneous wireless information and power transfer in modern communication systems,” *IEEE Communications Magazine*, vol. 52, no. 11, pp. 104–110, 2014.
- [8] L. R. Varshney, “Transporting information and energy simultaneously,” in *IEEE International Symposium on Information Theory*. IEEE, 2008, pp. 1612–1616.
- [9] M. A. Ullah, R. Keshavarz, M. Abolhasan, J. Lipman, K. P. Esselle, and N. Shariati, “A review on antenna technologies for ambient RF energy harvesting and wireless power transfer: Designs, challenges and applications,” *IEEE Access*, vol. 10, pp. 17 231–17 267, 2022.
- [10] Z. Popovic, “Far-field wireless power delivery and power management for low-power sensors,” in *IEEE Wireless Power Transfer (WPT)*, 2013, pp. 1–4.
- [11] R. Zhang and C. K. Ho, “MIMO broadcasting for simultaneous wireless information and power transfer,” *IEEE Transactions on Wireless Communications*, vol. 12, no. 5, pp. 1989–2001, 2013.
- [12] X. Zhou, R. Zhang, and C. K. Ho, “Wireless information and power transfer: Architecture design and rate-energy tradeoff,” *IEEE Transactions on Communications*, vol. 61, no. 11, pp. 4754–4767, Nov. 2013.
- [13] A. S. Boaventura and N. B. Carvalho, “Maximizing DC power in energy harvesting circuits using multisine excitation,” in *IEEE MTT-S International Microwave Symposium*, June 2011, pp. 1–4.
- [14] M. S. Trotter, J. D. Griffin, and G. D. Durgin, “Power-optimized waveforms for improving the range and reliability of RFID systems,” in *IEEE International Conference on RFID*, April 2009, pp. 80–87.

- 
- [15] P. Dhull, D. Schreurs, G. Paolini, A. Costanzo, M. Abolhasan, and N. Shariati, “Multitone PSK modulation design for simultaneous wireless information and power transfer,” *IEEE Transactions on Microwave Theory and Techniques*, vol. 72, no. 1, pp. 446–460, Jan. 2024.
- [16] P. Dhull, D. Schreurs, S. Pollin, M. Abolhasan, and N. Shariati, “Multitone ASK waveform design for simultaneous wireless information and power transfer,” *IEEE Access*, 2024.
- [17] P. Dhull, N. Shariati, S. Pollin, M. Abolhasan, and D. Schreurs, “Multitone QAM modulation design for simultaneous wireless information and power transfer,” *IEEE Access*, 2024.
- [18] P. Dhull, A. P. Guevara, M. Ansari, S. Pollin, N. Shariati, and D. Schreurs, “Internet of things networks: Enabling simultaneous wireless information and power transfer,” *IEEE Microwave Magazine*, vol. 23, no. 3, pp. 39–54, March 2022.
- [19] N. Shinohara, *Wireless power transfer via radiowaves*. Wiley Online Library, 2014.
- [20] H. Kim, H. Hirayama, S. Kim, K. J. Han, R. Zhang, and J. Choi, “Review of near-field wireless power and communication for biomedical applications,” *IEEE Access*, vol. 5, pp. 21 264–21 285, 2017.
- [21] C. R. Valenta and G. D. Durgin, “Harvesting wireless power: Survey of energy-harvester conversion efficiency in far-field, wireless power transfer systems,” *IEEE Microwave Magazine*, vol. 15, no. 4, pp. 108–120, 2014.
- [22] A. Boaventura, D. Belo, R. Fernandes, A. Collado, A. Georgiadis, and N. B. Carvalho, “Boosting the efficiency: Unconventional waveform design for efficient wireless power transfer,” *IEEE Microwave Magazine*, vol. 16, no. 3, pp. 87–96, April 2015.

- 
- [23] N. B. Carvalho, A. Georgiadis, A. Costanzo, N. Stevens, J. Kracek, L. Pessoa, L. Roselli, F. Dualibe, D. Schreurs, S. Mutlu *et al.*, “Europe and the future for WPT,” *IEEE Microwave Magazine*, vol. 18, no. 4, pp. 56–87, 2017.
- [24] B. Clerckx, A. Costanzo, A. Georgiadis, and N. B. Carvalho, “Toward 1G mobile power networks: RF, signal, and system designs to make smart objects autonomous,” *IEEE Microwave Magazine*, vol. 19, no. 6, pp. 69–82, 2018.
- [25] P. Grover and A. Sahai, “Shannon meets tesla: Wireless information and power transfer,” in *IEEE international symposium on information theory*. IEEE, 2010, pp. 2363–2367.
- [26] L. Liu, R. Zhang, and K.-C. Chua, “Wireless information and power transfer: A dynamic power splitting approach,” *IEEE Transactions on Communications*, vol. 61, no. 9, pp. 3990–4001, 2013.
- [27] Y. Zeng, B. Clerckx, and R. Zhang, “Communications and signals design for wireless power transmission,” *IEEE Transactions on Communications*, vol. 65, no. 5, pp. 2264–2290, May 2017.
- [28] S. Bi, C. K. Ho, and R. Zhang, “Wireless powered communication: Opportunities and challenges,” *IEEE Communications Magazine*, vol. 53, no. 4, pp. 117–125, 2015.
- [29] S. Bi, Y. Zeng, and R. Zhang, “Wireless powered communication networks: An overview,” *IEEE Wireless Communications*, vol. 23, no. 2, pp. 10–18, 2016.
- [30] H. Tabassum, E. Hossain, A. Ogundipe, and D. I. Kim, “Wireless-powered cellular networks: Key challenges and solution techniques,” *IEEE Communications Magazine*, vol. 53, no. 6, pp. 63–71, 2015.
- [31] I. Krikidis, S. Timotheou, S. Nikolaou, G. Zheng, D. W. K. Ng, and R. Schober, “Simultaneous wireless information and power transfer in modern communication systems,” *IEEE Communications Magazine*, vol. 52, no. 11, pp. 104–110, 2014.

- 
- [32] D. Niyato, D. I. Kim, M. Maso, and Z. Han, “Wireless powered communication networks: Research directions and technological approaches,” *IEEE Wireless Communications*, vol. 24, no. 6, pp. 88–97, 2017.
- [33] E. Boshkovska, D. W. K. Ng, N. Zlatanov, and R. Schober, “Practical non-linear energy harvesting model and resource allocation for SWIPT systems,” *IEEE Communications Letters*, vol. 19, no. 12, pp. 2082–2085, Dec 2015.
- [34] X. Xu, A. Özçelikkale, T. McKelvey, and M. Viberg, “Simultaneous information and power transfer under a non-linear RF energy harvesting model,” in *2017 IEEE International Conference on Communications Workshops (ICC Workshops)*, May 2017, pp. 179–184.
- [35] K. Xiong, B. Wang, and K. J. R. Liu, “Rate-energy region of SWIPT for MIMO broadcasting under nonlinear energy harvesting model,” *IEEE Transactions on Wireless Communications*, vol. 16, no. 8, pp. 5147–5161, Aug 2017.
- [36] J. Kang, I. Kim, and D. I. Kim, “Wireless information and power transfer: Rate-energy tradeoff for nonlinear energy harvesting,” *IEEE Transactions on Wireless Communications*, vol. 17, no. 3, pp. 1966–1981, March 2018.
- [37] B. Clerckx and E. Bayguzina, “Waveform design for wireless power transfer,” *IEEE Transactions on Signal Processing*, vol. 64, no. 23, pp. 6313–6328, Dec 2016.
- [38] B. Clerckx, R. Zhang, R. Schober, D. W. K. Ng, D. I. Kim, and H. V. Poor, “Fundamentals of wireless information and power transfer: From RF energy harvester models to signal and system designs,” *IEEE Journal on Selected Areas in Communications*, vol. 37, no. 1, pp. 4–33, Jan 2019.
- [39] K. S. Turitsyn and S. K. Turitsyn, “Nonlinear communication channels with capacity above the linear shannon limit,” *Optics letters*, vol. 37, no. 17, pp. 3600–3602, 2012.

- 
- [40] M. Sorokina and S. Turitsyn, “Nonlinear signal transformations: path to capacity above the linear AWGN shannon limit,” in *IEEE Photonics Society Summer Topical Meeting Series*, July 2014, pp. 136–137.
- [41] M. S. Trotter and G. D. Durgin, “Survey of range improvement of commercial RFID tags with power optimized waveforms,” in *IEEE International Conference on RFID*, April 2010, pp. 195–202.
- [42] A. Collado and A. Georgiadis, “Optimal waveforms for efficient wireless power transmission,” *IEEE Microwave and Wireless Components Letters*, vol. 24, no. 5, pp. 354–356, May 2014.
- [43] H. Matsumoto and K. Takei, “An experimental study of passive UHF RFID system with longer communication range,” in *Asia-Pacific Microwave Conference (APMC)*, Dec 2007, pp. 1–4.
- [44] C. Lo, Y. Yang, C. Tsai, C. Lee, and C. Yang, “Novel wireless impulsive power transmission to enhance the conversion efficiency for low input power,” in *IEEE MTT-S International Microwave Workshop Series on Innovative Wireless Power Transmission: Technologies, Systems, and Applications*, May 2011, pp. 55–58.
- [45] Y. Yang, C. Tsai, C. Yang, and C. Yang, “Using pulse width and waveform modulation to enhance power conversion efficiency under constraint of low input power,” in *Asia Pacific Microwave Conference Proceedings*, 2012, pp. 400–402.
- [46] C. Yang, C. Tsai, Y. Yang, and C. Lee, “Enhancement of wireless power transmission by using novel multitone approaches for wireless recharging,” *IEEE Antennas and Wireless Propagation Letters*, vol. 10, pp. 1353–1357, 2011.
- [47] Y. Yang, C. Yang, C. Tsai, and C. Lee, “Efficiency improvement of the impulsive wireless power transmission through biomedical tissues by varying the

- duty cycle,” in *IEEE MTT-S International Microwave Workshop Series on Innovative Wireless Power Transmission: Technologies, Systems, and Applications*, May 2011, pp. 175–178.
- [48] C. R. Valenta, M. M. Morys, and G. D. Durgin, “Theoretical energy-conversion efficiency for energy-harvesting circuits under power-optimized waveform excitation,” *IEEE Transactions on Microwave Theory and Techniques*, vol. 63, no. 5, pp. 1758–1767, May 2015.
- [49] A. S. Boaventura and N. B. Carvalho, “Spatially-combined multisine transmitter for wireless power transmission,” in *2013 IEEE Wireless Power Transfer (WPT)*, May 2013, pp. 21–24.
- [50] A. J. Soares Boaventura, A. Collado, A. Georgiadis, and N. Borges Carvalho, “Spatial power combining of multi-sine signals for wireless power transmission applications,” *IEEE Transactions on Microwave Theory and Techniques*, vol. 62, no. 4, pp. 1022–1030, April 2014.
- [51] J. C. Pedro and N. B. Carvalho, *Intermodulation Distortion in Microwave and Wireless Circuits*. Artech House, 2003.
- [52] A. Collado and A. Georgiadis, “Improving wireless power transmission efficiency using chaotic waveforms,” in *IEEE MTT-S International Microwave Symposium*, June 2012, pp. 1–3.
- [53] G. Fukuda, S. Yoshida, Y. Kai, N. Hasegawa, and S. Kawasaki, “Evaluation on use of modulated signal for microwave power transmission,” in *European Microwave Conference*, Oct 2014, pp. 425–428.
- [54] D. Belo, J. Muñoz-Ferreras, R. Gómez-García, and N. B. Carvalho, “Exploiting radar waveforms for wireless power transmission,” in *2015 IEEE Wireless Power Transfer Conference (WPTC)*, May 2015, pp. 1–4.
- [55] D. Belo and N. B. Carvalho, “Harmonic spaced multisines for efficient wireless power transmission,” in *IEEE Wireless Power Transfer Conference (WPTC)*,

- May 2015, pp. 1–4.
- [56] N. Pan, D. Belo, M. Rajabi, D. Schreurs, N. B. Carvalho, and S. Pollin, “Bandwidth analysis of RF-DC converters under multisine excitation,” *IEEE Transactions on Microwave Theory and Techniques*, vol. 66, no. 2, pp. 791–802, Feb 2018.
- [57] A. Boaventura, N. B. Carvalho, and A. Georgiadis, “The impact of multi-sine tone separation on RF-DC efficiency,” in *Asia-Pacific Microwave Conference*, Nov 2014, pp. 606–609.
- [58] N. Pan, A. S. Boaventura, M. Rajabi, D. Schreurs, N. B. Carvalho, and S. Pollin, “Amplitude and frequency analysis of multi-sine wireless power transfer,” in *Integrated Nonlinear Microwave and Millimetre-wave Circuits Workshop (INMMiC)*, Oct 2015, pp. 1–3.
- [59] M. Rajabi, N. Pan, S. Pollin, and D. Schreurs, “Impact of multisine excitation design on rectifier performance,” in *European Microwave Conference (EuMC)*, Oct 2016, pp. 1151–1154.
- [60] H. Sakaki, K. Nishikawa, S. Yoshida, and S. Kawasaki, “Modulated scheme and input power impact on rectifier RF-DC efficiency for WiCoPT system,” in *European Microwave Conference (EuMC)*, Sep. 2015, pp. 60–63.
- [61] K. Nishikawa and H. Sakaki, “Impact of modulation scheme on rectifier RF-DC efficiency and optimal signal control technique,” in *IEEE MTT-S International Microwave and RF Conference (IMaRC)*, Dec 2015, pp. 288–291.
- [62] F. Bolos, J. Blanco, A. Collado, and A. Georgiadis, “RF energy harvesting from multi-tone and digitally modulated signals,” *IEEE Transactions on Microwave Theory and Techniques*, vol. 64, no. 6, pp. 1918–1927, June 2016.
- [63] M. H. Ouda, P. Mitcheson, and B. Clerckx, “Optimal operation of multi-tone waveforms in low RF-Power receivers,” in *IEEE Wireless Power Transfer Conference (WPTC)*, June 2018, pp. 1–4.

- 
- [64] Z. Liu, Z. Zhong, and Y. Guo, "In vivo high-efficiency wireless power transfer with multisine excitation," *IEEE Transactions on Microwave Theory and Techniques*, vol. 65, no. 9, pp. 3530–3540, Sep. 2017.
- [65] H. Sakaki, S. Yoshida, K. Nishikawa, and S. Kawasaki, "Analysis of rectifier operation with FSK modulated input signal," in *IEEE Wireless Power Transfer (WPT)*, May 2013, pp. 187–190.
- [66] H. Sakaki, T. Kuwahara, S. Yoshida, S. Kawasaki, and K. Nishikawa, "Analysis of rectifier RF-DC power conversion behavior with QPSK and 16QAM input signals for WiCoPT system," in *Asia-Pacific Microwave Conference*, Nov 2014, pp. 603–605.
- [67] H. Shimamura, R. Tanaka, H. Sakaki, S. Yoshida, K. Nishikawa, and S. Kawasaki, "Impact of symbol rate and roll-off factor on rectifier RF-DC conversion efficiency for wicopt system," in *European Microwave Conference (EuMC)*, Oct 2016, pp. 934–937.
- [68] S. Claessens, M. Rajabi, N. Pan, S. Pollin, and D. Schreurs, "Measurement-based analysis of the throughput-power level trade-off with modulated multisine signals in a SWIPT system," in *89th ARFTG Microwave Measurement Conference*, June 2017, pp. 1–4.
- [69] R. Zhang, L. Yang, and L. Hanzo, "Energy pattern aided simultaneous wireless information and power transfer," *IEEE Journal on Selected Areas in Communications*, vol. 33, no. 8, pp. 1492–1504, Aug 2015.
- [70] J. Wu, W. Lu, H. Peng, X. Liu, and J. Hua, "Simultaneous wireless information and power transfer in OFDM systems based on subcarrier allocation," in *International Wireless Communications and Mobile Computing Conference (IWCMC)*, Sep. 2016, pp. 926–929.
- [71] W. Lu, Y. Gong, J. Wu, H. Peng, and J. Hua, "Simultaneous wireless information and power transfer based on joint subcarrier and power allocation in

- OFDM systems,” *IEEE Access*, vol. 5, pp. 2763–2770, 2017.
- [72] M. Konstantinos, A. Adamis, and P. Constantinou, “Receiver architectures for OFDMA systems with subband carrier allocation,” in *European Wireless Conference*, 2008, pp. 1–7.
- [73] B. Clerckx, “Waveform optimization for SWIPT with nonlinear energy harvester modeling,” in *International ITG Workshop on Smart Antennas (WSA)*, March 2016, pp. 1–5.
- [74] H. Kassab and J. Louveaux, “Simultaneous wireless information and power transfer using rectangular pulse and CP-OFDM,” in *IEEE International Conference on Communications (ICC)*, May 2019, pp. 1–6.
- [75] R. F. Buckley and R. W. Heath, “System and design for selective OFDM SWIPT transmission,” *IEEE Transactions on Green Communications and Networking*, vol. 5, no. 1, pp. 335–347, 2021.
- [76] M. N. Khormuji, B. M. Popović, and A. G. Perotti, “Enabling SWIPT via OFDM-DC,” in *IEEE Wireless Communications and Networking Conference (WCNC)*, April 2019, pp. 1–6.
- [77] K. W. Choi, S. I. Hwang, A. A. Aziz, H. H. Jang, J. S. Kim, D. S. Kang, and D. I. Kim, “Simultaneous wireless information and power transfer (SWIPT) for internet of things: Novel receiver design and experimental validation,” *IEEE Internet of Things Journal*, vol. 7, no. 4, pp. 2996–3012, 2020.
- [78] D. I. Kim, J. H. Moon, and J. J. Park, “New SWIPT using PAPR: How it works,” *IEEE Wireless Communications Letters*, vol. 5, no. 6, pp. 672–675, Dec. 2016.
- [79] M. Rajabi, N. Pan, S. Pollin, and D. Schreurs, “Impact of multisine excitation design on rectifier performance,” in *2016 46th European Microwave Conference (EuMC)*, 2016, pp. 1151–1154.

- 
- [80] J. J. Park, J. H. Moon, K. Lee, and D. I. Kim, "Dual mode SWIPT: Waveform design and transceiver architecture with adaptive mode switching policy," in *IEEE Vehicular Technology Conference (VTC Spring)*, June 2018, pp. 1–5.
- [81] J. JinPark, J. HoMoon, K. Lee, and D. InKim, "Adaptive mode switching algorithm for dual mode SWIPT with duty cycle operation," in *IEEE International Workshop on Signal Processing Advances in Wireless Communications (SPAWC)*, June 2018, pp. 1–5.
- [82] I. Krikidis and C. Psomas, "Tone-index multisine modulation for SWIPT," *IEEE Signal Processing Letters*, vol. 26, no. 8, pp. 1252–1256, Aug. 2019.
- [83] S. Claessens, D. Schreurs, and S. Pollin, "SWIPT with biased ASK modulation and dual-purpose hardware," in *IEEE Wireless Power Transfer Conference (WPTC)*, May 2017, pp. 1–4.
- [84] S. Claessens, N. Pan, M. Rajabi, D. Schreurs, and S. Pollin, "Enhanced biased ASK modulation performance for SWIPT with AWGN channel and dual-purpose hardware," *IEEE Transactions on Microwave Theory and Techniques*, vol. 66, no. 7, pp. 3478–3486, July 2018.
- [85] A. M. Jaradat, J. M. Hamamreh, and H. Arslan, "OFDM with subcarrier number modulation," *IEEE Wireless Communications Letters*, vol. 7, no. 6, pp. 914–917, Dec 2018.
- [86] C. Im, J.-W. Lee, and C. Lee, "A multi-tone amplitude modulation scheme for wireless information and power transfer," *IEEE Transactions on Vehicular Technology*, vol. 69, no. 1, pp. 1147–1151, 2020.
- [87] M. Rajabi, S. Pollin, and D. Schreurs, "Hybrid rectifier-receiver node," in *IEEE MTT-S International Microwave Symposium (IMS)*, June 2017, pp. 1038–1041.
- [88] M. Rajabi, N. Pan, S. Claessens, S. Pollin, and D. Schreurs, "Modulation techniques for simultaneous wireless information and power transfer with an

- integrated rectifier–receiver,” *IEEE Transactions on Microwave Theory and Techniques*, vol. 66, no. 5, pp. 2373–2385, May 2018.
- [89] D. Kim, H. Lee, K. Kim, and J. Lee, “Dual amplitude shift keying with double half-wave rectifier for SWIPT,” *IEEE Wireless Communications Letters*, vol. 8, no. 4, pp. 1020–1023, Aug. 2019.
- [90] S. Claessens, N. Pan, D. Schreurs, and S. Pollin, “Multitone FSK modulation for SWIPT,” *IEEE Transactions on Microwave Theory and Techniques*, vol. 67, no. 5, pp. 1665–1674, May 2019.
- [91] S. Claessens, M. Rajabi, N. Pan, D. Schreurs, and S. Pollin, “Two-tone FSK modulation for SWIPT,” in *IEEE Wireless Power Transfer Conference (WPTC)*, June 2018, pp. 1–4.
- [92] T. Ikeuchi and Y. Kawahara, “Peak to average power ratio based signal detection for frequency shift multitone SWIPT system,” *IEEE Access*, vol. 9, pp. 4158–4172, 2021.
- [93] S. Claessens, Y. T. Chang, D. Schreurs, and S. Pollin, “Receiving ASK-OFDM in low power SWIPT nodes without local oscillators,” in *IEEE Wireless Power Transfer Conference (WPTC)*, 2019, pp. 20–25.
- [94] J. J. Park, J. H. Moon, H. H. Jang, and D. I. Kim, “Performance analysis of power amplifier nonlinearity on multi-tone SWIPT,” *IEEE Wireless Communications Letters*, vol. 10, no. 4, pp. 765–769, 2021.
- [95] T. A. Zewde and M. C. Gursoy, “Simultaneous wireless information and power transfer with finite-alphabet input signals,” in *2015 IEEE 82nd Vehicular Technology Conference (VTC2015-Fall)*, Sep. 2015, pp. 1–5.
- [96] I. Kim and D. I. Kim, “Wireless information and power transfer: Rate-energy tradeoff for equi-probable arbitrary-shaped discrete inputs,” *IEEE Transactions on Wireless Communications*, vol. 15, no. 6, pp. 4393–4407, June 2016.

- 
- [97] R. Rajashekar, M. Di Renzo, L. Yang, K. V. S. Hari, and L. Hanzo, "A finite input alphabet perspective on the rate-energy tradeoff in SWIPT over parallel gaussian channels," *IEEE Journal on Selected Areas in Communications*, vol. 37, no. 1, pp. 48–60, Jan 2019.
- [98] M. Varasteh, B. Rassouli, and B. Clerckx, "Wireless information and power transfer over an AWGN channel: Nonlinearity and asymmetric gaussian signaling," in *IEEE Information Theory Workshop (ITW)*. IEEE, 2017, pp. 181–185.
- [99] B. Clerckx and J. Kim, "On the beneficial roles of fading and transmit diversity in wireless power transfer with nonlinear energy harvesting," *IEEE Transactions on Wireless Communications*, vol. 17, no. 11, pp. 7731–7743, 2018.
- [100] M. Varasteh, B. Rassouli, H. Joudeh, and B. Clerckx, "SWIPT signalling over complex AWGN channels with two nonlinear energy harvester models," in *IEEE International Symposium on Information Theory (ISIT)*, June 2018, pp. 866–870.
- [101] M. Varasteh, B. Rassouli, and B. Clerckx, "SWIPT signaling over frequency-selective channels with a nonlinear energy harvester: Non-zero mean and asymmetric inputs," *IEEE Transactions on Communications*, vol. 67, no. 10, pp. 7195–7210, Oct 2019.
- [102] A. Rajaram, D. N. K. Jayakody, B. Chen, R. Dinis, and S. Affes, "Modulation-based simultaneous wireless information and power transfer," *IEEE Communications Letters*, vol. 24, no. 1, pp. 136–140, 2020.
- [103] E. Bayguzina and B. Clerckx, "Modulation design for wireless information and power transfer with nonlinear energy harvester modeling," in *IEEE International Workshop on Signal Processing Advances in Wireless Communications (SPAWC)*, June 2018, pp. 1–5.

- 
- [104] E. Bayguzina and B. Clerckx, “Asymmetric modulation design for wireless information and power transfer with nonlinear energy harvesting,” *IEEE Transactions on Wireless Communications*, vol. 18, no. 12, pp. 5529–5541, 2019.
- [105] B. Clerckx, “Wireless information and power transfer: Nonlinearity, waveform design, and rate-energy tradeoff,” *IEEE Transactions on Signal Processing*, vol. 66, no. 4, pp. 847–862, Feb 2018.
- [106] B. K. Ng and C. T. Lam, “On joint modulation design in two-user non-orthogonal multiple access channels,” in *International Symposium on Wireless Communication Systems (ISWCS)*. IEEE, 2016, pp. 65–69.
- [107] Y. Zhao, J. Hu, Z. Ding, and K. Yang, “Constellation rotation aided modulation design for the multi-user SWIPT-NOMA,” in *IEEE International Conference on Communications (ICC)*, May 2018, pp. 1–6.
- [108] J. Hu, Y. Zhao, and K. Yang, “Modulation and coding design for simultaneous wireless information and power transfer,” *IEEE Communications Magazine*, vol. 57, no. 5, pp. 124–130, May 2019.
- [109] Y. Zhao, J. Hu, Z. Ding, and K. Yang, “Joint interleaver and modulation design for multi-user SWIPT-NOMA,” *IEEE Transactions on Communications*, vol. 67, no. 10, pp. 7288–7301, Oct 2019.
- [110] T. D. Ponnimbaduge Perera, D. N. K. Jayakody, S. K. Sharma, S. Chatzinotas, and J. Li, “Simultaneous wireless information and power transfer (SWIPT): Recent advances and future challenges,” *IEEE Communications Surveys & Tutorials*, vol. 20, no. 1, pp. 264–302, Firstquarter 2018.
- [111] N. Shariati, W. S. T. Rowe, and K. Ghorbani, “RF field investigation and maximum available power analysis for enhanced RF energy scavenging,” in *2012 42nd European Microwave Conference*, 2012, pp. 329–332.
- [112] M. Del Prete, A. Costanzo, M. Magno, D. Masotti, and L. Benini, “Optimum excitations for a dual-band microwatt wake-up radio,” *IEEE Transactions on*

- Microwave Theory and Techniques*, vol. 64, no. 12, pp. 4731–4739, Dec. 2016.
- [113] N. Decarli, M. Del Prete, D. Masotti, D. Dardari, and A. Costanzo, “High-accuracy localization of passive tags with multisine excitations,” *IEEE Transactions on Microwave Theory and Techniques*, vol. 66, no. 12, pp. 5894–5908, Dec. 2018.
- [114] L. Yao, G. Dolmans, and J. Romme, “Optimal operation of RF energy rectifiers by adaptive number of frequency selection using multisine excitation,” in *2021 51st European Microwave Conference (EuMC)*, 2022, pp. 833–836.
- [115] N. Shariati, J. R. Scott, D. Schreurs, and K. Ghorbani, “Multitone excitation analysis in RF energy harvesters—considerations and limitations,” *IEEE Internet of Things Journal*, vol. 5, no. 4, pp. 2804–2816, Aug. 2018.
- [116] N. Ayir and T. Riihonen, “Joint impact of input power, PAPR, and load resistance on the receiver efficiency of multisine waveforms in RF energy harvesting,” in *2021 IEEE Wireless Power Transfer Conference (WPTC)*, 2021, pp. 1–4.
- [117] R. Zhang and C. K. Ho, “MIMO broadcasting for simultaneous wireless information and power transfer,” *IEEE Transactions on Wireless Communications*, vol. 12, no. 5, pp. 1989–2001, May 2013.
- [118] J.-G. Kim, G. Wei, M.-H. Kim, H.-S. Ryo, P.-C. Ri, and C. Zhu, “A splitting frequencies-based wireless power and information simultaneous transfer method,” *IEEE Transactions on Circuits and Systems I: Regular Papers*, vol. 65, no. 12, pp. 4434–4445, Dec. 2018.
- [119] Z. Jiang, Z. Wang, M. Leach, E. G. Lim, H. Zhang, R. Pei, and Y. Huang, “Symbol-splitting-based simultaneous wireless information and power transfer system for WPAN applications,” *IEEE Microwave and Wireless Components Letters*, vol. 30, no. 7, pp. 713–716, July 2020.

- [120] J. Kim and B. Clerckx, “Wireless information and power transfer for IoT: Pulse position modulation, integrated receiver, and experimental validation,” *IEEE Internet of Things Journal*, vol. 9, no. 14, pp. 12 378–12 394, July 2022.
- [121] L. W. Couch, *Digital and Analog Communication Systems*. 8th ed. NJ, USA: Pearson, 2012.
- [122] G. Paolini, Y. Murillo, S. Claessens, D. Masotti, S. Pollin, A. Costanzo, and D. Schreurs, “RF energy harvesting from GFSK-modulated BLE signals,” in *IEEE Topical Conference on Wireless Sensors and Sensor Networks (WiS-NeT)*, 2021, pp. 27–29.
- [123] Y. Guo, C. Skouroumounis, and I. Krikidis, “Joint information and energy transfer of SWIPT-enabled mobile users in wireless networks,” *IEEE Transactions on Green Communications and Networking*, vol. 6, no. 2, pp. 1141–1156, 2022.
- [124] A. Olutayo, Y. Dong, J. Cheng, J. F. Holzman, and V. C. M. Leung, “Performance of wireless powered communication systems over beaulieu-xie channels with nonlinear energy harvesters,” *IEEE Open Journal of the Communications Society*, vol. 4, pp. 456–463, 2023.
- [125] Y.-H. Liu, X. Huang, M. Vidojkovic, A. Ba, P. Harpe, G. Dolmans, and H. de Groot, “A 1.9nJ/b 2.4GHz multistandard (Bluetooth Low Energy/Zigbee/IEEE802.15.6) transceiver for personal/body-area networks,” in *2013 IEEE International Solid-State Circuits Conference Digest of Technical Papers*, 2013, pp. 446–447.
- [126] K. Philips, “Ultra low power short range radios: Covering the last mile of the IoT,” in *ESSCIRC 2014 - 40th European Solid State Circuits Conference (ESSCIRC)*, 2014, pp. 51–58.
- [127] C. Pérez-Penichet, C. Noda, A. Varshney, and T. Voigt, “Battery-free 802.15.4 receiver,” in *2018 17th ACM/IEEE International Conference on Information*

- Processing in Sensor Networks (IPSN)*, 2018, pp. 164–175.
- [128] D. Alqahtani, Y. Chen, W. Feng, and M.-S. Alouini, “A new non-linear joint model for RF energy harvesters in wireless networks,” *IEEE Transactions on Green Communications and Networking*, vol. 5, no. 2, pp. 895–907, 2021.
- [129] R. Keshavarz and N. Shariati, “Highly sensitive and compact quad-band ambient RF energy harvester,” *IEEE Transactions on Industrial Electronics*, vol. 69, no. 4, pp. 3609–3621, 2022.
- [130] K. Matsuura, K. Shin, D. Kobuchi, Y. Narusue, and H. Morikawa, “Synchronization strategy for distributed wireless power transfer with periodic frequency and phase synchronization,” *IEEE Communications Letters*, vol. 27, no. 1, pp. 391–395, 2023.
- [131] M. Rashid and J. A. Nanzer, “Frequency and phase synchronization in distributed antenna arrays based on consensus averaging and kalman filtering,” *IEEE Transactions on Wireless Communications*, vol. 22, no. 4, pp. 2789–2803, 2023.
- [132] W. Jiang and Y. Cui, “Performance analysis of MPSK phase detectors for carrier synchronization plls at low snrs,” *IEEE Communications Letters*, vol. 18, no. 12, pp. 2133–2136, 2014.
- [133] A. Costanzo, D. Masotti, G. Paolini, and D. Schreurs, “Evolution of SWIPT for the IoT world: Near- and far-field solutions for simultaneous wireless information and power transfer,” *IEEE Microwave Magazine*, vol. 22, no. 12, pp. 48–59, Dec. 2021.
- [134] J. Kim, B. Clerckx, and P. D. Mitcheson, “Signal and system design for wireless power transfer: Prototype, experiment and validation,” *IEEE Transactions on Wireless Communications*, vol. 19, no. 11, pp. 7453–7469, 2020.
- [135] A. Hanif and M. Doroslovački, “Simultaneous terahertz imaging with information and power transfer (STIIPT),” *IEEE Journal of Selected Topics in Signal*

- 
- Processing*, vol. 17, no. 4, pp. 806–818, 2023.
- [136] S. Claessens, P. Dhull, D. Schreurs, and S. Pollin, “WiLO-OFDM transmission scheme for simultaneous wireless information and power transfer,” *IEEE Open Journal of the Communications Society*, vol. 5, pp. 6261–6278, 2024.
- [137] S. A. Maas, *Nonlinear Microwave Circuits Second Edition*. Artech House Microwave Library, 2003.
- [138] L. V. Nguyen, A. L. Swindlehurst, and D. H. N. Nguyen, “SVM-based channel estimation and data detection for one-bit massive MIMO systems,” *IEEE Transactions on Signal Processing*, vol. 69, pp. 2086–2099, 2021.

# Biography



**Prerna Dhull** (Graduate Student Member, IEEE) received the M.Tech. degree in Electronics and Communication Engineering from the Indian Institute of Technology (IIT) Roorkee, Roorkee, India, in 2017. She was the recipient of Postgraduate Scholarship, Ministry of Human Resource Development (MHRD), Government of India. She worked as an Assistant professor with the Department of Electronics and Communi-

cation Engineering, Maharana Pratap University of Agriculture and Technology, Udaipur, India, till 2019. She served under the Technical Education Quality Improvement Programme (TEQIP) by the National Project Implementation Unit, MHRD, Government of India, for the implementation of World Bank Assisted Projects in technical education.

She is currently pursuing double Ph.D. degrees in electronics, RF, and communication technologies at KU Leuven, Leuven, Belgium, and the University of Technology Sydney, Sydney, New South Wales, Australia. She is a recipient of the University of Technology Sydney Presidential Scholarship, International Research Scholarship, GRS Publication Fund, and Thesis Completion Support Grant for her Ph.D. Her research interests include simultaneous wireless information and power transfer (SWIPT) systems, waveform design, wireless power transfer (WPT), RF energy harvesting, and self-sustainable networks.

FACULTY OF ENGINEERING SCIENCE  
DEPARTMENT OF ELECTRICAL ENGINEERING  
WAVECORE ARENBERG  
Kasteelpark Arenberg 10 - box 2444  
B-3001 Leuven  
prerna.dhull@kuleuven.be  
<https://www.esat.kuleuven.be>

